SYNTHESIS AND PROPERTIES OF SUBSTITUTED POLYLACTIDES AND SURFACE FUNCTIONALIZATION OF SMALL SILICA NANOPARTICLES

By

Quanxuan Zhang

A DISSERTATION

Submitted to
Michigan State University
in partial fulfillment of the requirements
for the degree of

Chemistry - Doctor of Philosophy

2013

ABSTRACT

SYNTHESIS AND PROPERTIES OF SUBSTITUTED POLYLACTIDES AND SURFACE MODULATION OF SMALL SILICA NANOPARTICLES

By

Quanxuan Zhang

Polylactides have been widely studied as a degradable material in environmental and biomedical fields due to their biodegradability and biocompatibility. However, the applications of polylactide has been limited by its high crystallinity, hydrophobicity and lack of functionalization; so strategies that provide routes to functionalized polyesters are necessary to produce materials with the desired physical and chemical properties. Development of those strategies has been one of the major efforts to expand the application of polylactides, especially as degradable delivery vehicles.

A series of propargyloxy lactic acid derivatives using poly(ethylene glycol) with different lengths as spacers between propargyl group and lactic acid were prepared with high yield via hydrolysis of cyanohydrin from inexpensive starting materials without using column purification. The versatility of the developed method was also tested by the survival of alkene group in the synthesis of allyloxy lactic acid. An azido lactic acid was also prepared to act as an alternative approach to render click function to polylactides. This allows for easy access of building up a library of clickable α-hydroxy acids to prepare clickable substituted polylactides.

Post-polymerization modification via click chemistry provides a convenient route to functionalized polylactides with a variety of new properties. We prepared clickable polylpropargyloxylactide that have pendant propargyl groups available for the attachment of chemical functionality using click chemistry without degradation of

polymer backbones. The clicked degradable polylactides have thermo-responsive properties with lower critical solution temperatures (LCST) from room temperature to 68 ^{o}C. The prepared amphiphilic copolymers, mPEG-*b*-polypropargyloxylactide were self-assembled into micelles which were core cross-linked to improve the structural stability of the micelles with better controlled release of cargo molecules and response to the reducing reagent.

The relationship between the glass transition temperature (T_g) of polylactide and its backbone structure was studied. The direct attachment of rigid and bulky substituents can be used to tune the T_g and thermal properties of polylactides and broaden the scope of their physical properties.

Silica nanoparticles (SiNPs) have attracted much attention due to their chemical inertness, low or non toxicity, excellent thermal stability and especially, easy access of surface functionalization. A facile grafting route was developed to prepare stably mono-dispersed SiNPs in aqueous media via click chemistry. Different sized SiNPs were grafted with a broad range of surface chemistries (carboxylic acids, amines, alcohols and methoxy-terminated polyethylene glycol chains). The resulted SiNPs were purified by dialysis and stably dispersed in water and *in vitro* cell culture media with narrow size distributions and no aggregation.

ACKNOWLEDEMENTS

I would like to sincerely thank my advisor, Dr.Greg Baker, for his guidance and support during my graduate study. I value tremendously his training and encouragements in all these years. I would also like to thank my current advisor, Dr. William Wulff, for his scientific guidance and support when serving on my committee, especially during the finalization of my graduate work here at MSU. I would also like to thank Dr. Xuefei Huang, Dr. Mitch Smith and Dr. Christina Chan for their invaluable and helpful discussions and suggestions for my research.

Thanks to Dan Holmes, Kermit Johnson, Kathy Severin, Richard Staples, Lijun Chen and Xudong Fan for their help on the instruments and valuable discussions.

I would like to thank former and current Baker group members Feng, Qin, Tom, Hui, Gina, Wen, Heyi, Zhe, Greg, Salinda and Olivia for their friendship and profitable discussions. I would also like to thank all of my friends I have met here, for making my life at MSU enjoyable.

Finally, I would like to thank my wife Hong for her love and support, as well as our lovely daughter, Aimee. I would also like to thank my parents, sisters, brothers-in-law, and all other family members for their support and encouragement during my study.

TABLE OF CONTENTS

LIST OF TABLES

LIST OF FIGURES

LIST OF SCHEMES

LIST OF ABBREVIATIONS

TBBA	4-*tert*-Butylbenzylalcohol
br	Broad
CM	Cross-linked micelle
CMC	Critical micelle concentration
d	Doublet
δ	Chemical shift
DCC	N,N'-Dicyclohexylcarbodiimide
dd	Doublet of doublet
DLS	Dynamic light scattering
DMAP	4-Dimethylaminopyridine
DMF	N,N-Dimethyl-formamide
DMSO-d_6	Deuterated dimethyl sulfoxide
DSC	Differential scanning calorimetry
FT-IR	Fourier transform infrared spectroscopy
GPC	Gel permeation chromatography
HOBT	Hydroxybenzotriazole
J	Coupling constant
LCST	Lower critical solution temperature
m	Multiplet
M_n	Number average molecular weight
m.p.	Melting point

mPEG	Poly(ethylene glycol) monomethyl ether
M_w	Weight average molecular weight
MWCO	Molecular weight cutoff
HRMS	High resolution mass spectroscopy
NMR	Nuclear magnetic resonance
p	Pentet
PDI	Polydispersity index
PEG	Poly(ethylene glycol)
PLA	polylactide
q	Quartet
RPMI 1640 media	Roswell Park Memorial Institute 1640 media
rt	Room temperature
s	Singlet
SiNP	Silica nanoparticles
$Sn(Oct)_2$	Tin(II)-2-ethylhexanoate
t	Triplet
TBD	Triazabicyclodecene
TEM	Transmission electron microscopy
T_g	Glass transition temperature
T_m	Melting temperature
TGA	Thermal gravimetric analysis
THF	Tetrahydrofuran

UV-Vis	Ultraviolet-Visible

CHAPTER 1 INTRODUCTION

1.1 Structure and Properties of Polylactides

Polylactide (PLA) is a biodegradable thermoplastic derived from lactic acid. Both polylactide and poly(lactic acid) are abbreviated as PLA since they have the same chemical structure, and since they only differ from each other in means of production. PLA can be prepared either by ring-opening polymerization (ROP) of lactides or by condensation polymerization of lactic acid which are obtained from economical fermentation of corn, beet-sugar, cane-sugar etc.[1] PLA has high mechanical properties, thermal plasticity, fabric ability, excellent biodegradability and biocompatibility. Notably these polymers are not only biodegradable (the aliphatic polyester backbone is intrinsically sensitive to water and heat) but also bio-assimilative, since the lactic acids generated by hydrolysis under physiological conditions are nontoxic components and can be eliminated via the Krebs cycle as water and carbon dioxide.[2] Glass transition temperature (T_g) is another important physical characteristic of polymers since it defines the useful temperature range of polymers for many applications.[2,3] Heating polymers above their T_g affects many physical properties and causes increased permeability, loss of dimensional stability, and increased resilience. Due to fairly low T_g of PLA (50 – 60 °C), crystalline poly(L-lactide) (PLLA) has been used in structural applications such as fibers and packaging,[4] orthopedic and bone fragment fixations,[5,6] absorbable sutures,[7,8] and scaffolds for tissue engineering.[9] Rubbery polylactides (lower T_g) at

room temperature degrade faster, and are preferred for applications such as controlled drug delivery and sustained drug release.[10,11,12]

1.2 Polymerization Methods and Mechanism to Polylactides

1.2.1 Polycondensation to Polylactides

Polycondensation of lactic acids in the presence of acid catalysts yields PLA and water as byproduct. The mechanism (**Scheme 1**) is the step-growth esterification polymerization by removing water to favor equilibrium.[13] Recently, this approach has gained some attention and it has been reported that binary catalysts comprised of metal compounds activated by co-catalysts are more effective catalysts in polycondensation. Although the polycondensation of L-lactic acid using a single catalyst (titanium(IV) butoxide) was reported to give PLA with high molecular weight up to 130,000 Da, the elongated reaction time (> 40 h) and wide PDI (>3.5) hindered its application.[14] The combination of $SnCl_2$ and *p*-toluenesulfonic acid (TSA) in melt polycondensation of L-lactic acid resulted in PLA with molecular weight up to 100,000 Da with low PDI (~1.5) and little racemization.[15] Using triphenylphosphine (PPh_3) as a co-catalyst, polycondensation of lactic acid catalyzed by $SnCl_2$ could similarly provide PLA with high molecular weight and low PDI.[16] Although this approach is relatively simple and inexpensive, it has several disadvantages. It is difficult to control the molecular weight, the polydispersity index (PDI), the PLA end groups, and the syntheses of copolymers with controlled sequences. As a consequence, there is increasing interest in methods that allow for the preparation of PLA polymers in a more reproducible and controlled

fashion.

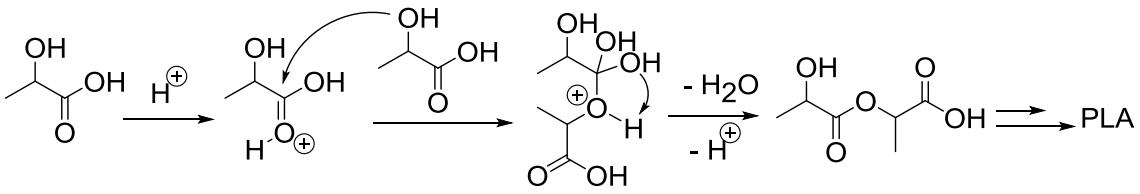

Scheme 1. Mechanism of polycondensation of lactic acid to PLA

1.2.2 Ring Opening Polymerization to Polylactides

The ring opening polymerization of lactide allows for a much higher control of lactide polymerization and remains by far the most widely used method for the synthesis of well-defined PLA materials. Mainly, there are five well-accepted polymerization mechanisms for lactide which are coordination-insertion, organo-catalysis, cationic, anionic and enzymatic mechanisms. The coordination-insertion and organocatalytic polymerizations are undoubtedly the most efficient and general methods reported so far for the ring opening polymerization of lactides.

1.2.2.1 Coordination-insertion Mechanism

There are a variety of catalysts which are studied and utilized in the effective polymerization of lactide, such as Al, Zn and Sn derivatives. Among them, tin(II) bis(2-ethylhexanoate) ($Sn(Oct)_2$) is the most widely used complex as catalyst for the preparation of PLA in industry and research due to its commercial availability, easiness of handling, low toxicity, and good solubility in common organic solvents and in melt monomers. It is highly active (from minutes to a few hours in bulk at 140-180 °C) and allows for the preparation of high-molecular-weight polymers (up to 10^5 or even 10^6 Da

in the presence of a alcohol co-initiator) with really low PDI. The mechanism is as shown in **Scheme 2**.[17] Two molecules of methanol coordinate to $Sn(Oct)_2$ with retention of the two octanoate moieties through hydrogen bonds formed between alcohol and octanoate ligands. Then lactide coordinates to the complex and induces a proton migration from methanol to the nearby octanoate ligand. Subsequently, the formed methoxy group on tin nucleophilically attacks the carbonyl of the coordinated lactide followed by ring opening to form the ring opening product with a hydroxyl end group which coordinates with the catalyst and allows for chain propagation. Several other research groups have also suggested that the alcohol added as co-initiator might substitute at least one octanoate group in a rapid equilibration, and the resulting Sn-alkoxide is then acting as the true initiator of the polymerization process, which also falls into the coordination-insertion mechanism.[18,19] Ring-opening polymerization of lactides with organometallic catalysts at high temperatures or with long reaction times often leads to both inter- and intra- molecular transesterification reactions resulting in an increase in PDI of the polylactides.

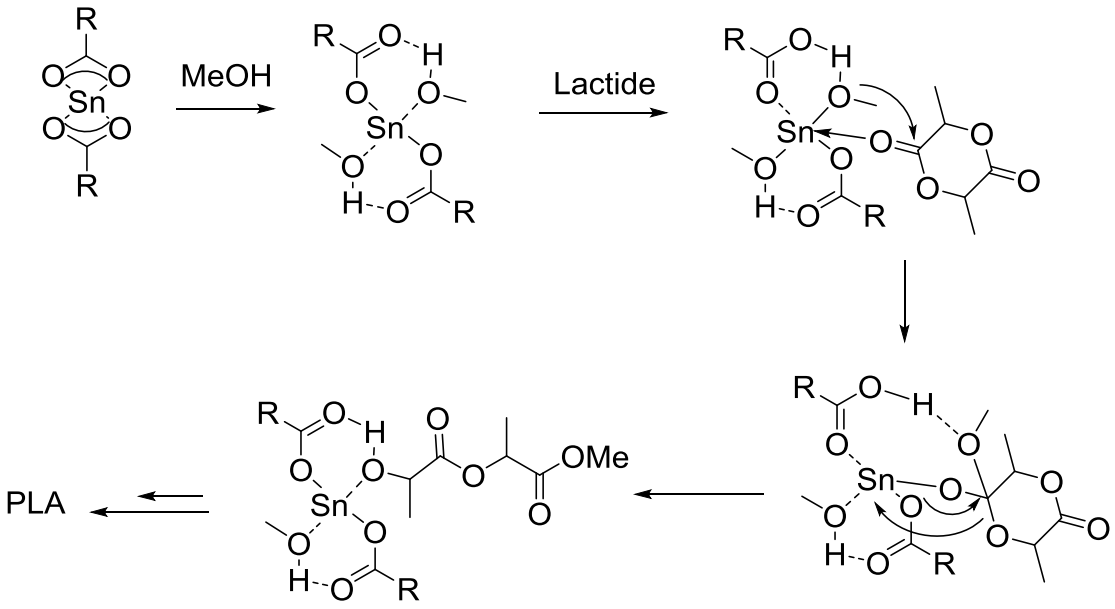

Scheme 2. Proposed Coordination-insertion mechanism for lactide ring-opening polymerization

1.2.2.2 Organo Catalysis Mechanism

Although $Sn(Oct)_2$ has been approved by the U.S. FDA, the toxicity related to most tin compounds is still one considerable drawback in biomedical applications. Thus organo-catalyzed lactide polymerization has been widely studied due to promising applications in the biomedical field and is considered to be one of the viable alternatives to organometallic approaches. Organo catalysts are easy to prepare, handle, and are typically nontoxic, and thus have generated much attention from both industry and academia.

Hedrick and co-workers reported the first use of the organic catalyst 4-(dimethylamino)pyridine (DMAP) in the ring opening polymerization of lactide which provided well controlled molecular weight and low PDI (~1.1).[20] Later on, other super bases, such as 1,8-Diazabicyclo[5.4.0]undec-7-ene (DBU), [21] 1,5,7-

Triazabicyclo[4.4.0]dec-5-ene (TBD)[22] and sparteine[23] were also reported to have excellent catalytic activity to afford polylactide with high yield, controlled molecular weight and narrow PDI. Taking DMAP as an example (**Scheme 3**), it serves to activate a carbonyl of the lactide ring and then nucleophilic attack of an alcohol gives a ring opened structure with an ester functionality on one end and a hydroxyl functionality on the other that reacts with the next lactide to continue chain propagation. Hedrick and coworkers also claimed that a secondary alcohol functionality is the best compromise for propagating lactide ROP without inducing undesirable transesterification of ring-opened products. This is supported by model reactions where primary alcohols react not only with lactide but also with ring-opened esters, whereas secondary alcohols only react with lactide and are inert toward ring opened products. This selectivity is responsible for the living character of nucleophilically catalyzed lactide polymerization.[24]

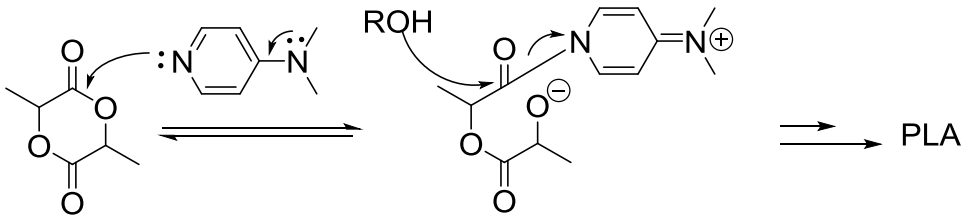

Scheme 3. Proposed mechanism of DMAP-catalyzed lactide ring opening polymerization

N-Heterocyclic carbenes (NHC) have showed high catalytic activity in ring opening polymerization of lactide[25] through a mechanism similar to that for DMAP by nucleophilically activating the lactide monomer, achieving near quantitative conversions for target degrees of polymerization (feed ratio: 30 to 200) within 24 hours with narrow PDI. The living nature of the polymerization was proved by charging additional lactide to

the system to afford further PLA chain growth with a final molecular weight close to theoretical value.[26,27] This type of catalyst also enables the selective construction of complex polymer architectures. For example, in the presence of alcohols/co-initiators, linear polylactides are generated using N-heterocyclic carbene catalysts, whereas in the absence of alcohols, N-heterocyclic carbene catalysts result in cyclic polylactides with high molecular weight and narrow PDI.

Hedrick and coworkers also utilized nucleophilic tertiary phosphines as a metal-free catalyst for the ring-opening polymerization of lactides.[28] The lactide was activated by the Lewis basic phosphine towards attack by the nucleophilic alcohol. However, tertiary phosphine catalysts only exhibit high activity in bulk polymerization at high temperature. The activity in solution is fairly low with polymerization requiring up to several weeks to achieve high conversion.

A bifunctional thiourea−tertiary amine catalyst was reported by Hedrick and coworkers in 2005 for living polymerization of lactide.[29] Polylactides with predictable molecular weights and extremely narrow PDI (~1.05) were produced under mild and highly selective polymerization conditions, which is the characteristic of a living polymerization. The bifunctional nature of the catalyst was proposed to be involved in the simultaneous activation of the initiating/propagating alcohol by an acid−base interaction with the tertiary amine moiety and the activation of the carbonyl of the lactide monomer via hydrogen bonding by the thiourea moiety of the catalyst (**Scheme 4**).

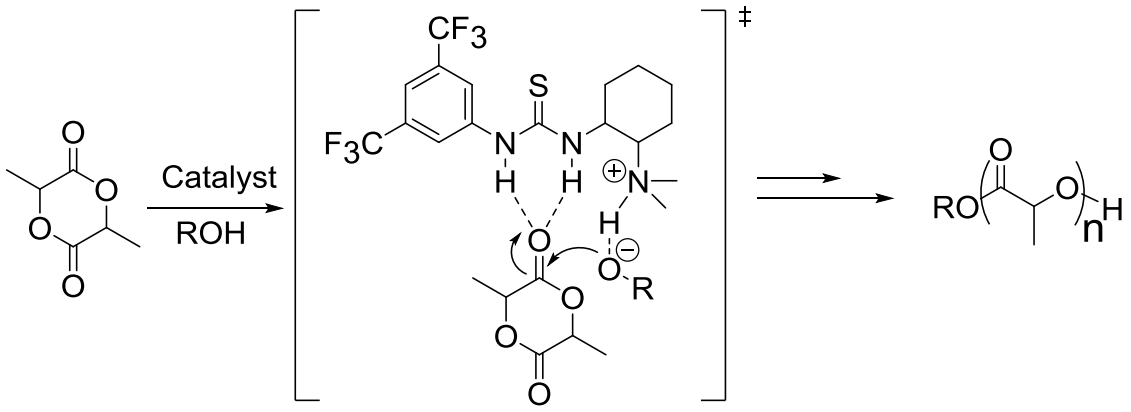

Scheme 4. Bifunctional thiourea-tertiary amine catalyst and its proposed intermediate

1.2.2.3 Cationic Mechanism

There are limited strong acids or carbenium ion donors capable of initiating a cationic polymerization of lactides, such as trifluoromethanesulfonic acid (HOTf) and methyl trifluoromethanesulfonate (MeOTf).[30] According to the fact that poly(L-lactide) with methyl ester end groups exhibit 100% retention of the optical purity of the lactide monomer as determined by ^{1}H NMR analysis and optical rotation measurements when using either MeOTf or HOTf as the initiator. Thus, the cationic mechanism was proposed to occur via a protonation or alkylation of the carbonyl *O*-atom of lactide with the consequence that the O–CH bond is subject to electrophilic activation. This activated O-CH bond is cleaved by the nucleophilic attack of another monomer which occurs repeatedly until a termination step is reached, ruling out the possibility that the polymerization occurs via cleavage of the acyl-oxygen bond (**Scheme 5**).

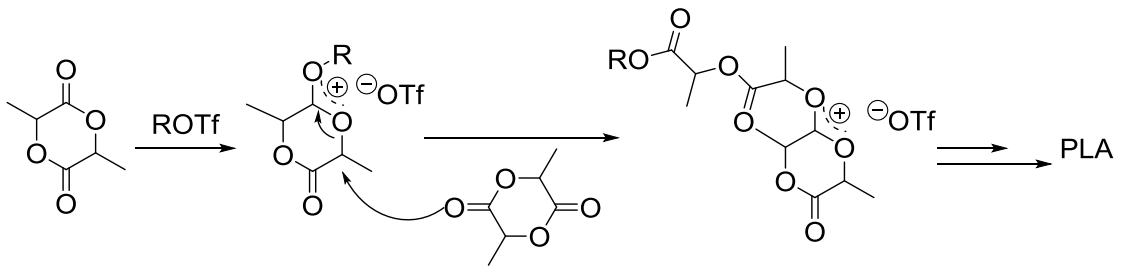

Scheme 5. Proposed cationic polymerization mechanism

However, it was reported[31] that the cationic copolymerization of lactide and glycolide was far from a living polymerization under the reported cationic polymerization conditions. By varying monomer-to-initiator ratios from 50 to 400, the resulting polymer samples showed very similar viscosities (0.15 - 0.27 dl/g), which indicates the nonliving nature of the polymerization.

1.2.2.4 Anionic Mechanism

The effective initiators used for anionic polymerization of lactides are alkali metals and alkali metal oxides, etc. The polymerization may proceed either by a living or a nonliving process depending on the reaction conditions, initiators, and monomers. The reaction may be initiated by either deprotonation of lactide[32] (**Scheme 6 (a)**) or nucleophilic attack on the carbon of the carbonyl group[33] (**Scheme 6 (b)**) followed by chain propagation resulting in formation of linear polylactide. These two initiation steps can be differentiated by end group analysis of the resulted PLA by whether or not initiator fragments are incorporated in the polymer. The reported experimental results strongly support both pathways depending on the basicity of the initiators.[34] Initiators formed in situ (such as metal alkoxides) can increase the efficiency of ring opening

polymerization compared to their commercial materials. The racemization and trans-esterification can also be minimized by carefully choosing the right initiators.

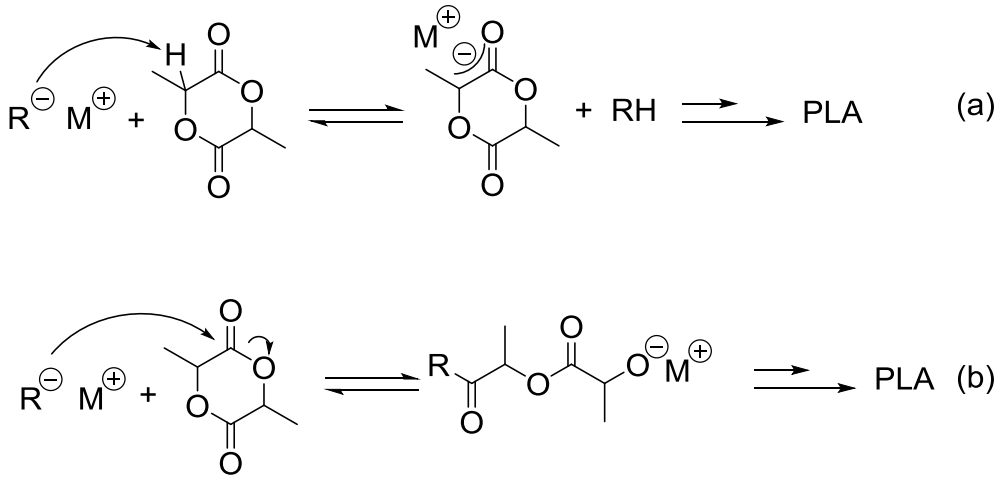

Scheme 6. Proposed anionic polymerization mechanism

Although higher activities can be anticipated for anionic initiators that typically display strong nucleophilic and/or basic character, the deleterious contributions from trans-esterification and racemization reactions are not neglectable when trying to achieve well controlled polymerizations when naked or loosely bonded anionic species are involved.

1.2.2.5 Enzymatic Mechanism

The use of enzymes as tools in *in vitro* catalysis is increasing interest. Enzymes have been recently used in ring opening polymerization to make polyesters.[35] Enzymes offer an advantage over conventional catalysts, namely, selectivity and biocompatibility. Most commerically available lipases have proved to be active in ring opening polymerization of lactide.[36, 37] The lipase-catalyzed polymerization of lactides is believed to share a mechanism similar to the organo catalysts discussed above. The

catalytic site of the lipase has a serine residue which activates the lactide to form an acyl-enzyme intermediate, and this intermediate suffers nucleophilic attack by terminal hydroxy group of the propagating polymer chain leading to chain propagation and regeneration of the enzyme.[38]

However, the reported PLAs from enzyme catalysis have either low molecular weights, relatively wide polydispersity indexes or elongated polymerization times of days, which currently limits the application of PLAs formed from enzyme catalysts.

1.3 Functionalization of Polylactides

However, due to the low solubility of polylactides in water, the applications of polylactides in an aqueous environment have been greatly restricted.[39] In addition, the lack of functional group diversity in the backbones and side chains in polylactide makes further modification extremely difficult. So functionalization of polylactides has been a major effort in expanding the application of polylactides, especially as degradable delivery vehicles. Three strategies have been developed to introduce functionality in the polylactide scaffold: the initiating/end group modification approach, the monomer derivative approach and the post-polymerization modification approach (**Scheme 7**). All three routes allow the incorporation of functional groups onto the polymer backbone or side chains or to introduce access points for further modification to tune the physical properties of PLA. The first approach has been widely investigated, and since it involves the conversion of lactide to polylactides, it is often an integral part of the other two approaches as well.

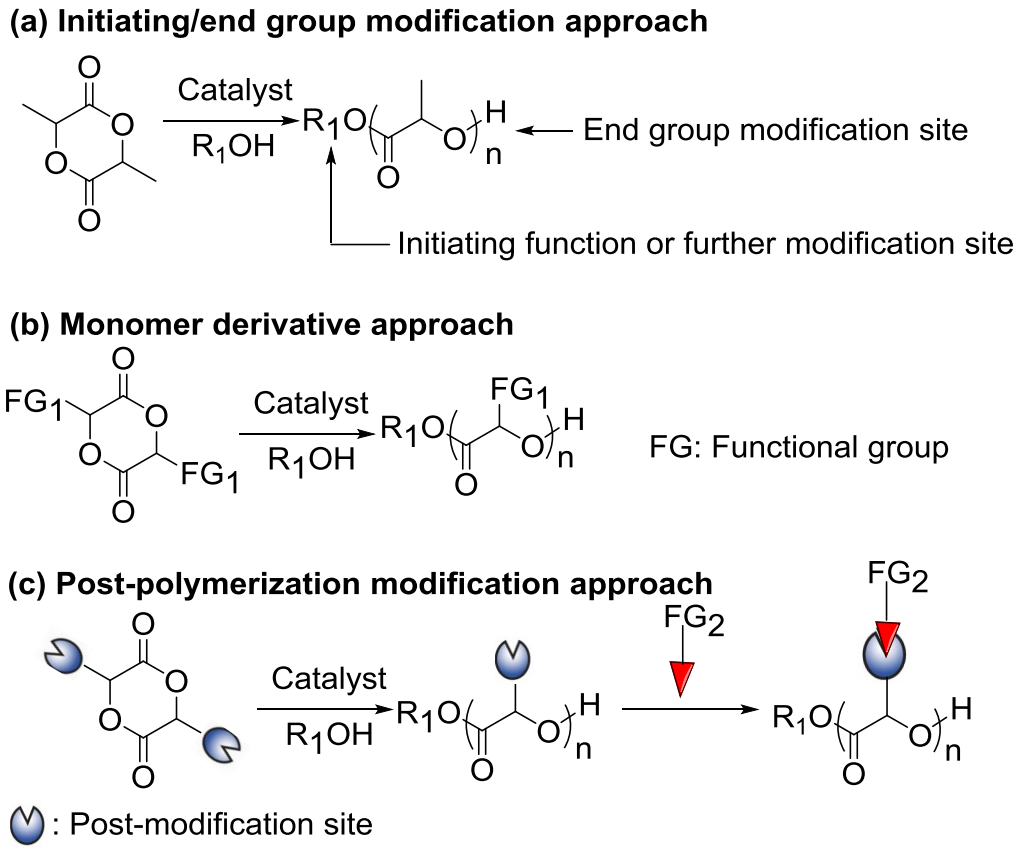

Scheme 7. Strategies to functionalized Polylactides. “For interpretation of the references to color in this and all other figures, the reader is referred to the electronic version of this dissertation.”

1.3.1 Initiating/End Group Modification Approach

Due to the limited scope of their applications, the properties of polylactides have been thoroughly modified and improved by the initiating/end group modification method. A variety of functionalities have been incorporated into polylactides either using different functional initiators during the polymerization or introducing different functionalities into the ω-hydroxyl group by treating with reactive functional molecules.

Polyethylene glycol-*co*-polylactide (PEG-*co*-PLA) block copolymers have gained much attention due to their amphiphilic properties, their ability to form nanoparticles and

their application as delivery vehicles (**Figure 1 (a)**). Li and coworkers prepared di-block and tri-block copolymers of PEG-*co*-PLA using mono- or di- hydroxy PEG as initiators.[40] The hydrophilicity of these copolymers was dramatically improved and hydrogels could be formed in water for both di-block and tri-block copolymers. Longer PEG segments could prevent the crystallization of PLA segments in the copolymer. PEG-PLA copolymers were also formulated into micelles and their degradation behavior was also studied.[41] Micelles made from the dialysis method are more stable than those from the direct dissolution method which showed a collapsed micellar structure. The composition of PLA-PEG copolymers greatly affects the degradation of micelles. Micelles with longer hydrophilic PEG blocks exhibit more size changes due to the less compact structure compared to copolymers with longer PLA segments. Polysaccharides (TMS protected Pulluan) and a monosaccharide (benzyl protected α-glucose) have also been introduced into polylactides (**Figure 1 (b)**) to improve hydrolytic degradability and surface wettability.[42,43] As expected, the higher hydrophilicity due to the presence of saccharides in the copolymer resulted in faster degradation. Amino, halide, pyrene (fluorescent) and other functionalities were also reported to have been incorporated into polylactides either through direct initiation of polymerization or post-deprotection of the polylacitdes (**Figure 1 (c)**).[44,45,46]

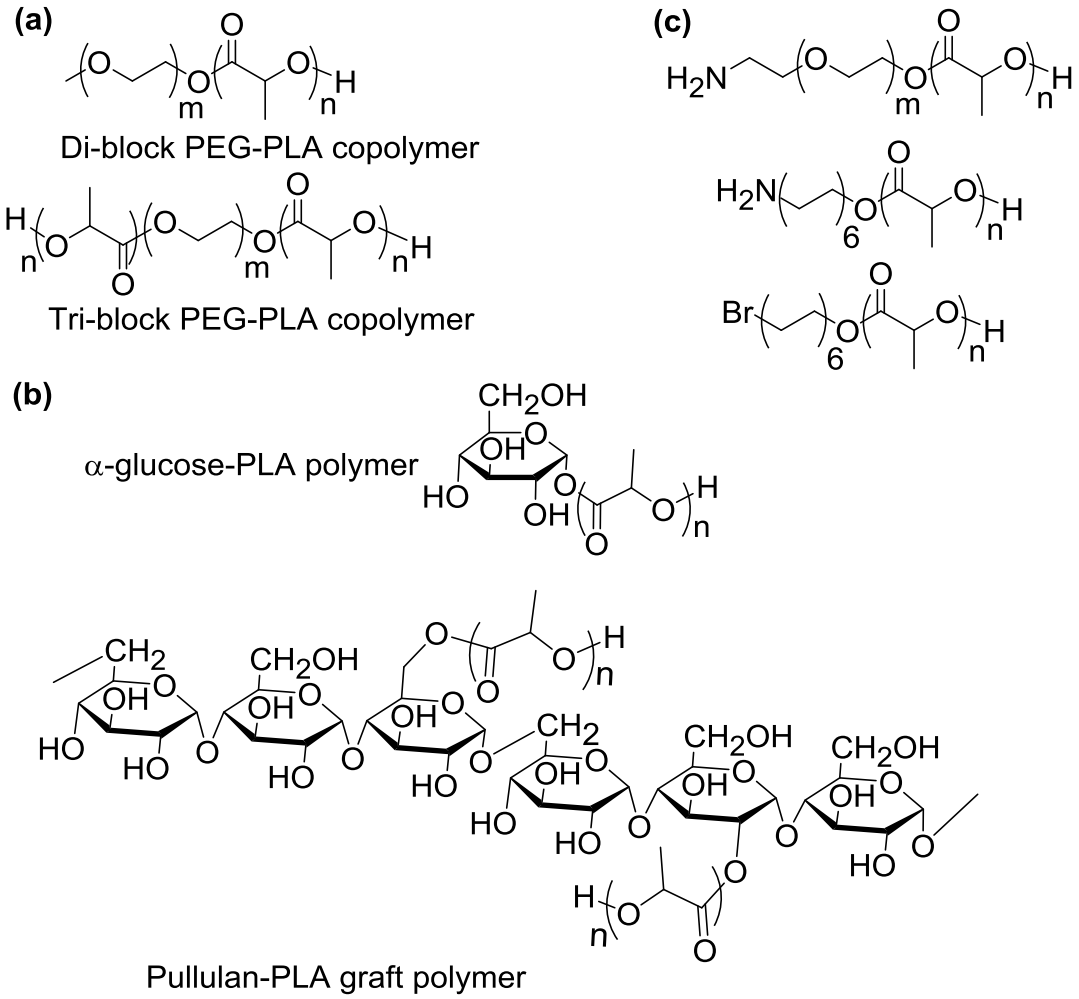

Figure 1. Examples of functionalized polylactides through initiating group approach

Another method for introducing functionality via initiating group modification is to first install a moiety that is capable of undergoing "click" chemistry, thus enabling further modification through super easy and efficient chemistry. If the polylactide chain end is caped with 1,6-heptadiyne, which it can be further cyclo-polymerized to afford brush polymers containing a semiconducting polyene backbone (**Scheme 8 (a)**). The incorporation of an alkyne into polylactides was not affected by the presence of terminal alkyne group and PLA was obtained with well controlled molecular weight and narrow PDI.[47] However, it was reported that the alkyne function could be affected in the

presence of $Sn(Oct)_2$ probably due to oxidative coupling. This deleterious result was avoided by adding *N,N,N′,N″,N″*-pentamethyldiethylenetriamine whose steric hindrance prevents interaction with the propargyl groups and affords polylactide with higher chain-end functionality (f = 86%) and low polydispersity (PDI = 1.22) (**Scheme 8 (b)**).[48] Propargyl alcohol initiated polylactides formation has also been used to prepare materials for click modification with other azido-polymers or small organic azides to prepare amphiphilic polymers promoting the study of their self assembly behavior in aqueous media (**Scheme 8 (c)**).[49,50] Thio-ene click chemistry (Michael addition of thiols) was also utilized to functionalize polylactides by capping a thiol at the polymer chain end. Molla and coworkers reported versatile chain end modification of polylactide containing pyridyl disulfide group which can be quantitatively reduced to a thiol by DTT. [51] This versatile methodology includes thiol−ene, thiol−maleimide, and thiol−acrylate “click” reactions, as well as chain-end modification by thiol−disulfide exchange reactions (**Scheme 8 (d)**). Thus the functionalities of the resulted polylactides can be greatly modified depending upon the nature of the attached molecules or polymers. Recently, one tetrazine-norbornene click modification was also applied in a mild and efficient manner to norbornene-initiated polylactide formation without degradation of the polymer backbone.[52]

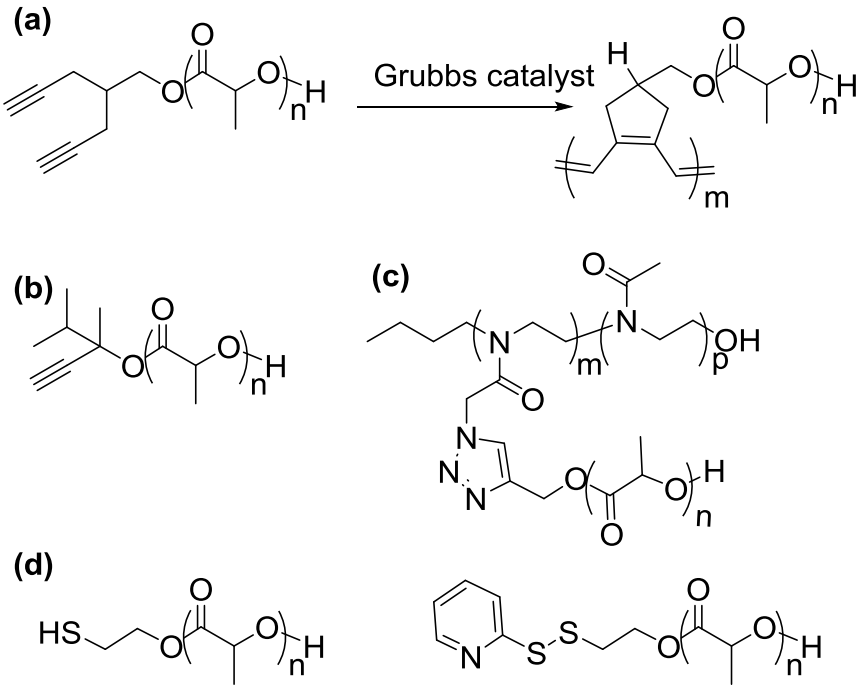

Scheme 8. Examples of chain-end clickable polylactides capable of further modification through initiating group approach

The ω-hydroxy group in polylactide chain ends is very important for end group modification to modulate the polymer's properties, most commonly via activated esterification to protect the hydrolytic PLA backbone. Stupp and coworkers prepared self-assembled polylactides initiated by cholesterol (Chol) to investigate the self-assembly behavior and the interactions of the resulting polylactides with cells. They further modified the Chol-PLA by reacting the ω-hydroxy group with different functionalized carboxylic acids to afford new ordered PLA scaffolds. The bulk Chol-PLA material could self-assemble to give layered structures through proper orientation of cholesterol moiety with the spacing distance corresponding to the short PLA chain length.[53]

End group modification of the secondary alcohol terminus of Chol-PLA was also

examined with the rodcoil L-lysine dendrons (3 generations, G1, G2 and G3) which could be coupled in high yield by double esterification (DIPC/DPTS) while maintaining the sensitive PLA part of the backbone without cleavage (**Figure 2**). The resulting amphiphilic molecules displayed very different self assembly behavior compared to their precursor (Chol-PLA). They exhibit very poor ordering in the dry state, which consisted of a lamellar self assembled structure with periodicities that depend on the degree of hydration (< 50%) and discrete nanosized aggregates at high degree of hydration (> 50%).[54] Significant improvement in water wettability, enhanced adhesion of 3T3 mouse calvaria cells and greater population growth rates were observed after coating the self-assembled layer structure onto poly(L-lactic acid) fibers.[55] These rodcoil dendron biomaterials could be of potential interest as temporary molecular scaffolds for cell and tissue engineering (**Figure 2**).

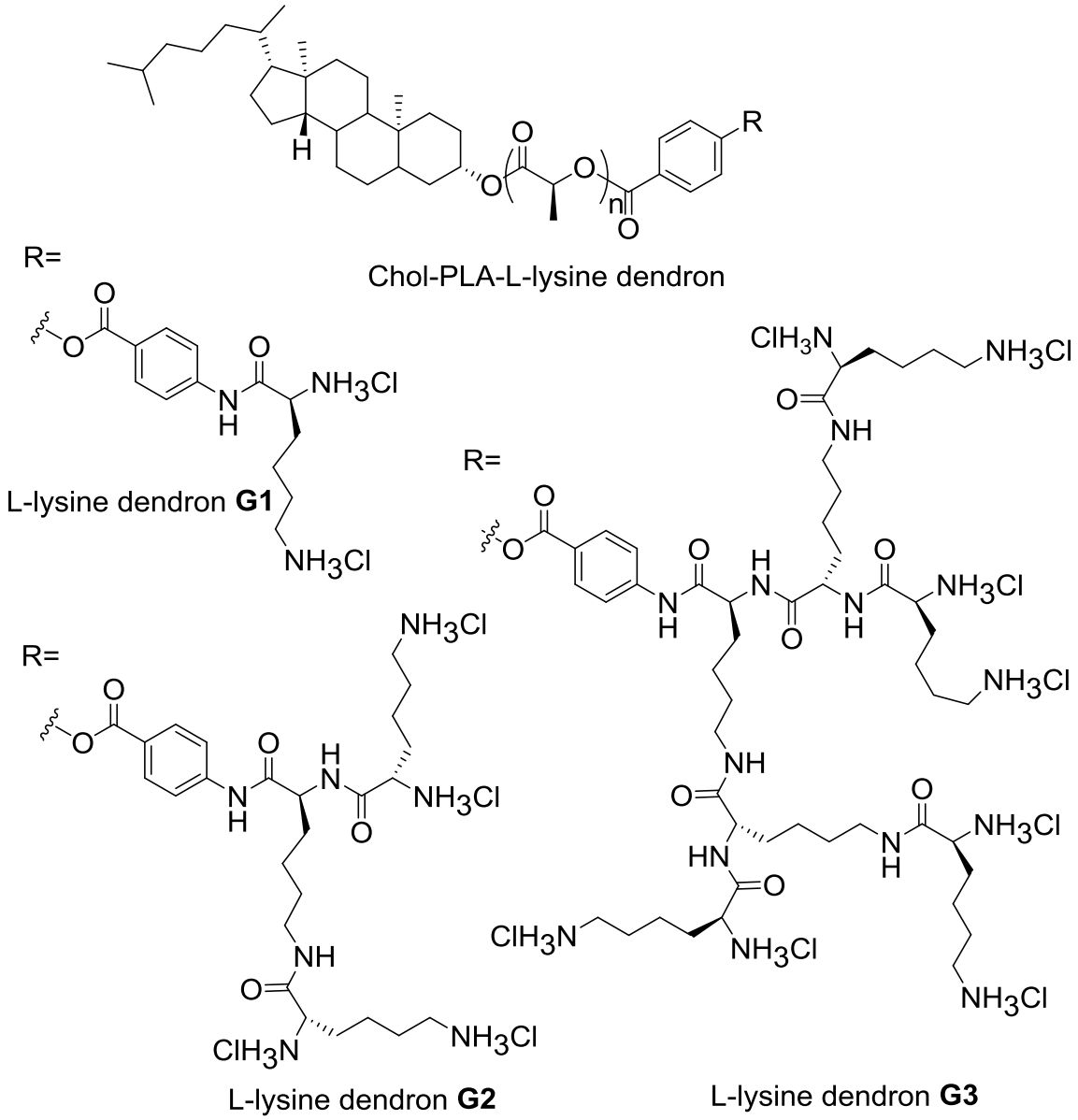

Figure 2. Examples of functionalized polylactides via end group modification

Furthermore, the secondary alcohol terminus of the Chol-PLA oligomers allows for the opportunity to introduce additional bioactive substituents such as cholesterol, indomethacin (an anti-inflammatory drug), pyrene and rhodamine B (fluorescent labels for bioimaging purposes) and various α-amino acids, which would dramatically increase the applications of PLA in the biomedical field. [56]

However, initiating/end group modification can only modulate the properties of PLA through two sole sites leaving the polylactide backbone inaccessible. Thus modification methods that lead to greater diversity are desired.

1.3.2 Monomer Derivative Approach

Since only a few α-hydroxy acids, such as lactic acid, 2-hydroxyisocaproic acid and β-phenyllactic acid, can be isolated via fermentation, access to most substituted α-hydroxy acids has to rely on synthetic preparation from other materials. Thus the substituted lactide monomers would be prepared via dimerization of those substituted α-hydroxy acids which requires highly diluted organic solutions under acidic conditions, and the dimerization step typically gives low isolated yields (**Scheme 9**). The resulting substituted polylactides produced from these substituted lactides have comb-like structures which can dramatically alter the physical properties of polylactides depending on the length and category of the attached functional group (FG_1), such as thermal and solubility properties, while retaining the degradability of the polylactide backbone.

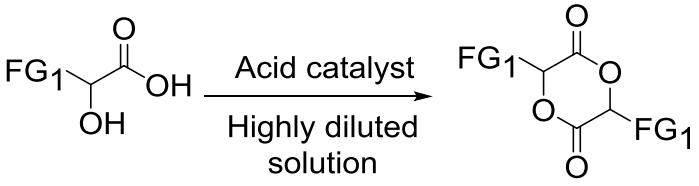

Scheme 9. General synthesis of functionalized lactide monomer derivative

Substituted polylactides have been prepared by polymerizing cyclic monomers derived from the corresponding α-hydroxy acids to give comb like structures. The preparation of this type of substituted polylactides typically begins by Grignard additions to oxalylic esters or by hydrolysis of cyanohydrins to afford α-hydroxy acids both of

which require harsh conditions (**Scheme 10**). However, due to the demanding requirements of some functional groups that would be of interest to introduce into polylactides, some mild reaction conditions were also developed in order to prepare a variety of functionalized polylactides and these will be discussed below.

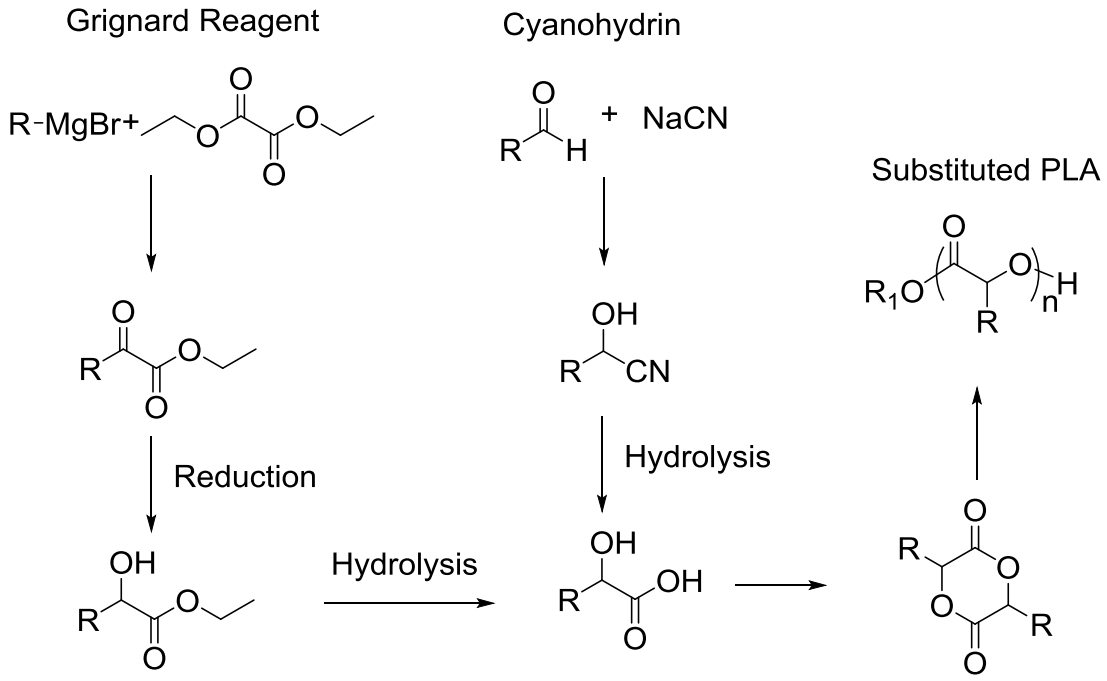

Scheme 10. General preparation routes to substituted polylactides

Baker and coworkers addressed the functionalization of PLA and studied the effect of both alkyl and aryl substitution of PLA on their thermal properties by preparing a series of alkyl and aryl groups tethered to the polylactide backbone.[57] There are three factors that affect the glass transition temperature (T_g) of polymers. The backbone rigidity, the rotation barrier along the backbone and the chain-chain interaction between the backbones all contribute to the T_g changes of polymers. By incorporating alkyl or aryl groups with different lengths or ring structures within the polylactides, the glass

transition temperature is dramatically affected by altering both the rotation barrier and chain-chain interaction as shown by the examples in **Figure 3**. It is believed that the rotation barrier would increase upon increasing the steric hindrance of the substituents attached to the backbone, and thus T_g would increase. This trend is clearly shown in **Figure 3** (**f** and **g**), where the incorporation of rigid phenyl and cyclohexyl rings onto the polylactide backbone dramatically increases the T_g of PLA from 55 ^{o}C to ~100 ^{o}C. A similar trend was also observed for **h** and **i** where bigger substituents were attached to polylactide backbone. The steric effect of tethered side chains decreases as the bulky groups move farther from the polymer backbone, thus, the T_g of **h** and **k** dropped significantly compared to **f** and **j**, respectively. This is thought to be due to the induction of a higher rotation barrier when the branch in the substituent is closer to the backbone. When increasing the length of the side chain from a methyl group on the lactide to ethyl, isopropyl, isobutyl, n-hexyl and n-octyl groups, one would expect a higher T_g for the polylactides based on the discussion above since longer alkyl chains are larger than a methyl group. However, the T_g of those substituted polylactides (**b**, **c**, **d**, **j** and **k**) were reported to have a lower T_g (-46 to 50 ^{o}C)[58,59,60,61] compared to polylactide (**a**, 55 ^{o}C). This clearly points out the importance of chain-chain interactions (dipole-dipole interaction) of polylactides in determining their T_g. By increasing the lengths of the side chains, the dipole-dipole interactions between polymer chains decrease, and thus T_g decreases, because the steric effects are overridden by a screening of the ester groups by the linear alkyl chains in the polymer backbone. This screening effect on dipole-

dipole interaction by alkyl groups was confirmed by the T_g of substituted polylactide (**e**) which comprised of both n-hexyl and cyclohexyl groups. The T_g of polylactide is only 13 ^{o}C which is much closer to the T_g of **c** (ΔT=50 ^{o}C) than **g** (ΔT= 85 ^{o}C).

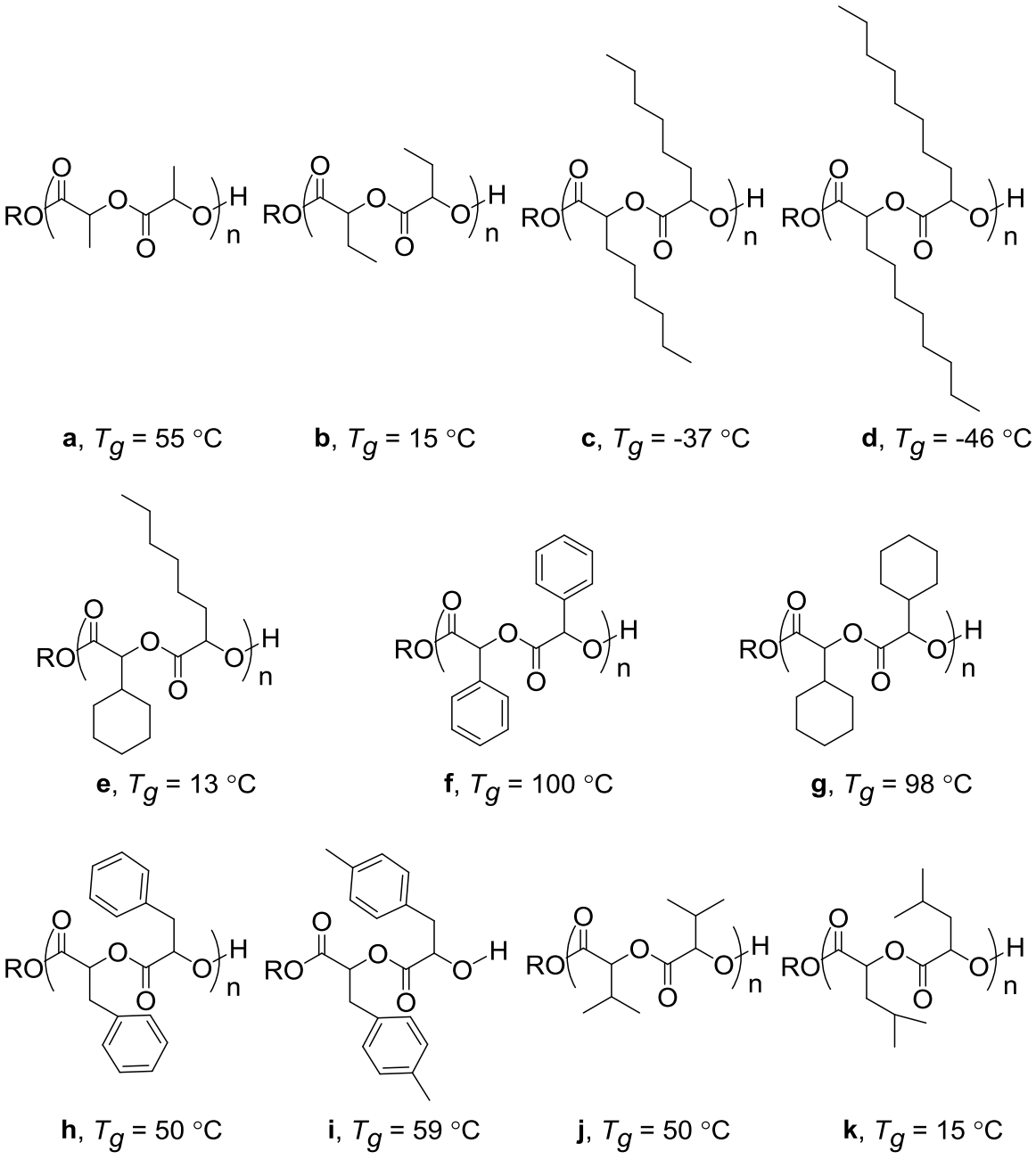

Figure 3. Substituted polylactides and their T_g

Although a variety of the substituted polylactides mentioned above were prepared and their thermal properties were investigated, functionalization of these polylactides is very limited due to the inert nature of the alkyl or aryl groups. So substituted lactide monomers with a great variety of functional groups were synthesized to provide highly functionalized polylactides, such as hydroxy, carboxylic acid, amine, saccharides and polyethylene glycol functions. This was done via protection-deprotection methods before and after polymerization due to the limited functional group tolerance in the polymerization step of polylactide preparation.

The introduction of hydroxy functions (-OH) tethered to the polylactide backbone has been reported by several groups through the monomer derivative approach. One of the most common starting materials is *O*-benzyl-L-serine which was converted to an α-hydroxy acid via diazotization for use in preparing homo- or hetero-substituted lactide dimers and thus in turn to various polylactide homo- or co-polymers (**Scheme 11**).[62,63,64] Notably, the monomer derivative approach usually requires extremely pure monomer to satisfy the polymerization conditions. The physical properties of hydroxy group tethered polylactides were reported to have significantly changed glass transition temperatures and degrees of crystallinity. They also have been shown to serve as delivery vehicles for sustained protein release with retained protein structural integrity while polymers degradation.[65] The tethered hydroxy groups also provide an opportunity for further grafting biotin/peptides to enhance the bio-applications, such as cell adhesion, and even in polymer grafting to produce more complex structures.

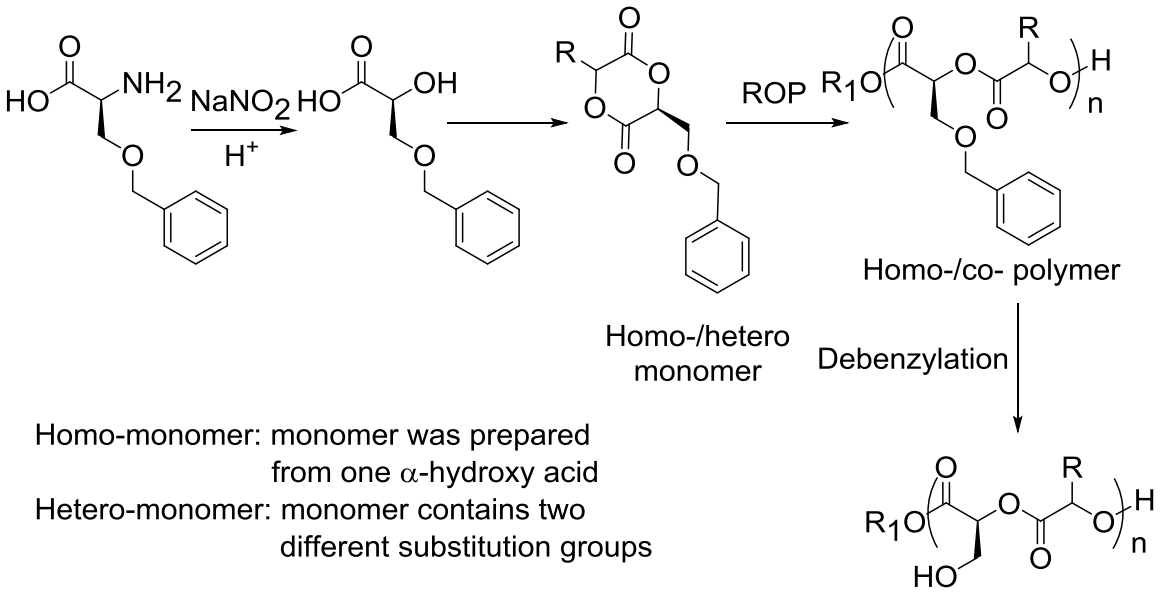

Scheme 11. Preparation of hydroxy group tethered polylactides

Another synthetic approach to prepare poly(α-hydroxy acids) with hydroxy groups tethered to the backbone is the polymerization of *O*-benzyl-*L*-serine carboxyanhydride, which is worth discussing here due to the fact that it provides the same polylactide structural polymer as that obtained from lactide via an alternative synthetic route. This can also be applied to the preparation of other poly(α-hydroxy acids) with functionalized tethers. [66] Starting from *O*-benzyl-L-serine, the synthesized α-hydroxy acid was converted to *O*-carboxyanhydride by phosgene followed by ring opening polymerization to afford protected polymers (**Scheme 12**). After the removal of the benzyl group, degradable, water-soluble poly(α-hydroxy acids) bearing pendant hydroxyl groups were obtained with excellent cell compatibility, suggesting their potential for use as novel materials in constructing drug delivery systems and as hydrogel scaffolds in tissue engineering.

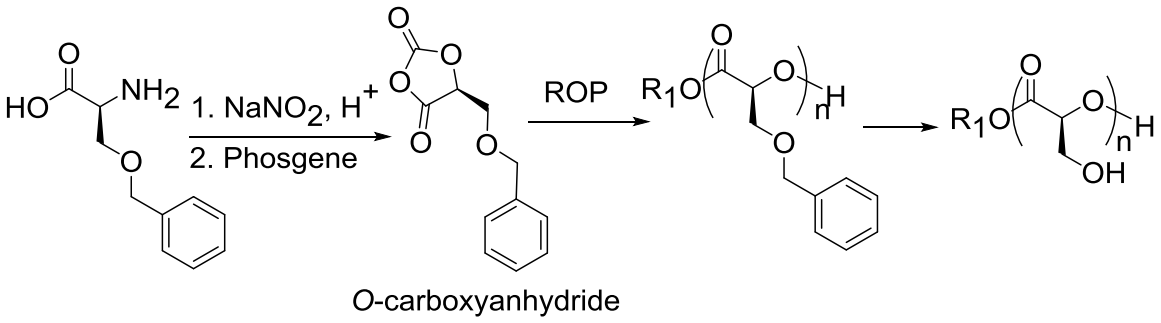

Scheme 12. Poly(α-hydroxy acids) (Polylactides) via *O*-carboxyanhydride routes

Amine tethered polylactides were also reported by Gerhard *et al.* via ring opening polymerization of carbamate-protected monomer derived from lysine followed by quantitative deprotection under acidic condition (HBr/AcOH). The deprotection was clean and resulted in no degradation of the backbone, which was confirmed by NMR analysis (**Scheme 13**).[62]

Several groups have investigated the preparation of polylactides tethered with carboxylic acid functions which were targeted to address solubility issues. As shown in **Scheme 14.**, starting from either malic acid or aspartic acid, homo- and hetero-monomers were both prepared and polymerized to the corresponding protected polylactides.[67,68] Catalytic hydrogenolysis using Pd/C provided the carboxylic acid tethered polylactides, which are water-soluble. More recently, Gerhardt and coworkers also reported similar substituted polylactides by polymerizing hetero-monomers with the carboxylic acid function protected by benzyl ester where glutamic acid was the starting material.[62] Deprotection was clean and quantitative without affecting the polymer backbone as determined by NMR analysis. However, GPC results were not reported due to the poor solubility of functionalized polylactides.

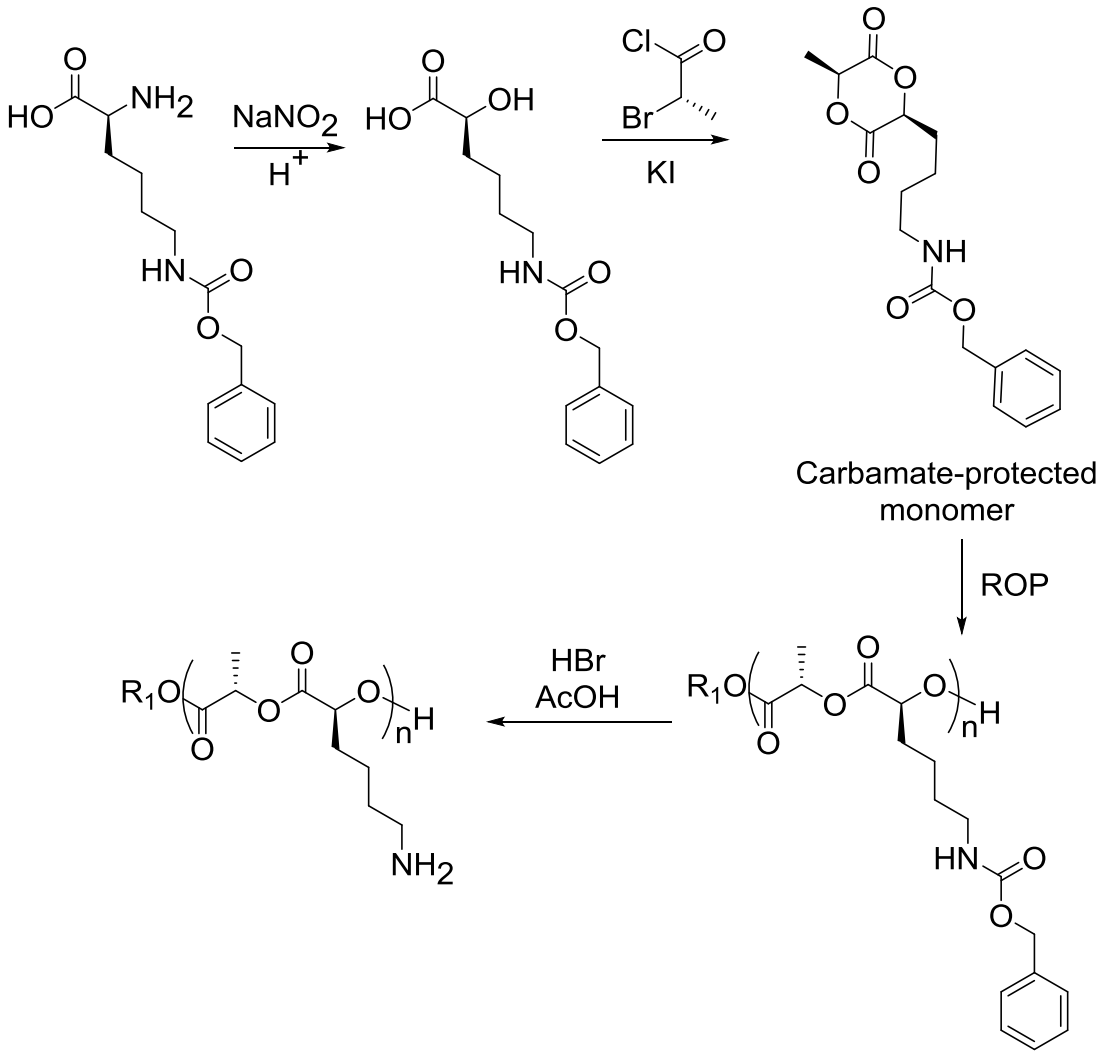

Scheme 13. Preparation of amine tethered polylactides

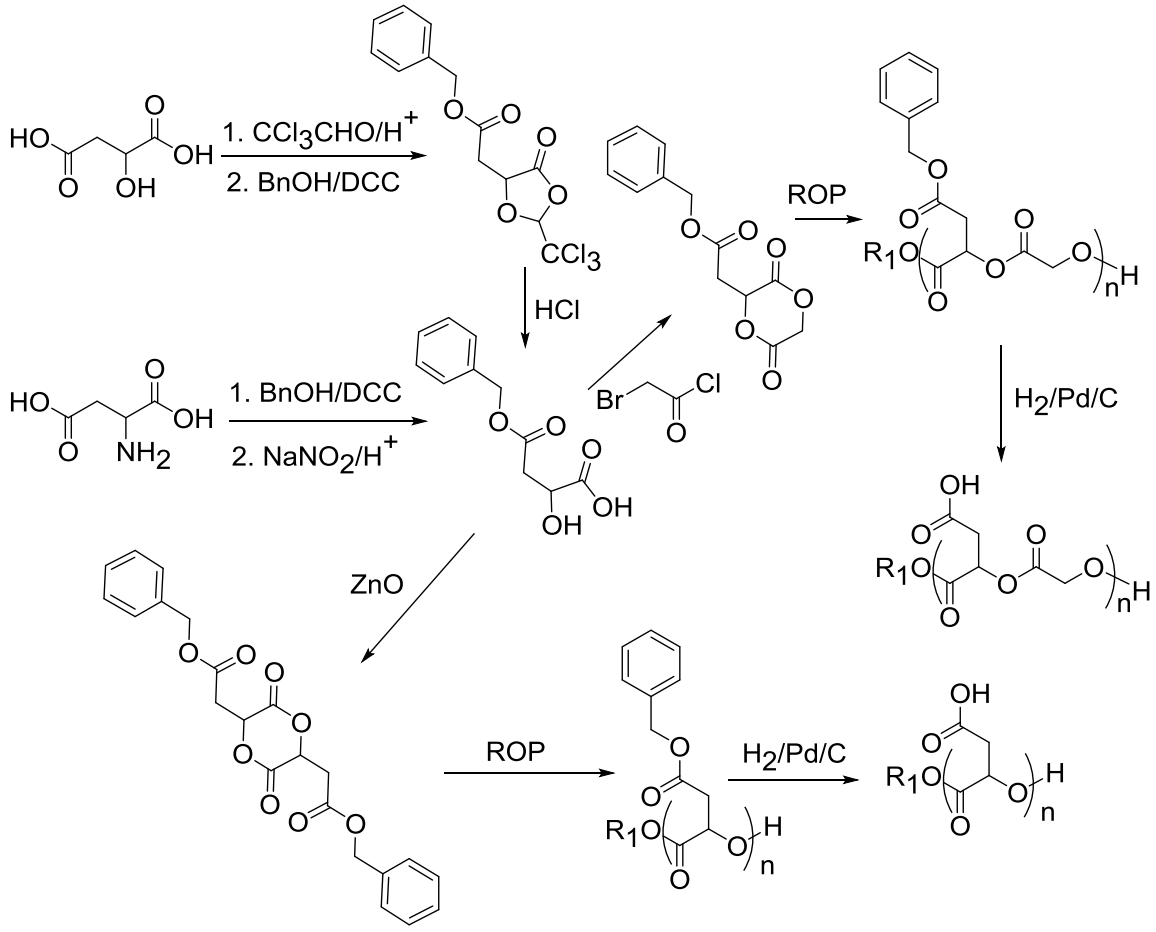

Scheme 14. Preparation of carboxylic acid tethered polylactides

Polyethylene glycol (PEG) was also tethered to the polylactide backbone to tune the physical properties through the monomer derivative approach. Recent reports have shown that introducing polyethylene glycol groups into hydrophobic polymers render them hydrophilic.[69,70] In addition, the thermo-responsive property of these polymers makes them ideal for drug delivery systems, smart surfaces, and bioseparations. These materials exhibit a solution-gel transition (a transition from a clear solution to a cloudy mixture) when heated through the lower critical solution temperature (LCST), which corresponds to the entropically driven expulsion of solvating water molecules from the

polymer. Recent research on thermoresponsive materials, especially those that contain mPEG segments, suggests that tuning the hydrophobic/hydrophilic balance in materials can shift the LCST over a broad temperature range.

Baker and coworkers have synthesized and polymerized lactide derivatives with 1-4 ethylene glycol segments using $Sn(Oct)_2$.[71, 72] The synthetic approach to the monomers uses poly(ethylene glycol) monomethyl ether (mPEG, 1-4 ethylene glycol segments), 1,6-dibromohexane and diethyl oxalate to generate the corresponding α-hydroxy acid, which was dimerized to the PEG-substituted lactide. The bulk polymerization at 130 ^{o}C afforded the alkyl/PEG substituted amphiphilic polylactides (**Scheme 15**). Polymers with short oligo(ethylene oxide) chains (1 or 2 ethylene glycol repeat units) are more hydrophilic than polylactide but nonetheless insoluble in water, whereas polymers having 3 or 4 ethylene glycol repeat units are water-soluble. Aqueous solutions of polymers with 3 and 4 ethylene oxide repeat units in each pendent chain are thermo-responsive, with LCSTs at 19 and 37 °C, respectively, which clearly indicates their promise in applications as thermo-triggered materials in the biomedical field.

More recently, Castillo *et al.* reported another approach to poly(ethylene glycol) (PEG) side-chain functionalized lactide analogues in four steps from commercially available L-lactide (**Scheme 16**).[73] The key step in the synthesis is a “click” reaction (1,3-dipolar cycloaddition) between mPEG-azides and a highly strained spirolactide–heptene monomer (Norbornene-lactide)[74] and occurs with high conversion. The ring-opening polymerization was affected with triazabicyclodecene (TBD) and gave well-defined tri- and hepta(ethylene glycol)–poly(lactide)s with molecular weights above 10

kDa and PDI around 2. mPEG–poly(lactide) (PLA) with mPEG chain M_n 2000 was also prepared, but GPC analysis showed a bimodal profile indicating the presence of starting macromonomer. Reduced MC3T3-E1 cell adhesion using tri(ethylene glycol)–poly(lactide) indicated the addition of mPEG chains to PLA modulates biological responses compared to the unfunctionalized PLA due to the nonspecific protein adsorption-resistant nature of PEG.

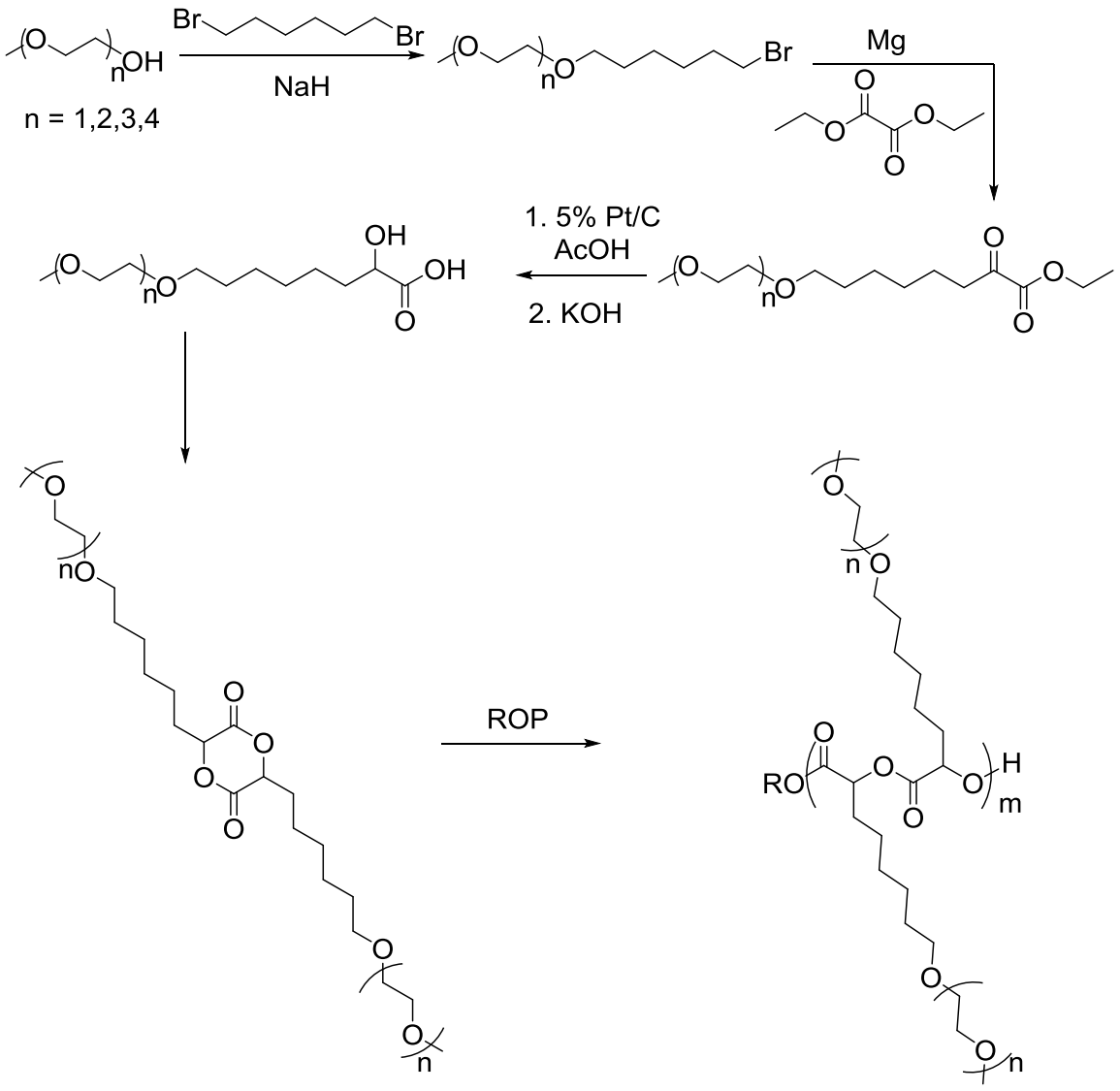

Scheme 15. Synthesis and polymerization of poly(ethylene glycol) monomethyl ether-modified polyglycolides.

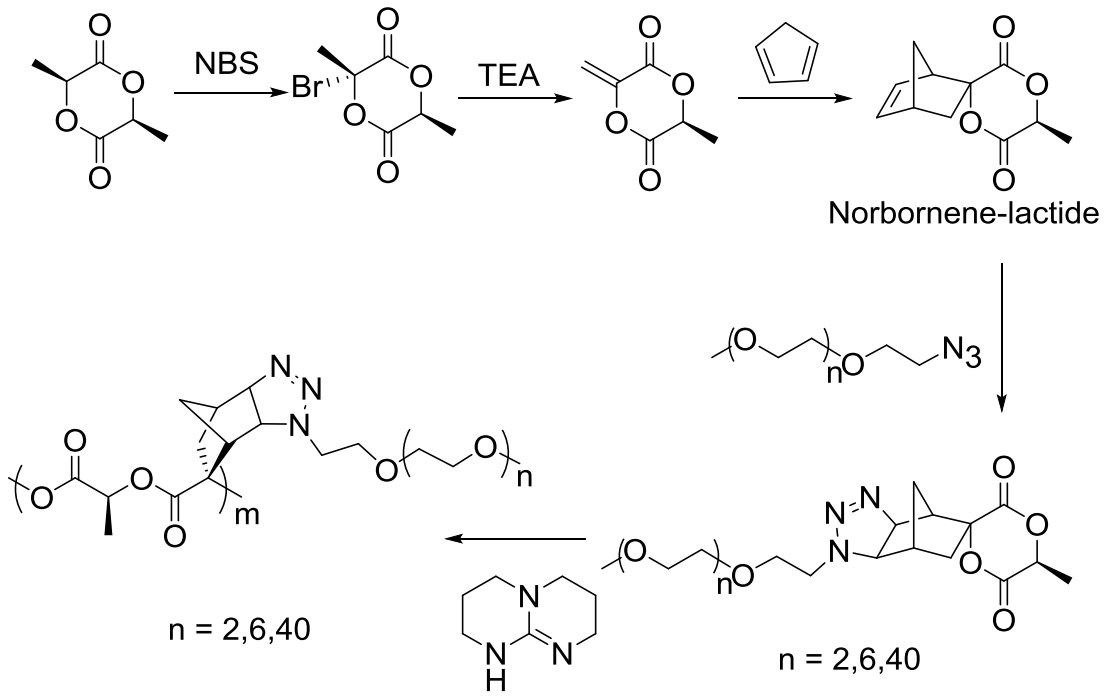

Scheme 16. Castillo's monomer derivative approach to poly(ethylene glycol) monomethyl ether-modified PLA

The general goal for the synthesis of substituted polylactides via the monomer derivative approach is to prepare novel monomers, not only for tethering new functional groups to the polylactide backbones but also for providing further access to modified polylactides via simple, efficient and versatile functionalization of existing functions within the polylactides themselves via simple and efficient chemistry. Alkenyl, azido and alkynyl functional groups have been incorporated into polyplactides via the monomer derivative approach, which enables subsequent efficient click chemistry on these polymers for further functionalization. Leemhuis *et al.* have prepared allyl functionalized lactide monomers in relative high yield (**Scheme 17**). Bulk polymerization at 110 ^{o}C afforded polymers in high conversion, high yields and good control over molecular weight, although the polydispersity index was moderate (~2.0).[75,76] The major issue in

the synthesis of functionalized lactide monomers is the low isolated yield (typically 20-40%) in the dimerization step due to the unfavorable ring formation, which wastes considerable amount of the precious α-hydroxy acid. So overcoming this issue in the dimerization step or developing a new approach to avoid this step would be highly desirable. The only example in the literature that avoids the dimerization step in the synthesis of substituted lactides is that of Jing *et al.* who prepared a tricyclic lactide (norbornene-lactide) from commercially-available lactide in high yield (>90%, **Scheme 16**).[74] Lactide was brominated, and following dehydrobromination, a Diels-Alder reaction to construct the norbornene-lactide monomer which was polymerized to give polymers with narrow PDI (1.1) using TBD as catalyst at -20 ^{o}C. The polymer can be further modified through click reactions,[52] which will be discussed later.

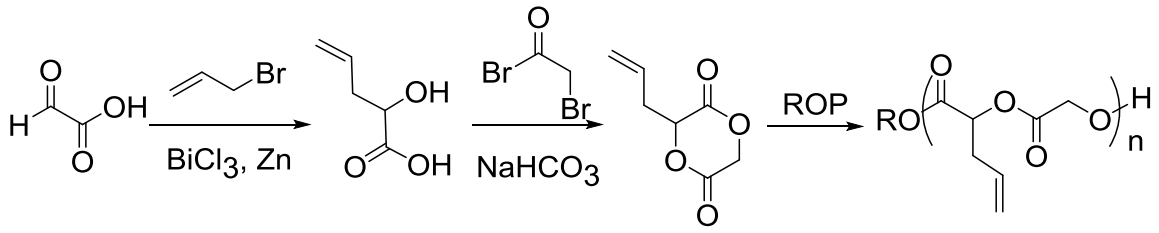

Scheme 17. Synthesis of allyl functionalized polylactides

Baker and coworkers synthesized and polymerized an alkynyl modified lactide monomer to click with different small functional molecules after polymerization (**Scheme 18**). The α-hydroxy acid was synthesized via a Reformatsky reaction between propargyl bromide in the presence of activated zinc and ethyl glyoxylate followed by mild hydrolysis in water. Then this α-hydroxy acid was converted to monomer which was polymerized to give homopolymers with good molecular weight control and narrow PDI.[77]

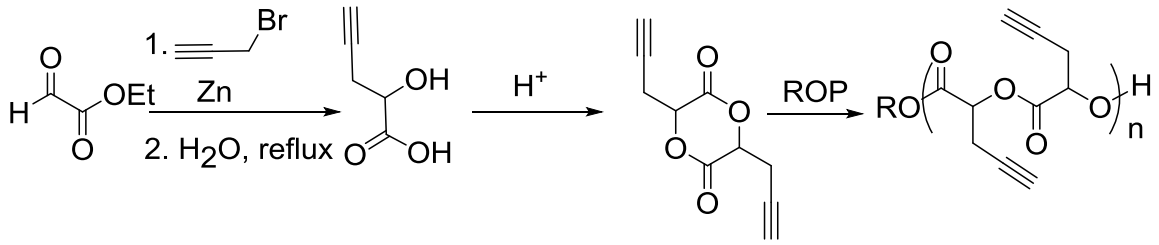

Scheme 18. Synthesis of alkynyl functionalized polylactides

Recently, a novel and versatile synthetic procedure to a variety of side chain functionalized lactide monomers was reported by Rubinshtein and coworkers using a Passerini-type condensation reaction.[78] The multicomponent reaction of isocyanide, aldehyde, and water afforded the *N*-acylindole of a substituted lactic acid in good yield in a one-pot fashion. Then, functionalized lactide monomers were prepared through hydrolysis of the *N*-acylindole under mild conditions followed by lactide ring construction in moderate yield (**Scheme 19**).

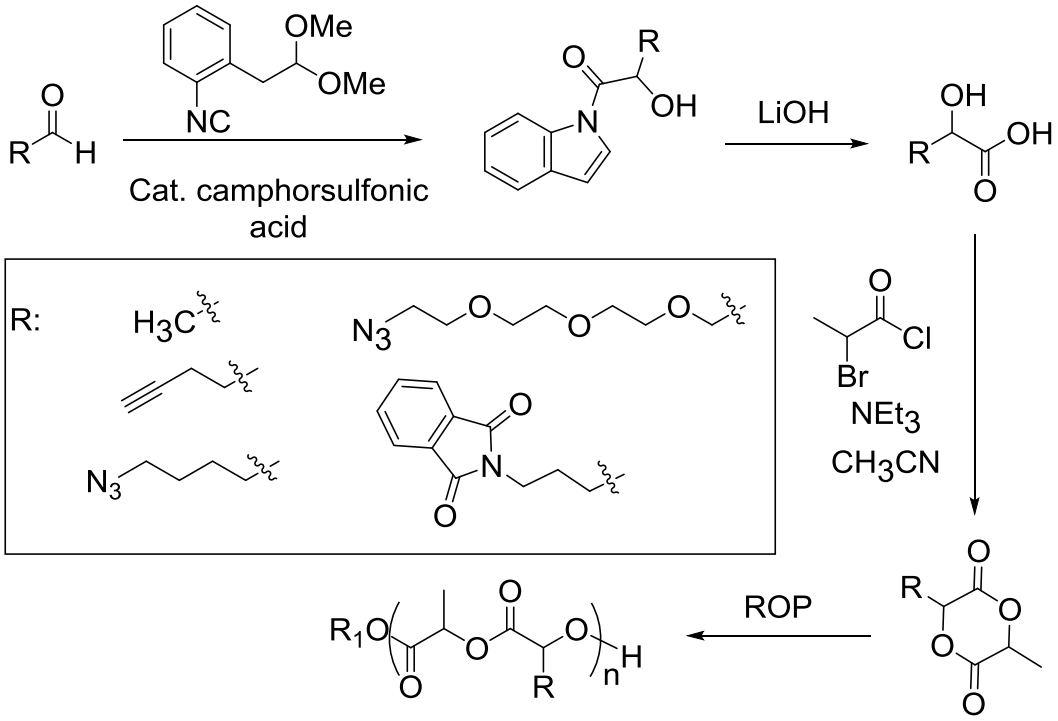

Scheme 19. Passerini-type condensation route to versatile functionalized lactide monomers

1.3.3 Post-polymerization Modification Approach

As shown in **Scheme 7 (c)** and discussed above, the monomer derivative approach to functionalize polylactides involves multi-step synthetic procedures to prepare the new substituted lactide monomers which consume a great deal of energy and time. Moreover, the functionality that is initially installed into the monomers must be compatible with the polymerization conditions. In contrast to the monomer derivative approach, post-polymerization approach offers the distinct advantage that a series of polymers with different functionalities tethered to the polymer backbone can in principle be accessed from a single monomer. Having a single, simple procedure for placing a broad range of pendant functional groups onto polylactide substrates is highly desirable. The ideal post-polymerization modification approach should utilize a chemical process that not only provides a simple synthesis of functional monomers but also does not degrade the polymer backbone. It should also be compatible with a wide range of functional groups, solvents, and conditions to achieve efficient and quantitative tethering.

1.3.3.1 Direct Post-polymerization Modification Approach

Due to the labile nature of the polylactide backbone towards degradation, there are limited literature reports regarding the direct post-polymerization modification of polylactides. The reported examples indicate that this approach is plausible for surface modification of polylactide films deposited on substrates.[79] Carlislf *et al.* used a pulsed plasma deposition strategy to attach a thin polyallyl amine layer onto polylactide films for tissue culture application. The polyethylene glycol-adhesion peptides (RGD or

YIGSR) were covalently grafted to the thin polyallyl amine layer to mimic the *in vitro* extracellular matrix and thus enhance the hepatocyte adhesion.[80] More recently, a single-step, nondestructive, and versatile technique for the covalent surface modification of a polylactide films was reported.[81] PLA films were subjected to three different vinyl monomers in the vapor phase: acrylamide, maleic anhydride, and N-vinylpyrrolidone. The solvent-free surface grafting was induced by photoinitiation by benzophenone under UV irradiation. The extent of surface grafting and the surface wettability increases upon elongating the UV treatment time. The grafted carboxylic acid groups remain functional and can subsequently be modified to provide altered desired properties. The in vitro degradation rate was enhanced by covalently grafting to the surface.[82] However, neither of the strategies discussed above didn't present the structural stability information of the polylactide films after pulsed plasma deposition or UV irradiation due to the difficult detachment of the surface layer and their low content for analysis.

Fortunately, Pan *et al.* have addressed the structural stability by measuring the M_n of polylactide materials before and after radical induced direct post-modification of bulk polylactide with maleic anhydride.[83] Radical reactions initiated by benzoyl peroxide, a radical initiator, provided for the covalent grafting of maleic anhydride to PLA (**Scheme 20**). The resulting bonded succinic anhydride could be ring-opened to give carboxylic acid and amine side chains via amidation with 1,6-hexanediamine. However, in the process, the modified PLA backbone significantly degraded, which was indicated by the loss of up to 20% of the original M_n. These results suggest that the direct post-

polymerization modification of PLA may not fulfill the general requirements of post-polymerization modifications, although it is a simple and convenient method for surface modification to tune the physical properties.

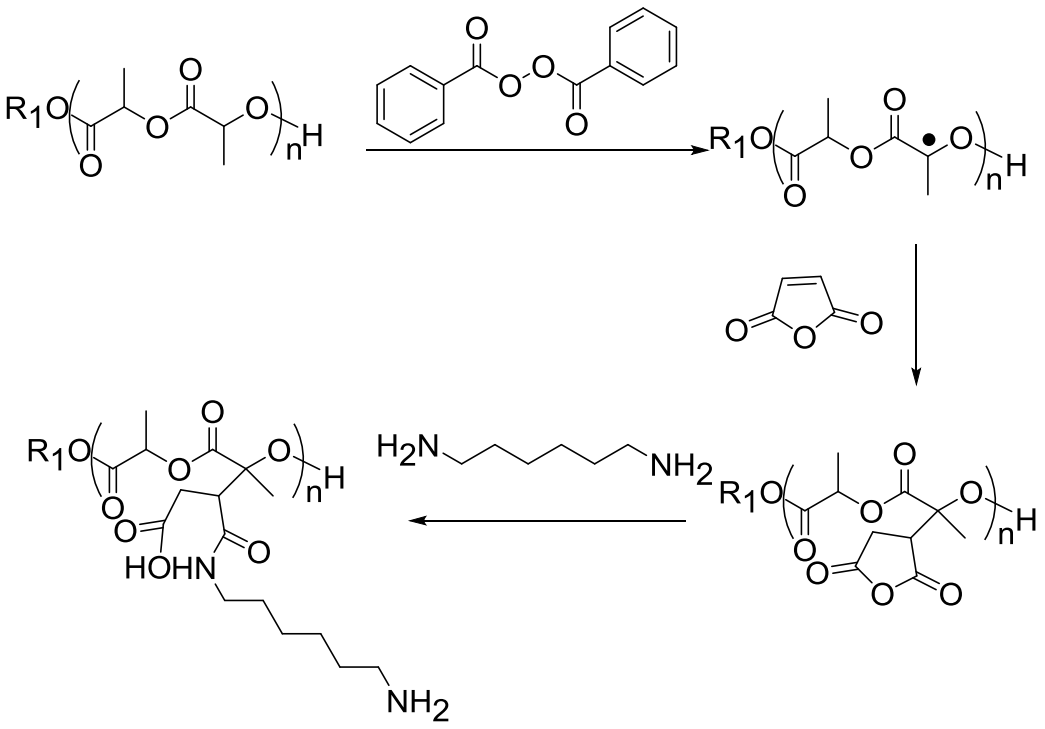

Scheme 20. Functionalization of bulk polylactide via direct post-polymerization modification using free radical initiator

1.3.3.2 Traditional Synthetic Coupling Approach via Side Functional Groups

Traditional synthetic methods have been applied to the post modification of polylactide since many functional groups, such as alcohol, amine and carboxylic acid, can be revealed after protection/deprotection strategies as discussed in monomer derivative approach. Those protected functional groups provide the opportunities for further access to modified polymers with desired unique properties. As shown in **Scheme 21**, hydroxylated polylactides with benzyl protected hydroxyl groups can be deprotected and coupled with succinic anhydride to afford carboxylated polylactides

which can be further coupled with biotin or RGD-peptide in the presence of EDC. This provides the opportunity for the fabrication of a variety of bioactive ligands onto PLA to improve biocompatibility.[64]

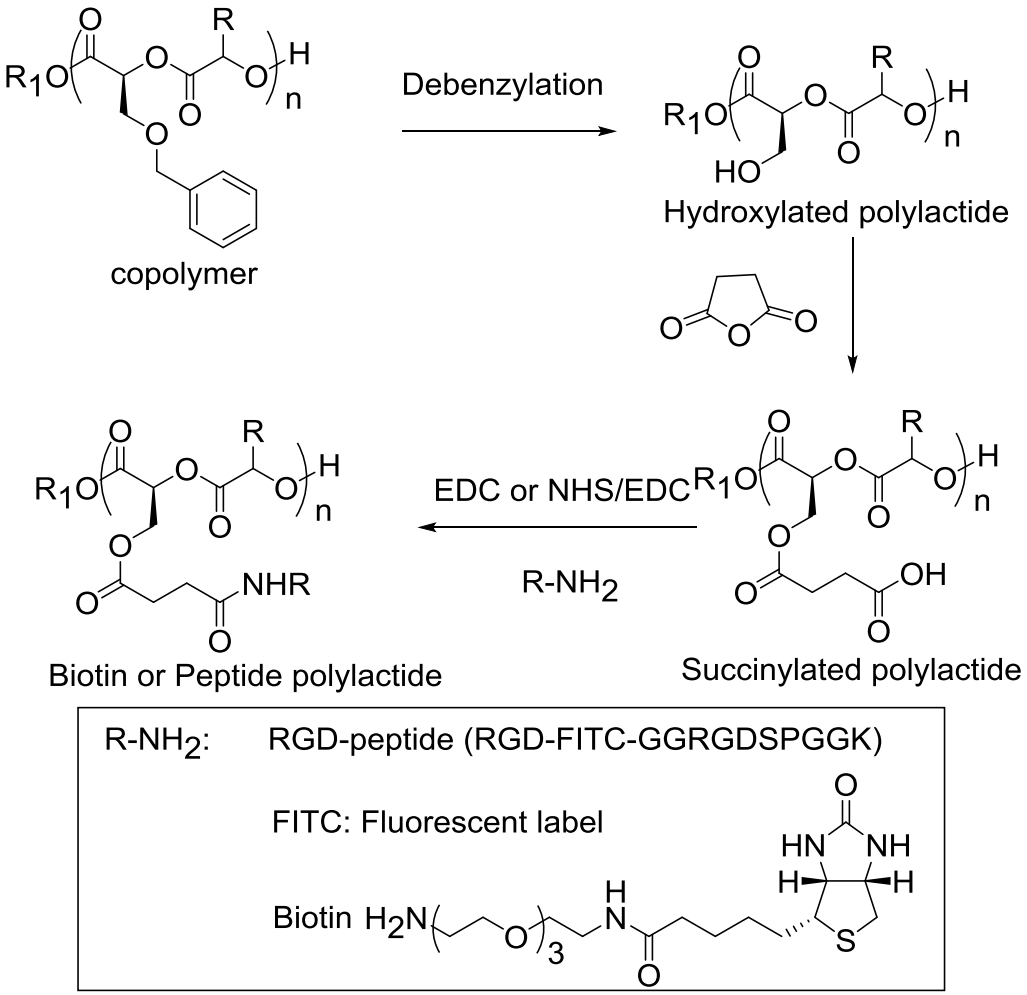

Scheme 21. Functionalization of hydroxylated polylactide via EDC coupling

Hydroxylated polylactides have also been prepared by the hydroboration-oxidation of poly(lactide-*co*-diallylglycolide)**Error! Reference source not found.**. The alkene-unctionalized PLA could be oxidized by 9-borabicyclo[3.3.1]nonane (9-BBN) and hydrogen peroxide to provide primary alcohol functions along the polymer chain without

interrupting the backbone. Subsequently, the hydroxylated polylactides could be coupled with different fatty acids using DCC coupling to afford polylactides with different long aliphatic chains again without backbone degradation (**Scheme 22**).[84]

Functionalized polylactides with carboxylic acids as pendent groups were also reported by du Boullay and coworkers through polymerization of *O*-carboxyanhydride derived from γ-benzyl L-glutamic acid in two steps.[85] The polymerization proceeded under mild condition using DMAP as the catalyst to produce well controlled polylactides. The pendent carboxylic acid groups protected with benzyl esters were readily recovered after hydrogenolysis. This procedure could provide well controlled homo, block and random polylactide polymers which cannot be achieved via polymerization of similar lactide derivatives probably due to their lower activity.

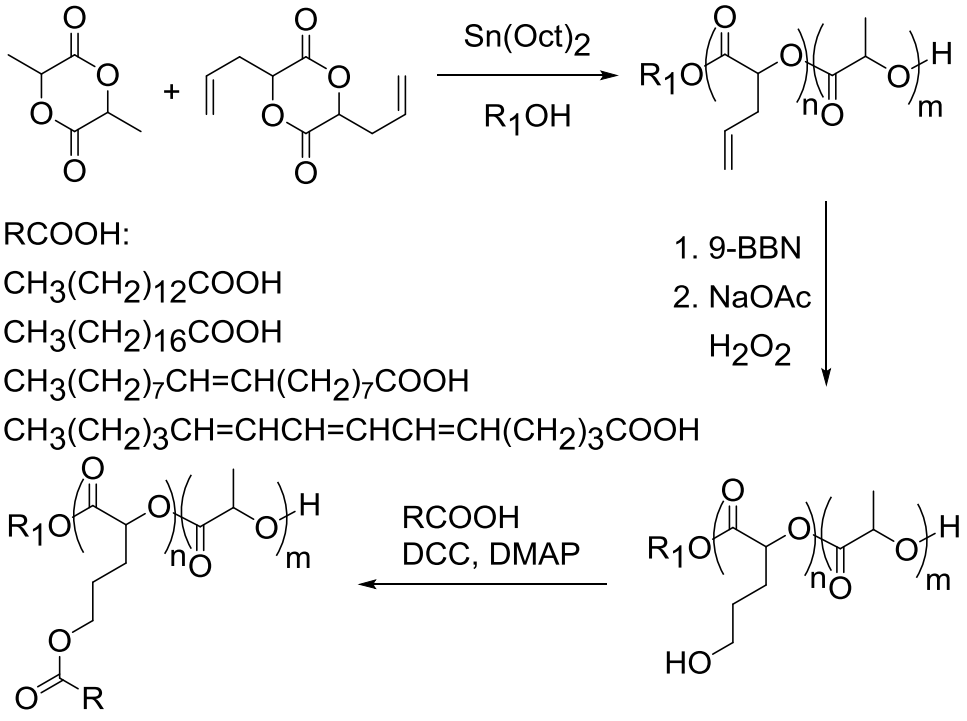

Scheme 22. Functionalization of hydroxylated polylactide via DCC coupling

1.3.3.3 Click Chemistry Approach via Side Functional Groups

Click chemistry is a chemical process introduced by K. Barry Sharpless in 2001[86] and describes chemical reactions that generate products quickly, reliably and in quantitative yield by joining small building blocks under mild conditions. Click chemistry is not limited to alkyne-azide 1,3-dipolar cycloadditions and can be extended to other highly efficient reactions, such as nucleophilic substitution,[87,88] radical additions,[89] Michael additions,[90,91] as well as Diels–Alder[92] and retro-Diels–Alder[52] reactions..

Norbornene pendant groups along the backbone of polylactides can be functionalized to give amine-functional PLAs and its copolymers by the addition of substituted 3,6-di-2-pyridyl-1,2,4,5-tetrazine via sequential and retro Diels-Alder reaction without degradation of the polymer backbone.[52] The tetrazine-norbornene click chemistry is fast, atom ecominical, catalyst free, air insensitive, and quantitative, and hence fulfils all of the requirements of the click concept. Due to the alkenyl side groups, it should be able to be subjected to alkene-azide, thiol-ene click chemistry as well for further post modification. However, there are no such reports in the literatures for modifying polylactides. They have been recently documented in the orthogonal post-modification of polycarbonate.[93]

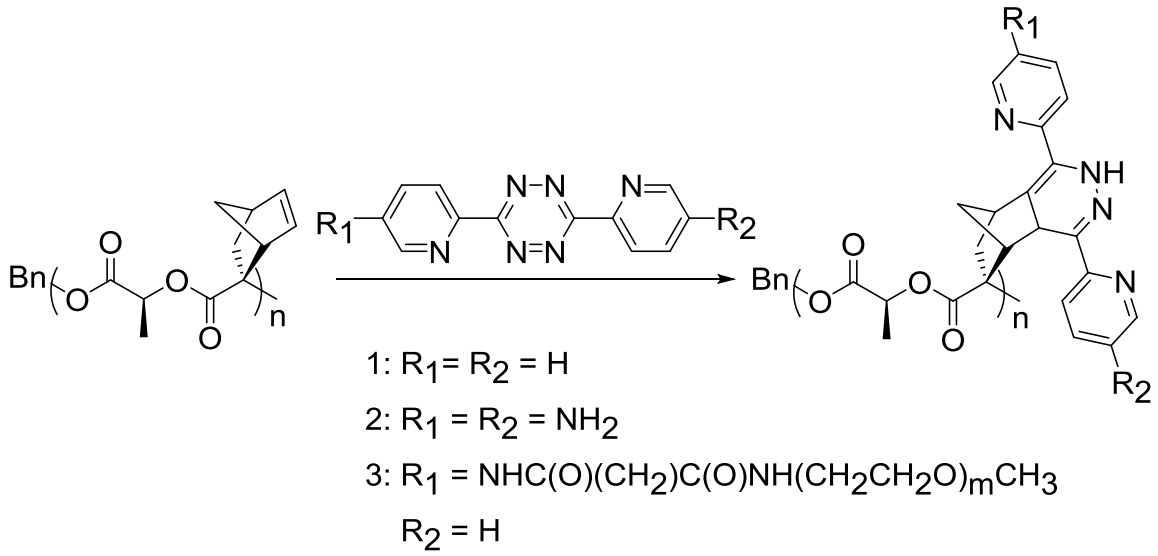

Scheme 23. Post-polymerization modification of polylactides via tetrazine-norbornene click chemistry

An allyl-functionalized polylactide prepared by Chen and coworkers was subjected to UV-induced thiol-ene click reaction with (diethylamino)ethanethiol hydrochloride (DEAET) in $CDCl_3$ using 2,2′-dimethoxy-2-phenylacetophenone (DMPA) as the photoinitiator at room temperature (**Scheme 24**).[76,94,95] To tune the polymer charge densities, the feed ratio of alkene, thiol and DMPA was altered and well-defined cationic polylactides (CPLA) with different amounts of tertiary amine groups were successfully synthesized. The CPLAs possess remarkable hydrolytic degradability with relatively low cytotoxicity. Prostate cancer cells can readily take up the CPLA- interleukin-8 siRNA nanoplexes, which results in significant - interleukin-8 gene silencing.[94]

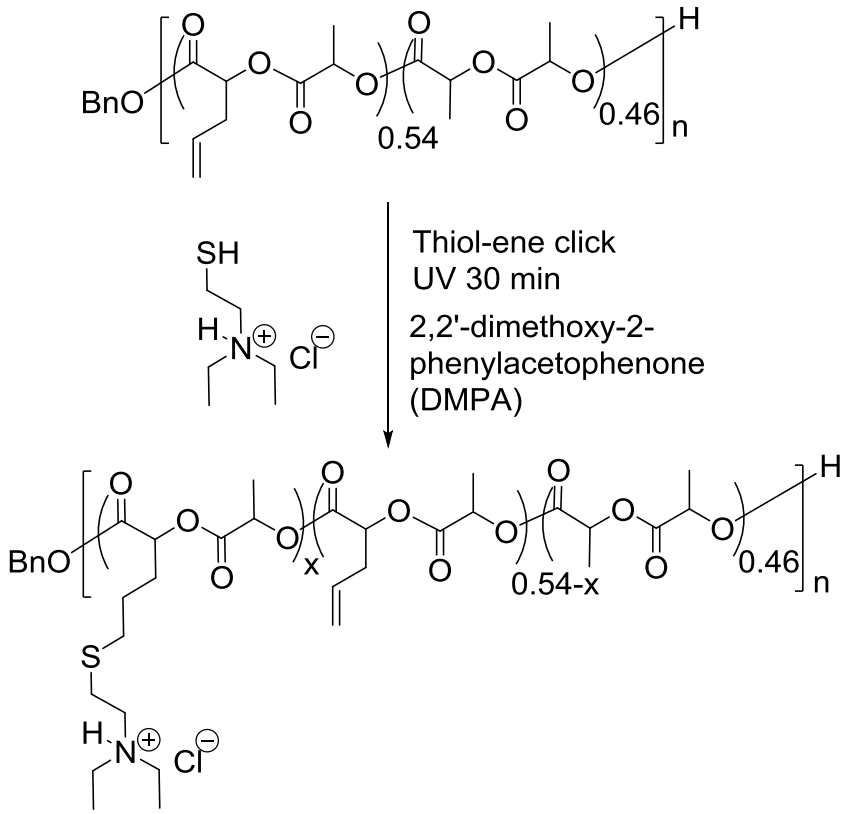

Scheme 24. Post-polymerization modification of polylactides via thiol-ene click chemistry

Alkyne-azide click chemistry has been applied to functionalize polylactides by several groups with quite different synthetic approaches involving either alkyne or azide substituted polylactides.[77,78, 96] Recently, Baker and coworkers introduced an acetylene modified lactide derivative capable of post-polymerization modification by Cu(I) catalyzed click chemistry to functionalize the polylactides with alkyl and poly(ethylene glycol) monomethyl ether branches under mild condition (**Scheme 25**). Their method showed good control over the degree of functionalization and no backbone degradation under the new click conditions was observed. The resulting functionalized polylactides exhibit thermo-responsive properties with the LCST 25-65 ^{o}C

depending on the mPEG/alkyl ratio in the polylactides.[77] When more hydrophilic mPEG segment was incorporated into polylactides, higher LCST was observed.

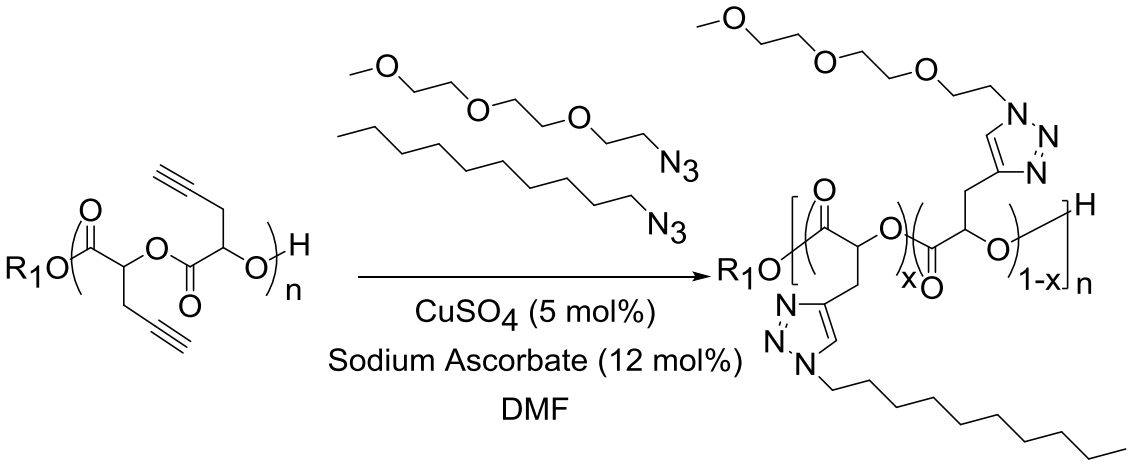

Scheme 25. Baker's synthesis of functionalized polylactides via Cu(I) catalyzed click chemistry

Both alkyne and azide functionalized polylactides were reported by Rubinshtein and coworkers using similar versatile synthetic routes (**Scheme 26**). The monomers were synthesized using a Passerini-type condensation reaction with broad functional group tolerance. The resulting polylactides were able to undergo click chemistry in the presence of Cu(I) catalyst while retaining the polymer structure.[78] This new methodology represents a significant step towards accessing biodegradable and biocompatible materials with improved functional and potentially tunable properties that may find utility in a variety of applications.

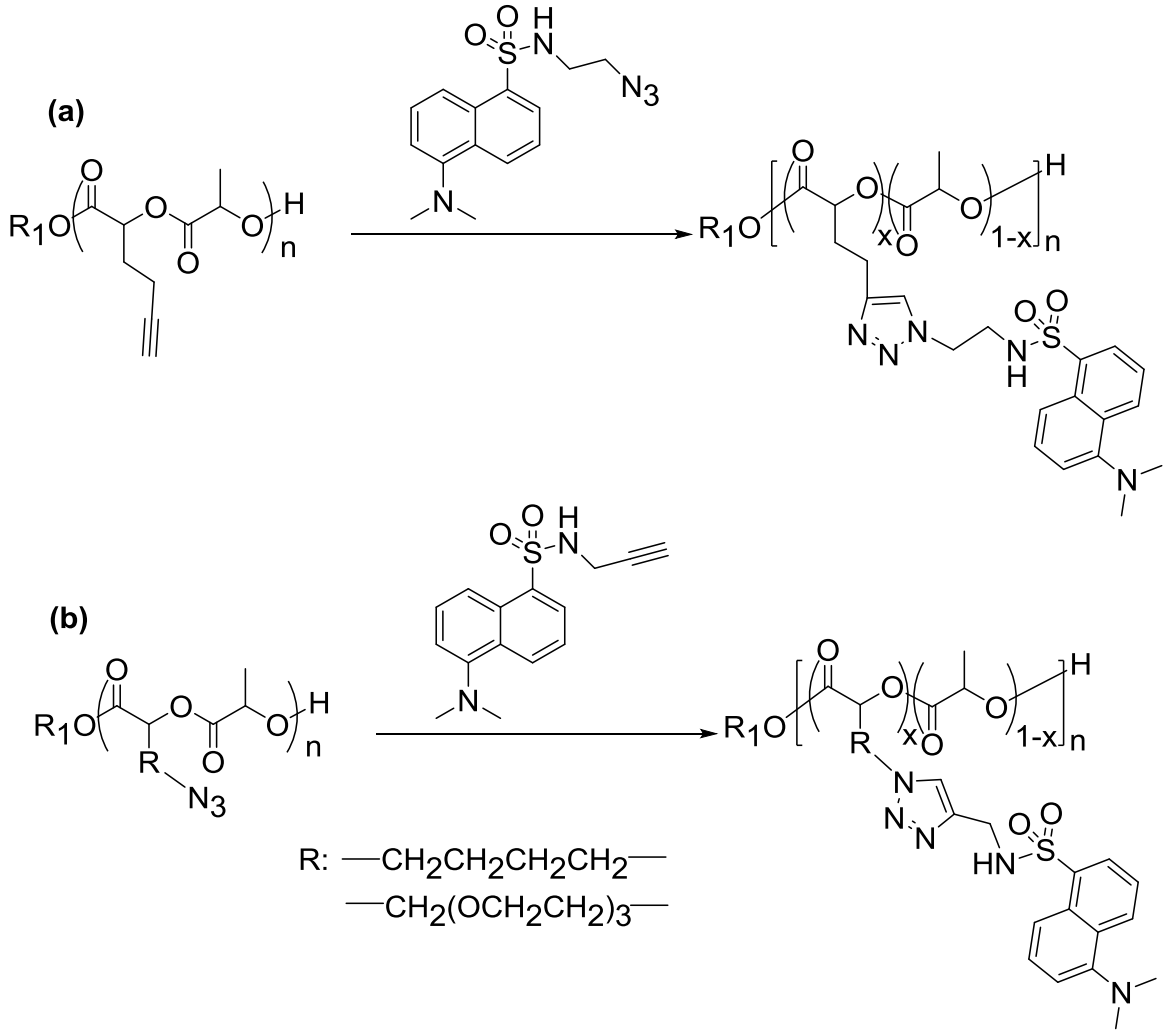

Scheme 26. Rubinshtein's synthesis of functionalized polylactides via Cu(I) catalyzed click chemistry

Polymerization of *O*-carboxyanhydride is an alternative procedure to produce polylactide polymers with exact same backbone as polylactides from lactide monomers. Zhang *et al.* synthesized an *O*-carboxyanhydride bearing an alkyne moiety to prepare clickable polylactides which could be further functionalized through either Cu(I) catalyzed click chemistry[96] or thiol-yne photo click chemistry.[97] As shown in **Scheme 27**, ring opening polymerization of *O*-carboxyanhydride resulted in amphiphilic clickable

polylactide which self assembled into micelles in water via nano precipitation method. The formed micelles was cross-linked in the cores using cross-linkers (1,4-diazdobutane and bis(azidoethyl) disulfide) via click chemistry. Core cross-linking not only improved the structural stability of the micelles, but also allowed controlled and triggered release of cargo molecules due to the fact that the disulfide cross-linkers can be cleaved by the reducing reagent DTT (dithiothreitol). Thiol-yne photo click chemistry of polylactides with 2-aminoethanethiol hydrochloride (AET) under UV irradiation provided side-chain aminated polylactides which displayed excellent cell penetration and gene delivery properties with low toxicities.

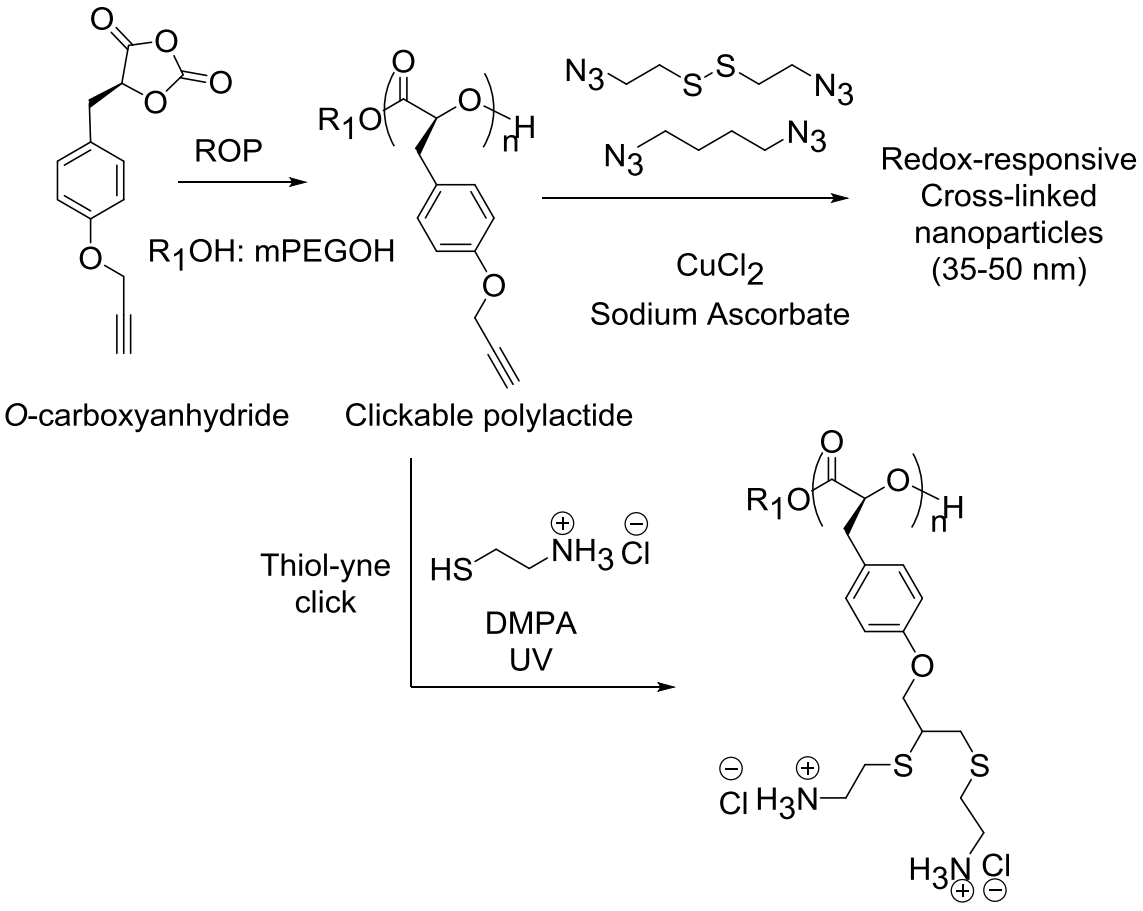

Scheme 27. Zhang's synthesis of functionalized polylactides via both Cu(I) catalyzed and thiol-yne click chemistry

1.4 Smart Polylactide Materials

Smart polymeric materials respond with a dramatic physical property change to a small change in their environment. Environmental stimuli include temperature, light, chemicals, and pH etc. “Smart” stimuli-sensitive materials from either synthetic or natural polymers can be used to solve biological problems such as drug delivery, biosensor design, tissue engineering and protein folding. The versatility and untapped potential of smart polymeric materials makes them one of the most exciting interfaces of chemistry and biology. Of all stimuli-responsive polymers, temperature-responsive (thermo-responsive),[77, 98] light-responsive [99] and redox-responsive[96, 100] polymers have been studied intensely because of the easiness to handle the corresponding small environmental change, such as temperature increase from room temperature to steady human body temperature at 37 ^{o}C and the common interconversion of thiol and disulfide in biological responses.

Post-polymerization modification of polymers via click chemistry provides advantages over traditional methods to smart polymeric materials, especially the functionalization of biodegradable polylactides due to the low chemical yield associated with synthesizing substituted lactide monomers and the extreme purity of the monomer that is required for the sequential polymerization. Post-modification with click chemistry in the preparation of smart polylactide materials would allow for the simple preparation of a series of functionalized polylactides from single clickable polylactides, which would improve the synthesis efficiency for specific smart property screening. It can also be used to tune the ratio of incorporation of different functionalities into the polylactides to modulate the stimuli-response at the desired level for a specific application. Both

thermo-responsive[71,72,77,101] and redox-responsive[96,102] properties of functionalized polylactides have drawn much attention and have been reported recently due to the interest in the biodegradable and stimuli-responsive properties of polylactides.

Thermo-responsive polymers exhibit a unique property which features a lower critical solution temperature (LCST) and/or an upper critical solution temperature (UCST). The LCST is a fascinating phenomenon found for various polymer solutions. At temperatures below the LCST, the polymer is completely miscible in water due to extensive hydrogen bonding interactions with the surrounding water molecules, whereas at temperatures above the LCST a phase separation occurs because hydrogen bonding with water is disrupted, and intra- and intermolecular hydrogen bonding/hydrophobic interactions of the polymer chains dominate, which results in a transition in solubility.[103] The ratio of hydrophilic and hydrophobic segments incorporated onto the polymer backbone can be used to tune LCST.[77,104,105] Higher LCST can be achieved by increasing the hydrophilic nature of the polymers due to the increased overall hydrogen bonding; whereas incorporating more hydrophobic groups lowers the LCST which could be rationalized by the disruption of hydrogen bonding and higher hydrophobic interaction.[106]

Redox-responsive polymers, especially thiol-sensitive polymers, are of particular interest, because the thiol-disulfide exchange reaction is one of the most important reactions in many biological processes including protection of important cellular components from reactive oxygen species. Polylactides with disulfide bonds are redox-responsive because the disulfide bonds can be reversibly converted to thiol groups in

the presence of reducing agents (such as Dithiothreitol (DTT)) via redox chemistry or by an excess of other thiol compounds via disulfide exchange. The result is that the original disulfide functionalized polylactides would undergo partial structural disruption and induce changes in certain physical properties. For example, Zhang *et al.* have prepared cross-linked polylactides nanoparticles with cross-linkers including disulfide cross-linkers. The cross-linked nanoparticles showed high morphologic stability, and they displayed controlled releas of entrapped cargo molecules upon treatment with DTT with increased nanoparticle size due to the thiol-disulfide exchange reaction.[96] This clearly indicates the redox-responsive property of disulfide functionalized polylactides. The most abundant reducing agent in cell, glutathione (GSH) has an intracellular concentration of 10 mM, 1000 times higher than that in the cellular exterior.[107] The development of redox-responsive and biodegradable polylactides as delivery vehicles to deliver and release therapeutics upon entry into cells due to the significant concentration difference of GSH is very promising in biomedical research. However, at this time there is limited research on delivery behavior using redox-responsive polylactides prepared from click post-modification of side chains of polylactides.

1.5 Conclusion

Functionalized polylactides greatly enhance the application of PLA in biomedical and structural applications. Three approaches to functionalized substituted polylactides have been intensely studied to explore their novel physical properties resulting from the functionalization and their applications in biomedical field. The polymerization mechanisms from substituted lactides to functionalized polylactides were also discussed

to address the choice of polymerization when new monomers are prepared. These new functionalized polylactides fall in the range of smart polymeric materials which would expand their promise in a variety of application.

In this thesis, we addressed the functionalization of polylactides via monomer derivative approach and post-polymerization modification approach. A series of novel and clickable α-hydroxy acid containing terminal alkyne groups and polyethylene glycol units were synthesized via a facile synthetic procedure without requiring column purification. We prepared the alkynyl substituted lactide monomers and the bulk polymerization of these monomers afforded the clickable polylactides. The post-modification of the resulting polylactides via click reactions provided thermo-responsive and redox responsive properties to polylactides. The spirolactide monomers were also prepared and polymerized into the corresponding polyspirolactides which displayed different thermal properties for different ring substituents attached to polylactide backbones.

CHAPTER 2 BUILDING UP A LIBRARY OF CLICKABLE α-HYDROXY ACIDS TO CLICKABLE SUBSTITUTED POLYLACTIDES

2.1 Introduction

At the present time, there are two kinds of monomers, substituted lactides and *O*-carboxyanhydrides which can be polymerized to give polylactides via ring opening polymerization. Theoretically, both of them can be prepared from either ring construction using substituted α-hydroxy acids as starting materials or direct functionalization of lactides or *O*-carboxyanhydrides (**Scheme 28**). The direct functionalization of lactides or *O*-carboxyanhydrides would be more advantangeous since it does not require additional synthesis of specific substituted α-hydroxy acids followed by ring construction which typically results in poor yield. However, due to the labile nature of both monomers under acidic or basic condition, there is only one reported method detailed in several reports to directly functionalize commercially-available lactides in high yields (55-90%).[52,73,74,108] Commercially-available L-lactide was brominated, dehydrohalogenated and the resulting double bond subjected to a Diels-Alder reaction with cyclopentadiene to construct a norbornene-lactide monomer. Although the polymerization of this monomer could provide alkenyl-substituted polylactides with narrow PDI, the polymerization in days with triazabicyclodecene (TBD) as the only known active catalyst gave poor molecular weight control and thus is not plausible to produce reliable and reproducible polymer for further applications. Due to the limitation of direct functionalization methods, the monomer synthesis for ring opening polymerization to polylactides is always based on dimerization through the

reaction between α-hydroxy acid and bromoacyl chloride derivatives followed by cyclization to give asymmetrical lactide monomers (hetero-monomer), or direct dimerization of α-hydroxy acids to symmetrical lactide monomers (homo-monomer). The first method usually gives low to moderate yields while the latter one always occurs with poor to low yields. So the synthesis of substituted lactide monomers is always the limiting step in the preparation of functionalized polylactides. Based on the discussion above, versatile methodologies which can directly functionalize commerically available lactides or dramatically improve the yield of the dimerization step from α-hydroxy acids to its lactide monomers would be highly desirable.

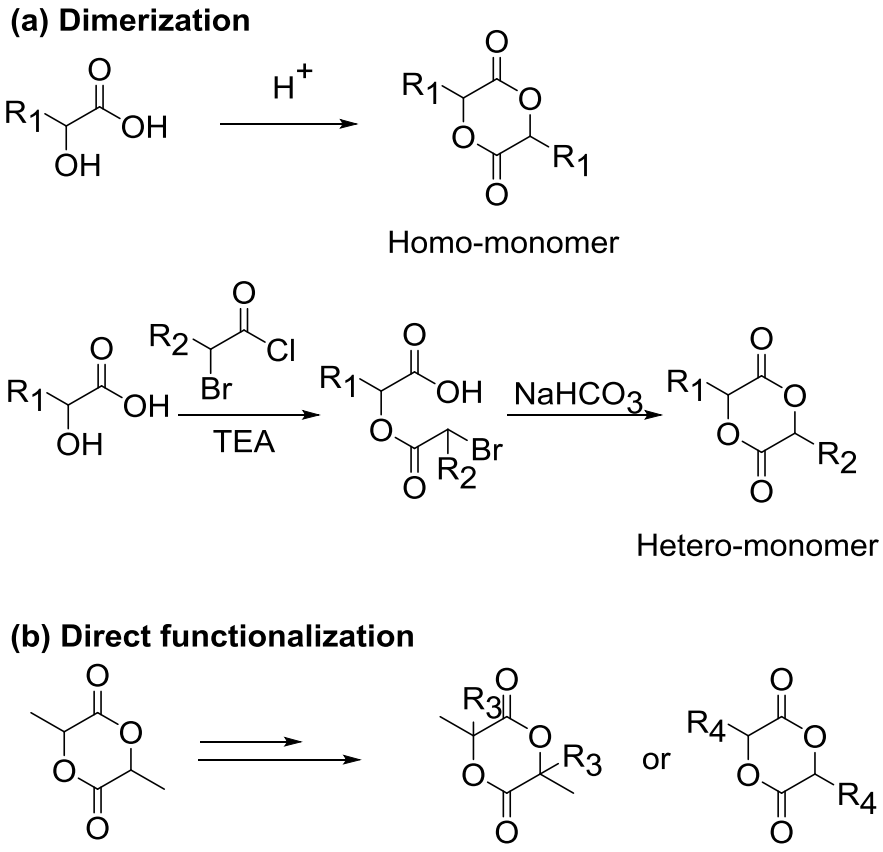

Scheme 28. General synthetic routes to substituted lactide monomers

Given the fact there is a lack of new methodologies to prepare substituted lactide

monomers in high yield, the pursuit of simple but versatile synthetic procedures to prepare a variety of α-hydroxy acids with different functional groups in high yield was considered to be the most practical way to produce a sufficient supply of monomers for the ultimate preparation of functionalized biodegradable polylactides. We are interested in building up a library of substituted α-hydroxy acids functionalized with different clickable moieties which can be converted to their lactide monomers and then to functionalized polylactides for exploring a variety of click post-modification process and the evaluation of the resulting polylactides for their potential in biological applications.

2.2 Results and Discussion

2.2.1 Synthesis of Propargyl Glycolic Acid

Our group was the first to develop a procedure to synthesize propargyl glycolic acid **1** to prepare alkyne functionalized polylactides for post-modification via click chemistry.[77] As shown in **Scheme 29**, a Reformatsky-type reaction of propargyl bromide with ethyl glyoxylate in the presence of activated zinc gives ethyl 2-hydroxy-3-butynoate, which was hydrolyzed in water to provide α-hydroxy acid **1** in 42% overall yield. Besides the low overall yield of **1**, propargyl bromide is very costly and is shock sensitive and subject to explosive thermal decomposition, which makes the preparation of **1** via this method impractical. Several other synthetic routes to **1** were examined in order to find a more convenient procedure that does not use propargyl bromide. However, all of the routes indicated in **Scheme 30** were determined not to be feasible.[109]

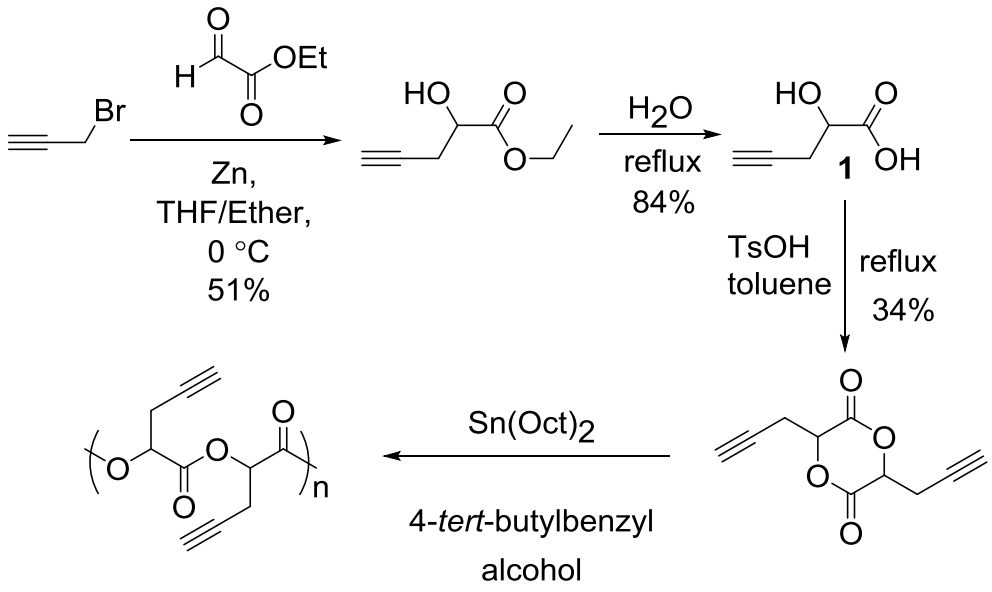

Scheme 29. Synthetic route for propargyl glycolide and its polymer

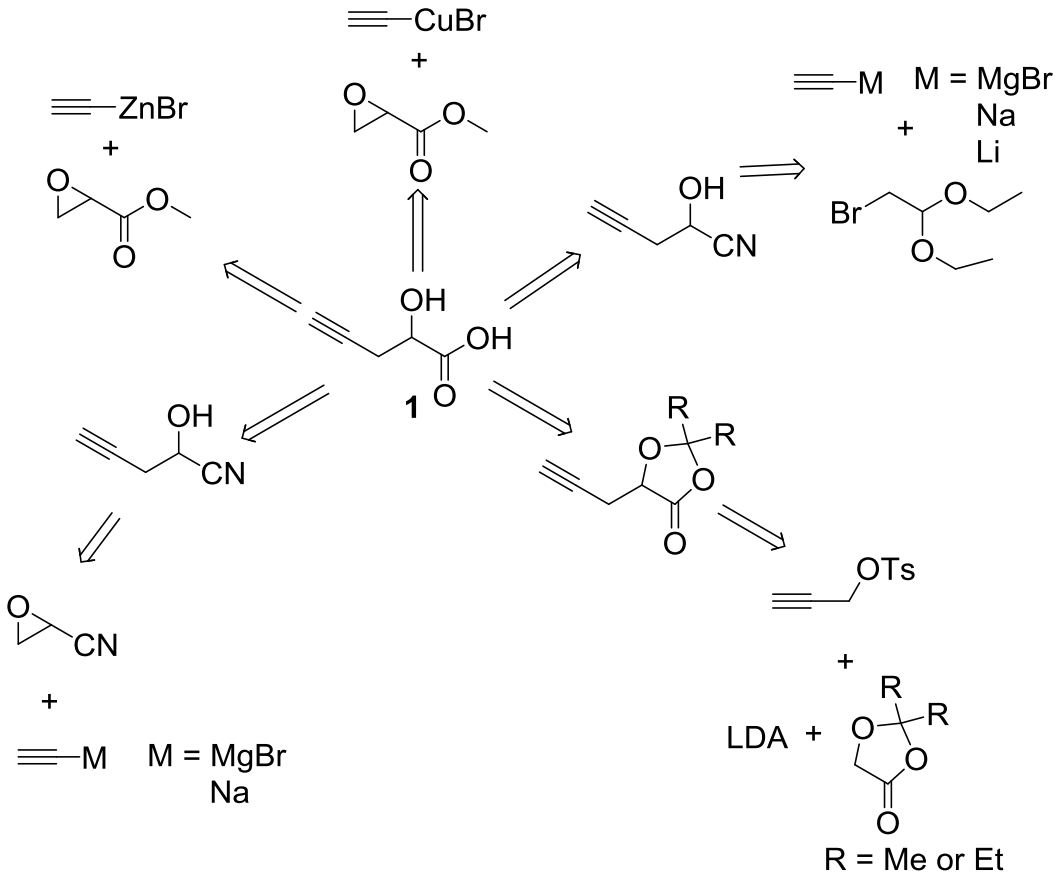

Scheme 30. Failed synthetic procedures conducted to synthesize **1**

2.2.1.1 Synthesis of Propargyl Glycolic Acid via an Organoalane

The intrinsic nucleophilicity of organoalanes is well below that of organolithium and magnesium compounds, which enables them to be better nucleophiles in reactions with base sensitive substrates.[110] Also, because of the Lewis acidic nature of aluminium, organoalane can coordinate with the epoxide oxygen leading to activation of the epoxide and transfer of the alkyl group and the opening of the epoxide ring.[111] However, ethynylaluminum compounds are unstable because of the acidic nature of the ethynyl proton, thus the use of a protecting group, such as TMS, is necessary.

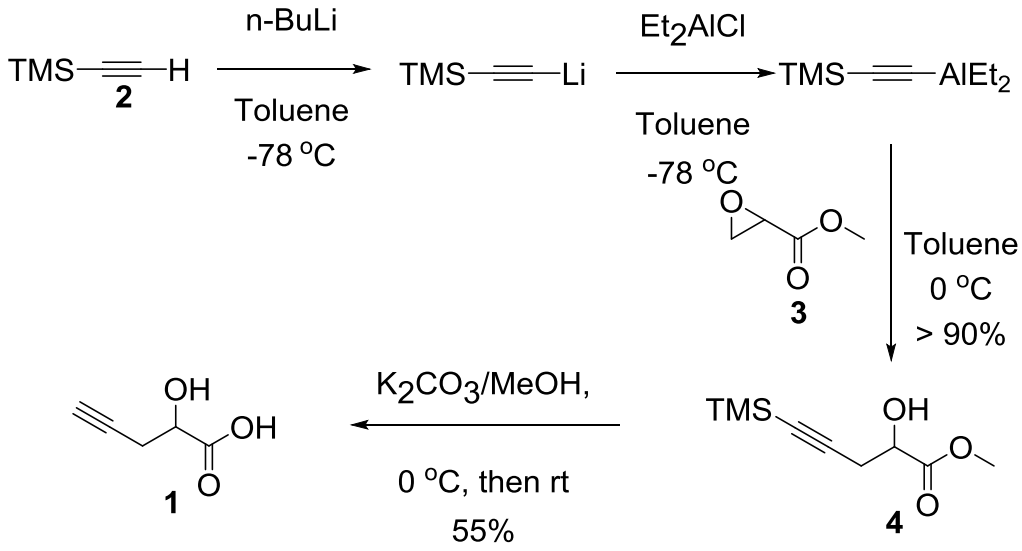

Scheme 31. Epoxide ring opening by organoalane in the synthesis of **1**

Trimethylsilyl acetylene (**2**), prepared from acetylene and trimethylsilyl chloride according to literature procedures,[112, 113] was deprotonated by butyl lithium and converted to trimethylsilylethynyldiethylaluminum by reaction with diethylaluminum chloride. Then methyl glycidate (**3**) was added. The epoxide ring opening was completed after stirring overnight (>90% yield) with no evidence for byproduct formation.

The product (**4**) was directly deprotected in MeOH in the presence of K_2CO_3 to give the propargylglycolic acid (**1**, 55% yield) where the methyl ester was hydrolyzed in the acidic workup (**Scheme 31**). However, at least 2 equivalent of the alanae is required to give high conversion; one equivalent of alane presumably coordinates to the carbonyl oxygen[114] and another equivalent of alane facilitates the ring-opening process after activating the epoxide.[115, 116, 117] An alternative reaction to prepare diethylethynylaluminium was also conducted where equal molar amounts of trimethylsilyl acetylene and triethylaluminium were heated to reflux in toluene.[118] However, a complex mixture was obtained with no obvious formation of product **1** after the addition of epoxide (**3**) and workup. However, this procedure is highly costly at about 1400$/mol compared to 600$/mol for the route from propargyl bromide (**Scheme 29**), since both trimethylsilyl acetylene and diethylaluminium chloride are expensive, although no propargyl bromide was involved.

2.2.1.2 Synthesis of Propargyl Glycolic Acid via the Enolate of a Malonate and Propargyl Tosylate

Two procedures discussed above suffered either from the use of expensive and explosive propargyl bromide or the low pKa of an acetylene proton which can be deprotonated under strong basic conditions. Malonate have a low pKa around 13 and can be easily deprotonated by mild bases such as sodium/potassium alkoxides without deprotonating a terminal alkyne. Thus it should be possible to alkylate a malonate containing a terminal alkyne function. Moreover, the resulting alkylated malonate can be converted to a carboxylic acid by simple decarboxylation upon heating. Propargyl

tosylate,[119] a safe analogue of propargyl bromide, can be prepared from propargyl alcohol and tosyl chloride. Conveniently, both malonates and propargyl alcohol starting materials are commercially available in bulk quantities and can be used to synthesize propargyl glycolic acid (**1**).

As shown in **Scheme 32**, the enolate of diethyl acetamidomalonate (**5**) will react with propargyl tosylate in dioxane under reflux to give **6** in 95% yield.[120] The final glycolic acid (**1**) was obtained in a sequential one-pot reaction with moderate yield (41%) from the combination of 4 steps, hydrolysis of ester (**6**), decarboxylation, hydrolysis of amide, and diazotization of the resulted amino acid (propargylglycine **7**) using $NaNO_2$ under acidic conditions.[121,122]

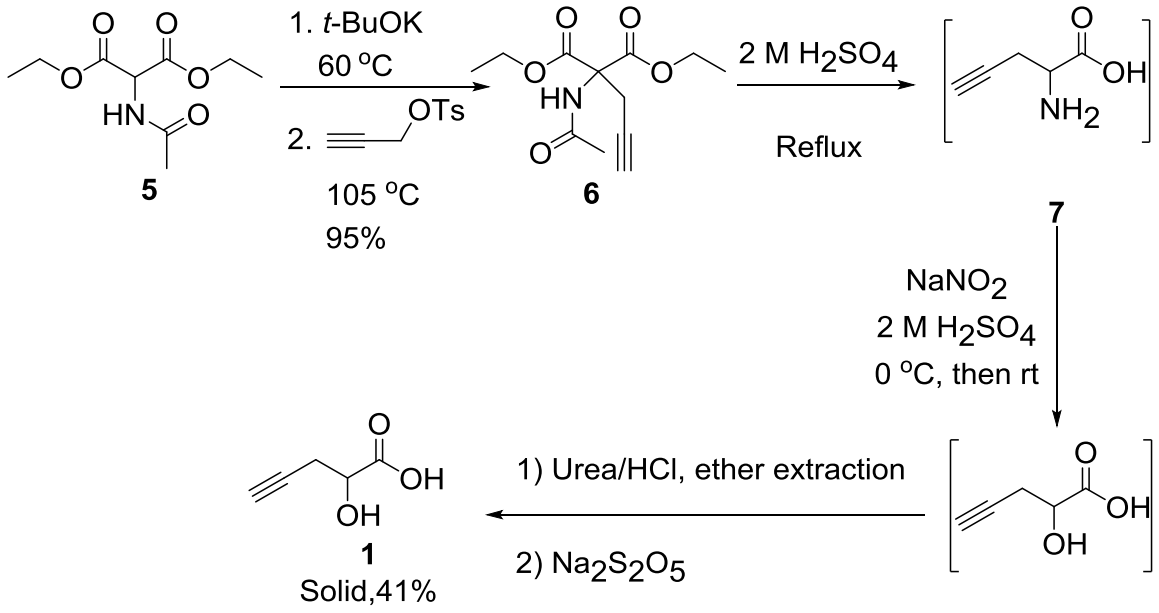

Scheme 32. Synthesis of propargyl glycolic acid from diethyl acetamidomalonate

Propargyl glycolic acid (**1**) prepared by this method rapidly decomposes under high vacuum after extraction from aqueous solution with ether (**Table 1**). This was surprising

since **1** prepared by other method does not decompose upon isolation.[77] The possible reason for this decomposition is that there might be certain oxidants present in the ether extract (verified by a rapid color change of KI-starch test paper, which destroys the product during concentration. However, neither the addition of urea (reacting with HNO_2) nor the passing of the crude product through a short silica gel column can stop the decomposition. So several reductants were examined which presumably would react with any possible oxidants. No product **1** was detected in the filtrate from an ether solution after addition of Na_2SO_3 to an ether solution of **1** and filtration to remove the solid. However, **1** can be recovered in low yield (<15%) as a light yellow solid after extracting the acidified aqueous solution of Na_2SO_3 with ether. Apparently, acid **1** can be converted to its sodium salt which precipitates from ether through an acid-base reaction with Na_2SO_3. This shows that it is not convenient to use Na_2SO_3 as a reductant to remove the possible oxidants. When the reductant $Na_2S_2O_3$ was added to an ether solution of acid **1**, both sulfur and acid **1** were obtained as yellow solid mixture after the removal of ether under vacuum. Dissolution of this mixture in water, filtration and removal of the water gave pure acid product **1** in 30% yield. However, pure product **1** could be obtained as light yellow solid in 41% yield by adding $Na_2S_2O_5$ solid to an ether solution of acid **1** followed by simple filtration, concentration and sublimation under vacuum. This indicates that $Na_2S_2O_5$ solid may remove any possible oxidants and provide product **1** as solid with a relatively uncomplicated procedure. Based on these results, we conclude that the reducing salts added to an ether solution of **1** probably act

as bases to remove the possible acidic oxidants (like HNO_2, HNO_3 and H_2SO_4) and enable the product **1** to form as solid without decomposition under vacuum. Despite the moderate yield, the overall cost to synthesize 1 mol of acid **1** is 220$, much lower than other procedures.

Table 1. Propargyl glycolic acid (**1**) after treatment with different reductants/bases

	Reductant/Base[a]			
	None	Na_2SO_3	$Na_2S_2O_3$	$Na_2S_2O_5$
Compounds in ether [b]	**1**	No **1**	**Sulfur** + **1**	**1**
Appearance of dry **1** [c]	Decomposition black	Light yellow solid [d]	Yellow solid	Light yellow solid

[a] Solid reductants/bases were added into ether extract containing **1** and stirred for 12 hours. [b] Compounds in ether extract before and after treatment with reductants/bases followed by filtration. [c] Product **1** obtained after removal of ether after treatment with reductants/bases followed by filtration. [d] The product **1** was recovered after extracting the acidified aqueous solution of solid Na_2SO_3.

However, several factors, like the use of dioxane as solvent, the requirement for toxic chemicals and especially the low atom economy, render this procedure unfeasible for a practical synthesis of the target acid **1**.

2.2.2 Synthesis of Propargyloxy Lactic Acid via Hydrolysis of a Cyanohydrin

Propargyl alcohol contains two functional groups, a terminal alkyne and a hydroxy group and it is possible to employ the hydroxy group as nucleophile under weak basic condition without affecting the terminal alkyne function. Bromoacetaldehyde diethyl acetal has a good leaving group (bromo group) and the protected aldehyde which can be later converted to a cyanohydrin. The use of propargyl alcohol and

bromoacetaldehyde diethyl acetal as starting materials to synthesize a cyanohydrin containing terminal alkyne would be able to provide a general and economic synthetic route to the corresponding α-hydroxy acid since both starting materials are widely used in industry and can be supplied in large quantities at low prices. However, the hydrolysis of cyanohydrins containing a terminal alkyne group is rare in the literature.[123]

The synthesis of propargyloxy lactic acid (**12**) is outlined in **Scheme 33**. An excess of propargyl alcohol was deprotonated by NaH in THF and the resulting alkoxide will nucleophilically attack the bromo group of the bromoacetaldehyde diethyl acetal (**8**) to afford propargyloxyacetaldehyde diethyl acetal (**9**) as pale red liquid in 92% yield without affecting the terminal alkyne (Further purification can be done through vacuum distillation, but this is not necessary). The optimized hydrolysis condition for the acetal **9** to aldehyde **10** was determined to be a biphasic mixture of trifluoroacetic acid (TFA), water and dichloromethane (1:1:4), which require vigorous stirring to achieve quantitative conversion (**Table 2**, entries 8 and 9). The resulting aldehyde **10** was used without further purification.[124, 125, 126] *p*-Toluenesulfonic acid (TsOH), HCl,[127] H_2SO_4[128] and acetic acid were not effective in the deprotection of diethyl acetal **9** (**Table 2**, entries 1-7).

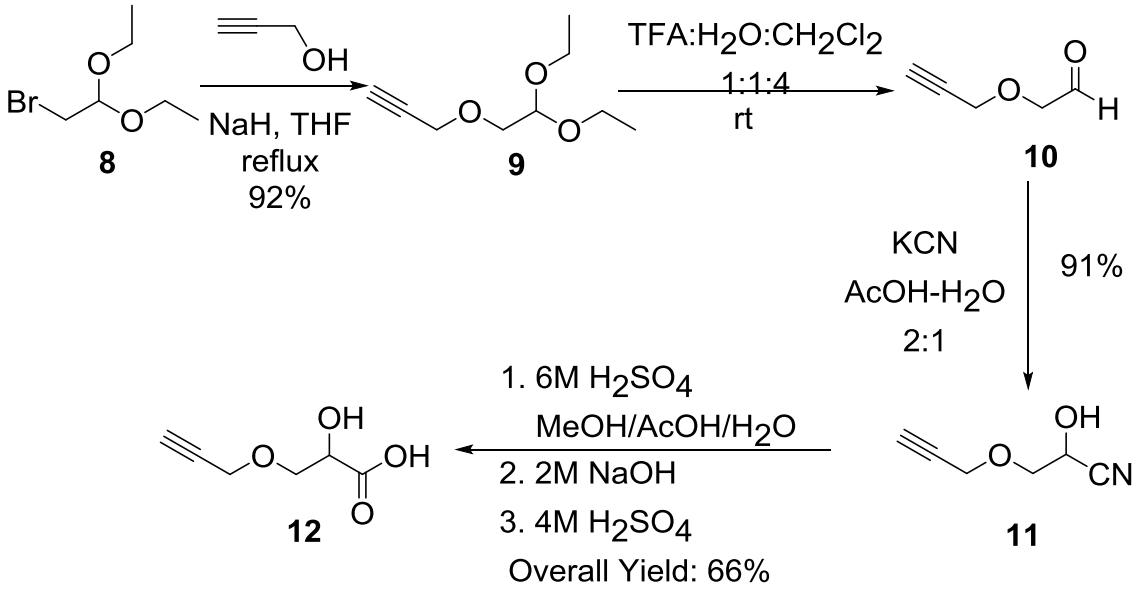

Scheme 33. Synthesis of propargyloxy lactic acid (**12**)

Table 2. Deprotection of **9** with various acids and solvents at room temperature

Entry	Acid	Solvent	Time / h	Conversion (%)[a]
1	TsOH (10%)	H_2O	20	0
2	TsOH (10%)	THF-H_2O	5	< 5%
3	AcOH (25%)	CH_2Cl_2-H_2O (4:1)	36	< 10%
4	HCl (2M)	Ether-H_2O	20	30%
5	HCl (2M)	THF-H_2O	20	35%
6	HCl (2M)	AcOH-H_2O	20	< 20%
7	H_2SO_4 (2M)	AcOH-H_2O	36	40%
8	TFA (2%)	CH_2Cl_2-H_2O (4:1)	36	< 10%
9	TFA (16%)	CH_2Cl_2-H_2O (4:1)	12	100%

[a] Conversion was measured by ^1H NMR.

The cyanation of aldehyde **10** was performed under acidic condition and the resulting aqueous solution of **11** was extracted continuously with CH_2Cl_2 to give cyanohydrin **11** in high yield (91%) and was used without further purification. The

hydrolysis of cyanohydrin **11** was first tried in aqueous HCl (2, 6 and 11 M) and resulted in decomposed starting material (not shown in **Table 3**). Considering the fact that the alkyne function can survive in refluxing 2 M H_2SO_4 (**Scheme 32**), hydrolysis of **11** at various concentrations of H_2SO_4 and at various temperatures was conducted in a mixture methanol and water to find the best condition (**Table 3**). The results of hydrolysis at different temperatures and concentrations of H_2SO_4 showed that hydrolysis can proceed much faster at higher reaction temperature and higher concentration of H_2SO_4. However, high temperatures also gave slightly lower yields (entries 7-10). Changing the solvent ratio between MeOH and H_2O did not show an effect on the yields (entries 9 and10). So the optimized conditions for hydrolysis of **11** were with 5~6 M H_2SO_4 at 70 ^oC for 24 h at (entries 3 and 4). The product consists of a mixture of the α-hydroxy acid and its methyl ester and was continuously extracted with ether and then hydrolyzed in 2 M NaOH for 12 h at room temperature followed by extraction with ether to remove mineral oil (from first step) and other organic impurities. After acidifiication back to pH<1, the final product was extracted with ether again and concentrated to give **12** as a light yellow solid with an overall yield of 66% from **8** (4 steps) which can be further decolorized with charcoal in water to give a white solid. These studies indicate that this procedure can be used to synthesize sufficient quantities of alkyne functionalized α-hydroxy acid **12** with low cost and convenient reaction conditions.

Table 3. Hydrolysis of **11** at various concentrations of H_2SO_4, temperatures and solvents

Entry	Temp (°C)	MeOH/H_2O	[H_2SO_4] (M)	Time (h)	Conv.[a]	Yield[b] **12**
1	70	1:1	3.6	160	98%	78%
2		1:1	4	31	94%	79%
3		1:1	5	25	91%	76%[c]
4		1:1	6	26	100%	81%
5		1:1	6	48	-	76%
6	80	1:1	4	24	91	80%
7		1:1	5	12	99	78%
8	98	3:1	2	65	84%	63%
9		1:1	5	16	98%	67%
10		3:1	5	18	100%	65%

[a] Conversions were measured by ^{1}H NMR; [b] Yield of **12** were measured by ^{1}H NMR by adding an internal standard, triphenylmethane after basic and acidic workup; [c] Isolated yield after basic and acidic workup followed by extraction with ether.

2.2.3 Synthesis of Poly(ethylene glycol) Monopropargyl Ether Lactic Acid via Hydrolysis of a Cyanohydrin

PEG is a biologically inert polymer which has been extensively used to alter the physical properties of polymer complexes, especially as electrolyte and therapeutic agents. Conjugation with PEG can confer many beneficial properties, such as increased solubility, reduced interaction with serum and proteins and thus significantly increasing the half-life *in vivo*.[129] Polylactides functionalized with hydrophilic PEG and/or hydrophobic alkyl chains as pendant groups have been reported to have thermo-responsive properties[71,72,77] and to influence the interactions of cells with polymer

materials[73]. They are prepared either by the monomer derivative approach or post-polymerization modification via click chemistry. Incorporating both terminal alkyne and polyethylene glycol chain pendant groups onto polylactides can enable functionalization of the polymer by click chemistry and enable PLA novel physical properties, such as thermo-responsive property. So a series of α-hydroxy acids (poly(ethylene glycol) monopropargyl ether lactic acids) (**Figure 4**) with different PEG unit lengths were synthesized to expand the library of clickable and thermo-responsive polylactides and their preparation will be discussed below.

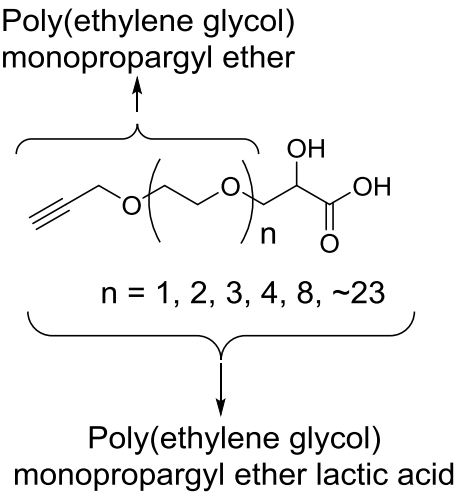

Figure 4. Structure of poly(ethylene glycol) monopropargyl ether lactic acid

2.2.3.1 Synthesis of Poly(ethylene glycol) Monopropargyl Ether Lactic Acid (23, n=1,2,3,4)

The synthesis of poly(ethylene glycol) monopropargyl ether lactic acid (n=1,2,3,4) starts from the corresponding oilgo(ethylene glycol) with 1 - 4 glycol units, all of which are commercially available. The synthetic strategy is based on the coupling of monoprotected oligo(ethylene glycol), propargyl alcohol and protected

bromoacetaldehyde (**8**) to generate a cyanohydrin which can be hydrolyzed to α-hydroxy acids of the type **23**. As shown in **Scheme 34**, the oligo(ethylene glycol) (**13**, n=1,2,3,4) were desymmetrized and monoprotected with trityl chloride to afford **14** as white solids (n=1,2) or viscous liquid (n=3,4) in high yield (>90%) which were used without further purification.[130, 131] Dityrityl protected oligo(ethylene glycol)s were obtained as minor side products with **14**, but were not removed since it was anticipated that it could be easily removed in derivatized forms while purifying the final α-hydroxy acids and this will be discussed later. Coupling of the propargyl group with **14** is not plausible due to the fact that deprotection of trityl group will employ a palladium catalyzed hydrogenolysis and due to possible side reactions of the terminal alkyne when NaH is used in subsequent steps. So the monotriytl protected PEG (**14**) was coupled with protected bromoacetaldehyde (**8**) to quantitatively give **15** which does not require further purification. After workup, excess **8** was simply removed under high vacuum at 40 ^{o}C overnight. However, due to the low solubility of the alkoxide of **14** (n=1), the coupling between ethylene glycol monotrityl ether (**14**, n=1) and **8** only proceeds to 66% conversion after refluxing for 48 h and this cause problems in the purification. This problem was solved by using the commerically available ethylene glycol monobenzyl ether (**16**) which was converted to pure **17** quantitatively following the same protocol used in the synthesis of **15**. The selective deprotection of trityl group of **15** and **17** in both THF and CH_2Cl_2 were not effective or required very high catalyst loading and long reaction times to give high conversion. However, the deprotection in an alcohol, such as ethanol, gave 100% conversion without affecting the acetal. So both **15** and **17** were selectively deprotected by hydrogenolysis in ethanol catalyzed by

palladium on carbon (≥ 2%) at 1400 psi H_2.[131] The resulting alcohol **18** was then carefully dried under vacuum to remove ethanol. However, the ethanol cannot be completely removed (5 - 10% left). If it is completely removed, the protected aldehyde will undergo alcohol exchange to give a mixture of compounds. This mixture can be converted to **18** by mixing with ethanol under high pressure in a steel autoclave reactor. However, the small amount of ethanol will not affect subsequent reactions since the by-product (propargyl ethyl ether) from ethanol can be easily removed at the end. The tosylation of **18**[131] followed by coupling with propargyl alcohol provided alkyne functionalized acetal **20** in quantitative yield. The deprotection of **20** by trifluoroacetic acid in CH_2Cl_2 and water gave aldehyde **21** which was subjected to cyanation directly without further purification to provide **22**. After continuous extraction of **22** from an aqueous solution and removal of CH_2Cl_2, cyanohydrin **22** was hydrolyzed in 6M H_2SO_4 in a mixture of MeOH and water then followed by extraction with CH_2Cl_2 and with aqueous NaOH treatment to hydrolyze methyl ester. Then the mixture was diluted and extracted with CH_2Cl_2 to remove all nonionic organic impurities, such as poly(ethylene glycol) dipropargyl ether, propargyl ethyl ether and mineral oil. After it was acidified with 4 M HCl, the pure target α-hydroxy acids (**23**, poly(ethylene glycol) monopropargyl ether lactic acids) were obtained via extraction as light yellow or pale red viscous liquid in 40-60% yields.

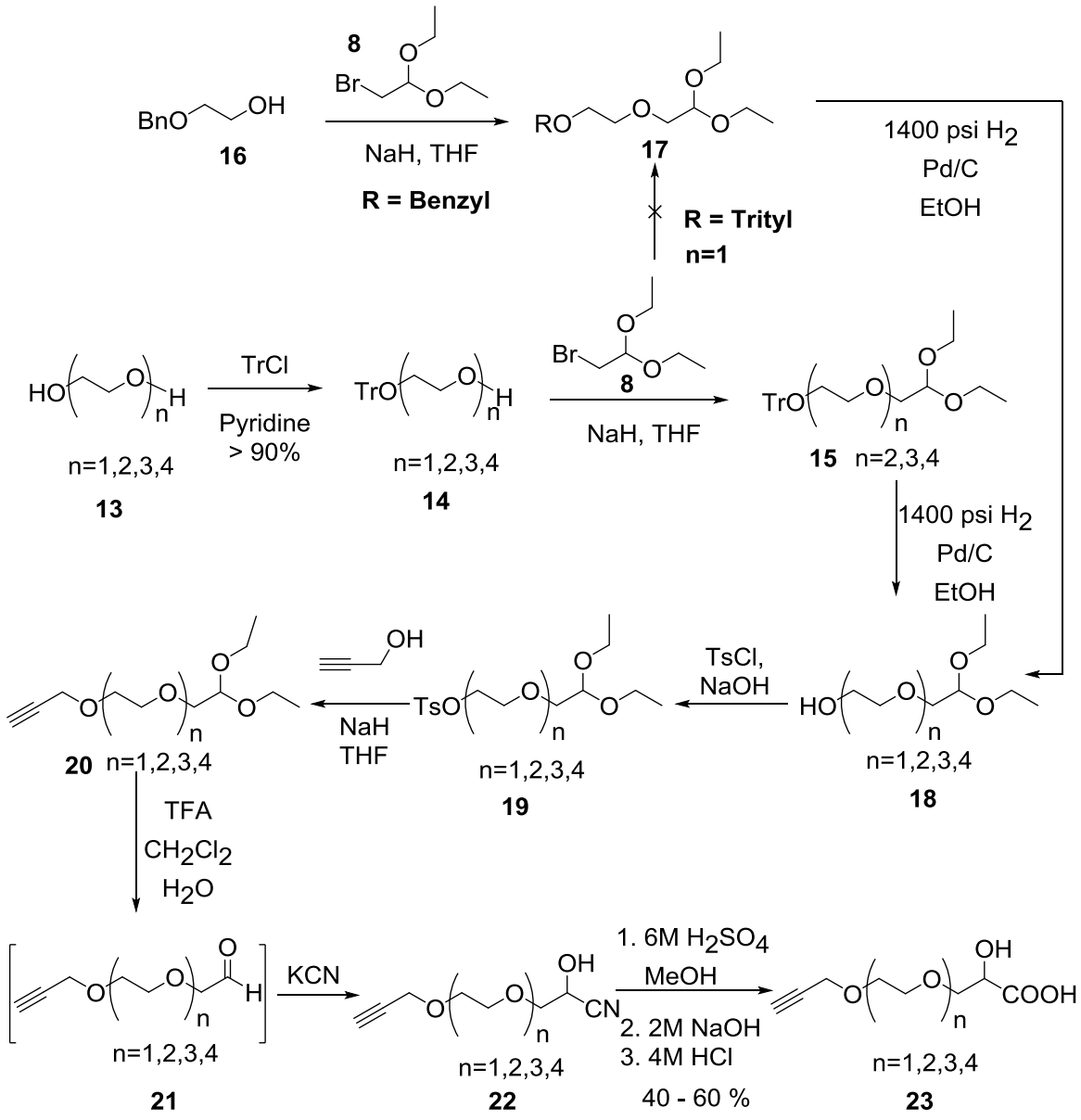

Scheme 34. Synthesis of poly(ethylene glycol) monopropargyl ether lactic acid (**23**, n=1,2,3,4)

Notably, the overall synthesis discussed above doesn't involve purification by column chromatography which is one of the advantages of this procedure and thus the synthesis can be easily scaled up. This also indicates that the step involving hydrolysis of cyanohydrin is compatible with the overall synthesis of terminal alkyne functionalized

lactic acids and should be general and useful.

2.2.4 Synthesis of Octa(ethylene glycol) Monopropargyl Ether Lactic Acid (n=8)

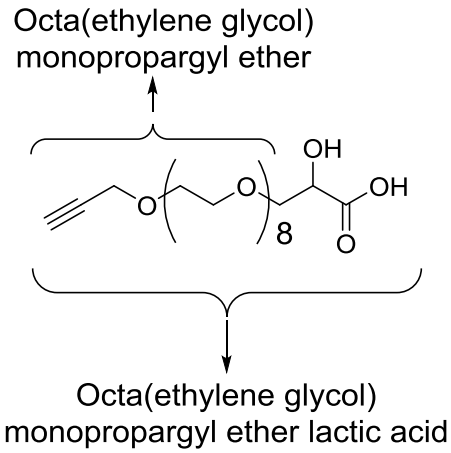

Figure 5. Structure of octa(ethylene glycol) monopropargyl ether lactic acid

Oligo(ethylene glycol)s with up to 4 glycol units (n=1,2,3,4) are available commerically in large scales and thus during the desymmetrization and mono-functionalization one can afford to waste these inexpensive diols. However, when extending the number of repeating units of the oligo(ethylene glycol) to greater than 5, it is not acceptable to start with oligo(ethylene glycol) in the synthesis of the corresponding α-hydroxy acid due to the extreme high cost. So it is necessary to synthesize these poly(ethylene glycol)s with an efficient route not involving complicated purifications, such as column chromatographic separations. Herein, we describe a simple procedure to produce longer well-defined bifunctional octa(ethylene glycol) (n=8) by introducing orthogonal protecting/functional groups to two shorter oligo(ethylene glycol)s and then coupling of the two for the purpose of synthesizing monopropargyl ether lactic acid (**Figure 5**). This method could potentially be used to synthesize various

longer poly(ethylene glycol)s with exact repeating units (n>8).

2.2.4.1 Synthesis of Tetraethylene Glycol Monobenzyl Ether (29)

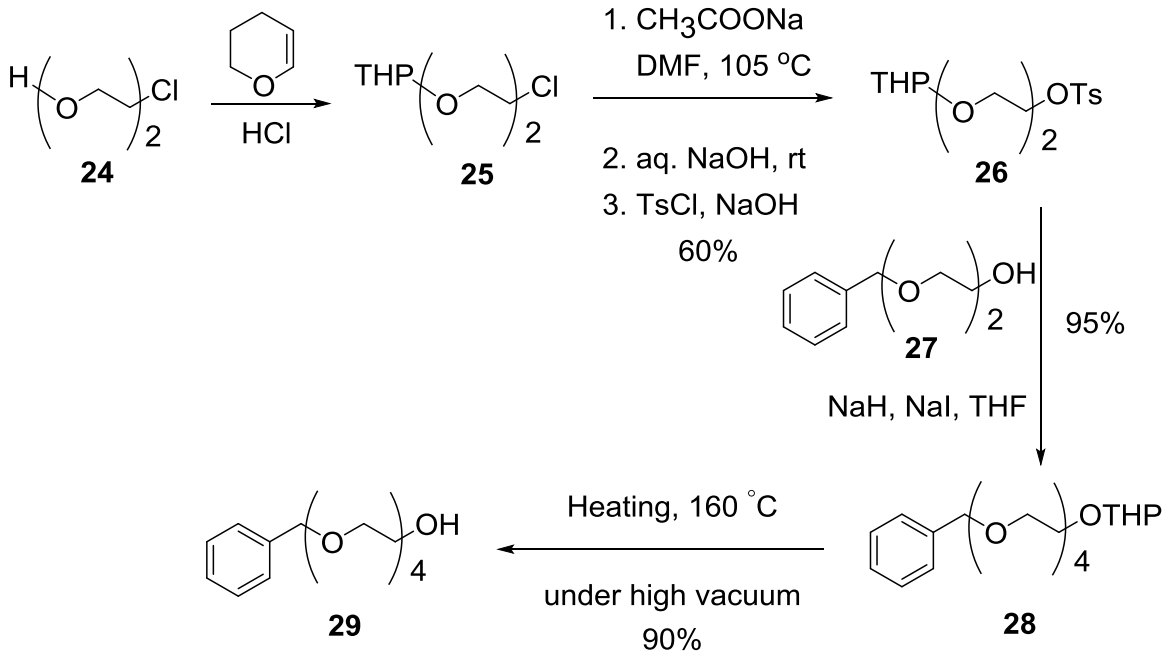

Scheme 35. Synthesis of tetraethylene glycol monobenzyl ether (**29**)

The synthesis of tosylate **26** started from the commercially available diethylene glycol monochlorohydrin (**24**) which was quantitatively protected with dihydropyran (DHP) to afford **25** which was isolated by drying under high vacuum at 50 °C.[132] Then the chloro group of **25** was substituted with sodium acetate in DMF followed by hydrolysis and tosylation to provide the pure protected tosylate **26** (60%, 4 steps).[133] Thus diethylene glycol monobenzyl ether (**27**) was coupled with **26** under basic conditions to provide **28** that contained negligible impurity (yield: 95%).[134] This indicates one efficient coupling step to prepare elongated bifunctional PEG chains with high conversion and high yield, which does not require column chromatographic

separation due to the negligible amount of by-product from the reaction. After heated in a 160 ^{o}C oil bath under high vacuum, the THP protecting group of **28** was efficiently removed to give the target compound tetraethylene glycol monobenzyl ether (**29**) in high yield of 90%.

2.2.4.2 Synthesis of Monotetrahydropyran-protected Tetraethylene Glycol Monotosylate (35)

Tetraethylene glycol (**30**) was monoprotected with dihydropyran (DHP) using a large excess of **30** in THF to give a mixture of **31** and **32** (8:1) which was quantitatively tosylated to tosylates **33** and **32** (**Scheme 36**).[134] After complete cleavage of the THP protecting groups of **33** and **32** under acidic conditions in MeOH, the crude product was concentrated and redissolved in CH_2Cl_2 and washed with aqueous NaCl solution to give the pure tetraethylene glycol monotosylate (**34**) as colorless liquid in 87% yield. The desired product **33** was achieved by protecting **34** using DHP under acidic condition (74%). Although di-THP protected tetraethylene glycol (**32**) was an impurity in the preparation of **31**, it can be simply removed by washing with water after deprotection due to the highly hydrophilic nature of tetraethylene glycol. The overall procedure allows for the synthesis of pure tetraethylene glycol monotosylate (**34**) in a simple and efficient manner.

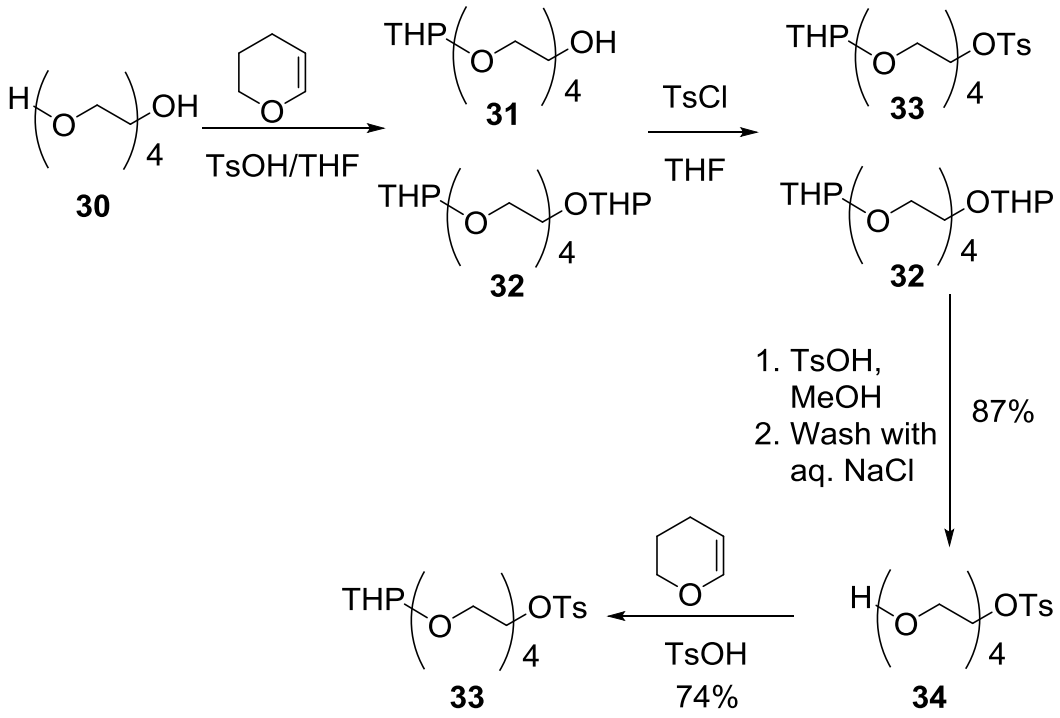

Scheme 36. Synthesis of monotetrahydropyran-protected tetraethylene glycol monotosylate (**33**)

2.2.4.3 Synthesis of Octa(ethylene Glycol) Monobenzyl Ether (36) and the Lactic Acid (40, n=8)

As shown in **Scheme 37**, tetraethylene glycol monobenzyl ether (**29**) and **33** were coupled together via a substitution reaction followed by deprotection of the THP group by heating at 55 ^{o}C under high vacuum to give pure octa(ethylene glycol) monobenzyl ether (**36**). The feed ratio of **29** to **33** (1:1.1 in our case) was found to be crucial to get **36** in a form which can be easily purified. Then tosylate **37** was synthesized from the coupling of **8** and **36**, and subsequent deprotection of the benzyl group and tosylation gave **37** at 91% yield (3 steps). Upon coupling with propargyl alcohol, **37** was quantitatively converted to **38** (90%) which was deprotected to give an aldehyde that was converted to cyanohydrin **39**. Then final pure product (**40**) was obtained in 65%

yield after hydrolysis of the cyanohydrin, hydrolysis of the methyl ester by NaOH, extraction from acidic solution and washing with 1 M HCl solution to remove all impurities. The washing of **40** using 1 M HCl was intended to wash out some of the organic byproducts that are more hydrophilic than **40** in water.

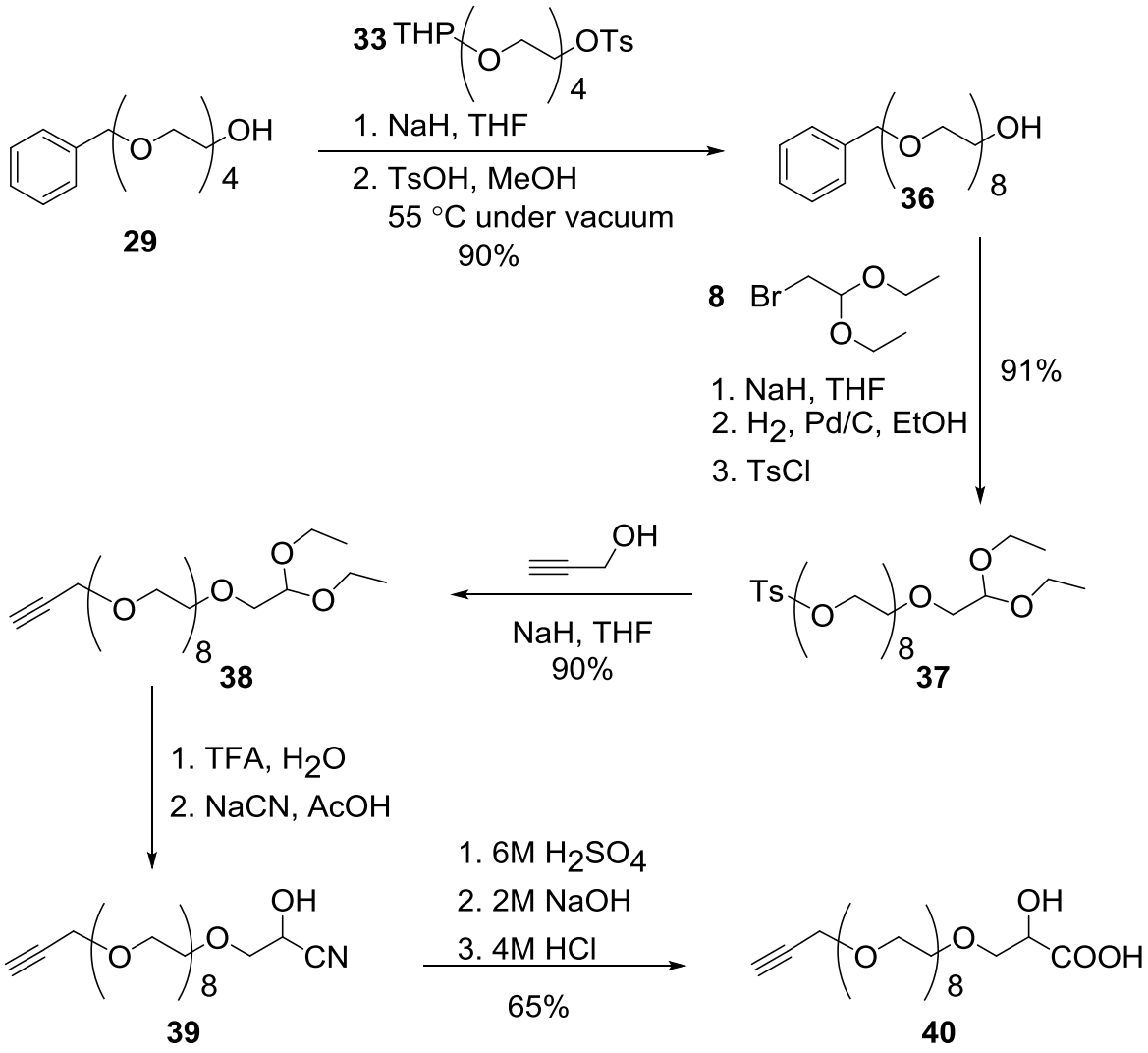

Scheme 37. Synthetic route to octa(ethylene glycol) monopropargyl ether lactic acid (**40**)

2.2.5 Synthesis of Poly(ethylene glycol) Monopropargyl Ether Lactic Acid (50, n≈23)

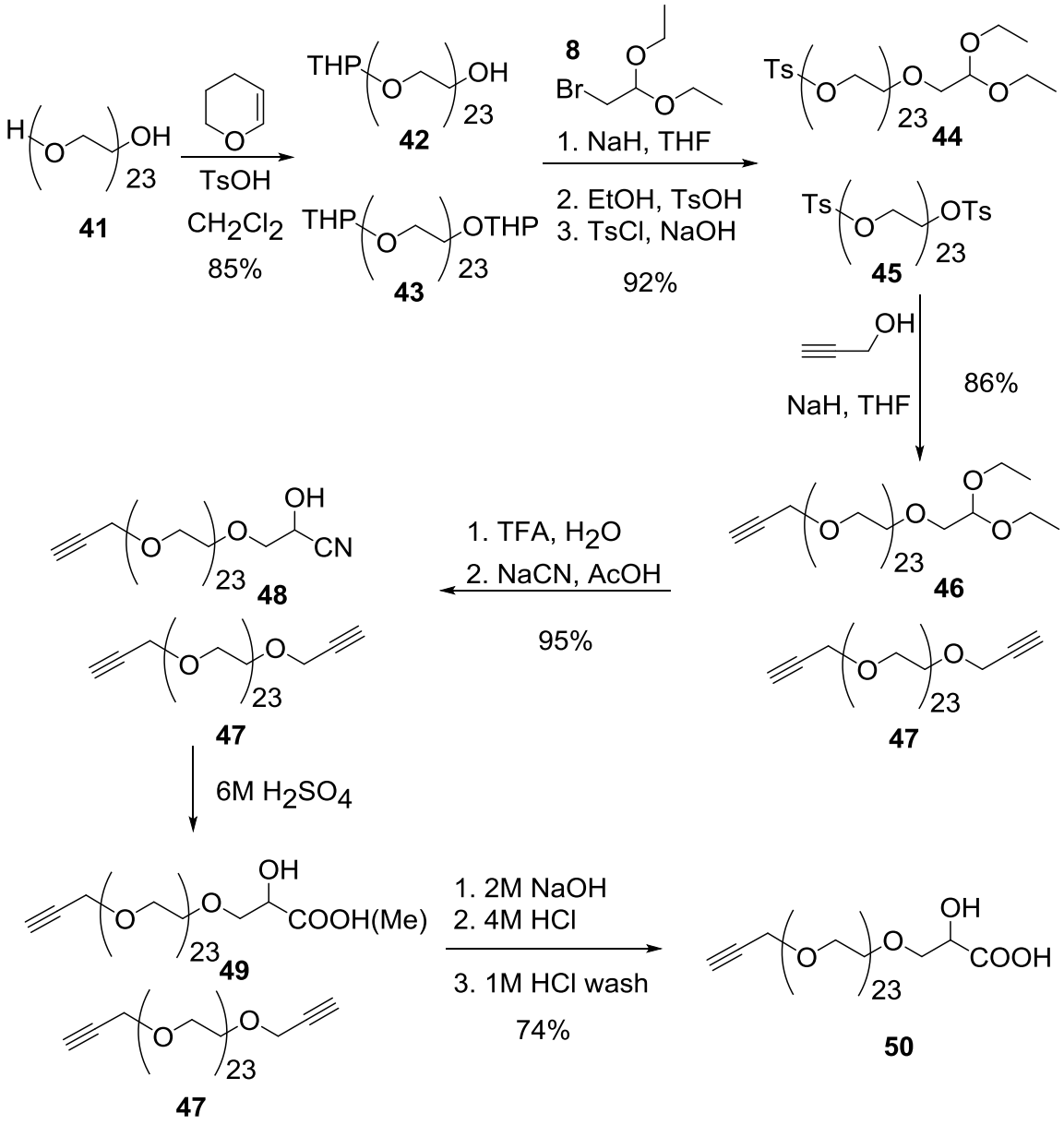

Scheme 38. Synthesis of poly(ethylene glycol) monopropargyl ether lactic acid (**50**, n≈23)

Using a procedure similar to that for the preparation of tetraethylene glycol monotosylate (**34**, **Scheme 36**), poly(ethylene glycol) (**41**, n≈23) was mono-protected by

DHP to give **42** as major product with bis-THP ether **43** as a minor product which can be carried through the synthesis and removed as its derivative (**47**) at the end (**Scheme 38**). The THP protection of **41** gives a ~10:1 mixture of **42** and **43** in 85% total yield after washing their dichloromethane solution with water for 40 times. Coupling **8** with **42** under basic condition followed by deprotection of the THP group and then tosylation resulted in the formation of desired product **44** containing **45** as minor product (92% total yield). The tosylate **44** was coupled with propargyl alcohol to install the alkyne function and give **46** in 86% yield. Acetal hydrolysis and cyanation gave cyanohydrin **48** (95% yield) which was hydrolyzed in 6 M H_2SO_4 to afford a mixture of **47** and **49**. After hydrolyzing the methyl ester, hexane/CH_2Cl_2 (1:1) was used to extract the aqueous solution twice to remove mineral oil, **47**, and some other nonionic impurities. The aqueous solution of **49** was acidified and extracte with CH_2Cl_2. The organic solutions was washed with 1M HCl solution 3 times to provide pure poly(ethylene glycol) monopropargyl ether lactic acid (**50**, n≈23, 74% yield) as white wax-like solid after drying under vacuum.

2.2.6 Synthesis of Allyloxy Lactic Acid (54) via Hydrolysis of Cyanohydrin

The versatility of the synthetic route to substituted lactic acids described above which involves a cyanohydrin hydrolysis was tested by the preparation of allyloxy lactic acid (**54**), since alkene is feared to undergo unexpected side reactions, such as H_2O addition under acidic conditions and polymerization by light or heat. As outlined in **Scheme 39**, the synthesis of allyloxy lactic acid (**54**) was prepared following a

procedure similar to prepare propargyloxy lactic acid (**12**, **Scheme 33**) using allyl alcohol and acetal (**8**) as starting materials. The coupling between **8** and allyl alcohol gave **51** in 76% yield after vacuum distillation. After hydrolysis to aldehyde **52** under acidic condition, cyanohydrin **53** was prepared as a pale red oil (>100%, with acetic acid) and isolated by continuous extraction. Following hydrolysis under acidic and basic conditions allyloxy lactic acid (**54**) was extracted from acidic solution in 55% yield (4 steps).

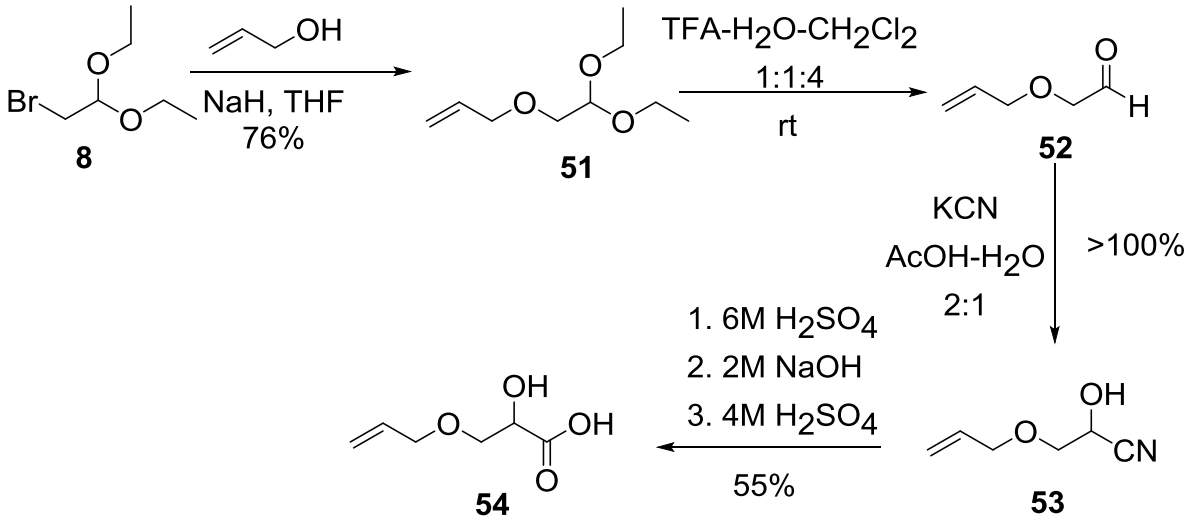

Scheme 39. Synthesis of allyloxy lactic acid (**54**)

2.2.7 Synthesis of Azido Lactic Acid (56)

Azide functionalized polylactides provide an alternative approach to render click function through Cu(I) catalyzed (CuAAC) or strain-promoted alkyne-azide cycloadditions (SPAAC). The azido lactic acid (**56**) was prepared as viscous liquid (59% yield) from methyl glycidate (**3**) and sodium azide in the presence of NH_4NO_3 (**Scheme 40**)under reflux followed by hydrolysis of the methyl ester with 1M aqueous NaOH solution.[135]

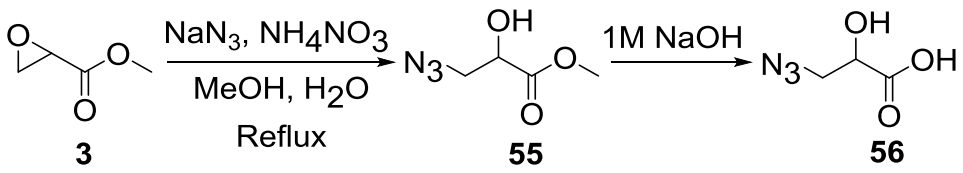

Scheme 40. Synthesis of azido lactic acid (**56**)

2.3 Conclusion

With the goal of development of a convenient synthetic process for preparation of propargyl glycolic acid (**1**), two synthetic processes were explored. The disadvantages of both processes promoted us to search for new substituted lactic acids and appropriate methods for their synthesis. Propargyloxy lactic acid was proposed as a clickable polylactide precursor and was synthesized from inexpensive starting materials in high yield with a method that involves a cyanohydrin hydrolysis. A series of propargyloxy lactic acids derivatives incorporating poly(ethylene glycol) units of different lengths as spacers between the propargyl group and the lactic acid were prepared. The synthesis featured by poly(ethylene glycol) desymmetrization and coupling methods without using column chromatographic purification. The versatility of the developed method was also tested for its tolerance of an alkene group in the synthesis of allyloxy lactic acid. Finally, azido lactic acid was also prepared to act as an alternative approach to incorporate click functions to polylactides.

2.4 Experimental Section

Materials. Butyl lithium (2.5 M in hexane), diethylaluminum chloride, propargyl alcohol, allyl alcohol, bromoacetaldehyde diethyl acetal, oilgo(ethylene glycol) (n=1,2,3,4), dihydropyran, dioxane, sodium hydride, trityl chloride and palladium on

activated charcoal (10%) were purchased from Sigma-Aldrich and used as received. Potassium *tert*-butoxide, diethyl acetamidomalonate, ethylene glycol monobenzyl ether, diethylene glycol monobenzyl ether, and 2-(2-chloroethoxy) ethanol were purchased from Alfa-Aesar and used directly. THF, dioxane and toluene were dried over sodium and distilled before use. All other reagents and solvents were ACS grade and used as received unless specified.

Characterization. Melting points were measured on Electrothermo® melting point apparatus. ^{1}H NMR and ^{13}C NMR were recorded on a Varian 300 MHz or VXR-500 MHz or 600 MHz instrument in $CDCl_3$ unless otherwise noted. $CDCl_3$ was used as the internal standard for both ^{1}H NMR (δ = 7.24) and ^{13}C NMR (δ = 77.0).

Synthesis of trimethylsilylacetylene (2). To a 500-mL 2-necked flask (flame-dried) was added 5.25 g (0.218 mol) of magnesium which was dried under vacuum overnight. After addition of 30 mL of dry THF and a piece of I_2, 15 mL (0.20 mol) of dry bromoethane in 100 mL of dry THF was added to the magnesium dropwise. After refluxing for 40 min and then cooling down to room temperature, the fresh Grignard reagent was titrated following Knochel's method [136] and the concentration was determined to be 0.76 M.

To a flame-dried 1000-mL 3-necked flask equipped with an addition funnel, reflux condenser, and a gas-inlet diffusion tube connected to an acetylene cylinder through two traps immersed into dry ice-acetone bath, 140 mL of dry THF was added and saturated with acetylene for 40 min in a 15 ^{o}C water bath. Then the freshly-made Grignard reagent was added dropwise. After addition of all the ethyl Grignard to the

flask, the acetylene was continuously introduced for another 3 hours. The concentration of ethynylmagnesium bromide was 0.38 M after titration and was used directly. Then 14 mL (0.11 mol) of trimethylsilyl chloride in dry THF was added rapidly to ethynylmagnesium bromide (260 mL, 0.100 mol) and the water bath was kept at 15 ^{o}C for another 30 min. The reaction mixture was refluxed for 1 h. Then the liquid mixture was distilled and the distillate was washed with water. The liquid was distilled to give **2** as liquid (11.7 g, 60%). b.p. 50-57 ^{o}C. ^{1}H NMR (500 MHz, $CDCl_3$): δ 2.34 (s, 1H), 0.17 (s, 9H).

Synthesis of methyl glycidate (3). To a 500-mL flask containing 146 mL (0.120 mol) of bleach solution, 8.6 g (0.10 mol) of methyl acrylate was added in one portion at 0 ^{o}C, and the resulted biphasic mixture was stirred vigorously for 35 min. Then the solution was slowly heated from room temperature to 35 ^{o}C for 1.5 h. After cooling with ice bath, the product was extracted with CH_2Cl_2 and the combined organic layers were dried over sodium sulfate and concentrated to give slightly yellow oil. Vacuum distillation gave the pure colorless liquid **3**, (4.0 g, 40%). b.p. 71-78 ^{o}C/60 Torr). ^{1}H NMR (500 MHz, $CDCl_3$): δ 3.74 (s, 3H), 3.39 (dd, 1H, *J* = 2 and 4 Hz), 2.90 (dd, 2H, *J* = 2 and 6 Hz).

Synthesis of propargyl glycolic acid methyl ester (4) via organoalanate. To a flame-dried 500 mL round bottom flask was added 20 mL of 2.5 M (50 mmol) of *n*-BuLi solution, then 7.6 mL (50 mmol) of trimethylsilyl acetylene (**2**) in 15 mL of toluene was added dropwise in 30 min at -78 ^{o}C under N_2. After stirring the resulted mixture for another 10 min under -78 ^{o}C and 15 min in ice bath, diethylaluminium chloride in

hexane (50 mL, 50 mmol) was added dropwise and stirred for 30 min at rt. Then the flask was cooled in ice bath, 5.2 mL (50 mmol) of methyl glycidate (**3**) in 5 mL of toluene was added dropwise and stirred for another 24 h. After quenching with saturated NH_4Cl solution, the product was extracted with ether (4x75 mL), dried over Na_2SO_4 and concentrated to give 4.5 g product (**4**), 90%. This product was used without further purification. ^{1}H NMR (500 MHz, $CDCl_3$) δ 4.3 (q, 1H, *J* = 5 Hz), 3.8 (s, 3H), 2.97 (d, 1H, *J* = 2 Hz), 2.7 (t, 2H, *J* = 5 Hz), 2.0 (s, 1H), 0.15(s, 9H); ^{13}C NMR (125 MHz, $CDCl_3$) δ 174.4, 100.5, 88.3, 67.0, 52.7, 26.4, 0.16; IR 3474, 2959, 2179, 1743, 1441, 1250 cm^{-1}.

Synthesis of propargyl glycolic acid (1) via organoalanate. A 250-mL flask was charged with 3 g of ester (**4**), 25 g of anhydrous K_2CO_3 and 150 mL of MeOH and stirred for 24 h at rt. Then 100 mL of water was added and the acid (**1**) was extracted with ether (3x40 mL), and the solvent was removed under vacuum to give light yellow oily product (**1**) (0.8 g, 55%). ^{1}H NMR (500 MHz, $CDCl_3$) δ 4.35 (t, 1H, *J* = *4.5* Hz), 2.69-2.82 (m, 2H), 2.08 (t, 1H, *J* = 2.5 Hz); ^{13}C NMR (125 MHz, $CDCl_3$) δ 177.1, 77.5, 72.1, 68.4, 24.5.

Synthesis of propargyl tosylate. A 1L round bottom flask was charged with 11.2 mL (0.200 mol) of propargyl alcohol, 50 g (0.26 mol) of tosyl chloride and 200 mL of ether. After cooled in a -5 ^{o}C ice-salt bath, NaOH (40 g, 1.0 mol) was added to the above stirred solution in 6 portions at -5 ^{o}C and stirred for another 4 h at rt. After the suspension was poured to cold water and extracted with ether (2x50 mL), the ether layer was dried over Na_2SO_4 and concentrated under vacuum to give pure propargyl

tosylate 37.0 g, 84%. The product was purified under vacuum distillation before use (100-105 ^{o}C/45 mtorr). ^{1}H NMR (500 MHz, $CDCl_3$) δ 7.77 (d, *J* = 8 Hz, 2H), 7.32 (d, *J* = 8.5Hz, 2H), 4.65 (d, *J* = 2.5Hz, 2H), 2. 48 (t, *J* = 2.5Hz, 1H), 2.47 (s, 3H).

Synthesis of diethyl α-propargyl-α-acetamidomalonate (6) from malonate and popargyl tosylate. To a solution of 105 g (0.480 mol) of diethyl acetamidomalonate (**5**) in 1.41 L of dioxane was added 61 g (0.54 mol) of potassium *t*-butoxide in 650 mL of dioxane dropwise via cannula over 2 h at rt. Then the suspension was warmed to 50 ^{o}C for 2 h followed by adding 83 mL (0.49 mol) of propargyl tosylate in 170 mL of dioxane dropwise at 50 ^{o}C over 1h. After the mixture was refluxed for 6 h, it was cooled and filtered to remove the solid. The filtrate was dried over Na_2SO_4, concentrates and dried under vacuum overnight to give solid diethyl α-propargyl-α-acetamidomalonate (**6**), 124 g, 100%. m.p. 85-88 ^{o}C. ^{1}H NMR (500 MHz, $CDCl_3$) δ 6.91 (s, 1H), 4.24 (dd, *J* = 3, 7.5 Hz, 4H), 3.26 (d, *J* = 2.5 Hz, 2H), 2.04 (s, 3H), 1.94 (t, *J* = 2.5 Hz, 1H), 1.24 (t, *J* = 7.5 Hz, 6H); ^{13}C NMR (125 MHz, $CDCl_3$) δ 169.7, 166.9, 78.6, 71.8, 65.6, 63.2, 24.1, 23.2, 14.3.

Synthesis of propargyl glycolic acid (1) from malonate and popargyl tosylate. A 3-L round bottom flask was charged with 110 g (0.430 mol) of **6**, 1.2 L of H_2SO_4 (2M) and heated to reflux for 36 h until full conversion to 2-aminopent-4-ynoic acid (**7**) which was used directly without further purification. Then 5 equiv. of $NaNO_2$ in water (40%) was added dropwise to the solution of amino acid (**7**) at 0 ^{o}C followed by addition of another 3 equiv. of $NaNO_2$ in water (40%). After stirring for 40 h at rt, urea in diluted HCl

was added dropwise until the mixture didn't make KI-Starch test paper blue or purple. Then the resulted solution was extracted with ether continuously for 30 h. The ether layer was treated with $Na_2S_2O_5$ and stirred for 12 h, then filtered to remove the $Na_2S_2O_5$. The ether layer was concentrated and dried under vacuum to give 22.8 g of crude propargyl glycolic acid (48%). Later, the product was purified by sublimation to give 19 g of acid (**1**) (41%). ^{1}H NMR (500 MHz, $CDCl_3$) δ 4.35 (t, 1H, *J*= 4.5 Hz), 2.68 (m, 2H), 2.08 (t, 1H, *J* = 2.5 Hz); ^{13}C NMR (125 MHz, $CDCl_3$) δ 177.5, 77.7, 71.9, 68.5, 24.4.

Synthesis of propargyloxyacetaldehyde diethyl acaetal (9). Propargyl alcohol (134 mL, 2.25 mol) in 200 mL of THF was added to NaH (97 g, 60%, 2.4 mol) in 1.1 L of THF dropwise over 1h at 0 ^{o}C and then stirred at rt for another 1h. **8** (234 mL, 1.50 mol) in 100 mL of THF was added to the mixture prepared above and the resulted suspension was refluxed for 4 days to achieve 96% conversion. Then the suspension was filter and the filtrate was concentrated and dissolved in 500 mL of dichloromethane which was washed with aqueous NaCl solution (1x200 mL). The dichloromethane layer was dried over sodium sulfate, concentrated and dried under vacuum for 24 h to give pale red liquid, **9** (237 g, 92%). ^{1}H NMR (500 MHz, $CDCl_3$) δ 4.65 (t, 1H, *J*= 5 Hz), 4.21 (d, 2H, *J* = 2 Hz), 3.70 (m, 2H), 3.58 (m, 4H), 2.43 (t, 1H, *J* = 2 Hz) 1.22 (t, 6H, *J* = 10 Hz).

Synthesis of propargyloxy lactic acid (12). Acetal (**9**, 222 g, 1.29 mol) in 180 mL of dichloromethane was added to a mixture of TFA (230 mL), water (230 mL) and dichloromethane (700 mL) dropwise and stirred for 3 days until full conversion. Then

dichloromethane was removed and 450 mL of acetic acid was added. After cooled in ice bath, KCN (256 g, 3.90 mol) in 420 mL of water was added dropwise and stirring continued for 18 h until no aldehyde signal in ^{1}H NMR. The resulted cyanohydrin (**11**) was extracted continuously with ether to provide a mixture of **11** and acetic acid (644 mL, 91% yield from ^{1}H NMR). The resulted solution was cooled in ice bath followed by the addition of concentrated H_2SO_4 and methanol (Final concentration of H_2SO_4 was 6 M). After heating for 24 h at 70 ^{o}C, the resulted dark red solution was continuously extracted with ether to give dark liquid after removing all acetic acid. Then the acid mixture was hydrolyzed by addition of 2M NaOH solution. Extraction with dichloromethane removes all impurities, such as mineral oil. After acidifying with 4 M H_2SO_4, the final acid (**12**) was obtained via continuous extraction as light yellow solid, 144 g, 66% (4 steps). m.p. 58-61 ^{o}C. ^{1}H NMR (500 MHz, $CDCl_3$) δ 4.44 (t, 1H, *J*= 4 Hz), 4.26 (d, 2H, *J*= 2 Hz), 3.92 (m, 2H), 2.50 (t, 1H, *J* = 2 Hz); ^{13}C NMR (125 MHz, $CDCl_3$) δ 176.14, 78.64, 76.75, 70.59, 70.17, 58.87; IR 3286, 2933, 2122, 1735, 1358, 1203, 1129, 1104, 1044; HRMS(m/z) calcd for $C_6H_7O_4$ 143.0343 $[M-H]^-$, found 143.0344.

General Procedure of Synthesis of oligo(ethylene glycol) (n=1,2,3,4) monotrityl ether (14). A 500 mL three-neck round-bottom flask was charged with oligo(ethylene glycol) (n=1,2,3,4) (3 mol) and pyridine (30 mL) and heated to 55 °C, then powdered trityl chloride (42 g, 0.15 mol) was added to the reaction mixture under vigorous stirring. After being stirred at 55 °C for 18 h, the suspension was poured into water and extracted with toluene (5x100 mL). The combined toluene layer was washed with 0.3 M

HCl (2x600 mL), aq. NaOH (1x600 mL) and water (5x600 mL), dried over sodium sulfate, concentrated to give white solid or viscous liquid.

Ethylene glycol monotrityl ether (n=1): white solid (5% dityrityl ether), 42 g, 91%, m.p. 95-98 ^{o}C. ^{1}H NMR (300 MHz, $CDCl_3$) δ 7.50 (m, 6H), 7.30 (m, 9H), 3.80 (t, 2H, *J* = 6 Hz), 3.32 (t, 2H, *J* = 6 Hz), 2.03 (s, br. 1H).

Diethylene glycol monotrityl ether (n=2): white solid (8% dityrityl ether), 48 g, 92%, m.p. 108-110 ^{o}C. ^{1}H NMR (500 MHz, $CDCl_3$) δ 7.50 (m, 6H), 7.29 (m, 9H), 3.62-3.82 (m, 6H), 3.30 (t, 2H, *J* = 6 Hz), 2.06 (s, br. 1H).

Triethylene glycol monotrityl ether (n=3): viscous liquid (4% dityrityl ether), 57 g, 98%. ^{1}H NMR (300 MHz, $CDCl_3$) δ 7.51 (m, 6H), 7.32 (m, 9H), 3.64-3.81 (m, 10H), 3.31 (t, 2H, *J* = 6 Hz).

Tetraethylene glycol monotrityl ether (n=4): viscous liquid (9% dityrityl ether), 62 g, 95%. ^{1}H NMR (300 MHz, $CDCl_3$) δ 7.50 (m, 6H), 7.30 (m, 9H), 3.60-3.80 (m, 14H), 3.29 (t, 2H, *J* = 6 Hz), 2.50 (s, br. 1H).

General Procedure of Synthesis of 15 and 17. 15 and **17** were synthesized according to the procedure as described for **9**.

17 (n=1): pale liquid, 96 g, 91%. ^{1}H NMR (600 MHz, $CDCl_3$) δ 7.31 (m, 5H), 4.62 (t, 1H, *J* = 6 Hz), 4.54 (s, 2H), 3.50-3.70 (m, 10H), 1.19 (t, 6H, *J* = 6 Hz), 2.50 (s, br. 1H).

15 (n=2): pale red liquid, 208 g, 100%. ^{1}H NMR (600 MHz, $CDCl_3$) δ 7.50 (m, 6H), 7.25-7.36 (m, 9H), 4.67 (t, 1H, *J* = 5 Hz), 3.55-3.80 (m, 12H), 3.27 (t, 2H, *J* = 5 Hz), 1.23 (t, 6H, *J* = 5 Hz).

17 (n=3): dark red liquid, 229 g, 91%. ^{1}H NMR (500 MHz, $CDCl_3$) δ 7.50 (m, 6H), 7.23-7.37 (m, 9H), 4.66 (t, 1H, *J* = Hz), 3.54-3.77 (m, 16H), 3.27 (t, 2H, *J* = 5 Hz), 1.24 (t, 6H, *J* = 7 Hz).

17 (n=1): light brown liquid, 276 g, 92%. ^{1}H NMR (600 MHz, $CDCl_3$) δ 7.52 (m, 6H), 7.22-7.36 (m, 9H), 4.68 (t, 1H, *J* = Hz), 3.52-3.78 (m, 20H), 3.30 (t, 2H, *J* = 5 Hz), 1.28 (t, 6H, *J* = 7 Hz).

General Procedure of Synthesis of 20. A high-pressure autoclave reactor with a glass insert was charged with tritylate **15** or **17**, 2% of catalyst (10% palladium on carbon) and 150 mL of ethanol. Hydrogenolysis was carried out with effective stirring at room temperature under 1400 psi of H_2 for 48 h. Upon completion of the reaction, the catalyst (which can be reused) and triphenylmethane were removed via filtration. The filtrate was concentrated and dried under vacuum carefully to give a mixture of **18**, triphenyl methane and ethanol (<10%) which was used without further purification. Then this mixture was tosylated by TsCl in THF/H_2O to give tosylate **19** quantitatively as light yellow liquid. Propargyl alcohol was then coupled with tosylate **19** under basic condition in THF to provide **20** with high yield (containing byproducts from impurities).

20 (n=1): light yellow liquid, 35 g, 95%. ^{1}H NMR (600 MHz, $CDCl_3$) δ 4.62 (t, 1H, *J* = 6 Hz), 4.18 (d, 2H, *J* = 2.5 Hz), 3.65-3.71 (m, 6H), 3.50-3.58 (m, 4H), 2.40 (t, 1H, *J* = 2.5 Hz), 1.19 (t, 6H, *J* = 6 Hz).

20 (n=2): pale liquid, 48 g, 92%. ^{1}H NMR (600 MHz, $CDCl_3$) δ 4.59 (t, 1H, *J* = 6 Hz), 4.16 (d, 2H, *J* = 2.5 Hz), 3.57-3.68 (m, 10H), 3.42-3.56 (m, 4H), 2.38 (t, 1H, *J* = 2.5 Hz),

1.17 (t, 6H, *J* = 6 Hz).

20 (n=3): pale red liquid, 62 g, 94%. ^{1}H NMR (600 MHz, $CDCl_3$) δ 4.62 (t, 1H, *J* = 6 Hz), 4.19 (d, 2H, *J* = 2.5 Hz), 3.60-3.73 (m, 14H), 3.48-3.58 (m, 4H), 2.41 (t, 1H, *J* = 2.5 Hz), 1.20 (t, 6H, *J* = 6 Hz).

20 (n=4): light brown liquid, 81 g, 90%. ^{1}H NMR (600 MHz, $CDCl_3$) δ 4.64 (t, 1H, *J* = 6 Hz), 4.20 (d, 2H, *J* = 2.5 Hz), 3.62-3.74 (m, 18H), 3.52-3.61 (m, 4H), 2.43 (t, 1H, *J* = 2.5 Hz), 1.22 (t, 6H, *J* = 6 Hz).

General Procedure of Synthesis of oligo(ethylene glycol) monopropargyl ether lactic acid (23, n=1,2,3,4). Following similar procedure as described in the synthesis of **11**, protected acetal **20** was hydrolyzed in a mixture of TFA, water and dichloro methane (1:1:4) followed by cyanation in acetic acid/water solution to give cyanohydrin **22** which was subjected to hydrolysis directly. To a solution of **22** in acetic acid and water (from hydrolysis and cyanation steps), was added a mixture concentrated sulfuric acid and methanol with final concentration of sulfuric acid adjusted to 6M in ice bath. After full conversion monitored by ^{1}H NMR, the resulted dark solution was diluted, extracted with dichloromethane, concentrated to remove acetic acid under vacuum. Then the acid mixture was hydrolyzed by 2M NaOH solution. Extraction with dichloromethane removes all impurities, such as mineral oil, propargyl ethyl ether and oligo(ethylene glycol) dipropargyl ether. After acidifying with 4 M HCl, the final acids (**23**, n=1,2) was obtained via continuous extraction and concentrated under vacuum as dark red liquids. The final acid (**23**, n=3,4) was further purified by washing their solution in dichloromethane with 1 M HCl three times to give pure products as dark red liquids.

23 (n=1): dark red liquid, 20 g, 53% (8 steps). ^{1}H NMR (600 MHz, $CDCl_3$) δ 5.05 (br. 1H), 4.38 (t, 1H, *J* = 5 Hz), 4.22 (d, 2H, *J* = 2.5 Hz), 3.82-3.92 (m, 2H), 3.70-3.76 (m, 4H), 2.48 (t, 1H, *J* = 2.5 Hz); ^{13}C NMR (125 MHz, $CDCl_3$) δ 174.5, 79.1, 75.0, 72.1, 70.8, 70.1, 68.9, 58.4; IR 3286, 2922, 2878, 2122, 1746, 1446, 1355, 1248, 1203, 1110, 1038; HRMS(m/z) calcd for $C_8H_{13}O_5$. 189.0763 $[M+H]^+$, found 189.0754.

23 (n=2): dark red liquid, 60 g, 56% (8 steps). ^{1}H NMR (600 MHz, $CDCl_3$) δ 5.55 (br. 1H), 4.37 (t, 1H, *J* = 5 Hz), 4.22 (d, 2H, *J* = 2.5 Hz), 3.80-3.92 (m, 2H), 3.64-3.76 (m, 8H), 2.47 (t, 1H, *J* = 2.5 Hz); ^{13}C NMR (125 MHz, $CDCl_3$) δ 174.1, 79.2, 74.9, 72.3, 71.0, 70.3, 70.2, 70.1, 70.0, 58.4; IR 3269, 2916, 2878, 2117, 1746, 1460, 1352, 1253, 1201, 1104, 1035; HRMS(m/z) calcd for $C_{10}H_{15}O_6$ 231.0869 $[M-H]^-$, found 231.0868.

23 (n=3): dark red liquid, 38.6 g, 49% (8 steps). ^{1}H NMR (600 MHz, $CDCl_3$) δ 4.34 (t, 1H, *J* = 5 Hz), 4.21 (d, 2H, *J* = 2.5 Hz), 3.78-3.89 (m, 2H), 3.59-3.74 (m, 12H), 2.45 (t, 1H, *J* = 2.5 Hz); ^{13}C NMR (125 MHz, $CDCl_3$) δ 174.26, 79.28, 74.73, 77.29, 70.93, 70.41, 70.38, 70.32, 70.15, 70.11, 68.90, 58.22; IR 3264, 2911, 2878, 2117, 1746, 1457, 1358, 1250, 1203, 1104; HRMS(m/z) calcd for $C_{12}H_{19}O_7$ 275.1131 $[M-1]^-$, found 275.1129.

23 (n=4): dark red liquid, 48 g, 46% (8 steps). ^{1}H NMR (600 MHz, $CDCl_3$) δ 4.35 (t, 1H, *J* = 5 Hz), 4.23 (d, 2H, *J* = 2.5 Hz), 3.81-3.93 (m, 2H), 3.60-3.79 (m, 16H), 2.46 (t, 1H, *J* = 2.5 Hz); ^{13}C NMR (125 MHz, $CDCl_3$) δ 173.47, 79.42, 74.66, 72.25, 70.92, 70.56, 70.51, 70.48, 70.45, 70.23, 70.22, 70.06, 68.91, 58.35; IR 3258, 2916, 2878,

2122, 1749, 1457, 1355, 1297, 1250, 1107, 947; HRMS(m/z) calcd for $C_{14}H_{23}O_8$ 319.1393 $[M-H]^-$, found 319.1390.

Synthesis of tetraethylene glycol monobenzyl ether (29). Alcohol **24** (187 g, 1.50 mol) was mixed with dihydropyran (1.3 equiv., 166 g, 2.00 mol) at room teperature and stirred for 10 mins at rt. Then 20 drops of concentrated HCl was added and stirred for another 14 h. Upon completion, 15 g of potassium carbonate and 25 g of sodium sulfate were added to remove HCl and water followed by filtration and drying under vacuum at 55 ^oC to give 310 g of colorless liquid (**25**), 98%. ^1H NMR (500 MHz, $CDCl_3$) δ 4.63 (t, 1H, *J* = 5 Hz), 3.82-3.90 (m, 2H), 3.72-3.80 (m, 2H), 3.69 (m, 2H), 3.57-3.65 (m, 3H), 3.49 (m, 1H), 1.76-1.87 (m, 1H), 1.66-1.75 (m, 1H), 1.45-1.62 (m, 4H). Then **25** was put into the flask containing NaI (0.1 equiv.), sodium acetate (738 g, 6 equiv.) and 2.5 L of DMF at 110 ^oC for 12 h while stirring. After removing the solid, the filtrate was concentrated, dissolved in 1.4 L of ethyl acetate and washed with water (5x 400 mL). After drying, concentrating, the dark red liquid was directly hydrolyzed under basic condition (5 M aq. NaOH solution) to give oily product, 175 g. Then this oily product was mixed with TsCl (262 g, 1.38 mol) in THF/water mixture followed by the addition of 362 g of KOH in water. After stirring overnight, the tosylate (**26**) was extracted with dichloromethane, dried over sodium sulfate and concentrated under vacuum to give light brown liquid, 309 g, 60% (3 steps). ^1H NMR (500 MHz, $CDCl_3$) δ 7.78 (d, 2H, *J* = 5 Hz), 7.32 (d, 2H, *J* = 5 Hz), 4.57 (t, 1H, *J* = 5 Hz), 4.15 (t, 1H, *J* = 5 Hz), 3.75-3.88 (m, 2H), 3.66-3.70 (m, 2H), 3.58 (m, 2H), 3.41-3.54 (m, 2H), 2.43 (s, 3H), 1.76-1.88 (m, 1H), 1.66-1.75 (m, 1H), 1.45-1.60 (m, 4H);); ^{13}C NMR (125 MHz, $CDCl_3$) δ 144.59, 132.96,

129.64, 127.77, 98.80, 77.25, 76.99, 76.74, 70.52, 69.13, 68.49, 66.43, 62.07, 30.40, 25.25, 21.43, 19.32.

Then **27** (195 g, 0.997 mol) in THF (320 mL) was added dropwise to ice-colded THF (1.8 L) containing NaH (1.05 equiv., 25.1 g, 60%) and NaI (2.5 g) and stirred for another 3 h. Then **26** (1.02 equiv., 350 g, 1.012 mol) in THF (1.2 L) was added over 4 h and stirred overnight. After refluxing for 24 h, the solid was filtered and concentrated. Then it was dissolved in hexane and washed with water followed by decolorization by charcoal to give slight reddish liquid, 396 g, which was directly subjected to be dried under high vacuum at 160 ^{o}C to provide pure tetraethylene glycol monobenzyl ether (**29**). ^{1}H NMR (500 MHz, $CDCl_3$) δ 7.36 (m, 5H), 4.59 (s, 2H), 3.62-3.75 (m, 16H), 2.57 (br., 1H); ^{13}C NMR (125 MHz, $CDCl_3$) δ 138.23, 128.29, 127.69, 127.53, 73.20, 72.45, 70.57-70.62 (br.), 70.35, 69.42, 61.72.

Synthesis of monotetrahydropyran-protected tetraethylene glycol monotosylate (35). To a flask charged with tetraethylene glycol (**30**, 970 g, 5 mol), dichloromethane (3 L) and TsOH (6 g) was added dihydropyran (109 mL, 1.15 mol) dropwise at rt. After stiring for 24 h, the reaction mixture was washed with aqueous NaCl solution (6x1 L) and dried over sodium sulfate to give a mixture of **31** and **32** after drying under vacuum, 276 g (8:1). Then this mixture (190 g) was reacted with TsCl (196 g, 1.03 mol) in THF/water mixture while adding saturated KOH solution. The product was extracted with dichloromethane and concentrated to give 258 g of light yellow viscous liquid (**32** and **33**).Then this mixture was dissolved in 450 mL of methanol containing 1 g of TsOH and stirred for 36 h. After removing methanol, it was dissolved in

dichloromethane (1 L) and washed with aqueous NaCl/HCl solution (5x300 mL). Then the organic layer was concentrated and dried under vacuum to give yellow liquid (**34**), 198 g. Then pure **34** (198 g, 0.6 mol) was protected with dihydropyran (71 mL, 0.78 mol) in dry THF (570 mL) in the presence of TsOH. After removing THF and excess of dihydropyran, it was washed with 10% NaCl solution (3x300 mL), dried over sodium sulfate and concentrated under vacuum to give a dark red liquid (**35**), 244 g, 74% yield (4 steps). ^{1}H NMR (500 MHz, $CDCl_3$) δ 7.82 (d, 2H, *J* = 10 Hz), 7.36 (d, 2H, *J* = 10 Hz), 4.65 (t, 1H, *J* = 5 Hz), 4.18 (t, 1H, *J* = 5 Hz), 3.85-3.92 (m, 2H), 3.58-3.75 (m, 13H), 3.52 (m, 1H), 2.47 (s, 3H), 1.80-1.90 (m, 1H), 1.68-1.77 (m, 1H), 1.48-1.66 (m, 4H); ^{13}C NMR (125 MHz, $CDCl_3$) δ 144.71, 133.07, 129.77, 127.95, 98.94, 70.76, 70.64, 70.58, 70.54, 69.20, 68.67, 66.63, 62.22, 30.57, 25.42, 21.60, 19.49.

Synthesis of octa(ethylene glycol) monopropargyl ether lactic acid (40). Benzyl ether (**29**, 71 g, 0.25 mol) in THF (200 mL) was added to NaH (1.2 equiv., 12.5 g, 60%), NaI (2 g) in THF (1.3 L) dropwise and stirred for 2 h. Then **35** (1.1 equiv., 121.7 g, 0.275 mol) in THF (300 mL) was added dropwise over 1 h at 0 ^{o}C. After refluxing for 12 h, the solid was removed via filtration and the filtrate was and dissolved in dichloromethane. After washed with aqueous NaCl/NaOH solution (1x300 mL) and dried over sodium sulfate, the organic layer was concentrated and dried and vacuum to give reddish viscous liquid, 147 g. The obtained liquid was mixed with TsOH (1 g) and 500 mL of anhydrous methanol and stirred for 36h. The methanol was removed and the oily product was dissolved in dichloromethane which was washed with saturated NaCl/NaOH solution (4x250 mL). After removing the dichloromethane, the product was

heated to 55 ^{o}C under high vacuum for 12h to provide 121 g of pure octa(ethylene glycol) monobenzyl ether (**36**) as pale viscous liquid quantitatively. ^{1}H NMR (500 MHz, $CDCl_3$) δ 7.36 (m, 5H), 4.59 (s, 2H), 3.60-3.77 (m, 32H), 2.60 (t, 1H, *J* =5 Hz); ^{13}C NMR (125 MHz, $CDCl_3$) δ 138.25, 128.28, 127.66, 127.51, 73.18, 72.45, 70.45-70.65 (br.), 70.32, 69.41, 61.69.

Then bifunctional **38** was synthesized from the coupling of **36** (121 g, 0.26 mol) and **8** following similar procedure to synthesize **20** from **14** to provide 101 g of **38** as amber liquid, 90% (4 steps). ^{1}H NMR (600 MHz, $CDCl_3$) δ 4.59 (t, 1H, *J* = 6 Hz), 4.17 (d, 2H, *J* = 2.5 Hz), 3.47-3.72 (m, 38H), 2.40 (t, 1H, *J* = 2.5 Hz), ^{13}C NMR (125 MHz, $CDCl_3$) δ 101.16, 79.64, 74.47, 71.88, 70.45-70.65 (br.), 70.38, 69.08, 62.25, 58.36, 15.32.

Octa(ethylene glycol) monopropargyl ether lactic acid (**40**) was synthesized following the procedure as described in the synthesis of **23** from **20** as light yellow viscous liquid, 58.0 g, 65% (3 steps). ^{1}H NMR (500 MHz, $CDCl_3$) δ 4.34 (t, 1H, *J* = 5 Hz), 4.21 (d, 2H, *J* = 2.5 Hz), 3.79-3.91 (m, 2H), 3.60-3.77 (m, 32H), 2.45 (t, 1H, *J* = 2.5 Hz); ^{13}C NMR (125 MHz, $CDCl_3$) δ 173.61, 79.66, 74.55, 72.42, 71.07, 70.3-70.6 (br.), 70.18, 69.10, 58.38; IR 3241, 2878, 2117, 1746, 1457, 1352, 1297, 1250, 1107, 950; HRMS(m/z) calcd for $C_{22}H_{39}O_{12}$ 495.2442 $[M-H]^{-}$, found 495.2437.

Synthesis of poly(ethylene glycol) monopropargyl ether lactic acid (50, n≈23). Poly(ethylene glycol) (**41**, 250 g, 0.250 mol) was stirred with dihydropyran (13 mL, 0.125 mol) for 4 h in 3 L of dichloromethane containing 0.5 g of TsOH. Then the mixture was

washed with water (60x500 mL), dried over sodium sulfate, concentrated to give white solid (mixture of **42** and **43**), 106 g, 85%. ^{1}H NMR (500 MHz, $CDCl_3$) δ 7.82 (d, 2H, *J* = 10 Hz), 7.36 (d, 2H, *J* = 10 Hz), 3.40-3.90 (m, 93H), 2.61 (t, 0.6H), 1.75-1.87 (m, 1H), 1.65-1.75 (m, 1H), 1.45-1.62 (m, 4H); The this mixture (106 g, 0.110 mol) was mixed with NaH (6.06 g. 60%, 0.160 mol) in THF (410 mL) and stirred for 40 mins before adding **8** (33.6 g, 0.260 mol). After refluxing for 30 h, the solid was removed via filtration and the filtrate was concentrated to dissolve in dichloromethane. The organic layer was washed with water, dried over sodium sulfate, concentrated and dried under high vacuum for 48 h to provide a mixture of **43** and **44**, 112 g, 92%. Then the resulted mixture (112 g, 0.110 mol) was dissolved in a mixture of TsOH (1 g), ethanol (450 mL) and dichloromethane (70 mL). After stirring for 24 h, 3 g of K_2CO_3 was added before the solvents were removed. Then it was dissolved in dichloromethane and washed with aqueous NaCl/NaOH solution (1x450 mL). The organic layer was dried over sodium sulfate, concentrated and dried under high vacuum at 50 ^{o}C for 6 h to give 105 g of white sold. This solid was then reacted with TsCl (72 g, 0.40 mol) in THF/water in the presence of KOH. After workup following similar procedure used before, 120 g of a mixture of **44** and **45** were obtained. Then this solid product mixture in 570 mL of THF was added to the suspension prepared from propargyl alcohol (17 g) and NaH (10 g) in 400 mL of THF. After refluxing for 15 h, 80 ml of water was added and THF was removed followed by the addition of 400 mL of $CHCl_3$ and 500 mL of NaCl solution (10%). Then the product was extracted with $CHCl_3$ to give 112 g of a mixture of **46** and **47** after drying under high vacuum at 52 ^{o}C, 86%. ^{1}H NMR (500 MHz, $CDCl_3$) δ 4.54 (t,

1H, *J* = 5 Hz), 4.12 (d, 2H, *J* = 2.5 Hz), 3.45-3.68 (m, 95H), 2.38 (t, 1H, *J* = 2.5 Hz), 1.13 (t, 6H, *J* = 2.5 Hz). Then poly(ethylene glycol) monopropargyl ether lactic acid (**50**, n≈23) was synthesized as white solid (86 g, 74%, 3 steps) using similar procedure to synthesize **23** from **20** as discussed above. ^{1}H NMR (500 MHz, $CDCl_3$) δ 4.34 (t, 1H, *J* = 5 Hz), 4.21 (d, 2H, *J* = 2.5 Hz), 3.79-3.91 (m, 2H), 3.60-3.77 (m, 32H), 2.45 (t, 1H, *J* = 2.5 Hz); ^{13}C NMR (125 MHz, $CDCl_3$) δ 173.41, 79.67, 74.50, 72.42, 71.06, 70.30-70.65 (br.), 70.17, 69.11, 58.39; IR 3252, 2872, 2111, 1749, 1463, 1355, 1300, 1248, 1112, 955.

Synthesis of allyloxy lactic aicd (54). The synthesis of **54** used exactly same procedure as described in the synthesis of propargyloxy lactic acid (**12**).

Allyloxyacetadehyde diethyl acetal (**51**): vacuum distillation, 46 ^{o}C/2 Torr., colorless liquid, 198 g, 76%. ^{1}H NMR (600 MHz, $CDCl_3$) δ 5.84 (m, 1H), 5.22 (m, 1H), 5.12 (m, 1H), 4.58 (t, 1H, *J* = 6 Hz), 3.98 (m, 2H), 3.65 (m, 2H), 3.52 (m, 2H), 3.42 (d, 2H, *J* = 6 Hz), 1.15 (t, 6H, *J* = 6 Hz); ^{13}C NMR (150 MHz, $CDCl_3$) δ 134.52, 117.01, 101.08, 72.28, 70.55, 62.12, 15.22.

Allyloxy cyanohydrin (**53**): crude product was extracted from aqueous solution, no further purification, 145 g, 100%. ^{1}H NMR (500 MHz, $CDCl_3$) δ 5.92 (m, 1H), 5.30 (m, 2H), 4.61 (t, 1H, *J* = 5 Hz), 4.14 (m, 2H), 3.73 (m, 2H), 3.52 (m, 2H); ^{13}C NMR (150 MHz, $CDCl_3$) δ 133.31, 118.49, 118.15, 72.65, 70.35, 60.73.

Allyloxy lactic aicd (**54**): light yellow liquid, 120 g, 55%. ^{1}H NMR (500 MHz, $CDCl_3$) δ 5.83-5.93 (m, 1H), 5.17-5.33 (m, 2H) 4.40 (t, 1H, *J* = 5 Hz), 4.08 (m, 2H), 3.74-3.85 (dq,

2H, *J* = 5 Hz, *J* = 10 Hz); ^{13}C NMR (125 MHz, $CDCl_3$) δ 175.97, 133.72, 118.06, 72.62, 70.80, 70.23; IR 3407, 3093, 2977, 2933, 2872, 2500-3500 (br.), 1744, 1424, 1352, 1206, 1123, 1041, 931; HRMS(m/z) calcd for $C_6H_9O_4$ 145.0511 $[M-H]^-$, found 145.0499.

Synthesis of azido lactic aicd (56). To a solution of methyl glycidate (**3**) (26 g, 0.26 mol) in a mixture of 224 mL of MeOH and 11.2 mL of water was added 55 g (0.84 mol) of NaN_3 and 24 g (0.37 mol) of NH_4NO_3. After refluxing overnight, methanol was removed and methy ester (**55**) was extracted with CH_2Cl_2. After removal of CH_2Cl_2, the crude product (**55**) was purified by vacuum distillation to give 19.2 g of colorless liquid, 51%. b.p. 47-50 ^oC/70 mTorr., ^{1}H NMR (500 MHz, $CDCl_3$) δ 4.36 (t, 1H, *J*= 3 Hz), 3.80 (s, 3H), 3.63-3.45 (dq, 2H, *J* = 3, 13 and 85 Hz), 3.24 (br. s, 1H); ^{13}C NMR (125 MHz, $CDCl_3$) δ 172.6, 70.4, 53.7,50.1; IR 3470, 2959, 2110, 1743, 1442, 1224; HRMS, cal. 168.0385 $[M+Na]^+$, found 168.0351.

The above methyl ester (**55**, 16 g, 0.11 mol) was hydrolyzed overnight in a mixture of 1 M NaOH solution (180 mL) and methanol (200 mL). After removal of methanol, the solution was acidified and the product was extracted continuously with ether to give 8.5 g of light yellow liquid after dried under vacuum, 59%. ^{1}H NMR (500 MHz, DMSO-d_6) δ 5.90 (br. s), 4.20 (q, 2H, *J*= 4 and 6 Hz), 3.80 (s, 3H), 3.40 (dq, 2H, *J* = 4, 13 and 35 Hz); ^{13}C NMR (125 MHz, $CDCl_3$) δ 173.7, 70.4, 54.2; IR 3360, 2514, 2075, 1732, 1443, 1271; HRMS, calcd for $C_3H_4N_3O_3$ 130.0253 $[M-1]^-$, found, 130.0208.

CHAPTER 3 SYNTHESIS OF CLICKABLE POLYLACTIDES AND THEIR SMART PROPERTIES

3.1 Introduction

Polylactides have been extensively studied for biomedical applications due to their biodegradability and biocompatibility. However, their application is limited by their hydrophobic nature and the lack of chemical functionality along the polymer backbone to support further modification. The monomer derivative approach typically involves complex and tedious synthetic procedures, requires careful control of conditions in post-polymerization modifications to avoid backbone degradation, and limits the versatility of pendant functional groups. So having a single procedure that allows the introduction of a family of pendant functional groups onto a polylactide polymer would be highly desirable.

Polymeric micelles have been extensively studied as drug delivery carriers because they can enhance drug stability and solubility, elongate *in vivo* circulation time, and target specific tissues.[137] "Smart" stimuli-responsive materials can be designed to mimic nature in solving biological problems, such as those associated with biological self-response and self-defense. The versatility and untapped potential of smart polymeric materials makes them one of the most exciting new tools at the interface of chemistry and biology. Conventional polymeric micelles disintegrate at concentrations below their critical micelle concentrations (CMCs), which results in premature release of the encapsulated cargo before exerting specific functions. One effective approach to solve this problem is to stabilize micellar structures by cross-linking.[138] Approaches to

cross-linking in the shell of micelles have been reported and the resulting micelles were more stable than uncross-linked micelles (UCMs) upon dilution.[139] However, cross-linking of micelles with hydrophilic shells may affect the surface mobility, and requires a highly diluted solution to avoid undesired intermicellar cross-linking. So core cross-linked micelles (CMs) have been developed as an effective alternative. Most of the existing UCMs are based on nondegradable polymeric cores such as polyacrylate or polyacrylamide. [140] Considering the requirement for biocompatibility and biodegradability in clinical applications, CMs composed entirely of polyesters would be ideal candidates as drug delivery vehicles. The choice of the cross-linkers is also important because they can render specific properties to CMs, such as stimuli responsive properties, and thus facilitate the release of encapsulated drugs.

Because of its high selectivity, reliability, and tolerance to a broad range of functional groups and reaction conditions, “click” chemistry, specifically the copper(I)-mediated 1,3-dipolar cycloaddition of azides and alkynes, is an excellent strategy for elaborating polymer architectures. “Click” chemistry has been used for the preparation of block copolymers, [141] dendrimers, [142] and for the introduction of pendant and terminal functional groups into various polymers including polyesters.[143]

Polylactides with clickable side chains would enable them to be efficiently modified with different functionalities through click chemistry under mild conditions and thus impart polylactides with novel solution behavior which would enhance their biomedical application. Thus, we prepared and polymerized propargyloxy-functionalized lactide monomers. The subsequent polymerization of lactide monomers (**58** and **59**) provided the homopolymer of lactide monomers, random copolymers with lactide as well as

block copolymer with poly(ethylene glycol) (mPEG) that have pendant propargyl groups available for the attachment of functionalities using click chemistry.

3.2 Results and Discussion

3.2.1 Monomer Synthesis

As shown in **Scheme 41**, hetero- and homo- monomers (**58** and **59**) of propargyloxylactic acid were synthesized for the purpose of making polylactide polymers. Hetero-monomer (**58**) was synthesized as a colorless viscous liquid or a waxy solid by cyclization of **57** under basic conditions which was prepared from **12** and bromoacetyl bromide in 39% yield after flash column chromatography. Homo-monomer (**59**) was prepared in 32% yield from **12** in refluxing toluene with azeotropic removal of water and then purified by column chromatography on silica to as a white solid. Notably, the purification on silica gel should be completed quickly to avoid decomposition of the monomer. The ^{1}H NMR spectra of **58** and **59** (shown in **Figure 6**) show significant chemical shift change for the methine protons (~5.2 ppm for d and i) of both monomers, and are the characteristic of methine protons in lactide rings. The stereochemistry of **59** as a *meso* (R, S) stereoisomer was also confirmed by an X-ray study (**Figure 7**). The latide **59** was only isolated as *trans* isomer which avoids any stereochemistry effect on the polymerization of monomer.

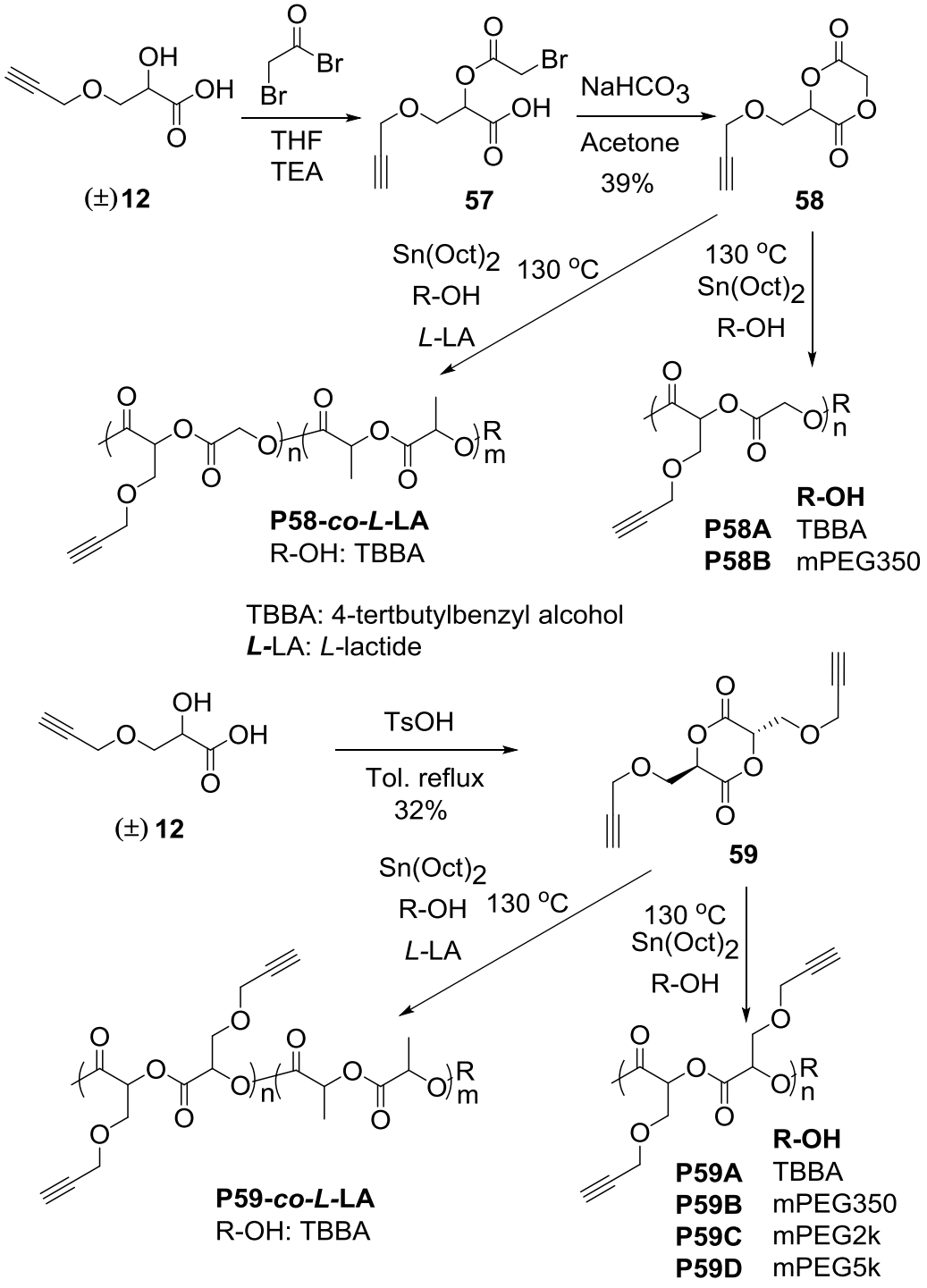

Scheme 41. Synthesis of propargyloxy lactides and their polymers

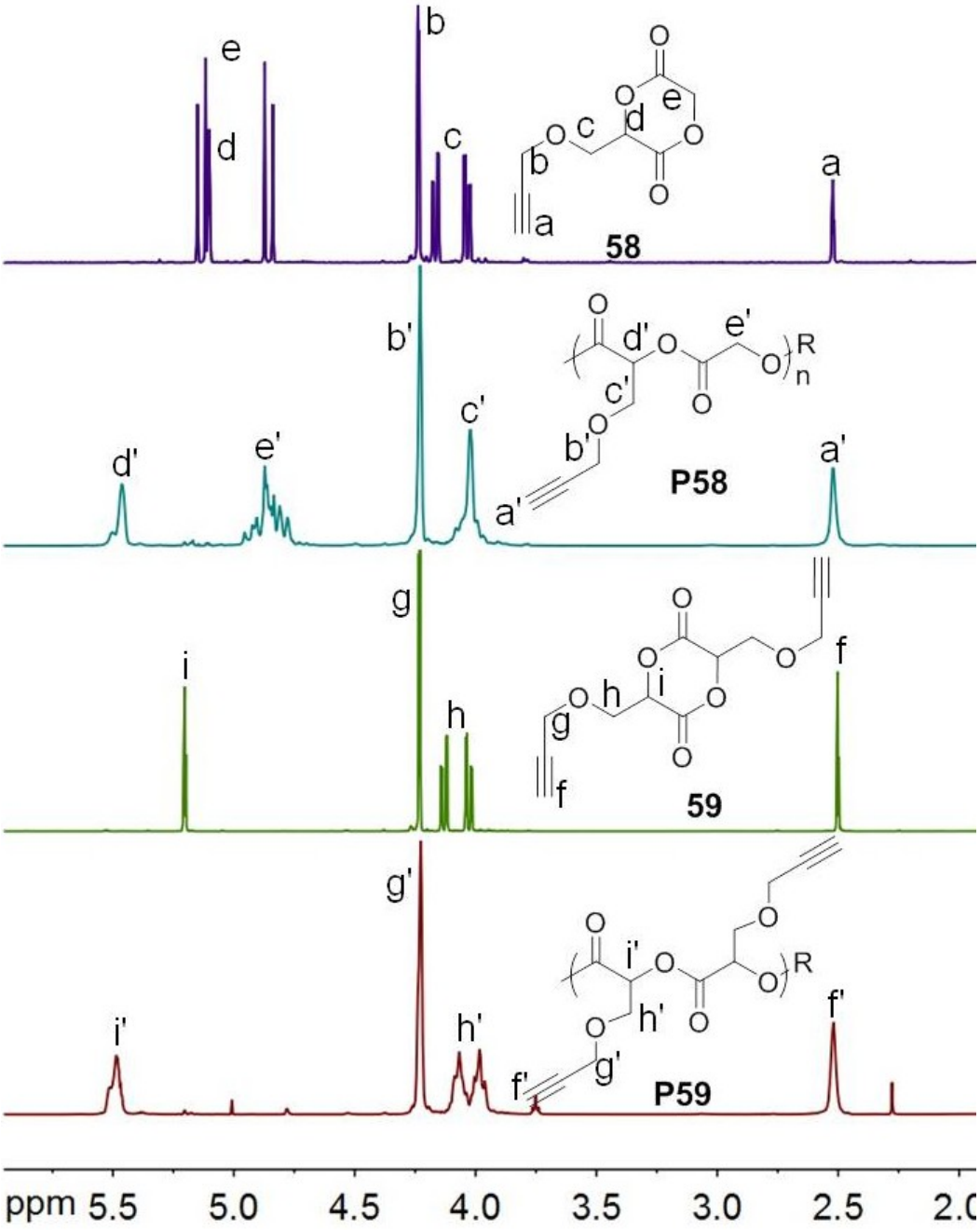

Figure 6. ^{1}H NMR spectra of **58**, **P58A**, **59** and **P59A**. Slovent: $CDCl_3$.

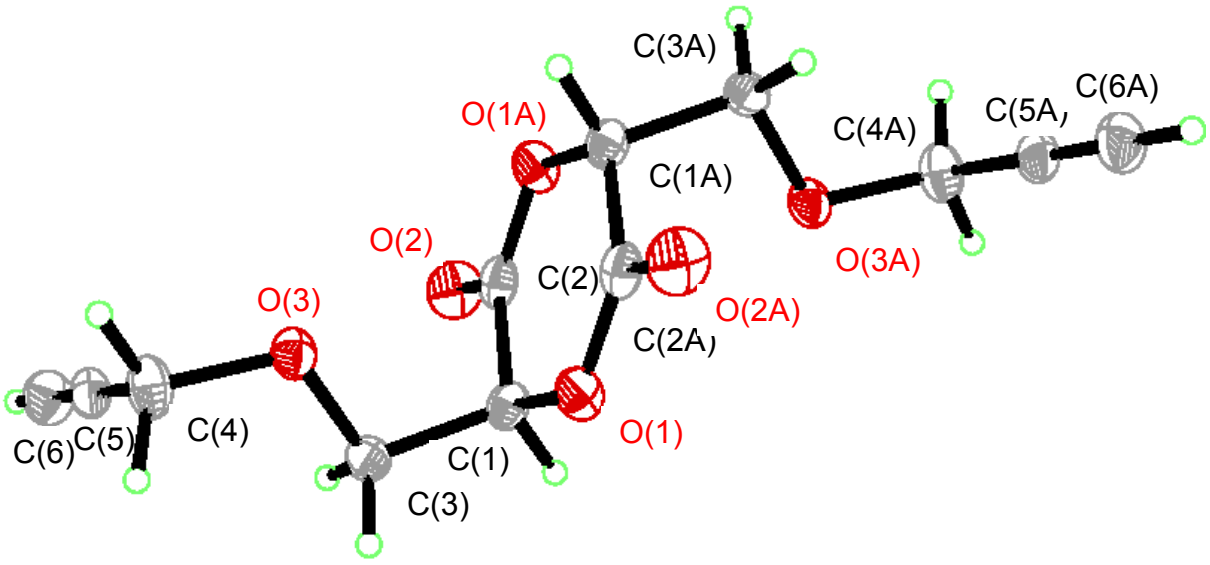

Figure 7. Molecular drawing of **59** with 50% thermal ellipsoids from X-ray crystallography. "For interpretation of the references to color in this and all other figures, the reader is referred to the electronic version of this thesis (or dissertation)."

3.2.2 Bulk Polymerization

3.2.2.1 Kinetics of Bulk Polymerization

Due to the low solubility of the monomers **58** or **59** in organic solvents, as well as the low solubility of the polymers in organic solvents, the solution polymerization of **58** or **59** in toluene or THF proceeded very slowly, which leads to poor molecular weight control. This is also true when copolymerization of **58** or **59** with *L*-lactide (*L*-LA) was attempted. So the bulk polymerization process without solvent was used to polymerize **58** and **59**.

Bulk polymerizations of **58** and **59** were performed at 130 °C and were catalyzed by $Sn(Oct)_2$ using 4-*tert*-butylbenzyl alcohol (TBBA) as the initiator in sealed polymerization bulbs, yielding polymers, **P58A** and **P59A** (**Scheme 41**). The catalyst-to-initiator ratio was 1:1 for all polymerizations, and the monomer-to-initiator ([M]/[I]) ratio

was varied from 25:1 to 200:1 to provide different molecular weight materials. The extent of conversion of the monomer to polymer was calculated by comparing the ^{1}H NMR integration of the methine protons in the monomer at 5.2 ppm with those in the polymer at 5.5 ppm (**Figure 6**). The ring-opening polymerizations of lactides are typically first-order in monomer[144] and can be expressed as

$$R_p = -d[M]/dt = k_p [M][cat] \quad \textbf{(1)}$$

where [M] and [cat] are the concentration of the monomer and the catalyst, respectively, and k_p is the rate constant for propagation. Assuming that the catalyst concentration is constant, integration of (1) provides equation (2)

$$-\ln([M]_t/[M]_0) = k_p[cat]_0 t \quad \textbf{(2)}$$

where the subscripts 0 and *t* refer to initial concentrations at time = *t*. Data from such a living polymerization should be linear when plotting-ln($[M]_t/[M]_0$ versus time *t* with a slope $k_p[cat]_0$. Lactide polymerizations run to high conversions often deviate from linearity due to the establishment of an equilibrium between the propagation and depropagation steps, leaving an equilibrium monomer concentration $[M]_e$.[145] To simplify evaluation of experimental data, equation (2) is revised to account for $[M]_e$ by subtracting $[M]_e$ from $[M]_0$, giving equation (3).

$$-\ln\{([M]_t - [M]_e)/([M]_0 - [M]_e)\}=k_p[cat]_0 t \quad \textbf{(3)}$$

The $[M]_e$ was determined from the limiting monomer conversion reached during the polymerization at 130 ^{o}C. As shown in **Figure 8**, 3% and 6% of **58** and **59** were

determined to be left in the system, respectively, and with these numbers equation (3) was used as $[M]_e$ to plot the kinetics of bulk polymerization for both **58** and **59**. As shown in **Figure 9**, a linear relationship between $-\ln\{([M]_t - [M]_e)/([M]_0 - [M]_e)\}$ and polymerization time *t* was observed which indicates that the bulk polymerization of propargyloxy substituted lactides exhibits a kinetic pattern similar to that of lactide, and that the ring-opening polymerization of **58** and **59** is controlled and facile. The slope of the linear fitting which is the apparent rate constant values ($k_p[cat]_0$) for **58** and **59** clearly indicates that monomer **58** undergoes polymerization much faster than **59** presumably due to the reduced steric hindrance present in **58**.

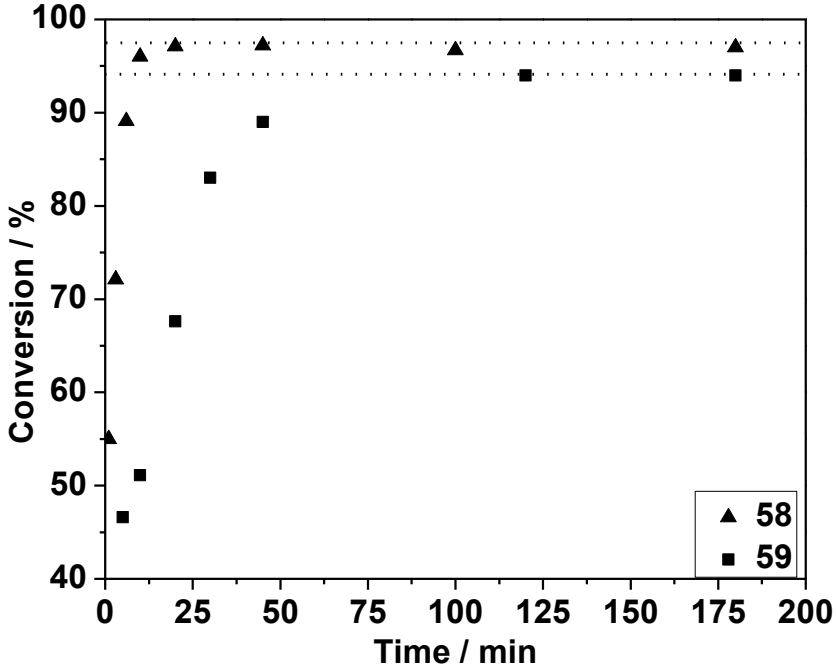

Figure 8. Percent conversion for the bulk polymerization of **58 and 59**. Conditions: 130 ^{o}C, [M]:[Sn(Oct)$_2$]:[TBBA] = 50:1:1.

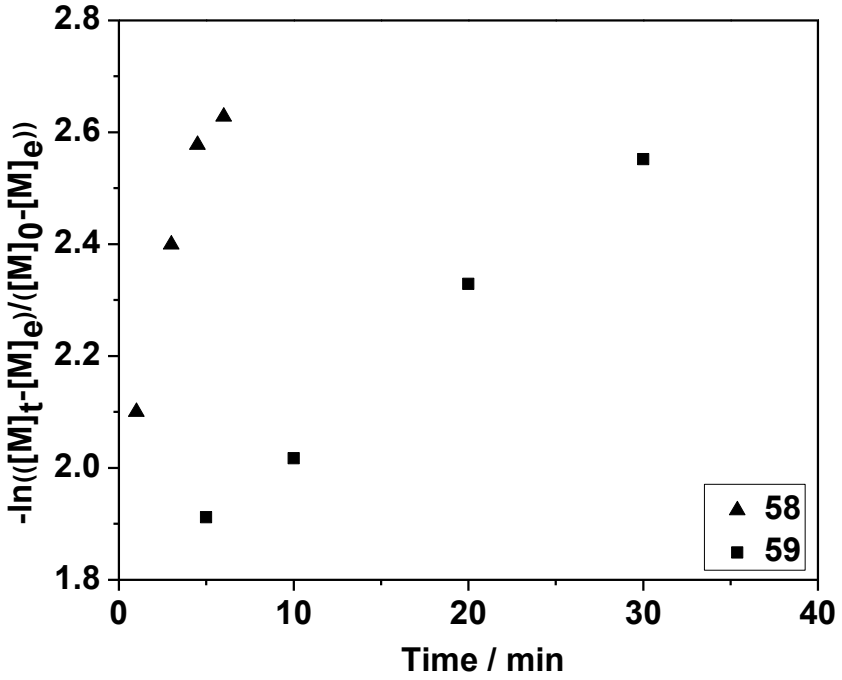

Figure 9. Bulk polymerization kinetics for **58 and 59**. Conditions: 130 ^{o}C, [M]:[$Sn(Oct)_2$]:[TBBA] = 50:1:1.

Figure 10 shows the evolution of the number-average molecular weight (M_n) and polydispersity index (PDI) from gel permeation chromatography (GPC) with time during the bulk polymerization. As the time increases and the percent conversion increases (**Figure 8**), M_n increases, reaches a maximum at high conversion (<90%) and then drops. The unexpected high M_n of the **P59A** at polymerization time t=180 mins is probably due to the cross-linking of the alkyne group at high temperature which will be discussed in next section. The PDI is in the range of 1.2-1.5 when conversions are below 90% and then rapidly increases when conversions get higher (**Figure 8** and **Figure 10**). This behavior has been reported to be typical characteristic of ring-opening polymerization of lactides.[58,61] M_n increases linearly with a narrow PDI while

conversion increases at low conversion due to the living nature of the ring-opening polymerization. However, intermolecular or intramolecular transesterification will compete with propagation at high conversion (>90% in our case) and results in an increase of PDI and a change in M_n.[145]

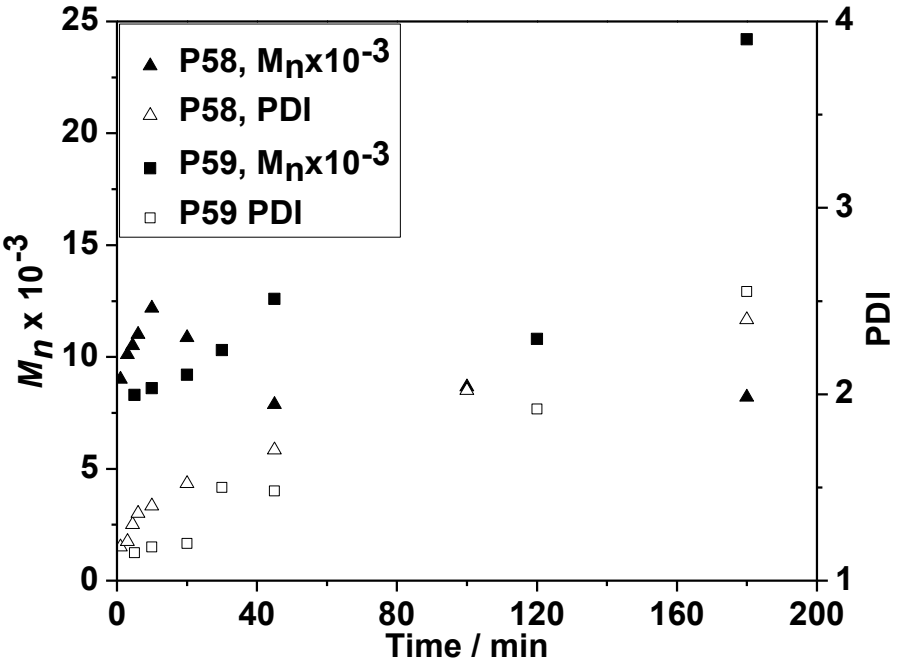

Figure 10. The evolution of molecular weight (M_n) from GPC (▲, **P58**; ■, **P59**) and PDI (△, **P58**; □, **P59**) with time for bulk polymerization of **58** and **59**. Conditions: 130 ^{o}C, [M]:[Sn(Oct)$_2$]:[TBBA] = 50:1:1.

The results of the bulk polymerization of **58** and **59** at different ratios of [M]/[I] were collected and are listed in **Table 4**. All results showed that X_n (number of repeating units) calculated from ^{1}H NMR spectra are close to their theoretical values after correcting for conversion by NMR at low [M]/[I] ratios; however, X_n calculated from the ^{1}H NMR at high [M]/[I] ratios shows lower values compared to the theoretical values

after correcting for conversion and this is probably due to the low integration accuracy of ^{1}H NMR at high molecular weight and with increased amounts of transesterification at longer polymerization times as evidenced by the slightly higher PDI. M_n from GPC is listed to show that the molecular weight increases with increasing [M]/[I] ratios; however, the data are not matching to the ratios of [M]/[I] due to the calculation accuracy of GPC software in our lab. This is consistent with GPC profiles which shift to shorter elution times with increasing [M]/[I] ratios as shown in **Figure 11** and **Figure 12**, since large polymers elute out of GPC faster by traveling less in size exclusion chromatography (SEC).[146] The PDI as determined from GPC is around 1.4-1.6 for all of the polymers and is not affected by the GPC calculation.

Table 4. Bulk Polymerizations of **58** and **59** at 130 ^oC[a]

entry	M	[M]/[I]	t/min	Conv.(%)[b]	X_n[c]	X_n[d]	M_n x 10^{-3} [e]	PDI[e]
1	**58**	30	8	86	26	25	6.9	1.40
2	**58**	50	15	89	44	45	10.8	1.42
3	**58**	100	30	88	88	75	18.2	1.51
4	**58**	200	30	86	172	126	27.9	1.59
5	**59**	25	30	90	23	22	9.9	1.48
6	**59**	50	40	87	44	48	10.1	1.46
7	**59**	100	60	80	80	65	11.4	1.55
8	**59**	200	100	85	170	135	17.2	1.60

[a] Using $Sn(Oct)_2$ as the catalyst and TBBA as initiator. [b] Measured by ^{1}H NMR. [c] Calculated from the [M]/[I] and corrected for conversion. [d] Calculated from ^{1}H NMR using end group analysis. [e] g/mol, measured by GPC in THF.

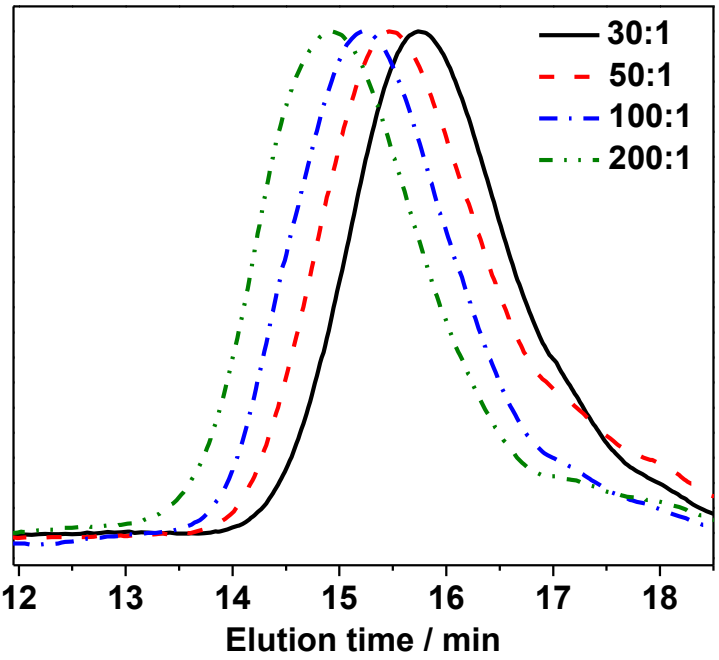

Figure 11. GPC curves of polymers from bulk polymerization of **58** with different [M]/[I] (130 ^{o}C).

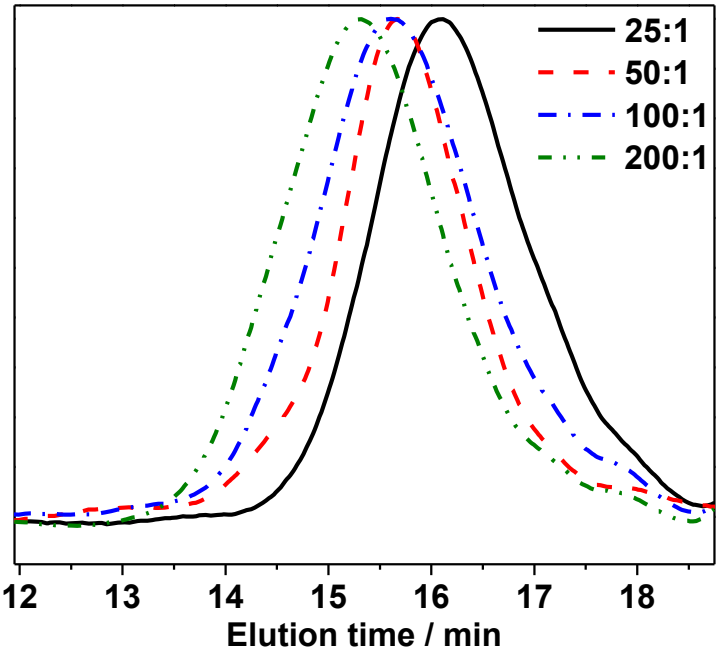

Figure 12. GPC curves of polymers from bulk polymerization of **59** with different [M]/[I] (130 ^{o}C).

3.2.2.2 Thermal Properties of Homopolymers

The thermal stability of the polymers **P58** and **P59** are shown in **Figure 13** and **Figure 14**. The onset decomposition temperature (5% weight loss) for **P58** starts at ~196 ^{o}C for [M]/[I] at a 30:1 feed ratio and gradually increases to ~230 ^{o}C when increasing [M]/[I] to 100:1 and 200:1. A similar trend was observed for **P59** but with higher temperature values. The onset decomposition temperature (5% weight loss) for **P59** starts at ~210 ^{o}C for [M]/[I] at a 25:1 feed ratio and gradually increases to ~255 ^{o}C upon increasing [M]/[I] to 100:1 and 200:1. This indicates that the thermal stability of **P59** is higher than **P58**. This behavior is more evidenced in the 100% decomposition temperature with 600 ^{o}C for **P58** and 750 ^{o}C for **P59**: a nearly 150 ^{o} C difference. This might be due to the pendant terminal alkyne groups which might act as a stabilizing agent if they undergo cross-linking upon heating. Indeed, alkyne groups are known to act as cross-linkers where this is used to make materials flame-retardant.[147,148,149]

The increased number of pendant propargyl groups on **P59** may result in increased cross-linking upon heating. The thermal decomposition of **P59** is delayed and shows a plateau from 335 – 620 ^{o}C with much higher polymer weight retention than **P58**, and this is followed by a second rapid decomposition (**P59**, **Figure 14**). Notably, the weight retention at the plateau after cross-linking of **P59** is doubled compared to that of **P58**, This indicates that the propargyl group content accounts for the doubled weight retention at the plateau.

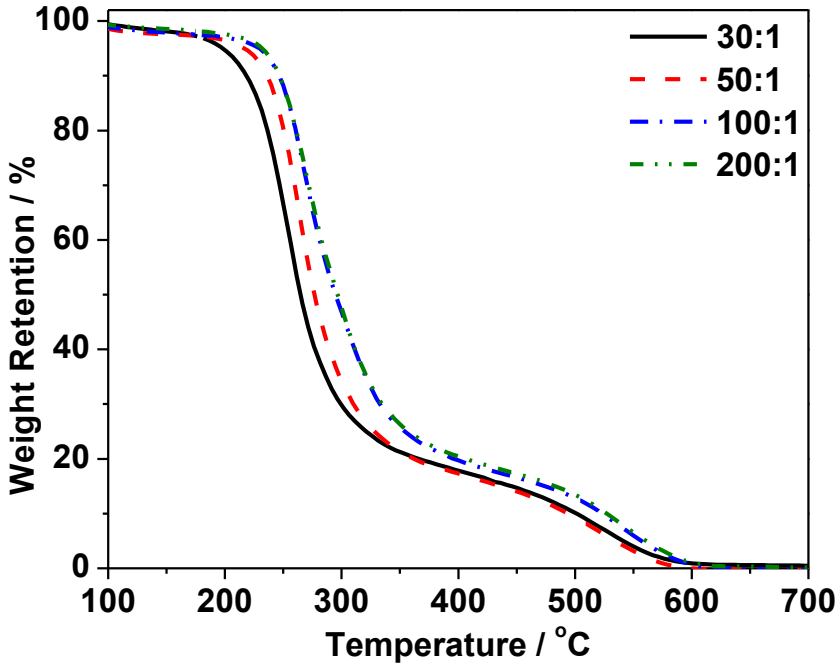

Figure 13. TGA curves of polymers from the bulk polymerization of **58** with different [M]/[I] (130 °C).

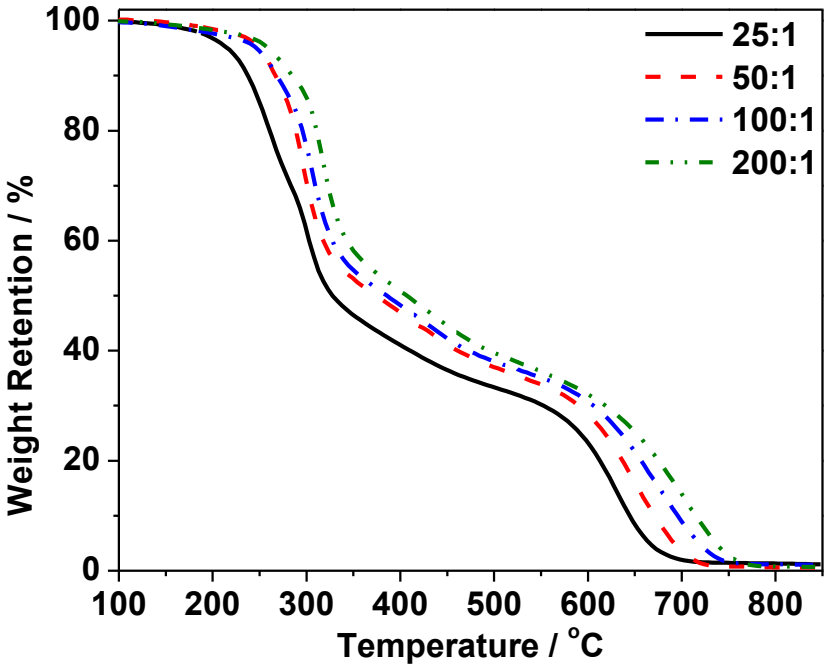

Figure 14. TGA curves of polymers from the bulk polymerization of **59** with different [M]/[I] (130 °C).

DSC traces of polymers **P58** and **P59** are shown in **Figure 15** and **Figure 16**. **P58** has a glass transition temperature (T_g) around 21 ^{o}C at a low [M]/[I] ratio of 30:1 and the T_g increases to ~ 25 ^{o}C upon increasing the molecular weight of the polymers. Due to the flexible chains (propargyloxy groups) along the polymer backbone which disrupts backbone-backbone interaction, the T_g decreases fairly rapidly compared to that of polylactide which has a T_g of 55-60 ^{o}C. This is even more obvious when homopolymer **P59** is considered. The T_g observed from the DSC for **P59** ranges from ~3 to 9 ^{o}C depending on the molecular weight. No melting/crystallizing transitions were observed for both **P58** and **P59** in either the heating or cooling scans, which indicates the amorphous state of the polymers.

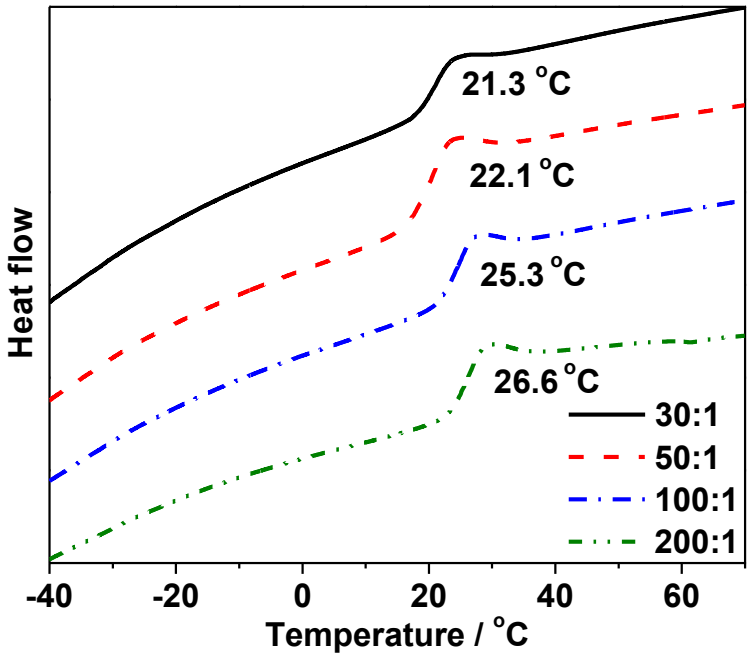

Figure 15. DSC traces of polymers from the bulk polymerization of **58** with different [M]/[I]. (second heating scan, 10 ^{o}C/min in N_2)

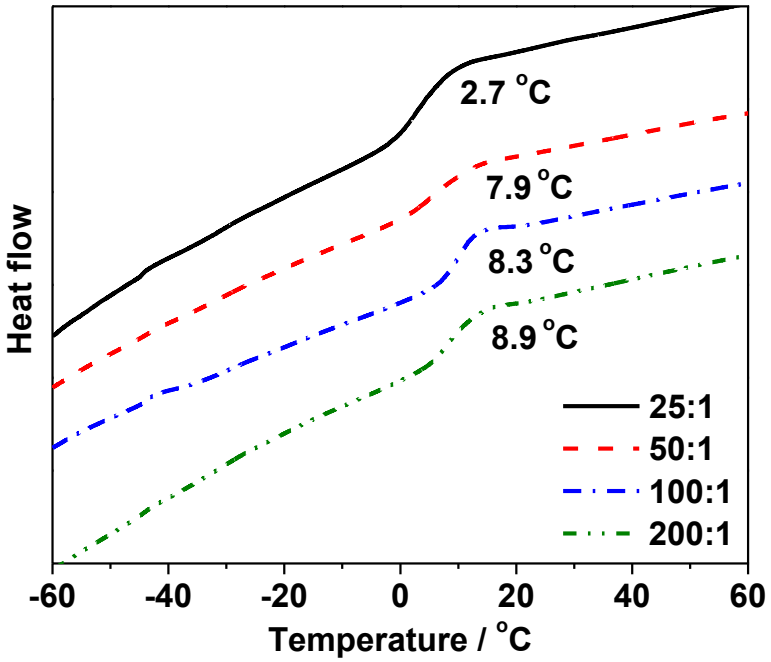

Figure 16. DSC traces of polymers from the bulk polymerization of **59** with different [M]/[I]. (second heating scan, 10 °C/min in N_2)

3.2.3 Copolymers of P58, P59 and *L*-Lactide

Copolymerization is a common strategy for synthesizing polymers with properties different from the corresponding homopolymers since it can be used to control the density and position of functional groups along the polymer backbones. A series of copolymers (**P58-*co*-*L*-LA**, **P59-*co*-*L*-LA**) of **58**, **59** and *L*-lactide were prepared in the melt of a mixture of *L*-lactide (*L*-LA) and either **58** or **59** (M) under the same conditions as was used for preparing homopolymers, i.e. using $Sn(Oct)_2$ as catalyst and TBBA as initiator (**Table 5**). The [M]/[I] ratio was kept at 100 while monomer feed ratios ranged from 25%, 50% to 75% lactide content. The percent conversions of *L*-LA were high (>93%) while the percent conversions of **58** were higher than 80%. Due to the overlap of peaks in the NMR spectra, the percent conversions of **59** were estimated to be 85%

from **Table 4**. As shown in **Table 5**, the calculated molecular weights closely match the experimental molecular weights.

Table 5. M_n and T_g of copolymers (**P58-*co*-*L*-LA**, **P59-*co*-*L*-LA**)

Polymer	Conv. (%)[a]		Feed ratio LA:M	Polymer LA:M	M_n[b] Calc. ($\times 10^{-3}$)	M_n[c] Exp. ($\times 10^{-3}$)	T_g (^oC)
	LA	M					
P58-*co*-*L*-LA	95	86	1:3	21:50	15.2	12.2	30.8
	97	86	1:1	38:39	14.8	12.6	36.6
	93	80	3:1	52:19	13.7	11.0	46.1
P59-*co*-*L*-LA	97	85[d]	1:3	32:53	19.1	18.0	19.9
	96	85[d]	1:1	47:41	17.7	17.1	26.4
	96	85[d]	3:1	71:21	15.8	15.5	34.0

[a] Determined by ^{1}H NMR. [b] g/mol, calculated from the [M]/[I] and corrected for conversion. [c] g/mol, calculated from ^{1}H NMR using end group analysis. [d] estimated from **Table 4** due to the overlap in ^{1}H NMR.

The onset decomposition temperature of both copolymers was about 230-240 ^{o}C which is similar to their homopolymers (**Figure 17** and **Figure 18**). The pendant alkyne groups along the polymer backbone act as a stabilizer and slows down the decomposition at 300 ^{o}C via cross-linking as discussed before. A higher alkyne group content leads to higher weight retention at 300 ^{o}C and thus a higher temperature for 100% decomposition.

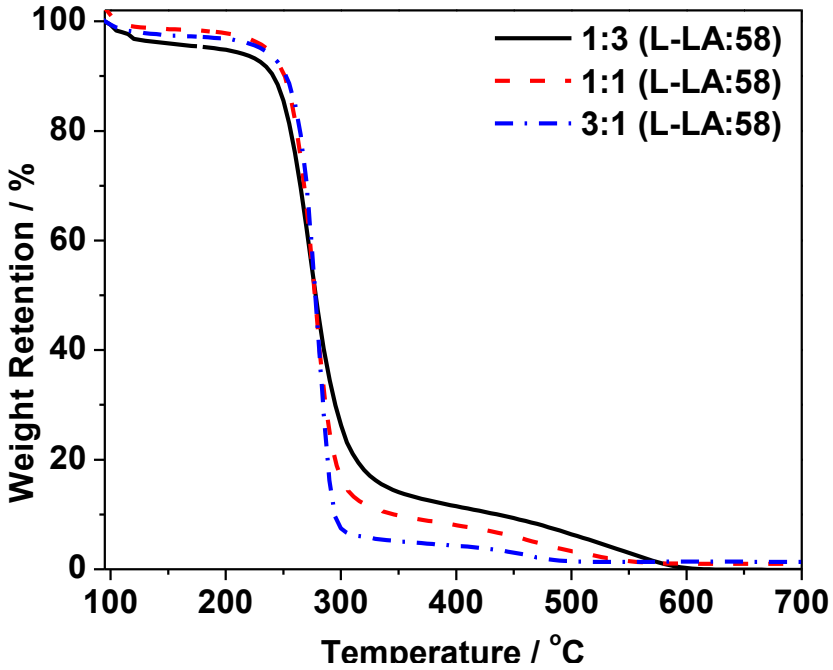

Figure 17. TGA curves of **P58-*co*-*L*-LA** with different feed ratios of L-LA to **58**. Conditions: 130 °C, [M]:[$Sn(Oct)_2$]:[TBBA] = 50:1:1.

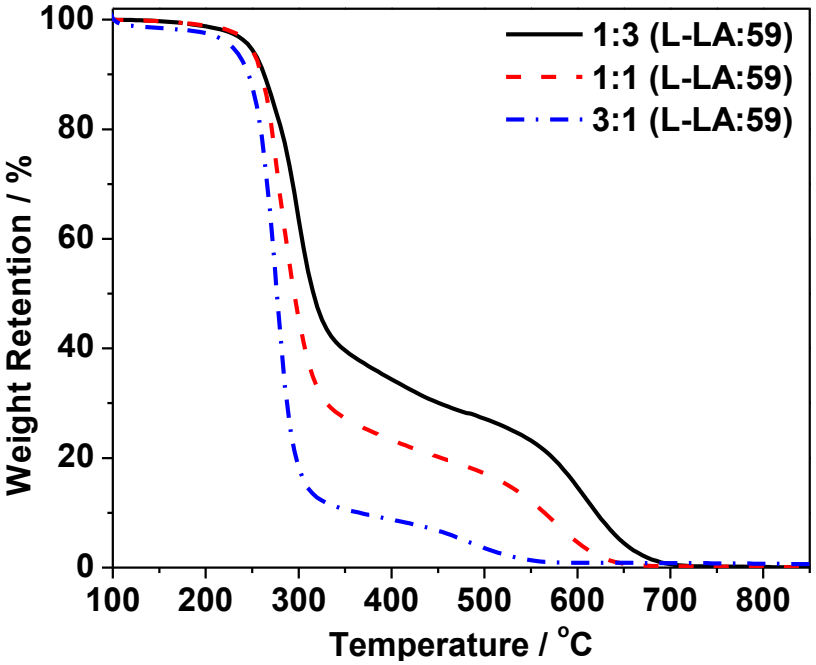

Figure 18. TGA curves of **P59-*co*-*L*-LA** with different feed ratios of L-LA to **59**. Conditions: 130 °C, [M]:[$Sn(Oct)_2$]:[TBBA] = 50:1:1.

As shown in **Figure 19** and **Figure 20**, DSC analysis shows that the T_g of both of the two series of copolymers increases with increasing lactide content (from 30 to 46 ^oC and 20 to 34 ^oC for **P58-*co-L*-LA** and **P59-*co-L*-LA**, respectively). No melting peaks were observed in any of the DSC scans up to 200 ^oC (not shown here), indicating that the copolymers are completely amorphous. The absence of any crystallinity, even at the highest level of lactide feeding (75%) reveals that the lactide units/blocks are of insufficient length to crystallize (usually at least 12 lactic acid units are required).[75,150] In addition, there was only one glass transition observed for all of the copolymers with different lactide contents, which indicates that the distribution of the propargyloxy lactides and L-LA is statistical in nature (more random than blocks).[108] Specifically, the alkyne groups are not concentrated in block segments, but instead are distributed along the polymer backbone. The Fox equation (**4**) can be applied to determine the glass transition temperature in polymer blends[151] and statistical copolymers[152] based on the weight fractions of monomers, and the T_g values of the respective homopolymers.[153,154]

$$(W_{L\text{-}LA}/T_{g,PLLA}) + (W_M/T_{g,\,PM}) = 1/T_{g,\,copolymer} \qquad (\mathbf{4})$$

$W_{L\text{-}LA}$, W_M and M denote the weight percentage of L-lactide and monomer **58** or **59** in our case. The inverse T_g values of the copolymers as a function of the weight percentage of **58** and **59** are shown in **Figure 21**. The theoretical lines were generated using the Fox equation (**4**) based on the measured T_g values of the homopolymers (9

°C for **P58** and 25 °C for **P59**) and poly(L-lactide) (PLLA, 59 °C). The experimental values fit well with the theory suggesting that the T_g of these copolymers can be tuned and predicted by varying the molar ratios of L-LA and **58** and **59** in the feed during the polymerization, because the proximity of a given temperature to the glass transition temperature is one of the most important factors in determining physical properties of an amorphous polymer.[155]

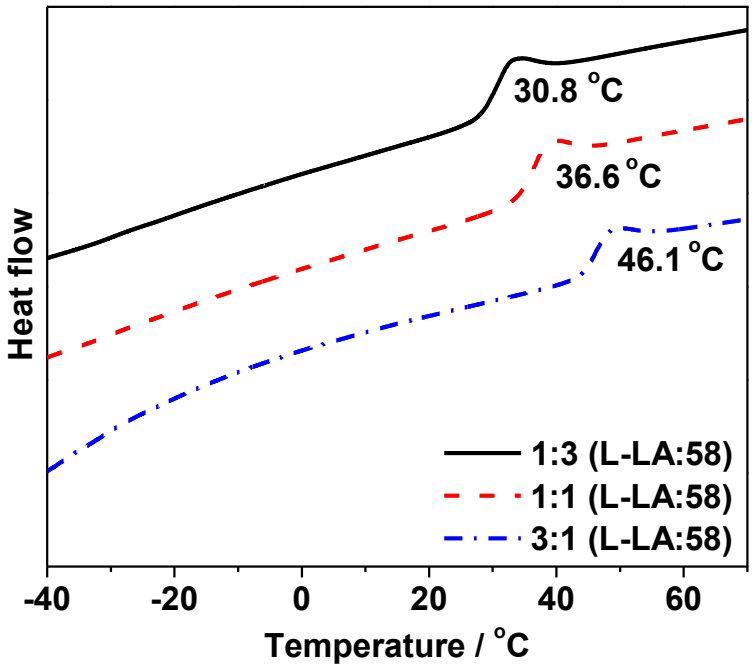

Figure 19. DSC curves of **P58-*co*-*L*-LA** with different feed ratios of L-LA to **58**. Conditions: 130 °C, [M]:[$Sn(Oct)_2$]:[TBBA] = 50:1:1.

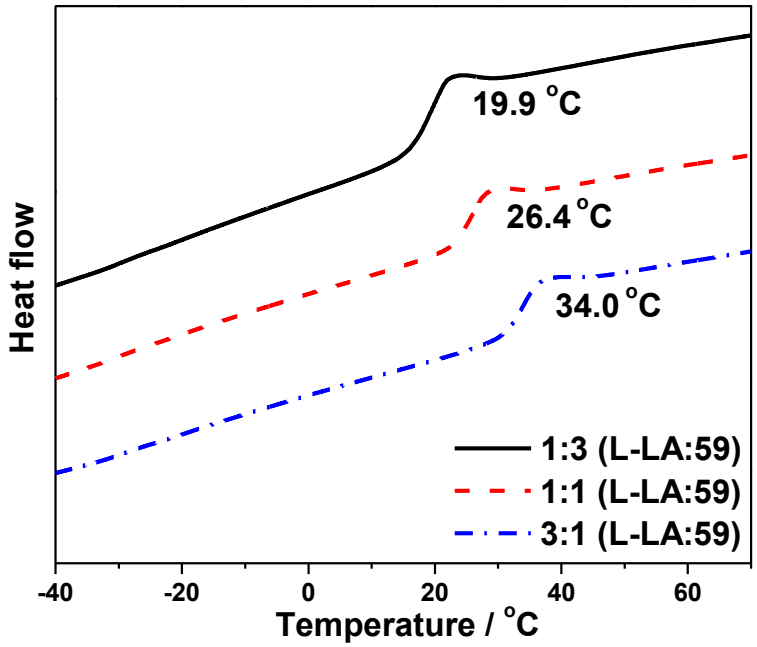

Figure 20. DSC curves of **P59-*co*-*L*-LA** with different feed ratios of L-LA to **59**. Conditions: 130 °C, [M]:[$Sn(Oct)_2$]:[TBBA] = 50:1:1.

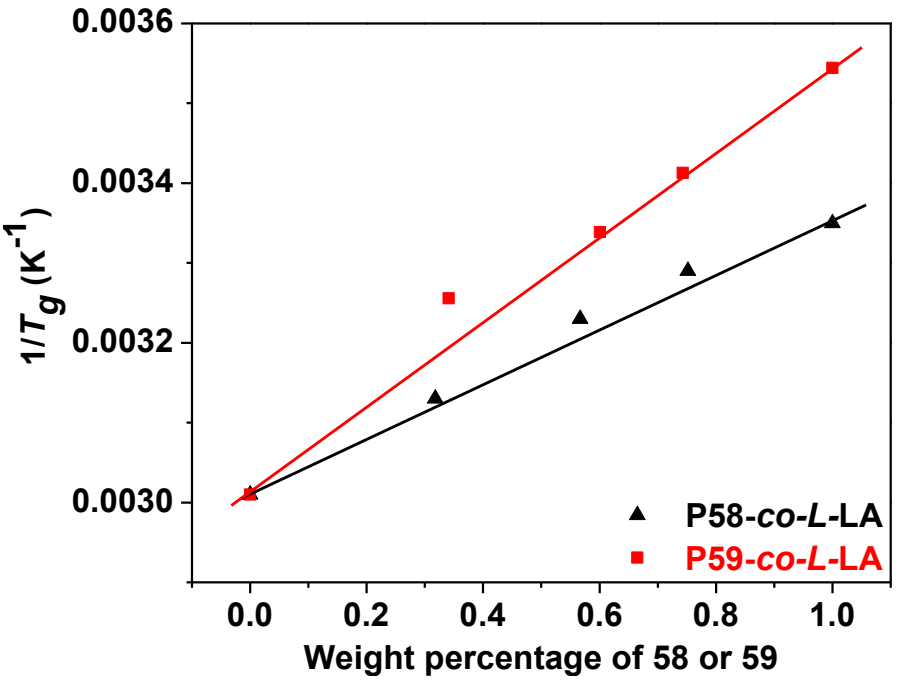

Figure 21. Plot of $1/T_g$ *versus* weight percentage of **58** and **59** in their copolymers. (Solid lines were generated using Fox equation (4) based on the measured T_g values of homopolymers)

This statistical nature of the copolymers was also confirmed by comparing the chemical shift changes in the carbonyl region of the ^{13}C NMR spectra from homopolymers PLLA, **P58**, **P59** and their copolymers **P58-*co-L*-LA**, **P59-*co-L*-LA**, as shown in **Figure 22** and **Figure 23**.[77,156,157] The carbonyl signals from **P58** and **P59** and PLLA are well-separated, with resonances of **P58** and **P59** shifted ~3.0 ppm upfield relative to PLLA. For both **P58-*co-L*-LA** and **P59-*co-L*-LA**, the "lactide" carbonyl shows new broad resonances shifted upfield ~ 0.3 ppm (marked with "*"). The carbonyls of **P58** or **P59** exhibit either new broad resonances shifted downfield ~ 0.2 ppm or a more highly split resonance pattern (marked with "+"). These results indicate a random distribution of the incorporated propargyl groups along copolymer backbone. Although there are remaining carbonyl resonances in copolymers which might be from block PLLA segments and **P58** or **P59** segments, those block segments should be short enough to be omitted to account for the statistical nature of the copolymers due to the single glass transition observed in DSC analyses.

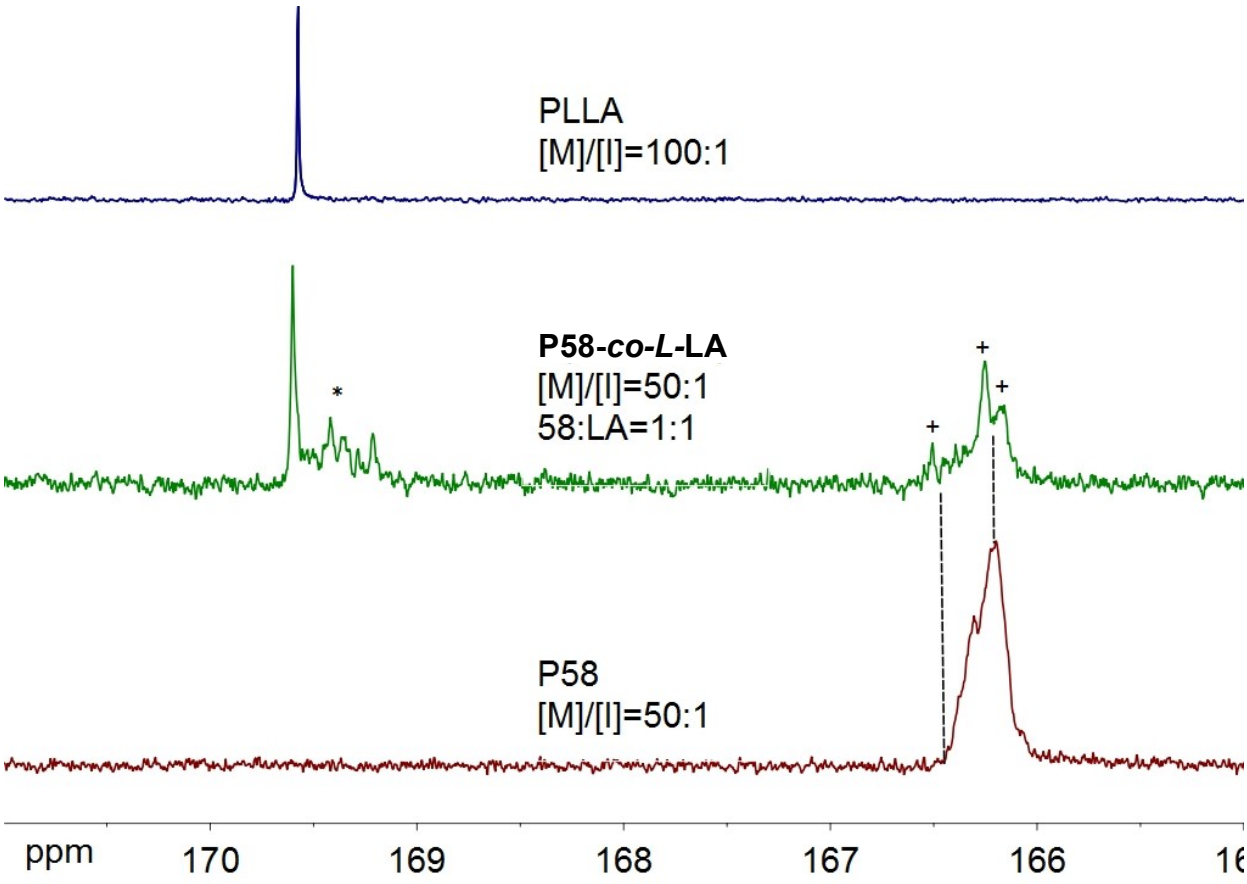

Figure 22. 125 MHz ^{13}C NMR carbonyl region of homopolymers PLLA, **P58** and copolymer **P58-*co*-*L*-LA**. Solvent: $CDCl_3$.

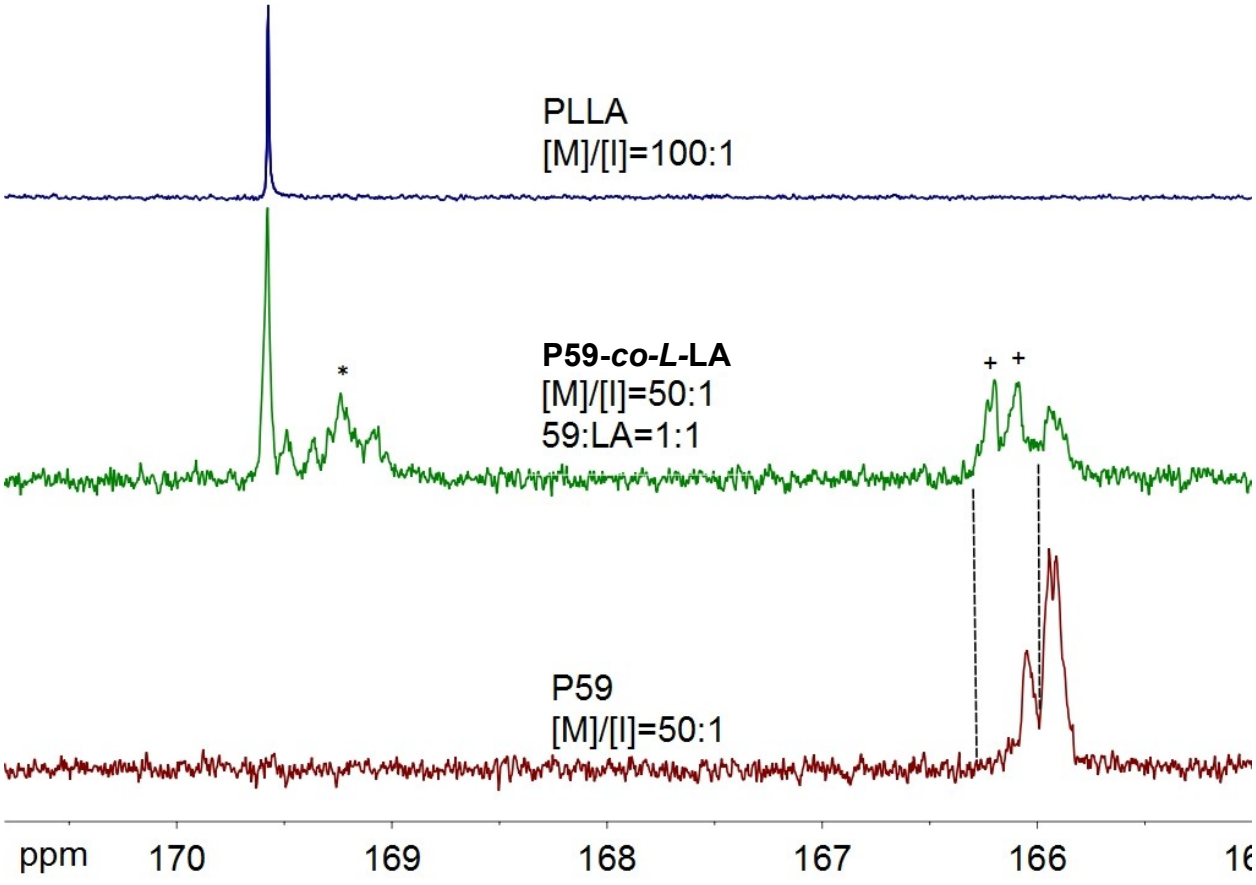

Figure 23. 125 MHz ^{13}C NMR carbonyl region of homopolymers PLLA, **P59** and copolymer **P59-*co*-*L*-LA**. Solvent: $CDCl_3$.

3.2.4 Thermo-responsive Properties of mPEG/Alkyl-Grafted Polymers from P59 via Click Chemistry

Emrick et al. were the first to report the Cu-catalyzed click functionalization of polyesters in the form of poly(α-propargyl-δ-valerolactone).[158] Since then, a variety of clickable polyesters have been reported[159,160,161] which were readily functionalized with different groups to afford new materials with tunable smart properties. Thermo-responsive polymers that show a lower critical solution temperature (LCST) have widely

been investigated due to their potential applications such as in controlled drug delivery, biomimetic actuators and gene-transfection agents. At LCST, polymers undergo a solution-gel transition and expulse the solvating water molecules from the polymer. It has been reported that the LCST can be tuned easily over a broad range of temperatures by adjusting the hydrophilic/hydrophobic balance.[77,162,163,164]

As shown in **Scheme 42**, the clickable polylactide **P59** was reacted with 1-(2-azidoethoxy)-2-(methoxyethoxy) ethane (m3PEGN_3), 1-azidodecane ($C_{10}H_{21}N_3$) or a mixtures thereof with different molar ratios (2:1 and 7:2) in the presence of $CuSO_4$ and sodium ascorbate using DMF as solvent for 12 h at room temperature after removal of oxygen. The ^{1}H NMR spectra of these polymers were recorded and are shown in **Figure 24**. The disappearance of the resonances at 2.5 ppm (-CH_2-C*CH*) and 4.20 ppm (-*CH_2*-CCH) and the appearance of a new peak at 7.6 ppm (*H* on the triazole ring) indicate the success of the click functionalization of **P59**. This is also confirmed by the appearance of characteristic proton resonances corresponding to m3PEG (3.4-3.7 ppm), methoxy (3.3 ppm) and alkyl groups (0.8-1.5 ppm) in the ^{1}H NMR spectra of P59-*g*-m3PEG (**P60**), P59-*g*-$C_{10}H_{21}$ (**P61**) and P59-*g*-$C_{10}H_{21}$/m3PEG (**P62**, 2 : 1 feed ratio of m3PEGN_3 : $C_{10}H_{21}N_3$). The click reaction of **P59** and m3PEGN_3 did not run to completion as shown in ^{1}H NMR and FT-IR spectra. The click functionalization was further tested by FT-IR which showed the disappearance of the triple bond stretching (2117 cm^{-1}) and the terminal alkyne C-H stretching (3282 cm^{-1}) accompanied by the

appearance of a triazole ring stretching vibration at 3150 cm^{-1} and 1460 cm^{-1} in fingerprint region (**Figure 25**). The incorporation of m3PEG and alky chains can account for the stronger absorbance at 2852-2970 and 1100 cm^{-1} compared to the parent polymer **P59** after normalizing the FT-IR spectra.

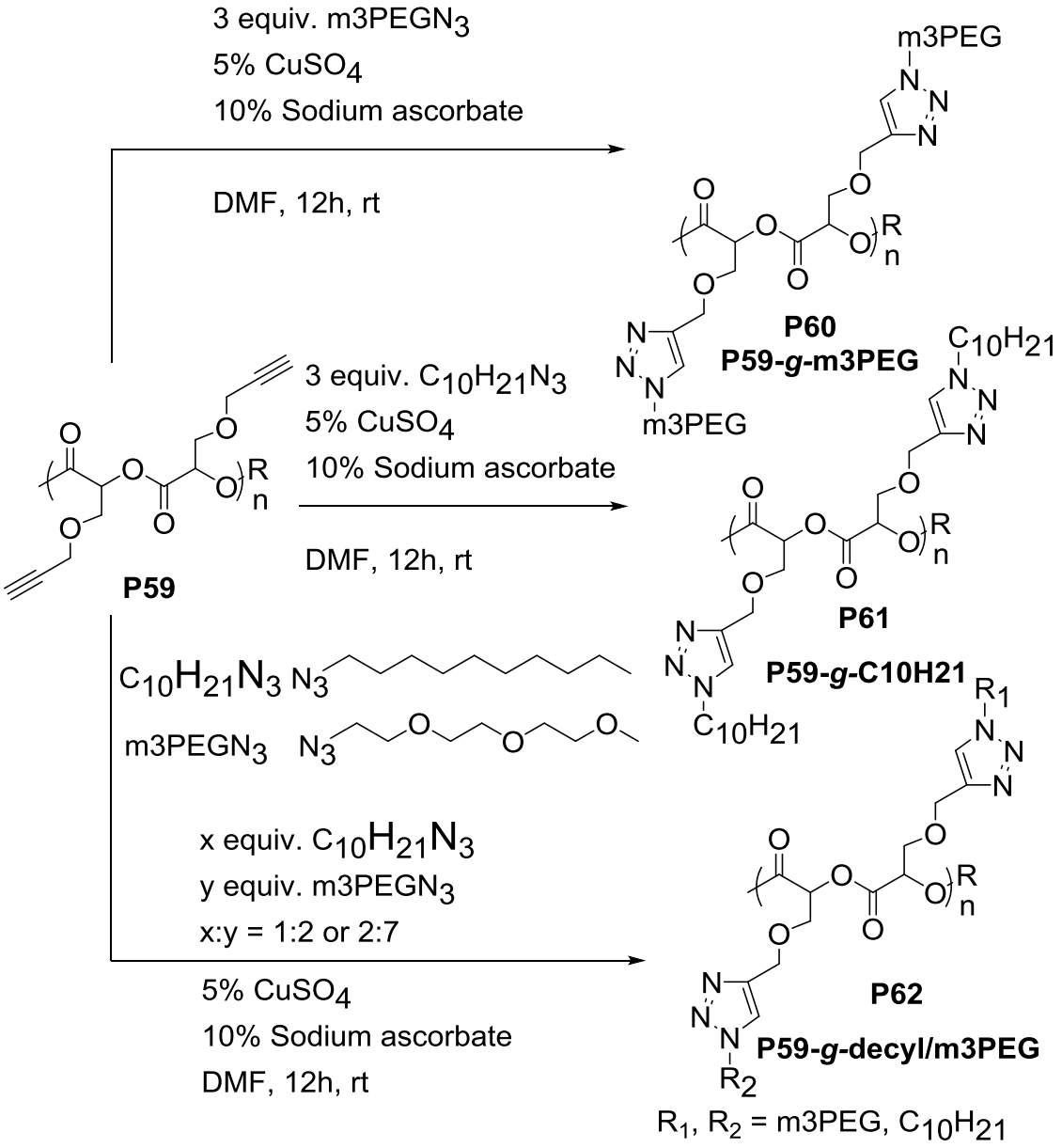

Scheme 42. Click functionalization of **P59** with alkyl and PEG azides

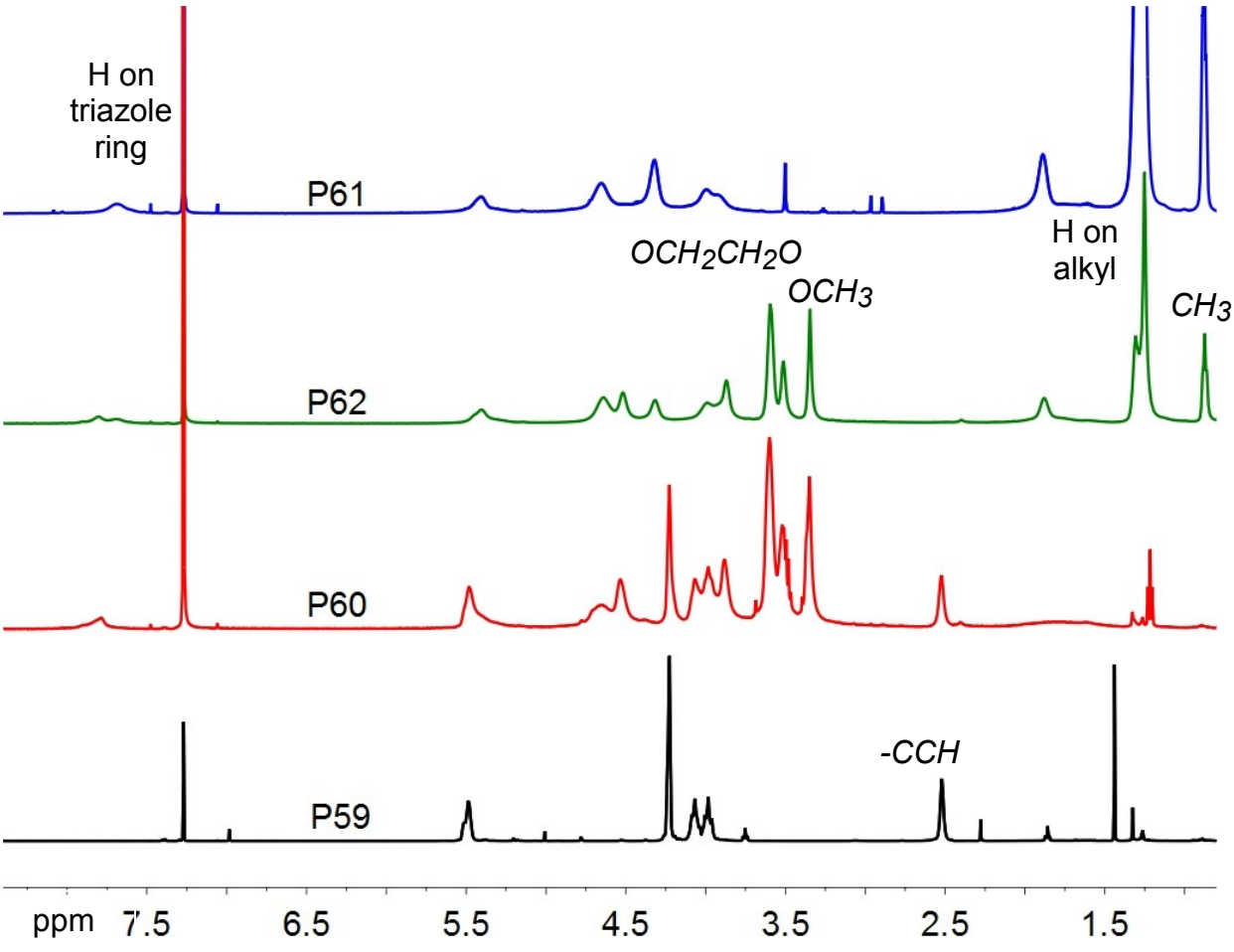

Figure 24. ^{1}H NMR spectra of **P59** and its click-grafted polymers **P60** (P59-*g*-m3PEG), **P61** (P59-*g*-$C_{10}H_{21}$) and **P62** (P59-*g*-$C_{10}H_{21}$/m3PEG, 2 : 1 feed ratio of m3PEGN_3 : $C_{10}H_{21}N_3$). Solvent: $CDCl_3$.

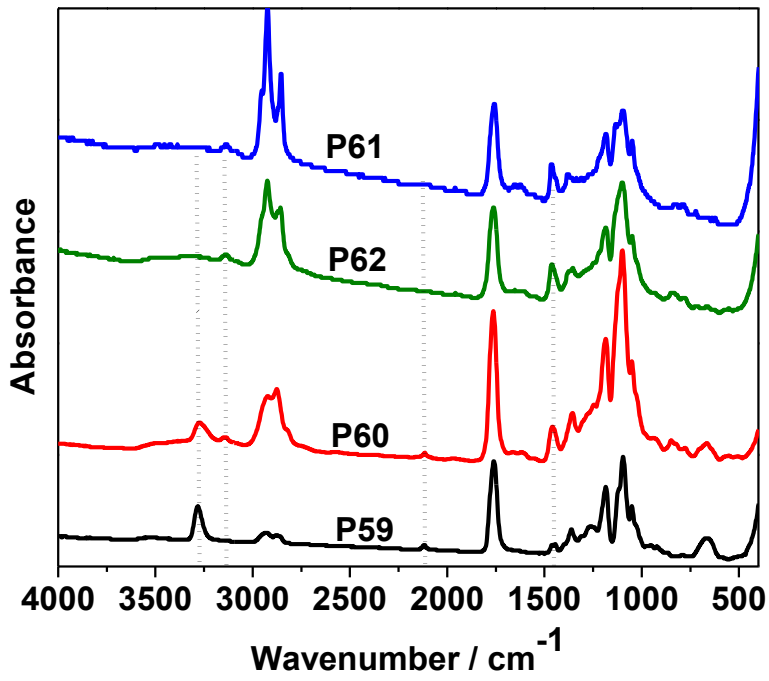

Figure 25. FT-IR spectra of **P59** and its click-grafted polymers **P60** (P59-*g*-m3PEG), **P61** (P59-*g*-$C_{10}H_{21}$) and **P62** (P59-*g*-$C_{10}H_{21}$/m3PEG, feed ratio of m3PEGN_3 and $C_{10}H_{21}N_3$ is 2 : 1).

By changing the feed ratios of m3PEGN_3 and $C_{10}H_{21}N_3$, one polymer **P60** with only pendant hydrophilic side chains and two polymers **P62** with different ratios of hydrophilic and hydrophobic pendant chains (2:1 and 7:2) were obtained and used to study their thermo-responsive properties and to measure LCST using the cloud point method. The composition of the pendant chains of the mix-clicked polymers were determined by ^{1}H NMR spectroscopy to be 58% m3PEG chains and 42% decyl chains from a 2:1 feed ratio, and 63% m3PEG chains and 37% decyl chains from a 7:2 feed ratio, which indicates that the 1-azidodecane reacts faster than m3PEGN_3. This also supports the orthogonal nature of click functionalization via simple mixing the azido compounds to afford polymers with different functionalities. Aqueous solution s(~3 wt%) of these

polymers were used to measure the absorbance at 450 nm at different temperatures using a UV-visible spectrophotometer. As shown in **Figure 26**, two polymers **P62** with different ratios of hydrophilic and hydrophobic pendant chains (2:1 and 7:2) exhibit very sharp solution-gel transitions at ~ 22 and 27 ^{o}C which were recorded as a rapid increase of absorbance due to the dramatic change in light scattering. **P60** with only hydrophilic chains has a moderate phase transition through LCST at ~68 ^{o}C. This higher LCST resulting from incorporation of more hydrophilic side chains could be attributed to the increased overall hydrogen bonding which requires higher temperature to be disrupted. Notably, those samples remained unchanged after performing more than 8 heating-cooling cycles in order to take pictures of the clear phase transition by a camera in the lab, which indicates their relative high stability upon heating and cooling (data is not shown here). For medical applications, it would be more interesting to have the LCST around body temperature (37 ^{o}C) and this presumably could be controled by tuning the hydrophobic/hydrophilic balance. The relationship between LCST and the molar fraction of m3PEG in polymers **P60** and **P62** is plotted in **Figure 27**, which shows a nearly linear relationship. This should allow for tuning the LCST to the desired temperature required for different applications simply by adjusting the side chain composition during the click functionalization. The dramatic increase in light scattering for all samples is directly visualized in **Figure 28** as the transition from a transparent solution to a cloudy mixture which can be re-dissolved upon cooling.

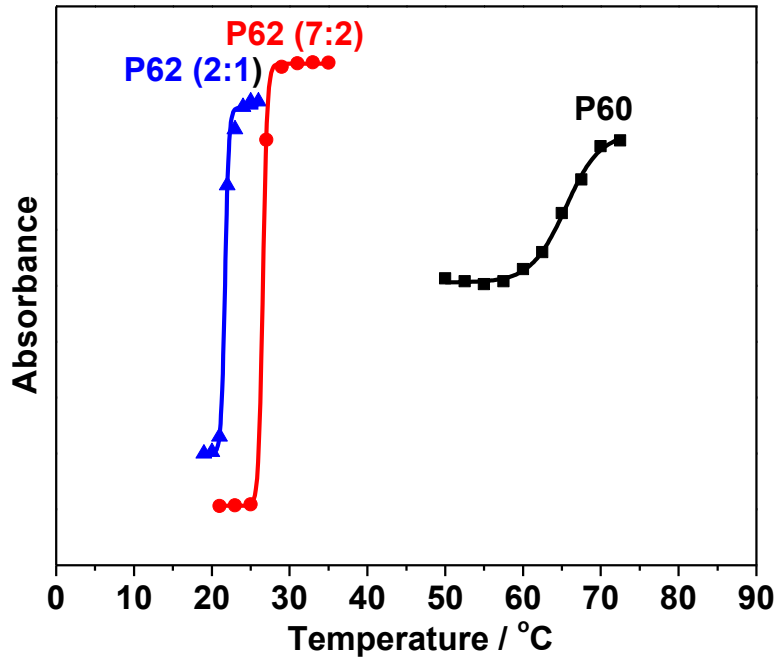

Figure 26. Plots of absorbance as a function of temperature for aqueous solutions (~3 mg/mL, in D_2O) of **P60** and **P62**. The solid lines are the non-linear curve fit to the data.

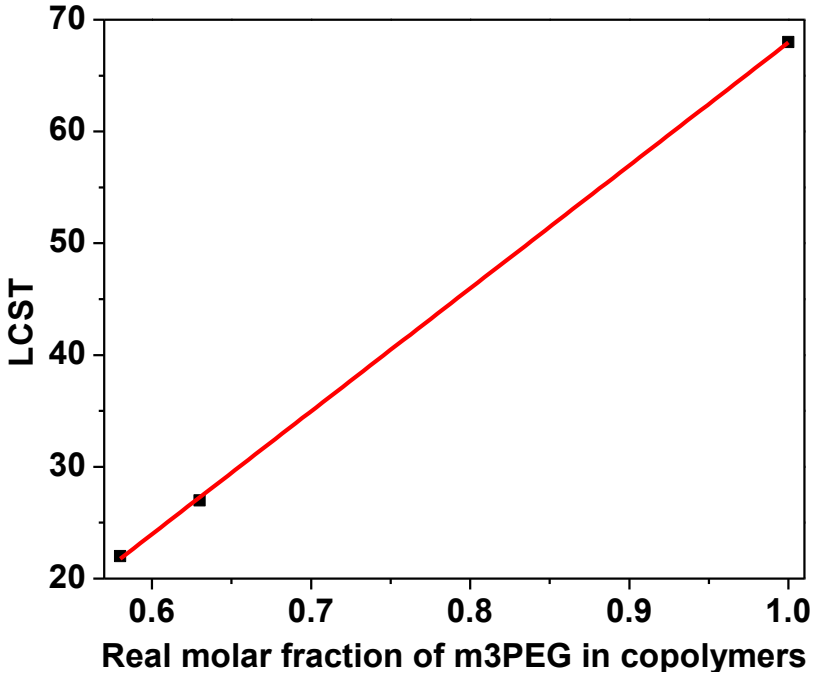

Figure 27. Plot of LCST as a function of mole fraction of m3PEG in polymers **P60** and **P62**. The solid line is the linear fit to the data.

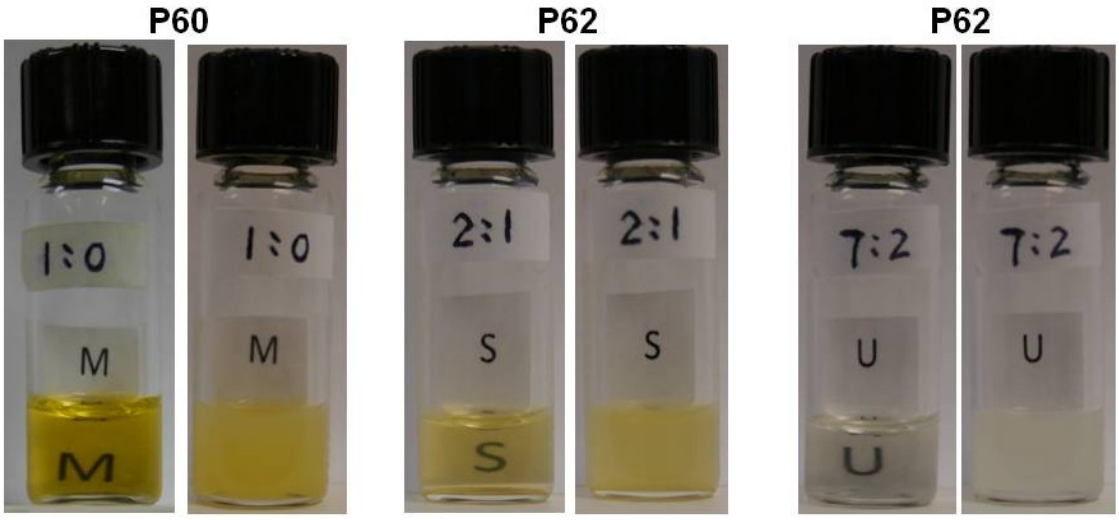

Figure 28. Visualization of thermo-responsive properties of **P60** (P59-*g*-m3PEG), **P62** (P59-*g*-$C_{10}H_{21}$/m3PEG, 2:1 and 7 : 2 feed ratio of m3PEGN_3 : $C_{10}H_{21}N_3$) at temperatures below (left) and above (right) their LCST. Solvent: D_2O.

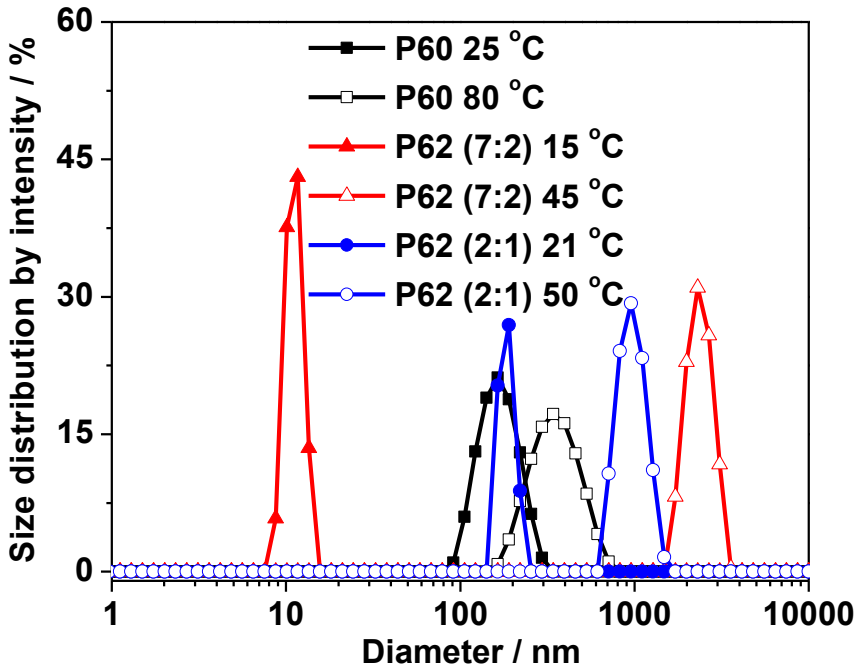

Figure 29. DLS of **P60** (P59-*g*-m3PEG), **P62** (P59-*g*-$C_{10}H_{21}$/m3PEG, 2:1 and 7 : 2 feed ratio of m3PEGN_3 : $C_{10}H_{21}N_3$) at temperatures below (filled symbol) and above (open symbol) their LCST. Solvent: D_2O.

The dynamic light scattering (DLS) curves in **Figure 29** show that the hydrodynamic sizes of all samples rapidly increased from ~10-150 nm to hundreds of nanometers when heating through the LCST, which suggests a transition from a hydrated state to an agglomerated insoluble state.

In general, the PEG segments of the polymer can form hydrogen bonding with water to facilitate the dissolution and exhibit reversible dehydration and hydration process with variations in the temperature, which changes the local environment around the polymers and results in a shift of their NMR resonances. Indeed, when heating aqueous solutions of **P60** and **P62** through their LCST, the proton chemical shifts of the triazole ring (~7.6 ppm), of the mPEG unit (3.4-3.7 ppm), of the methoxy group (3.3 ppm) and of the alkyl groups (0.8-1.5 ppm) are all shifted downfield in a similar pattern as shown in their ^{1}H NMR spectra (**Figure 30**). Each of these proton resonances is broader above the LCST due to the phase transition from a soluble to an insoluble state. This clearly further confirms the solution-gel phase transition of the clicked polymers when heated through the LCST.

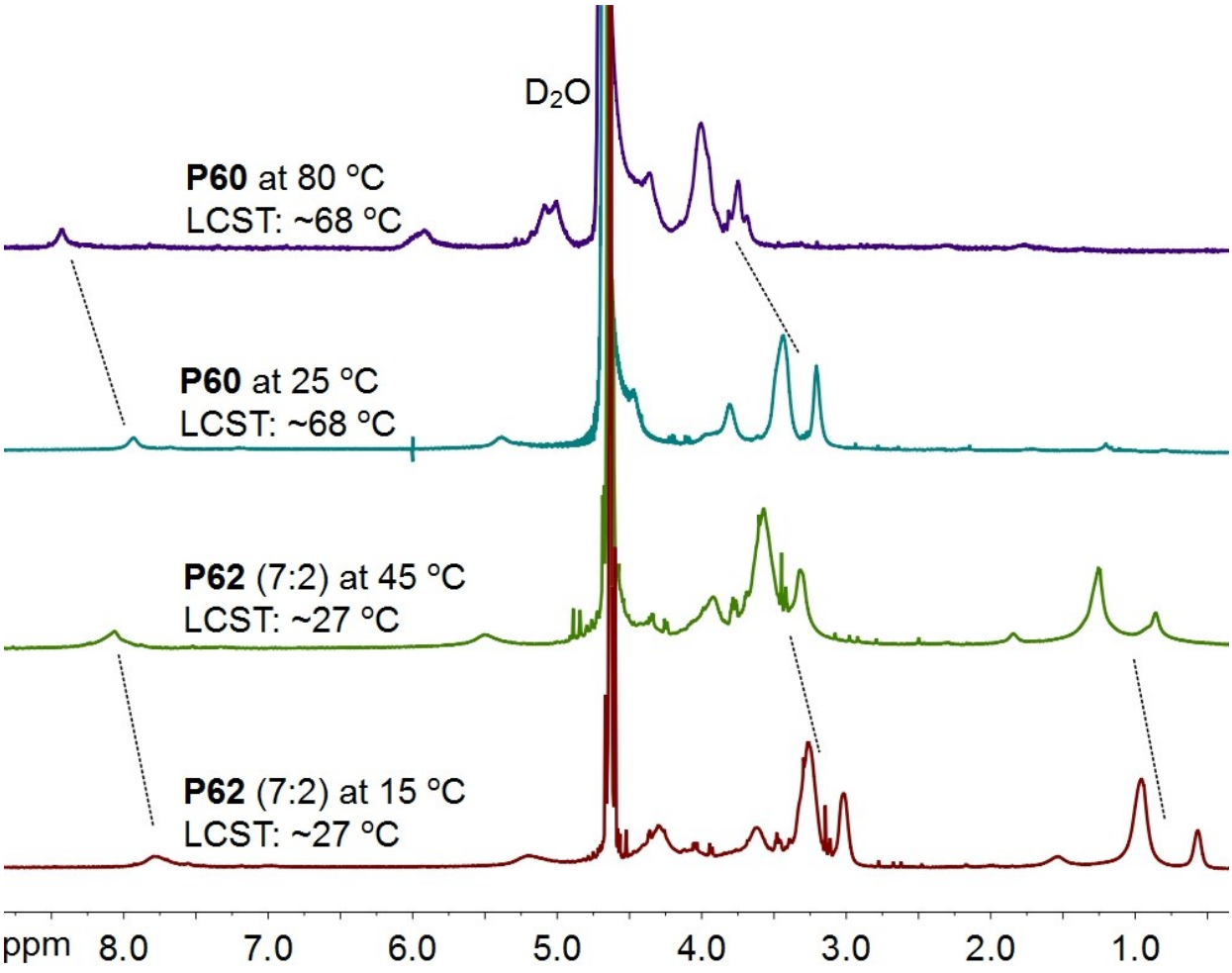

Figure 30. ^{1}H NMR spectra of **P60** (P59-*g*-m3PEG), **P62** (P59-*g*-$C_{10}H_{21}$/m3PEG, 7 : 2 feed ratio of m3PEGN_3 : $C_{10}H_{21}N_3$) at temperatures below and above their LCST. Solvent: D_2O. The broken line denotes the significant changes of chemical shift.

3.2.5 Formation of Core Cross-linked Biodegradable Micelles and the Modulation of Redox-Responsive Properties of PEG Block Copolymers of 58 and 59 via Click Chemistry

The application of amphiphilic block copolymers as drug carriers has been an active research area, and among the materials surveyed, polylactide (PLA) based copolymers are the most widely studied due to their easy availability. Amphiphilic block copolymers

of PEG and PLA form micelles in aqueous solution via self-assembly arising from the large solubility differences between hydrophilic and hydrophobic moieties and these micelles have been investigated in a variety of delivery systems. Typically, the hydrophobic blocks of the copolymers form the core of the micelles through hydrophobic interactions, electrostatic interactions or stereocomplex formation while the hydrophilic blocks of the copolymers form the corona shell all leading to the stabilization of the micellar structure.[165] These structures consist of water-insoluble cores and water-soluble corona shells each of which can be used to modify the micelle and thus improve the delivery performance. The amphiphilic polymers could form micelles in water when their concentrations are above the critical micelle concentrations (CMCs); However, the micelles will dissemble back to free polymer chains when their concentrations are below the CMCs. Due to the amphiphilic nature and low application concentration of the formed micelles, core cross-linking approach has been used to maintain their shape and structure under a variety of conditions. The utilization of functional or reversible cross linkers can give cross-linked micelles stimuli responsive properties depending on the functionalities of the cross linkers.

In order to synthesize amphiphilic copolymers, monomers **58** and **59** were polymerized at 130 ^{o}C using $Sn(Oct)_2$ as catalyst and mPEG as initiators of different molecular weights (M_n = 350, 2k and 5k) to give block copolymers (**P58B**, **P59B**, **P59C** and **P59D**) (**Scheme 41**). As shown in **Table** 6, the polymerization using mPEG as initiator achieved high conversion and the molecular weights calculated from ^{1}H NMR analysis are close to the feed ratio of [M]/[I] after taking percent conversion into account.

Table 6. Block copolymers of mPEG (initiator) and monomers **58** and **59**.[a]

entry	P	I	[M]/[I]	t (min)	Conv. (%)[b]	X_n[c]	X_n[d]	M_n (x 10^{-3}) [e]	T_g °C
1	**P58B**	mPEG350	50	15	96	48	47	9.0	16
2	**P59B**	mPEG350	50	45	95	48	44	11.4	5
3	**P59C**	mPEG2k	30	20	91	27	30	9.6	-22
4	**P59D**	mPEG5k	30	20	88	26	29	12.3	-33

[a] $Sn(Oct)_2$ used as the catalyst, 130 °C. [b] Measured by ^1H NMR spectra. [c] Calculated from the [M]/[I] and corrected for conversion. [d] Determined by ^1H NMR spectra using end group analysis. [e] g/mol, calculated from X_n[d].

The critical micelle concentration (CMC), an effective indicator of the micellar stability, was determined with nile red (NR) as fluorescence hydrophobic probe.[166] All amphiphilic copolymers generated for the study summarized in **Table 7** have relatively low CMC values and the CMC values decreased with decreasing hydrophilic PEG content. Water contact angle measurement is the one of the most common methods for determining a material's wettability and hydrophilicity. The materials with lower contact angle have greater tendency for water to wet the solid, and thus are more hydrophilic. The copolymers **P59C** and **P59D** showed similar water contact angles, but which were much lower than those of their homopolymer **P59** and the copolymer **P59B**. This is consistent with the observed CMC values. Based on the observed higher CMC and smaller contact angle than those of **P59** and **P59B**, homopolymer **P58** and its copolymer **P58B** were more hydrophilic compared to other polymers due to the lack of one side chain on each monomer unit.

Table 7. CMC and contact angles of polymers **P59** and **P59B**, **P59C** and **P59D**

	Substrate	P58	P58B	P59	P59B	P59C	P59D
CMC ($\times 10^{-2}$ mg/mL)	--	--	6.6	--	5.7	11	15
Contact angle (^{o})	32	86	72	95	82	25	23

The amphiphilic copolymers **P58B**, **P59B**, **P59C** and **P59D** were used to prepare uncross-linked micelles (UCMs) by nano-precipitation method.[167, 168] Acetone solutions of copolymers **P58B** and **P59B** were added to deionized water dropwise under vigorous stirring to give **UCMP58B** and **UCMP59B**, respectively. All UCMs of copolymers **P59C** and **P59D** were prepared by adding water dropwise to their DMF solution under vigorous stirring to give **UCMP59C** and **UCMP59D**, respectively. The final UCM/copolymer concentration in water was set to 0.5 mg/mL for all samples which is above their CMC.

The formation of a core–shell structure of the UCMs was characterized by ^{1}H NMR spectra of polymeric micelles as shown in **Figure 31**. The ^{1}H NMR spectra only show the proton signals of the mPEG component (3.2 ppm for terminal methoxy group and 3.6 ppm for methylene groups from the mPEG) in solvent D_2O (PEG segment is dissolved). This indicates that the PEG segment is in an extended solvated state to form the hydrophilic corona shell to protect UCMs in water. Since D_2O is a nonselective solvent of **P59** segment and it cannot dissolve **P59** segment, the protons in the **P59** segment (refer to **P59** in **Figure 24** for proton resonances in $CDCl_3$) have almost disappeared, implying that **P59** segment forms the central hydrophobic cores of

micelles and **P59** segment has restricted motion within the inner core.[169] The zeta potential, the charge that develops at the interface between a colloid particle surface and its liquid medium, is most often used as an indicator of dispersion stability. Surface functionalities of the colloid particles will change the zeta potential values of particles. The fact that PEG shell staying on the surface of UCMs was verified by the increase of UCMs' zeta potential (ζ) from -50 mV to about -10 mV when PEG composition in copolymers increased as shown in **Table 8**. Compared to the zeta potential (-50 mV) reported for PLA nanoparticles,[170] the increase of the non-ionic and hydrophilic corona shell thickness shields the core better and thus reduces the ionization degree of carbonyl groups, resulting in a higher zeta potential.

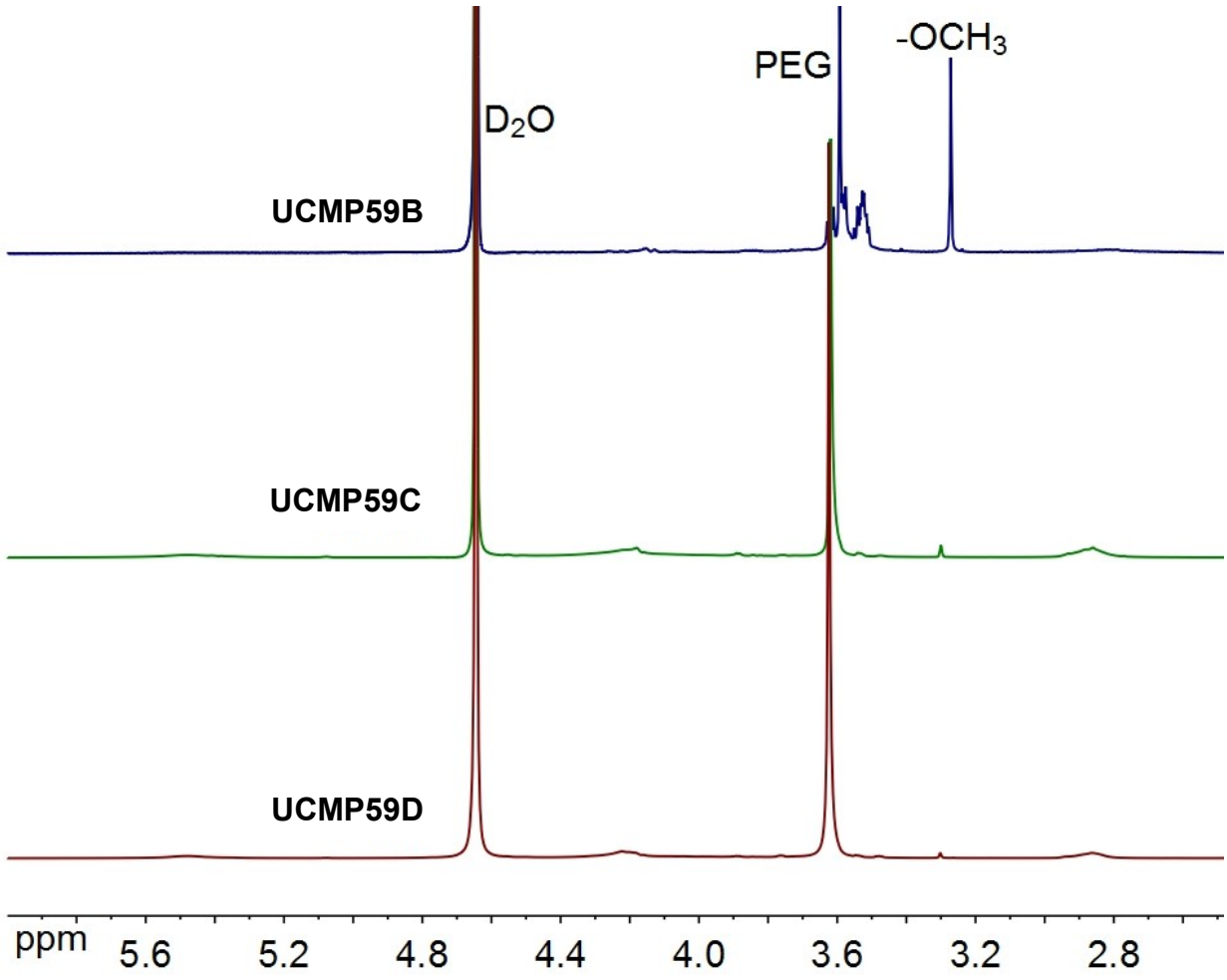

Figure 31. ^{1}H NMR spectra of UCMs prepared from **P59B**, **P59C** and **P59D** in D_2O.

Table 8. Properties of UCMS and CMs

UCM [a]				CM[b] Cross-linker: **63**				CM[b] Cross-linker: **64**			
	D[c]	D[d]	ζ[e]		D[c]	D[d]	ζ[e]		D[c]	D[d]	ζ[e]
UCMP58B	52	45	-50	--	--	--	--	--	--	--	--
UCMP59B	55	32	-30	--	--	--	--	--	--	--	--
UCMP59C	61	58	-11	CMP59C	51	28	-25	CM*P59C	67	27	-20
UCMP59D	128	59	-7	CMP59D	114	29	-14	CM*P59D	134	50	-10

[a] UCMs were dialyzed against water. [b] CMs were dialyzed against water. [c] Diameter, nm, measured by DLS in water. [d] Diameter, nm, measured by TEM. [e] Zeta potential, -mV, measured by DLS in water.

To maintain the original micelles shape and structure, core cross-linking requires the micelles to be dispersed well in solution after addition of the chemicals and catalysts required for core cross-linking to the micelle solution. However, different dispersion stability of the UCMs was observed upon addition of aqueous $CuSO_4$ (10% equiv. to alkyne groups). As shown in **Figure 32**, all UCM suspensions in water were clear. However, the suspensions of **UCMP58B** and **UCMP59B** immediately turned cloudy after adding $CuSO_4$ and a precipitate formed upon standing overnight, which indicates their low dispersion stability. The suspensions of **UCMP59C** and **UCMP59D** remained unchanged after adding $CuSO_4$. This phenomenon might be due to the different amounts of PEG composition in the copolymers with a lower degree of stabilization associated with a lower percentage of PEG in the copolymer. The addition of $CuSO_4$ might reduce ionization degree of carbonyl groups on hydrophobic core segment and thus the increased hydrophobic interaction between micelles can be dominant and induce aggregation due to the much lower micelle surface coverage by PEG chains in **P58B** and **P59B** compared to **P59C** and **P59D**.

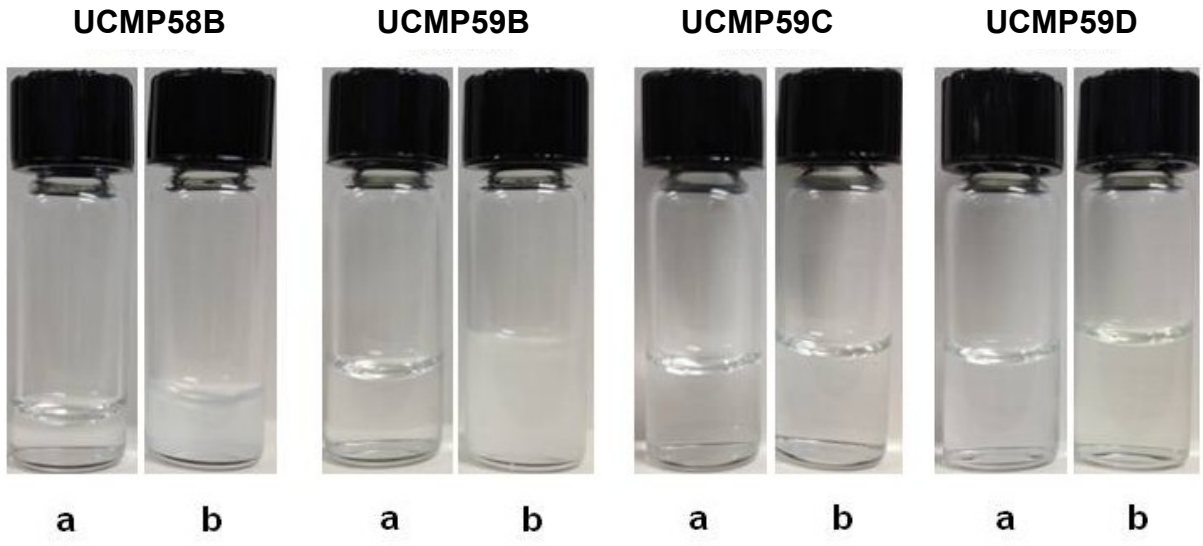

Figure 32. Visualization of UCMs' integrity stability prepared from **P58B**, **P59B**, **P59C** and **P59D** in D_2O without (**a**) and with (**b**) addition of aqueous $CuSO_4$.

Core cross-linking via click chemistry was performed only on those UCMs that were stable to the addition of $CuSO_4$. The cross-linking of **UCMP59C** and **UCMP59D** was carried with 1,5-diazidopentane (**63**), bis(azidoethyl) disulfide (**64**) or a mixture (2:8) of the two in the presence of $CuSO_4$ and sodium ascorbate to afford the core cross-linked micelles (**CMP59C** and **CMP59D** using **63** as cross-linker, **CM*P59C** and **CM*P59D** using **64** as cross-linker, **CM**P59C** and **CM**P59D** using a mixture (2:8) of **63** and **64** as cross-linker, **Scheme 43**). As shown in **Table 8**, after cross-linking, the diameters of all CMs as measured from DLS remained close to their precursor UCMs, indicating that the cross-linking was occurring in the core and did not substantially affect the micelle dispersion stability. The larger DLS diameters of **UCMP59D** and **CMP59D** were probably due to the more extended PEG brush chains and due to the higher viscosity of the DMF solution during the micelle preparation.[171] All micelles showed medium or high

negative zeta potentials (ζ), which is indicative of their high stability in water (**Table 8**). Indeed, they were stable in water for up to 5 days during the test period, and their stability for longer periods was not tested. This indicates that aging did not induce aggregation of the micelles (**Figure 33**). Micelle diameters measured by TEM were smaller than those measured by DLS due to the fact that dried samples are required for the TEM tests, whereas the extended micelle structure in water were measured by DLS. The cross linking only occurring in the core was also confirmed by the ^{1}H NMR spectra of **UCMP59D** and **CMP59D** in DMSO-d_6. This is because DMSO can dissolve both PEG and **P59** segments of **UCMP59D** to give all proton signals for both of segments in ^{1}H NMR spectra, whereas DMSO can only dissolve PEG segment of **CMP59D** to give PEG proton signals in ^{1}H NMR spectra without dissolving the cross-linked **P59** core segment. As shown in **Figure 34**, only hydrophilic PEG resonances (3.2 and 3.5 ppm) could be observed for **CMP59D** cross-linked by **63**, whereas **UCMP59D** also showed **P59** core segment (3.5, 3.9, 4.1 and 5.5 ppm), indicating the limited molecular motion of the **P59** backbone in the core and also that the micelle structure is maintained in DMSO.

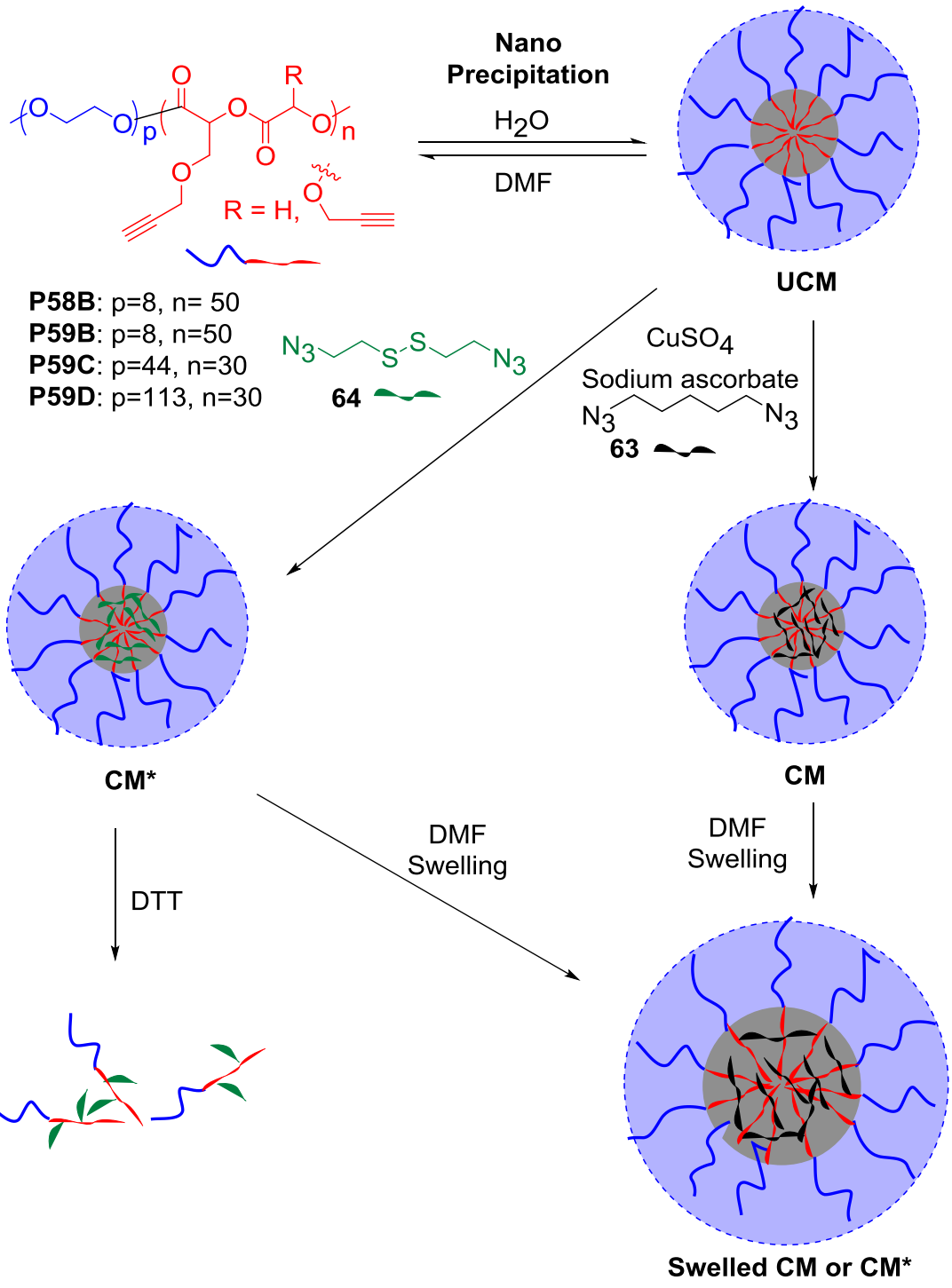

Scheme 43. Preparation of UCMs and CMs via click chemistry and their response to environment change.

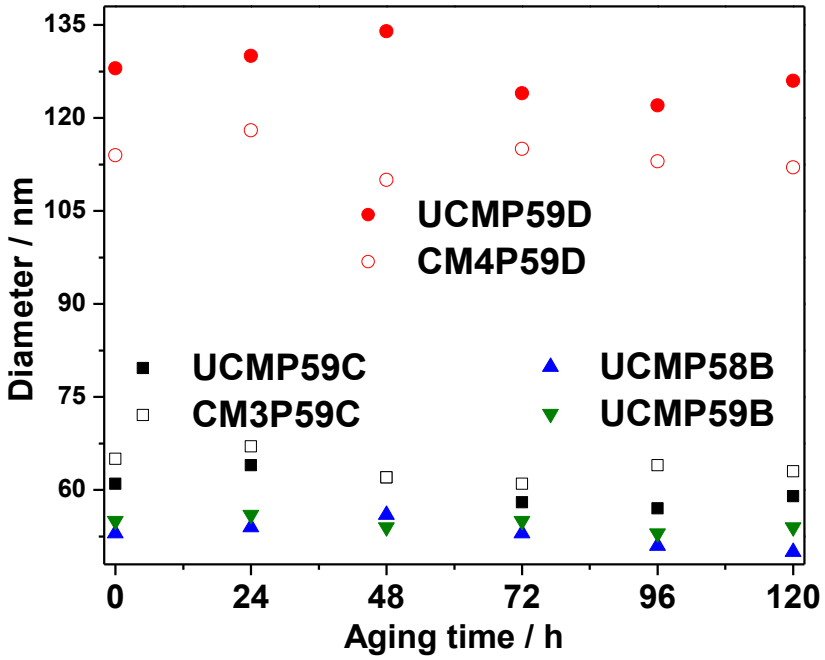

Figure 33. Hydrodynamic diameters of prepared UCMs and CMs *versus* aging time (Cross-linker: **63**).

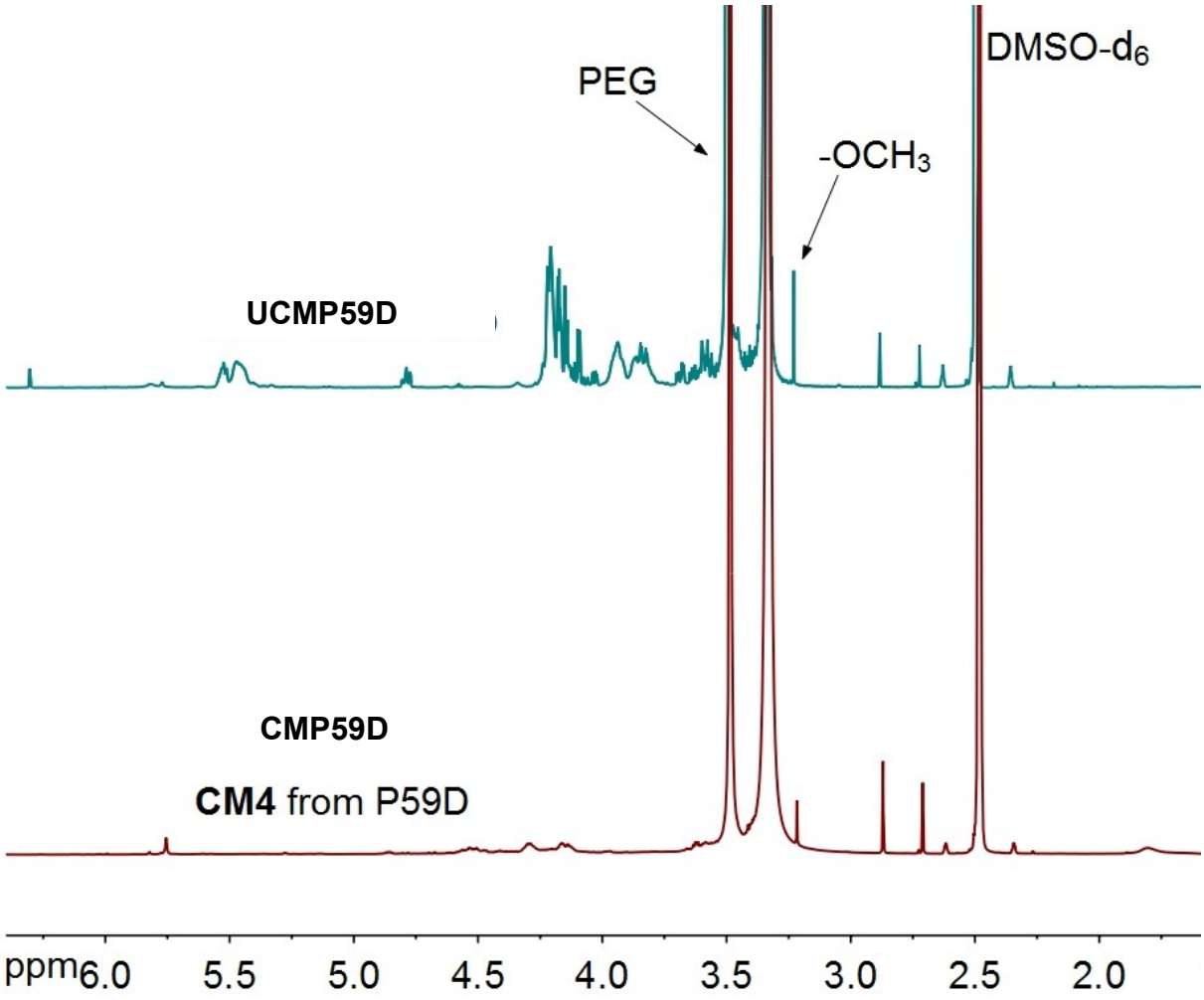

Figure 34. ^{1}H NMR spectra of **UCMP59D** and **CMP59D** (cross-linker: **63**) in DMSO-d_6.

To further demonstrate that the cross-linking of the micelles occurred in the hydrophobic core and to demonstrate their redox-responsiveness to reducing agent (DTT), the changes in the hydrodynamic diameters of both UCMs and CMs as a response to the environmental changes was evaluated by DLS in water or DMF in the presence or absence of DTT. The results of these studies will be described below.

DMF is capable of dissolving both outspread PEG segment and buried hydrophobic core segment of the micelles. Therefore DMF would be expected to completely disrupt the UCMs by dissolution, whereas CMs would maintain the micelle structure in DMF,

although a larger diameter as measured by DLS would be expected due to the swelling effect of the cross-linked micelle core DMF. As shown in **Figure 35**, both UCM3 and UCM4 were disrupted by 10-fold dilution with DMF which is confirmed by the disappearance of DLS peaks (**Figure 35**, (a)). However, the micellar structure of **UCMP59C** and **UCMP59D** was preserved after core crossing-linking with 1,5 diazidopentane **63** as evidenced by the presence of DLS peaks for **CMP59C** and **CMP59D** after dilution with DMF (**Figure 35**, (b)). These with the fact that DLS signals are shifted to a larger diameter, indicates that the micelles underwent swelling in DMF. These swelled micelles were unchanged after 24h (data shown in **Table 9**, and stability was not tested over longer times). These results also indicate the high micelle structure stability of the core cross-linked micelles.

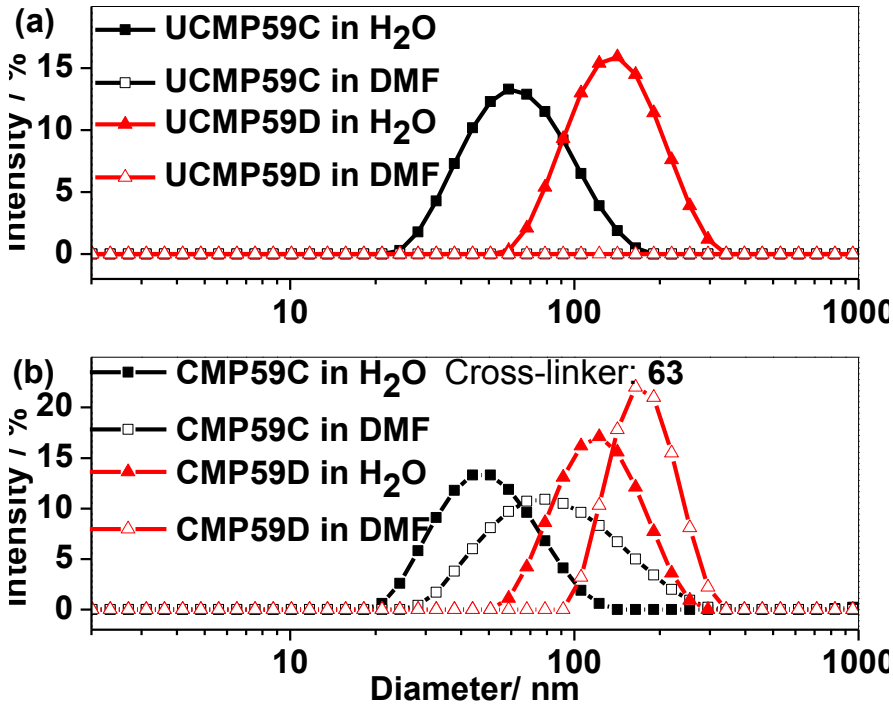

Figure 35. DLS size distribution of hydrodynamic diameters of (a) UCMs and (b) CMs in water before and after 10-fold dilution with DMF (Cross-linker: **63**).

To track the release of nile red (NR, used as a drug substitute to study the cargo release behavior of the micelles in the present study) from **UCMP59C**, **UCMP59D**, **CMP59C** and **CMP59D**, the NR-loaded micelles were placed in a dialysis bag (molecular weight cutoff (MWCO) = 3.5 kD; concentration 0.25 mg/mL, 2 mL) and dialyzed with DI water. The fluorescence spectra of the NR-loaded micelles were measured by removing aliquots of the micelle solution from the dialysis bag, which allowed us to monitor the continual release of nile red over 70 hours. As shown in **Figure 36**, all micelles exhibited a burst release of NR in the first 2 h period. But the cross-linked micelles **CMP59C** and **CMP59D** only released ~45% of their original loading, which is much lower than ~ 65% release from the uncross-linked micelles **UCMP59C** and **UCMP59D**. After burst release, NR release was monitored with time and it was observed that NR release from the cross-linked micelles **CMP59C** and **CMP59D** was more controlled and slower compared to the uncross-linked micelles **UCMP59C** and **UCMP59D** which continued until almost all of the entrapped nile red was released. This clearly indicates that core cross-linking has no adverse effect on cargo release; instead, it can slow down but not ultimately inhibit cargo release.[172] The structural stability of micelles after nile red release was complete was also investigated using DLS to study the cross-linking/cargo release effect on particle size distribution. As shown in **Figure 37** (a and b), both **UCMP59C** and **UCMP59D** showed a bimodal size distribution after NR release different from **UCMP59C** and **UCMP59D** without NR loading and release. However, the cross-linked micelles **CMP59C** and **CMP59D** showed almost no change compared to **CMP59C** and **CMP59D** without NR loading and release. These results again indicate that the micelles structural stability is greatly

enhanced by core cross-linking without affecting their cargo release behavior.

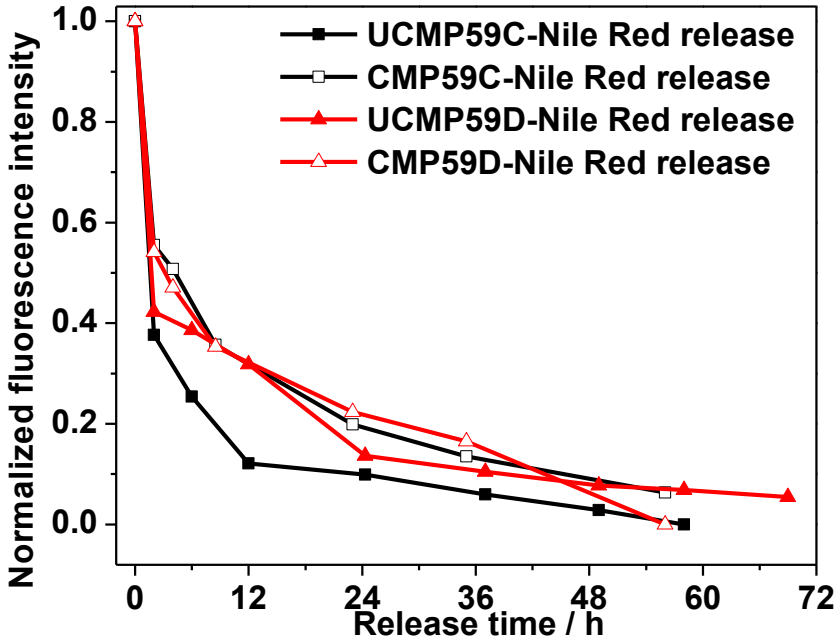

Figure 36. Continual release profiles of Nile red from NR-loaded uncross-linked micelles and cross-linked micelles.

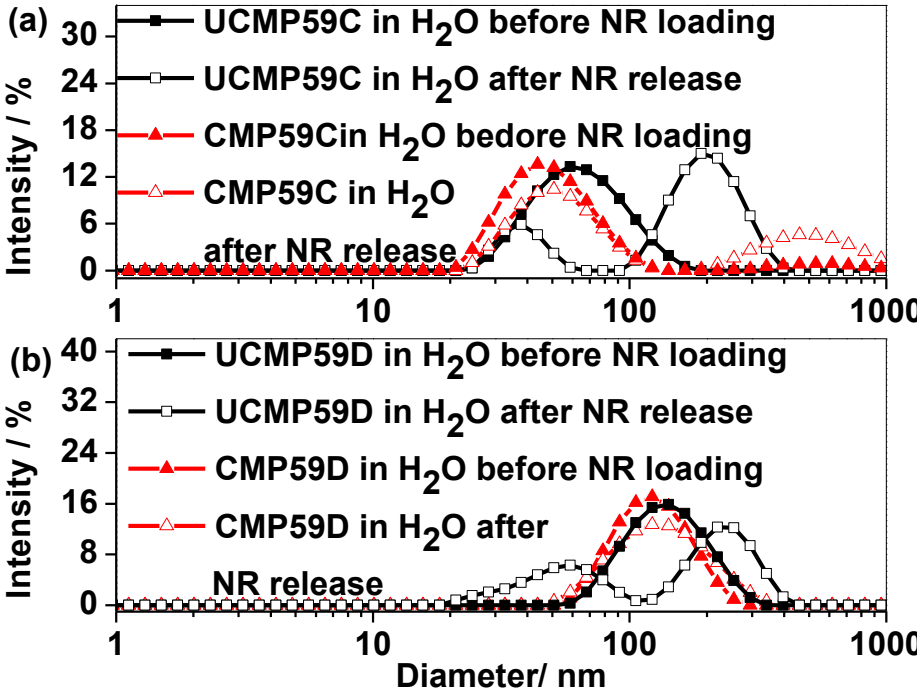

Figure 37. DLS size distribution of both uncross-linked and cross-linked micelles before and after nile red release.

The thiol-disulfide exchange reaction is an important reaction in many biological processes and protects important cellular components from reactive oxygen species. Cross-linkers that respond to external triggers such as redox agents would provide an element of control in the design and disassembly of crosslinked micelles and of control cargo release (**Scheme 43**). So cross-linker **64**, which should be responsive to the reducing agent (DTT) was used for cross linking. As shown in **Figure 38** and **Table 9**, the resulted cross-linked **CM*P59C** and **CM*P59D** showed an obvious size increase as indicated by DLS peaks which shifted after a 10-fold dilution with DMF. Upon treatment with 10 nM DTT, the diameters of both **CM*P59C** and **CM*P59D** in DMF further increased. Due to the fact that the swelled micelles **CM*P59C** and **CM*P59D** using cross-linkers **63** or **64** remained the same in DMF without DTT after 24h, the further diameter increase of **CM*P59C** and **CM*P59D** can be attributed to cleavage of the disulfide bond of cross-linker **64** via thiol-disulfide exchange which partially and gradually breaks the core cross linking, resulting in further swelling of the cross-linked micelles **CM*P59C** and **CM*P59D**. That the cross-linked core was only partially and gradually broken down was confirmed by the further size increase after a DMF solution of **CM*P59C** and **CM*P59D** micelles that had been treated with DTT were allowed to stand for 24h. Theoretically, the micelles should be disrupted completely and show no obvious DLS signals; however, DLS profiles showed light scattering of particles with diameters and PDI as 571 nm, 0.70 and 518 nm, 0.49 for CM3 and CM4, respectively (**Table 9**). These diameters were even larger than the corresponding DLS peak values. Further extending the reaction time or adding more DTT did not change the DLS traces. The micelle quality report from the DLS measurement indicated that the samples were

too poor or polydisperse for proper distribution analysis. So it is reasonable to conclude that DTT breaks all of the disulfide cross-linkers and disrupts the core cross-linked micelles in DMF. The reason why DLS still shows light scattering after DTT treatment remains unclear at this point.

In order to control the level of core cross-linking and thus the degree of disassembly upon treatment with DTT, a mixture of the inert cross-linker **63** and redox active cross-linker **64** (2:8) was used to give a mixed cross-linked core. As shown in **Figure 39** and **Table 9**, both mix cross-linked **CM**P59C** and **CM**P59D** swelled upon dilution with 10-fold DMF. After addition of DTT to the DMF solution of micelles, both the crosslinked **CM**P59C** and **CM**P59D** showed further hydrodynamic diameter increase which is attributed to disulfide bond cleavage of the cross-linker **64**. This reduces the level of core cross linking, and induces further swelling and size increases in the micelles **CM**P59C** and **CM**P59D**. In contrast to the micelles with only the redox active cross-linker **64**, the mix cross-linked **CM**P59C** and **CM**P59D** maintained micelle structure as evidenced by the DLS profiles after 24h in the presence of DTT at room temperature. This clearly demonstrates that the level of core cross-linking can be tuned by changing the feed ratios of the cross-linkers and thus can be used to control cargo release through tunable redox responsive properties of CMs.

Table 9. Hydrodynamic diameters and PDI of UCMs and CMs in different solvent

	Cross-linker	Solvent [a]									
		H_2O[b]		DMF[c]		DMF 24h[d]		DMF[e] (DTT)		DMF (DTT) 24h[f]	
		D	PDI	D	PDI	D	PDI	D	PDI	D	PDI
UCMP59C	--	61	0.23	--	--	--	--	--	--	--	--
UCMP59D	--	128	0.14	--	--	--	--	--	--	--	--
CMP59C	**63**	51	0.26	85	0.35	87	0.33	--	--	--	--
CMP59D	**63**	114	0.13	166	0.06	162	0.09	--	--	--	--
CM**P59C	**63**:**64** (2:8)	65	0.32	78	0.25	76	0.28	148	0.26	245	0.37
CM**P59D	**63**:**64** (2:8)	138	0.22	168	0.22	162	0.24	256	0.21	346	0.23
CM*P59C	**64**	67	0.33	75	0.28	76	0.25	113	0.28	571[g]	0.70[g]
CM*P59D	**64**	134	0.18	220	0.19	224	0.18	300	0.21	518[g]	0.49[g]

[a] Dispersion media of micelles. [b-f] Diameter (D, nm) and particle polydispersity index (PDI) of micelles were measured by DLS. [b] Micelles were dialyzed against water. [c] Micelles were diluted 10-fold with DMF and measured immediately by DLS. [d] Micelles were measured by DLS after dilution with 10-fold DMF and standing for 24 h in lab. [e] Micelles were diluted with 10-fold DMF in the presence of 10 nM DTT and measured immediately by DLS. [f] Micelles were measured by DLS after 10-fold dilution with DMF in the presence of 10 nM DTT and standing for 24 h in lab. [g] DLS reports were noted as poor or too polydisperse for distribution analysis. These data were the reported diameter and PDI.

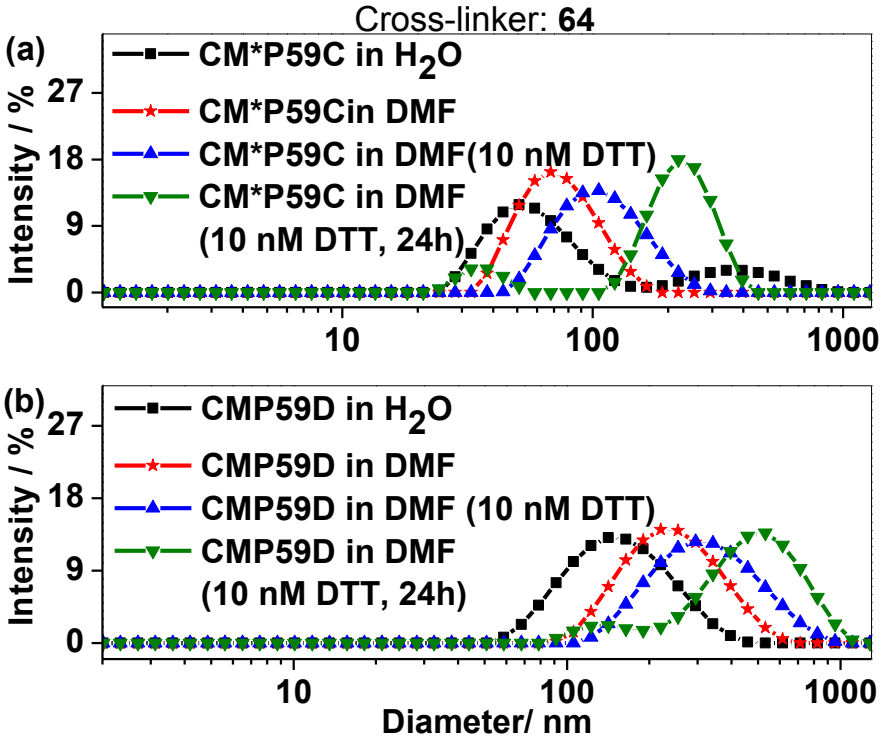

Figure 38. DLS size distribution of (a) **CM*P59C** and (b) **CM*P59D** in water before and after 10-fold dilution in DMF with or without 10 nM DTT (Cross-linker:**64**).

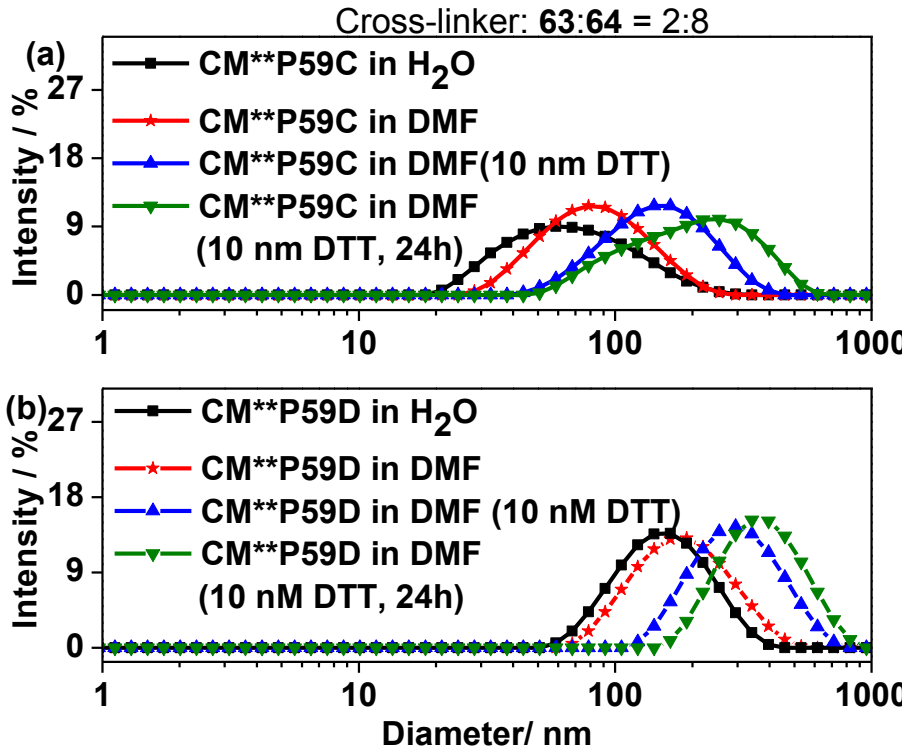

Figure 39. DLS size distribution of (a) **CM**P59C** and (b) **CM**P59D** in water before and after 10-fold dilution in DMF with or without 10 nM DTT (Cross-linker: **63**:**64** = 2:8).

3.3 Conclusion

The facile synthesis of propargyloxylactic acid (**12**) provides a convenient approach to the preparation of clickable polylactides (**P58** and **P59**) by the polymerization of hetero- and homo- monomers **58** and **59**. The kinetics of bulk polymerization was studied and clickable polylactides with pendant propargyl groups were obtained for further post-modification. The random copolymerization of monomers **58** and **59** with L-lactide was also successful to afford statistical copolymers as evidenced by DSC and ^{13}C NMR analysis. The click grafting of PEG chains, alkyl chains and a mixture of both to these polylactides provides side-chain grafted amphiphilic polylactides which exhibit thermo-responsive properties with LCST ranging from 22 to 65 ^{o}C depending on the ratio of incorporated PEG and alkyl chains that were grafted to the polymer. The greater the percentage of PEG chain that is incorporated onto the polylactide, the greater would be the increase in LCST due to the stronger hydrogen bonding with water. The amphiphilic block copolymers of PEG with **58** and **59** were also prepared to study their solution assembly behavior and the cross-linking of the core in the self-assembled micelles. The cross-linking of the core was confirmed by DLS and ^{1}H NMR spectra. The core cross-linked micelles have high dispersion stability in different solvents and provide controlled cargo release without affecting the micellar structure. Core cross-linked micelles with the disulfide cross-linker **64** conferred a redox-responsive property to the micelles which was triggered upon treatment with the reducing agent (DTT). These observations are suggestive potential application of this new class of cross-linked micelles in delivering pharmaceutical agents in a controlled release.

3.4 Experimental Section

Materials. Sodium azide, tosyl chloride (TsCl), tosylic acid (TsOH), bromoacetyl bromide, 1,5-dibromopentane, 2,2'-dithiodiethanol, D,L-dithiothreitol (DTT), 4-*tert*-butylbenyl alcohol (TBBA), triethylene glycol monomethyl ether (m3PEG) and 1-bromodecane were purchased from Sigma-Aldrich, Poly(ethylene glycol) monomethyl ether (M_n = 350, mPEG350; M_n = 2000, mPEG2k; M_n = 5000, mPEG5k) were purchased from Sigma-Aldrich and dried under high vacuum for 40h before use. Stannous octoate ($Sn(Oct)_2$) was freshly distilled under vacuum and kept in dry box before use. THF and toluene were dried over sodium and distilled before use. Triethylamine (Et_3N) was dried over calcium hydride and distilled before use The silica gel (60 Å porosity) for column chromatography was purchased from SiliCycle Inc. All other reagents and solvents were ACS grade and used as received unless specified.

Characterization. Melting points were measured on Electrothermo® melting point apparatus. ^1H NMR and ^{13}C NMR were recorded on a Varian 300 MHz, VXR-500 MHz or 600 MHz instrument in $CDCl_3$ unless otherwise noted. $CDCl_3$ was used as the internal standard for both ^1H NMR (δ = 7.24) and ^{13}C NMR (δ = 77.0). Analytical thin-layer chromatography (TLC) was performed on silica gel plates with F-254 indicator. FT-IR spectra were taken with Mattson Galaxy FT-IR 3000. HRMS were taken on Waters Xevo G2-S TOF UPLC/TOF MS. Thermogravimetric analysis (TGA) was recorded on Perkin-Elmer TGA 7 at a heating/cooling rate of 10 $^{\circ}C$ under air. Differential scanning calorimetry analysis of the polymers (DSC) was recorded on DSC-Q100 at a

heating/cooling rate of 10 °C under nitrogen and the second heating scan was used for analysis. Dynamic Light Scattering (DLS) was performed in a Malvern NanoZS ZetaSizer with a 178 degree backscattering detection (Malvern, UK) to give both size and zeta potential of the samples. TEM images were collected on a JOEL 2200FS electron transmission microscope. The micelle was deposited by putting one drop of the solution on the carbon-coated copper grid and then the solution was sucked away after 5 mins to keep the micelle integrity.

Polymer molecular weights were determined by GPC-MALLS 35 °C using two PLgel 10μ mixed-B columns in series (manufacturer-stated linear molecular weight range of 500-10×10^6 g/mol). The eluting solvent was THF at a flow rate of 1 mL/min. A Waters 2410 differential refractometer was used as the detector and an Optilab rEX (Wyatt Technology Co.) and a DAWN EOS 18-angle light scattering detector (Wyatt Technology Co.) with a laser wavelength of 684 nm were used to calculate absolute molecular weights. Uv-vis spectra were recorded with Evolution 600 BB Uv-visible spectrophotometer (Thermo Electron Corporation) with a polymer concentration at ~3 mg/mL.

Fluorescence was recorded using E4500 fluorescence spectrophotometer from Hitachi and the fluorescence emission spectra were observed from 580-900 nm with excitation wavelength at 561 nm. Contact angle was measured on VCA2000 (video contact angle system) with Fostec controller.

Synthesis of hetero-monomer (58). Propargyloxylactic acid (7.5 g, 52 mmol) and 200 mL of dry THF were added to a 500 mL 3-neck flask under nitrogen. After cooled to

0 °C, 2-bromoacetyl bromide (5.7 mL, 65 mmol) was added. Then a solution of Et_3N (11 mL) in THF (50 mL) was added dropwise. After stirring for 5 h at 0 °C, the mixture was filtered to remove white precipitate and the filtrate was concentrated to remove THF and redissolved in ethyl acetate (200 mL). After washed with 1 M HCl (4 x 100 mL) and saline (8 × 100 mL) and dried over $MgSO_4$, filtration and removal of the solvent *in vacuo* gave the crude linear acid ester as a viscous liquid (13.8 g). Then this ester was dissolved in a acetone (1.5 L) and refluxed for 24 h in the presence of $NaHCO_3$. The solids were removed by filtration and the filtrate was concentrated *in vacuo*. The residue was dissolved in ethyl acetate (250 mL), washed with 1 M HCl (2 x 100 mL), saturated $NaHCO_3$ (2 x 100 mL) and saturated NaCl (5 × 50 mL), and then dried over $MgSO_4$. The product was purified by flash chromatography with CH_2Cl_2/EtOAc (19:1) and dried under vacuum to give viscous liquid which turned to wax solid upon standing in the dry box, 1.86 g, 39%. R_f = 0.42. ^{1}H NMR (500 MHz, $CDCl_3$) δ 5.12 (d, 1H, *J* = 15 Hz), 5.10 (t, 1H, *J* = 5 Hz), 4.84 (d, 1H, *J* = 15 Hz), 4.24 (d, 1H, *J* = 5 Hz), 4.16 (dd, 1H, *J* = 10 and 5 Hz), 4.03 (dd, 1H, *J* = 10 and 5 Hz), 2.52 (t, 1H, *J* = 5 Hz); ^{13}C NMR (125 MHz, $CDCl_3$) δ 164.22, 163.32, 77.46, 76.34, 76.23, 70.38, 65.39, 59.03; IR 3286, 2944, 2878, 2122, 1763, 1443, 1374, 1286, 1237, 1107, 1068, 1038, 848 cm^{-1}; HRMS(m/z) calcd for $C_8H_9O_5$ 185.0451, $[M+1]^+$, found 185.0457.

Synthesis of homo-monomer (59). Racemic propargyloxylactic acid (10.5 g, 73 mmol) and *p*-toluenesulfonic acid monohydrate (1 g) were added to a 2-L round bottom

flask charged with 1.5 L of toluene. The flask was heated gently overnight until all acids were dissolved in toluene to give a slight yellow solution (Note: fast heating could decompose the propargyloxylactic acid). Then the mixture was heated to reflux for 11 days to achieve a conversion of 69% while removing water azeotropically using a Dean-Stark trap. After cooled to room temperature, the toluene was removed and the residue was dissolved in 500 mL of CH_2Cl_2, washed with saturated aqueous $NaHCO_3$ (3 x 150 mL) and dried over $MgSO_4$. Filtration and removal of the CH_2Cl_2 gave the product as a light brown liquid as a mixture of trans-diasteremer (RS) and cis-diastereomers (RR, SS), 5.51 g, ~60% yield. This brown liquid was purified by flash chromatography with CH_2Cl_2/EtOAc (19:1) to give white solid as the pure trans-diastereomer which was dried under vacuum and kept in dry box, 2.90 g, 32%. R_f = 0.60. m.p. 125-128 °C. ^{1}H NMR (500 MHz, $CDCl_3$) δ 5.20 (t, 2H, *J* = 2.5 Hz), 4.23 (d, 4H, *J* = 3 Hz), 4.14 (dd, 2H, *J* = 10 and 2.5 Hz), 4.03 (dd, 2H, *J* = 10 and 2.5 Hz), 2.50 (t, 2H, *J* = 2.5 Hz); ^{13}C NMR (125 MHz, $CDCl_3$) δ 164.09, 77.94, 76.43, 75.94, 69.52, 59.01; IR 3291, 2933, 2878, 2122, 1760, 1463, 1446, 1361, 1311, 1278, 1231, 1198, 1123, 1057, 922 cm^{-1}; HRMS(m/z) calcd for $C_{12}H_{13}O_6$ 253.0712, $[M+1]^+$, found 253.0711.

Synthesis of 1-(2-azidoethoxy)-2-(methoxyethoxy) ethane (m3PEGN_3). A saturated aqueous solution of NaOH (40 g, 1.0 mol) was added to a mixture of triethylene glycol monomethyl ether (34.0 g, 210 mmol) and tosyl chloride (TsCl) (59.0 g, 300 mol) in 400 mL of THF dropwise at 0. The mixture was stirred overnight at room

temperature. The mixture was poured into ice water and the water layer was extracted with ether (3 x 150 mL). The combined organic layer was washed with saturated aqueous NaCl, dried over Na_2SO_4 and concentrated. The resulted tosylate was used without further purification (60 g, 91 %). The prepared tosylate (29 g, 91 mmol), NaI (1 g) and sodium azide (9.50 g, 137 mmol) were mixed in 150 mL of DMF and stirred at 60 °C for 24 h. After cooled and added 100 mL of water, the product was extracted with ether (4 x 100 mL) and was washed with saturated aqueous NaCl (5x 100 ml) and dried over Na_2SO_4. After removal of ether, the product was purified via vacuum distillation to provide 1-(2-azidoethoxy)-2-(methoxyethoxy) ethane (m3PEGN_3) as a colorless liquid, b. p. 78 °C, 38 mTorr, 10.6 g, 62 %. ^{1}H NMR (500 MHz, $CDCl_3$) δ 3.65-3.62 (m, 8H), 3.53-3.51 (m, 2H), 3.36-3.34 (m, 5H); ^{13}C NMR (125 MHz, $CDCl_3$) δ 71.88, 70.66, 70.61, 70.57, 69.98, 58.89, 50.57; IR 2920, 2872, 2096, 1445, 1338 cm^{-1}.

Synthesis of 1-azidodecane ($C_{10}H_{21}N_3$). 1-bromodecane (22.1 g, 100 mmol), NaI (1 g) and sodium azide (9.50 g, 137 mmol) in DMF (100 mL) were stirred at 60 °C overnight. After cooled, the mixture was filter and dissolved in CH_2Cl_2, washed with water (6x 100 mL) and dried over Na_2SO_4. After removal of the solvent, the product was obtained as a colorless liquid, 16.2 g, 88 %. ^{1}H NMR (500 MHz, $CDCl_3$) δ 3.26 (t, 2H, *J* = 7.5 Hz), 1.61 (m, 2H), 1.22-1.42 (m, 14H), 0.89 (t, 2H, *J* = 7.5 Hz); ^{13}C NMR (125 MHz, $CDCl_3$) δ 51.49, 31.86, 29.49, 29.47, 29.27, 29.14, 28.83, 26.71, 22.65,

14.07; IR 2927, 2856, 2100, 1457, 1352, 1286, 892, 727 cm^{-1}.

Synthesis of 1,5-diazidopentane (63). 1,5-dibromopentane (11.4 g, 50.0 mmol), NaI (1 g) and sodium azide (14.2 g, 218 mmol) were dissolved in DMF (75 mL) and stirred overnight in 60 °C oil bath. Water (100 mL) was added and the solution was extracted with diethyl ether (2 x 75 mL). The organic phase was combined, washed with water (2 x 30 mL), and dried over $MgSO_4$. After filtration and solvent evaporation, a colorless oil was obtained, 5.0 g, 65 %. ^{1}H NMR (500 MHz, $CDCl_3$) δ 3.25 (t, 4H, J = 7.5 Hz), 1.61 (m, 4H), 1.44 (m, 2H); ^{13}C NMR (125 MHz, $CDCl_3$) δ 51.07, 28.28, 23.80; IR 2946, 2878, 2104, 1458, 1351, 1266, 900, 858 cm^{-1}.

Synthesis of bis-azidoethyl disulfide (64). 2,2'-dithiodiethanol (6.1 g, 40 mmol) and triethylamine (TEA, 11.1 g, 110 mmol) were dissolved in chloroform (65 mL) and cooled to 0 °C. TsCl (22.8 g, 120 mmol) in chloroform (30 mL) was added dropwise. After stirring at room temperature for 16 h, the reaction mixture was filtered, washed with saturated sodium carbonate solution (3 × 40 mL) and then with DI water (3× 50 mL). The organic phase was dried over $MgSO_4$, filtered, and evaporated under vacuum to give the tosylate which was used directly, 11.4 g, 62 %. Sodium azide (9 g, 65 mmol) in DI water (30 mL) was added to the acetone solution (150 mL) containing the obtained tosylate. Then the mixture was stirred at 80 ^{o}C overnight followed by removal of acetone under reduced pressure. The product was extracted with dichloromethane (4 × 50 mL), and the combined organic layer was dried over $MgSO_4$, filtered, and concentrated under vacuum to afford a light yellow oil, 4.2 g, 51 %. ^{1}H NMR (500 MHz,

$CDCl_3$) δ 3.61 (t, 4H, *J* = 5 Hz), 2.88 (t, 4H, *J* = 7.5 Hz); ^{13}C NMR (125 MHz, $CDCl_3$) δ 49.94, 37.62; IR 2927, 2872, 2104, 1448, 1413, 1346, 1291, 1256, 1224, 903 cm^{-1}.

General procedure for bulk polymerizations. In a dry box, a small magnetic stir bar was put into a bulb prepared from a 3/8 in. diameter glass tubing with a 1-inch diameter bulb blown on one end. Then weighed monomer in 5-mL vial was dissolved in THF followed by the addition of predetermined toluene solution (0.04 M) of catalyst ($Sn(Oct)_2$) and initiator (TBBA) separately. Then this solution was transferred to the bulb via pipette. After the bulb was connected to a T-shape vacuum adapter via cajon fitting, it was taken out of the dry box and connected to vacuum to remove the solvent carefully followed by holding under high vacuum for 10 h at room temperature. After the bulb was filled back with nitrogen, it was immersed in 130 ^oC oil bath for polymerization. At the desired period of time, the bulb was removed from the bath, quenched in ice water and opened. A portion of the polymer was analyzed by ^1H NMR for conversion. The remaining polymer was dissolved in CH_2Cl_2, precipitated from cold methanol/hexanes twice and dried under high vacuum at room temperature for 24 hours.

Polymerization of Hetero-monomer (58). 58 (92 mg) was polymerized for 15 min with [M]/[I] = 50. The conversion calculated from ^1H NMR was 89%. Precipitation and drying under vacuum gave 65 mg **P58** as a pale red sticky solid (70.6%). ^1H NMR: δ 5.37-5.55 (br, 1H), 4.72-4.97 (br, 2H), 4.20-4.27 (br, 2H), 3.95-4.10 (br, 2H), 2.44-2.58 (br, 1H); $M_{n,\ NMR}$ = 8,300 g/mol; GPC (THF): M_n = 10,800 g/mol, PDI = 1.42. Other

ratios at 25, 100 and 200 were also prepared.

Polymerization of Homo-monomer (59). 59 (126 mg) was polymerized for 40 min with [M]/[I] = 50. The conversion calculated from ^{1}H NMR was 87%. Precipitation and drying under vacuum gave 95.0 mg **P59** as a wax-like sticky solid (75.4%). ^{1}H NMR: δ 5.37-5.60 (br, 1H), 4.17-4.27 (br, 2H), 3.90-4.12 (br, 2H), 2.45-2.58 (br, 1H); $M_{n,\ NMR}$ = 13,000 g/mol; GPC (THF): M_n = 10,100 g/mol, PDI = 1.46. Other ratios at 25, 100 and 200 were also prepared.

Copolymerization of 58 and *L*-lactide. A mixture of **58** (23.0 mg, 0.125 mmol) and *L*-lactide (18.0 mg, 0.125 mmol) was polymerized for 15 min with [M]/[I] = 100 Precipitation and drying under vacuum gave 30.0 mg of copolymer **P58-*co*-LA** as a light yellow solid (73.2%). ^{1}H NMR: δ 5.38-5.56 (br, 1H), 5.17-5.32 (br, 2H), 4.66-4.98 (br, 2H), 4.20-4.27 (br, 2H), 3.90-4.10 (br, 2H), 2.45-2.56 (br, 1H), 1.45-1.62 (br, 3H); $M_{n,\ NMR}$ = 12,600 g/mol. Other feed ratios of **58** to lactide at 3:1 and 1:3 were also conducted.

Copolymerization of 59 and *L*-lactide. A mixture of **59** (31.0 mg, 0.125 mmol) and *L*-lactide (18.0 mg, 0.125 mmol) was polymerized for 40 min with [M]/[I] = 100 Precipitation and drying under vacuum gave 30.0 mg of copolymer **P59-*co*-LA** as a light yellow solid (77.6%). ^{1}H NMR: δ 5.40-5.56 (br, 2H), 5.17-5.33 (br, 2H), 4.18-4.28 (br, 2H), 3.89-4.12 (br, 2H), 2.45-2.56 (br, 1H), 1.45-1.62 (br, 6H); $M_{n,\ NMR}$ = 17,100 g/mol. Other feed ratios of **59** to lactide at 3:1 and 1:3 were also conducted.

Amphiphilic block copolymers of 58 and 59 with mPEGs as initiators. **P59D** was prepared from initiator mPEG5k (150 mg) and **59** (151 mg, 0.600 mmol) with [M]/[I] = 30. The conversion was 88%. The isolated polymer was as light yellow solid, 260 mg, 86.4%. ^{1}H NMR: δ 5.36-5.55 (br, 1H), 4.17-4.26 (br, 2H), 3.89-4.12 (br, 2H), 3.45-3.78 (br, 420H), 3.35 (s, 3H), 2.42-2.54 (br, 1H); $M_{n,\ NMR}$ = 12,300 g/mol. **P58B, P59B** and **P59C** were also prepared with high conversions (>90%) and good yield.

General procedure for "click" functionalization. The desired amount of propargyl functionalized polymer, three equivalents of azide and 10 mol % of sodium ascorbate (10 mg/mL in water) were dissolved in DMF in a 20-mL vial, and the solution was deoxygenated by two freeze-pump-thaw cycles. Then 5 mol % of $CuSO_4$ (10 mg/mL) was added to the frozen mixture under a nitrogen purge followed by evacuation. After backfilled with nitrogen, the solution was stirred at room temperature under nitrogen for 12 h. At the end of the reaction, DMF was blown away by gentle nitrogen flow and the viscous liquid was then washed with hexane and ether to remove the impurities and then dried under vacuum.

1-Azidodecane ($C_{10}H_{21}N_3$)-grafted P59. P59 (([M]/[I] = 50, 9.2 mg) and 40 mg of 1-azidodecane were dissolved in 6 mL DMF for the click reaction. The decane-grafted **P59** was isolated as a sticky solid, conversion: 100%, 19 mg, 81.2%. ^{1}H NMR: δ 7.5-7.9 (br, 1H), 5.2-5.6 (br, 1H), 4.5-4.8 (br, 2H), 4.2-4.4 (br, 2H), 3.7-4.15 (br, 2H), 1.8-2.0 (br, 2H), 1.1-1.4 (br, 14H), 0.8-0.9 (br, 3H); $M_{n,\ NMR}$ = 20,900 g/mol.

1-(2-azidoethoxy)-2-(methoxyethoxy) ethane (m3PEGN_3)-grafted P59. P59

(([M]/[I] = 50, 7.5 mg) and 34 mg of m3PEGN_3 were dissolved in 5 mL DMF for the click reaction. The m3PEG-grafted **P59** was isolated as a sticky solid, conversion: 69%, 11 mg, 73.3%. ^{1}H NMR: δ 7.5-7.9 (br, 1H), 5.2-5.6 (br, 1H), 4.5-4.8 (br, 2H), 4.2-4.4 (br, 2H), 3.7-4.15 (br, 4H), 3.4-3.68 (br, 8H), 3.2-3.4 (BR, 3H), 2.5 (br, 0.4H, leftover terminal alkyne), 1.1-1.4 (br, 14H), 0.8-0.9 (br, 3H); $M_{n,\ NMR}$ = 18,300 g/mol.

m3PEGN_3/$C_{10}H_{21}N_3$ (2:1 and 7:2)-grafted P59. Two ratios of m3PEGN_3/$C_{10}H_{21}N_3$ were used to graft both PEG and alkyl chains on to **P59**. Conversions were quantitative for both of them.

Measurement of LCST. The LCST of the grafted polymer samples was tested by measuring the absorbance of the solution at 450 nm while varying the temperature. The aqueous polymer solution (1 mL) was placed in cuvette and put into Uv-vis spectrophotometer with a programmed temperature control function. Then the absorbance at 450 nm was taken and plotted as a function of temperature. The midpoint of the solution-gel transition was taken as the LCST.

Preparation of uncross-linked micelles (UCM) and measurement of critical micelle concentration (CMC).

A. Acetone solution method: **P58B** or **P59B** (1.8 mg each) was dissolved in acetone (0.6 mL; 3 mg/mL polymer) and it was added to water (3.6 mL; 0.5 mg/mL UCM) slowly added under vigorous stirring in 20-mL vial. After vigorous stirring for another 10 mins at room temperature, the UCM micelles were purified by dialysis against DI water for 24 h to remove acetone (MWCO of 3.5k Da).The CMC of the micelle was tested using Nile Red as a fluorescence probe. Excess of Nile Red in chloroform (0.1 mg/mL, 10 μL) was

added to a glass vial and dried completely. Then a micelle solution (1 mL) with different concentration was added and shaken before settling down for 1 h. Then the fluorescence of the polymer solutions excited at 557 nm was taken and the peak fluorescence intensities were plotted versus concentration to give their CMC.

B. DMF solution method: In a 20-mL vial, water (10 mL) was slowly added to the solution of **P59C** or **P59D** (5 mg each) in DMF (1 mL; 5 mg/mL polymer) dropwise under vigorous stirring. The final concentration of polymers was 0.5 mg/mL. After vigorous stirring for another 10 mins at room temperature, the UCM micelles were purified by dialysis against DI water for 24 h to remove DMF (MWCO of 3.5k Da). The CMC of the micelle was tested similar as discussed above.

Preparation of cross-linked micelles (CM) of P59C and P59D. Water (10 mL) was slowly added to the solution of **P59C** or **P59D** (5 mg each) and 0.6 equiv. of cross-linker (**63**, **64** or a mixture **63** and **64** (**2:8**)) in DMF (1 mL; 5 mg/mL polymer) dropwise under vigorous stirring to afford UCM solution at 0.5 mg/mL. The vigorous stirring was kept for another 10 mins at room temperature before the UCM micelles were purified by dialysis against DI water. Then the UCM solution was deoxygenated by two freeze-pump-thaw cycles followed by the addition of 5 mol % of $CuSO_4$ (10 mg/mL) and 10 mol % of sodium ascorbate (10 mg/mL in water) to the frozen mixture under nitrogen flow. After another freeze-pump-thaw cycle, the vial was filled with nitrogen and stirred at room temperature for 12 h. After the cross-linking, the CMs were purified by dialysis (MWCO of 3.5k Da) and subjected for further characterization.

Nile Red release experiment. Nile Red loaded UCMs or CMs were placed into dialysis tubing and dialyzed with deionized water. Removing aliquots of the micelle

solution from the dialysis bag and measuring their fluorescence to monitor the continual release of Nile Red over 70 hours. After analysis, the micelle solution was returned to the dialysis bag and the surrounding water was replaced. And after Nile Red released, the hydrodynamic diameter of the micelles were measured by DLS.

CHAPTER 4 SYNTHESIS OF POLYSPIROLACTIDES

4.1 Introduction

Thermal properties of the polymeric materials define their process and application temperature range. Glass transition, one important concept in polymer science, is a function of polymer chain flexibility and mobility when there is enough vibrational/thermal energy to create sufficient free-volume to permit the polymer chain movement. A polymer behaves in an increasingly rigid and brittle manner, termed as glassy state, when temperature is below its T_g. Above the T_g of one polymer, the polymer would be more tough and leathery as rubbery state. All polymers have some temperature range where their physical properties are rigid and glassy. In glassy state, the structural and mechanical behavior of polymers is relatively stable and do not change significantly with temperature due to the restricted chain diffusion.

Several approaches can be used to tune the T_g of polymer, including molecular weight, tacticity, polymer architecture and the presence of plasticizer. In addition, the T_g of polymers can be raised by increasing the rotational barrier or interaction of polymer backbone. Increasing the polymer chain-chain interaction to make the polymer chains more “sticky” and thus raise the T_g, such as including polar groups or hydrogen bonding in the polymer structure. Incorporating rigid elements or bulky ring structures in or along polymer backbone, such as *para*-aromatic rings, would restrict the single bond rotation to raise the T_g. For PLA, replacing the methyl group on the lactide ring with bulky substituents, such as branched or cyclic groups can increase the bond rotation barrier

and thus the T_g. Baker and co-workers have prepared a series of lactide monomer derivatives with substituents ranging from linear, cyclic alkyl groups to phenyl groups to explore monomer structural effect on the thermal properties of PLA based materials, whose T_g increased to 100 and 98 ^{o}C for phenyl or cyclohexyl substituents, respectively.[61, 173] More recently, Hillmyer and coworkers have reported that spirolactide monomers can be prepared by Diels-Alder reaction to afford norbornane, cyclohexadiene and isoprene substituted lactides with high yield.[74,108] The polyspirolactides containing different cyclic structures on polymer backbones after polymerization exhibit much higher T_g than polylactide in the range of 76 to 119 ^{o}C.

We are interested in the synthesis of polyspirolactides incorporated with different sized cyclic rings and their effect on thermal properties, such as T_g, of the corresponding polylactides due to the essentially rigid ring structure of cyclic rings.

4.2 Results and Discussion

4.2.1 Monomer Synthesis

The spirolactide monomers (**72a-c**) were prepared using cyclic ketones (**69a-c**) as starting materials. The ketones were treated with KCN in the presence of $Na_2S_2O_5$ to give cyanohydrins after extraction which were directly hydrolyzed to their α-hydroxy acids (**70a-c**) at ~ 80% overall yield after continuous extraction and recrystallization. Then they were condensed with bromopropionyl bromide to form linear esters (**71a-c**) which were cyclized under mild basic condition in acetone to afford crude spirolactide

monomers (**72a-c**). The monomers were purified by recrystallization from ethyl acetate/hexane and flash column chromatography using dichloromethane as eluent to give white solid at ~55-62% yield. It is worth noting that sublimation after recrystallization cannot supply monomers pure enough for polymerization.

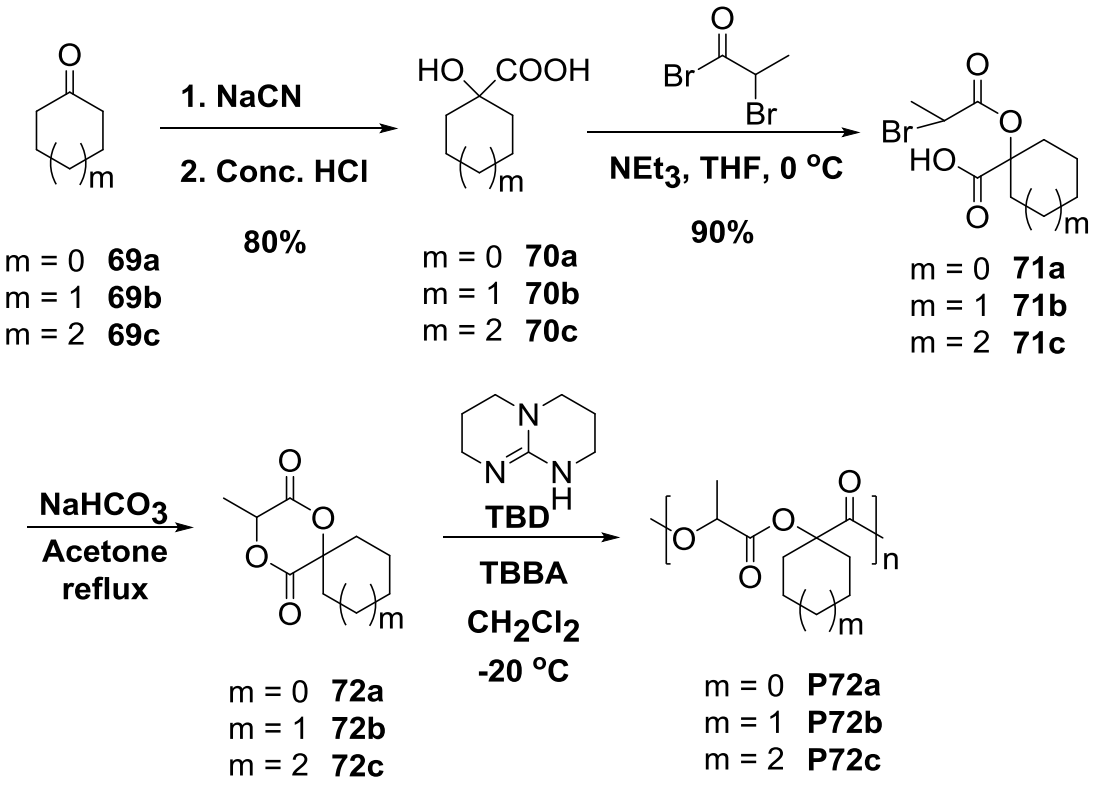

Scheme 44. Synthesis of spirolactide monomers and polyspirolactides

4.2.2 Solution Polymerization

The solution polymerization was conducted in dichloromethane using triazabicyclodecene (TBD) as catalyst and TBBA as initiator. Due to the basic and nucleophilic nature of the catalyst TBD and the slight acidic and electrophilic nature of the solvent dichloromethane, we conducted the stability experiments of TBD in dichloromethane at different temperature by recording their ^{1}H NMR spectra in CD_2Cl_2

in order to search for the best condition. As shown in **Figure 40**, TBD right after dissolved in CD_2Cl_2 showed only three sets of well splited proton resonances at 1.9, 3.1 and 3.2 ppm which correspond to three methylene groups at 25, 5 and -20 ^oC. After standing for 96 h at 25 and 5 ^oC, TBD gave completely different proton resonances in ^1H NMR spectra, which indicates the TBD lost its original structure and catalytic activity. This is confirmed by the very low yield and low molecular weight of the resulted polymers (data is not shown here). However, TBD displayed very high stability by showing exact same three sets of proton resonances as those at 0 h after standing for 96 h at -20 ^oC. The preliminary polymerization of **72b** gave polymer at 43% yield. Apparently, TBD and solvent CD_2Cl_2 reacted with each other more likely through SN2 reaction to give one inactive catalyst.[174,175]

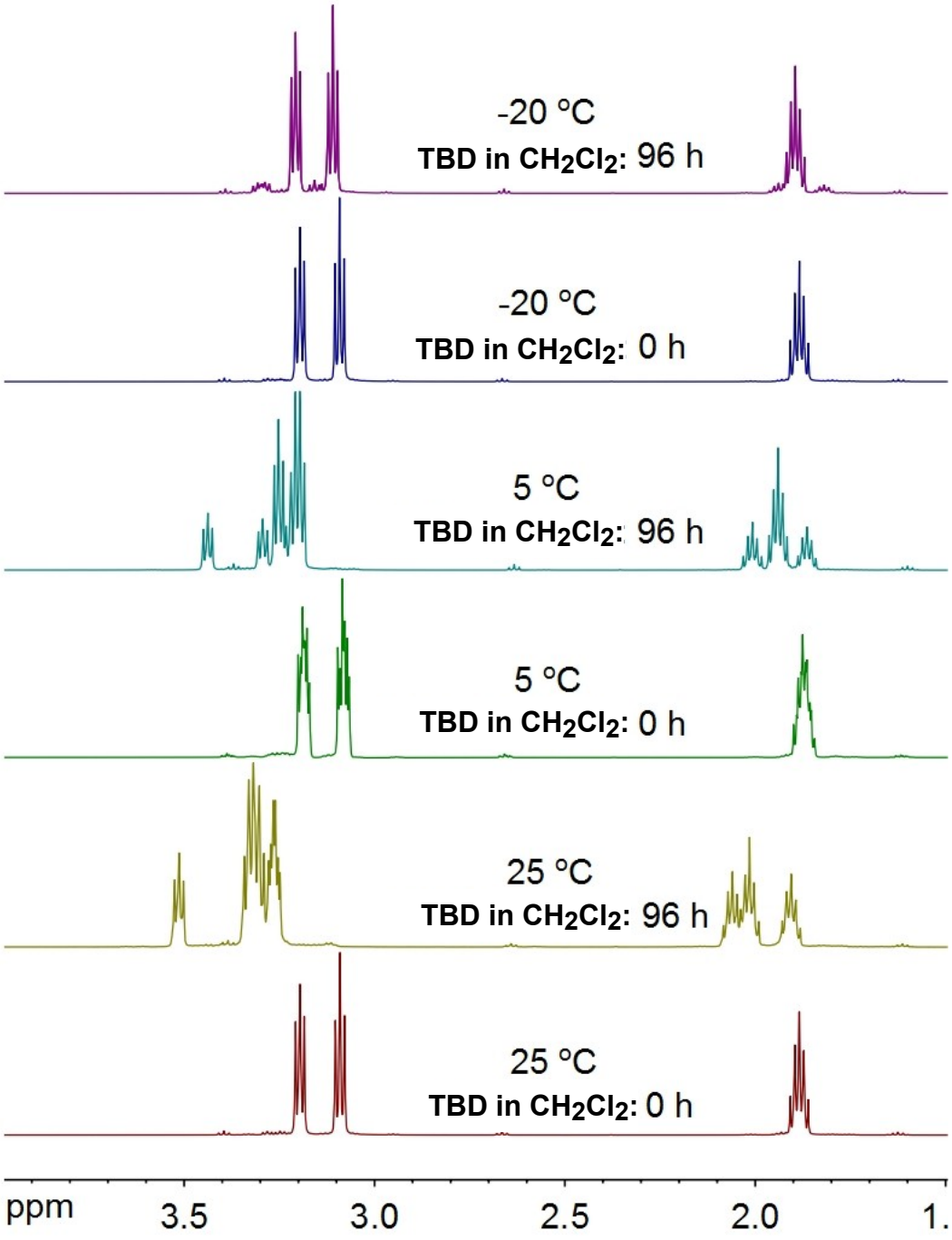

Figure 40. ^{1}H NMR spectra of TBD in CD_2Cl_2 at different time and temperature.

The kinetics was conducted in dichloromethane in order to optimize the polymerization conditions. Solution polymerizations were carried out using TBD as catalyst and TBA as initiator with fixed [M]/[I] ratio at 100:1 but slight different catalyst

feeding in order to obtain polymer products. The ratio of catalyst to initiator ([cat]/[I]) is 1:1 for **72a** and **72b**, and 1.5:1 for **72c**. Due to the steric hindrance of spirolactide monomers, the solution polymerizations proceeded fairly slow compared to lactide which was polymerized too fast under same conditions (less than 1 min in our case) and kinetics data were failed to be taken. The solution polymerization of lactide catalyzed by TBD at room temperature was reported to give 99% conversion after 20s (**Figure 41**).[22] The polymerization of **72a** and **72c** achieved higher conversions (up to 95%) than **72b** which only gave 83% after 100 h. And the polymerization rates depend on the ring size of the lactide ring substituents. Solution polymerization of the spirolactides should also follow first order kinetics as described by equation (**2**, Chapter **3**), and plots of $-\ln([M]_t/[M]_0)$ versus time *t* should be linear for low monomer conversions as shown in **Figure 42**. The apparent rate constant values were extracted from the slope of the linear fitted plots and listed in **Table 10**. As we can see from **Table 10**, ring size of the substituents showed significant effect on their polymerization rates with **72a** about 6x and 9x times faster than **72b** and **72c**, respectively. The much smaller size of cyclopentyl group compared to cyclohexyl and cycloheptyl groups enables **72a** to polymerize faster; however, increasing ring size to cycloheptane did not slow down the polymerization too much compared to **72b**, which is probably due to the more flexible ring structure in cycloheptane than cyclohexane, though the steric hindrance is bigger.[176] This effect was also reflected in reversed glass transition temperature trend which will be discussed later.

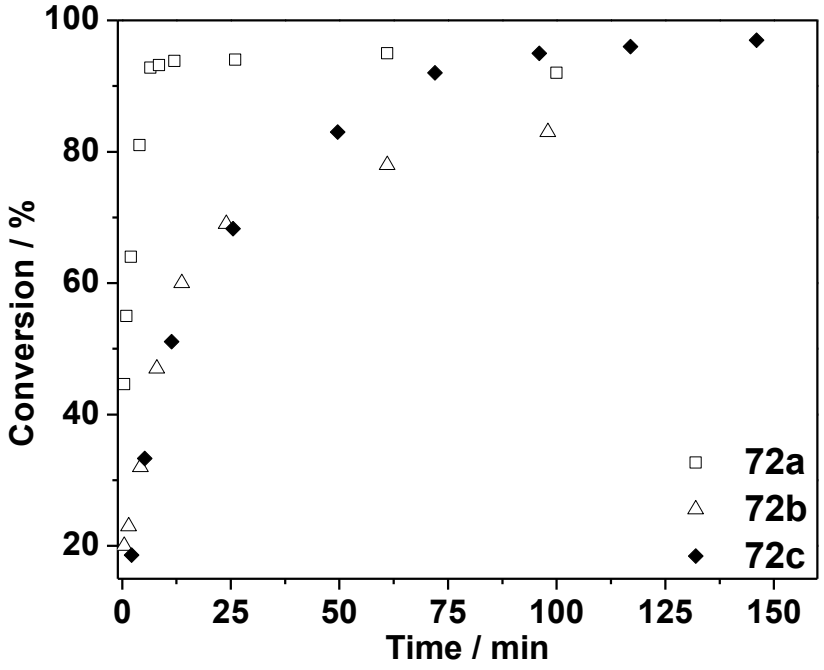

Figure 41. Conversions for solution polymerization of **72a**, **72b** and **72c**. Conditions: -20 ^{o}C in CH_2Cl_2, [M] = 1 M, [M]/[cat]/[I] = 100:1:1 for **72a** and **72b**; [M]/[cat]/[I] = 100:1.5:1 for **72c**.

Table 10. Solution polymerization rates of **72a**, **72b** and **72c**.

monomer	K_p (L S^{-1} mol^{-1}) x 10^2
72a	9.28
72b	1.49
72c	1.08

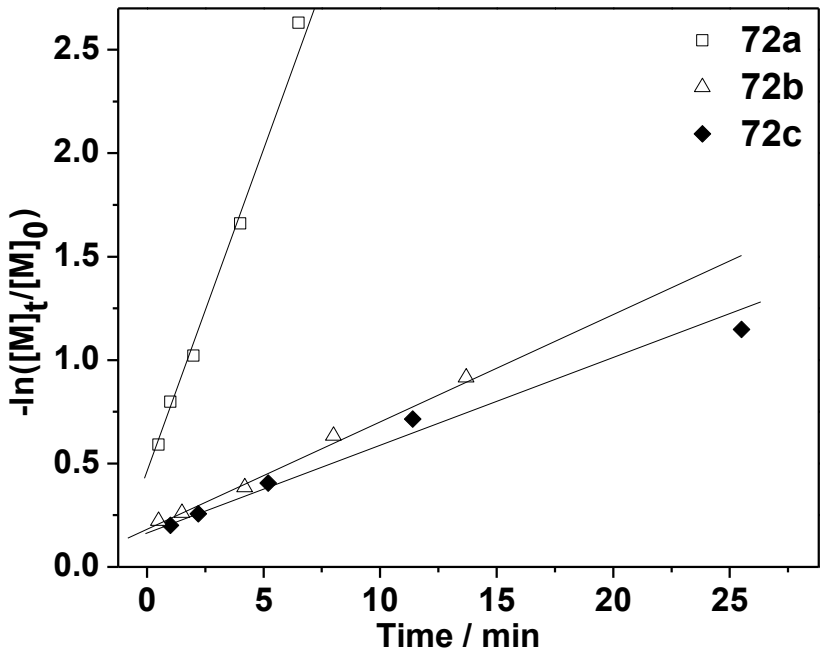

Figure 42. Solution polymerization kinetics of **72a**, **72b** and **72c**. Conditions: -20 ^{o}C in CH_2Cl_2, [M] = 1 M, [M]/[cat]/[I] = 100:1:1 for **72a** and **72b**; [M]/[cat]/[I] = 100:1.5:1 for **72c**.

As shown in **Figure 43**, M_n of polyspirolactides increased with increasing the polymerization time until it reached high conversions. The PDI also remains narrow (~1.1) and then raised gradually when high conversions were achieved. These results indicate that ring-opening polymerization by TBD at low conversions is living “in nature” and intra- and intermolecular transesterification happen at high conversions which results in the drop of M_n and increase of PDI. The polymerization of these spirolactide monomers with different [M]/[I] ratios were carried out using the optimized condition for each monomer. The results are listed in **Table** 11, which showed relatively good agreement between feed ratio and X_n from NMR with higher deviation at higher [M]/[I] ratio. GPC results indicate the increase of M_n and narrow PDI for all the polymer

samples. GPC profiles of the polymers shift to shorter elution times with increasing [M]/[I] ratios as shown in **Figure 44**, **Figure 45** and **Figure 46**, since large polymers elute out of GPC faster by traveling less in size exclusion chromatography (SEC).[177] These results indicate polymers with higher molecular weight were obtained by changing feed ratio of monomer to initiator. The PDI as determined from GPC is around 1.4-1.6 for all of the polymers and is not affected by the GPC calculation.

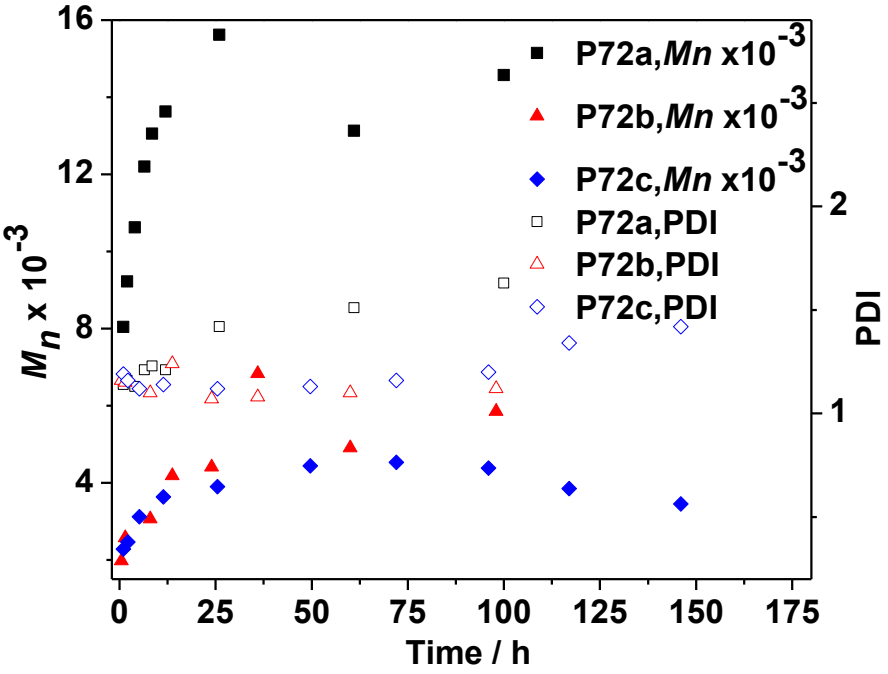

Figure 43. The evolution of molecular weight (M_n) from GPC and PDI with time for **72a**, **72b** and **72c**. Conditions: -20 ^{o}C in CH_2Cl_2, [M] = 1 M, [M]/[cat]/[I] = 100:1:1 for **72a** and **72b**; [M]/[cat]/[I] = 100:1.5:1 for **72c**.

Table 11. Solution polymerizations of **72a**, **72b** and **72c** at -20 °C.[a]

entry	M	[M]/[I]	t/h	Conv. (%)[b]	X_n[c]	X_n[d]	M_n (x 10^{-3}) [e]	PDI[e]	T_g °C
1		100	24	94	94	91	24.0	1.32	63
2	**72a**	200	50	95	190	175	30.7	1.32	64
3		300	90	93	279	242	36.0	1.37	65
4		100	50	72	72	60	10.6	1.16	69
5	**72b**	200	110	75	150	132	12.5	1.09	70
6		300	230	79	247	200	14.2	1.28	71
7		100	90	89	89	74	9.2	1.11	53
8	**72c**	200	200	85	170	127	9.6	1.12	55
9		300	300	87	261	202	10.2	1.15	56
10	**LA**	--	--	--	--	--	--	--	55[f]

[a] TBD as the catalyst and TBBA as initiator, -20 °C in CH_2Cl_2, [M] = 1 M, [cat]/[I] = 1:1 for **72a** and **72b**; [cat]/[I] = 1.5:1 for **72c**. [b] Measured by ^{1}H NMR. [c] Calculated from [M]/[I] and corrected for conversion. [d] Calculated from ^{1}H NMR using end group analysis. [e] g/mol, measured by GPC in THF using 0.03 as dn/dc for samples. [f] ref. 57.

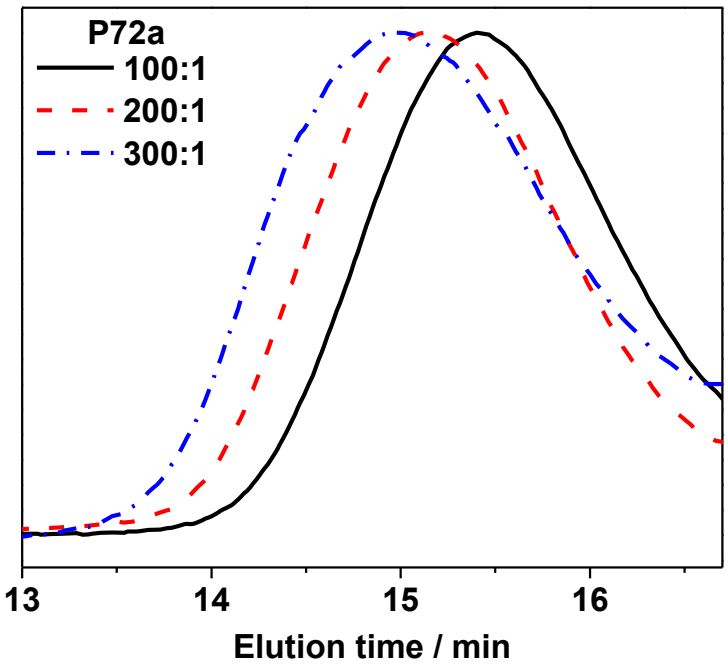

Figure 44. GPC profiles of P72a with different [M]/[I].

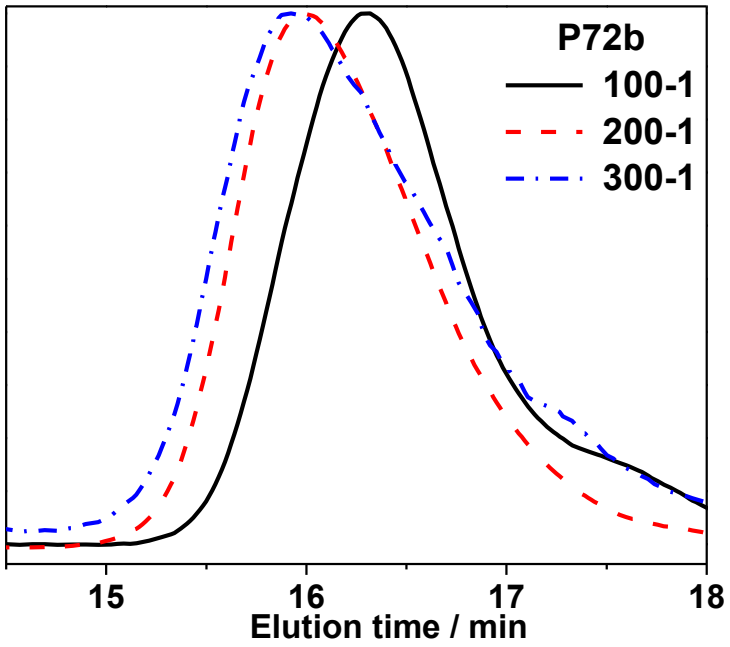

Figure 45. GPC profiles of P72b with different [M]/[I].

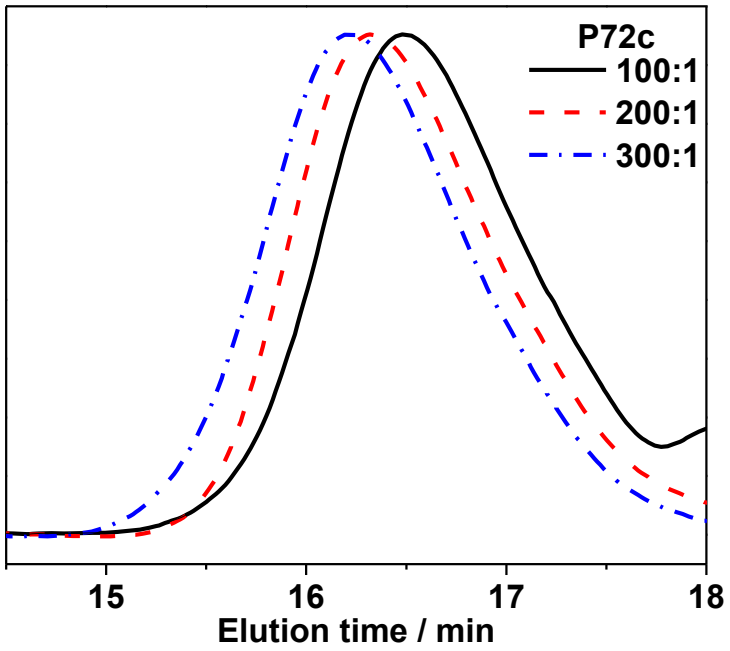

Figure 46. GPC profiles of P72c with different [M]/[I].

The obtained polymer samples were analyzed by TGA under air and DSC under

nitrogen to measure their decomposition temperature and glass transition temperature. The TGA curves are shown in **Figure 47**, which showed the onset of decomposition temperatures of **P72a**, **P72b** and **P72c** was 290, 275 and 255 ^{o}C, respectively. The 100% decomposition temperatures were very close to each other at 350 ^{o}C. Both the onset of and 100% decomposition temperatures were higher than polylactide (235 ^{o}C for onset and 300 ^{o}C for 100%, prepared from [M]/[I] ratio at 100, data not shown here), which indicates slight higher thermal stability than PLA probably due to the more rigid polymer architecture and restricted polymer backbone rotation from the cyclic rings along backbone. This is consistent with previous report where polyspirolactides exhibited higher thermal stability than PLA.[108] **Figure 48** showed the DSC traces of three polymers prepared with [M]/[I] at 300 and all other T_gs were listed in **Table 11**, which showed a significant effect of ring structure on T_g of polymers. The incorporation of bulky substituents along polymer backbone can increase the rotation barrier and thus increase the T_g. **P72a** introduced cyclopentyl group onto polylactide which increased T_g to 65 ^{o}C, and introducing more bulky cyclohexyl group onto **P72b** further increased its T_g to 71 ^{o}C. This clearly confirms the assumption of raising T_g by increasing backbone rotational barrier with bulky substituents. However, when further increase the ring size to cycloheptyl group, somewhat surprising was a T_g of 56 ^{o}C for **P72c** which fell into the same T_g range as PLA (**Table 11**, entry 10) which showed unexpected reverse trend based on the assumption. It has been known that the intermolecular dipole-dipole interaction between chains of PLA determine its T_g.[178] When dipole−dipole interactions

of polylactides become important, bulky substituents not only increase rotation barriers (higher T_g), but also interrupt dipole−dipole interactions (lower T_g) by shielding ester groups. One other factor which cannot be neglected is the higher flexibility of cycloheptyl group than cyclopentyl and cyclohexyl groups. Cycloheptyl group is more flexible than cyclopentyl and cyclohexyl groups,[61] and the rotational barrier increased by cycloheptyl group is lower than those by cyclopentyl and cyclohexyl groups, which also tends to decrease T_g. Apparently, the increase of rotational barrier of **P72c** to give higher T_g caused by the cycloheptyl groups might be compensated by the decrease of dipole−dipole interactions and the increase of ring flexibility, which leads to a similar T_g to PLA.

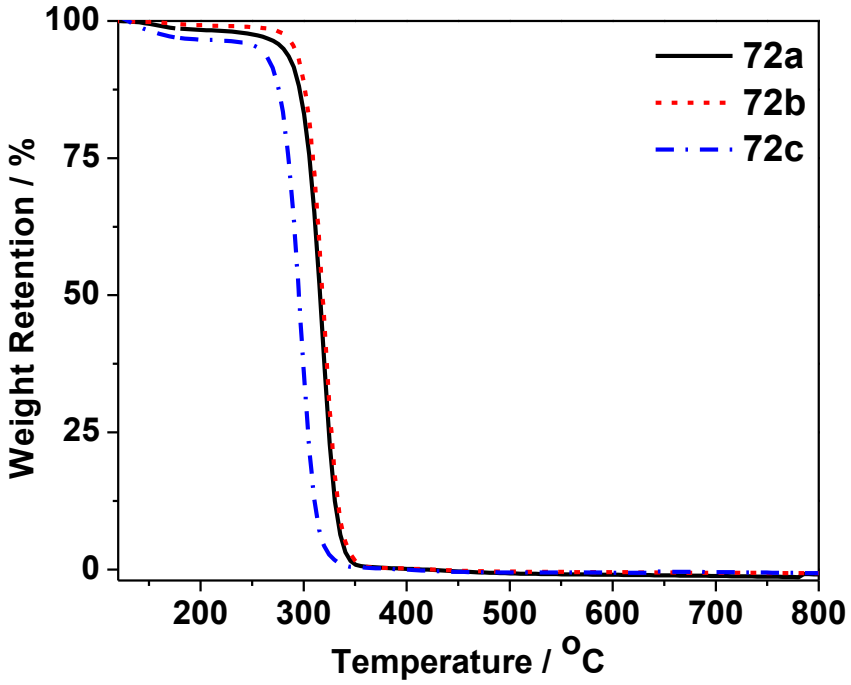

Figure 47. TGA curves of **P72a**, **P72b** and **P72c**. Conditions: [M] = 1 M, [M]/[I] = 300:1 for **72a**, **72b** and **72c**, -20 °C in CH_2Cl_2.

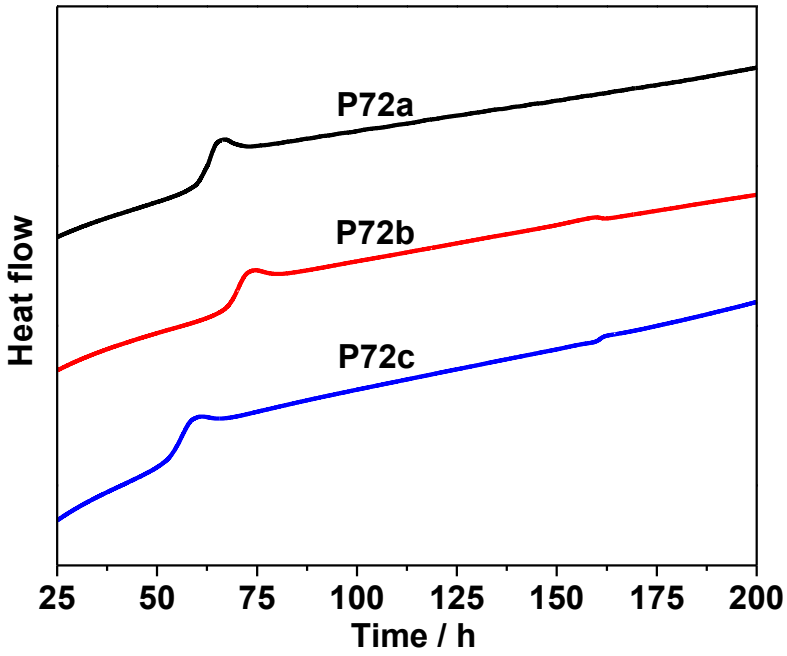

Figure 48. DSC scans of **P72a**, **P72b** and **P72c**. Conditions: [M] = 1 M, [M]/[I] = 300:1 for **72a**, **72b** and **72c**, -20 ^{o}C in CH_2Cl_2.

4.3 Conclusion

A series of spirolactide monomers (**72a**, **72b** and **72c**) were prepared from condensation of corresponding cyclic ring substituted α-hydroxy acid and bromopropionyl bromide followed by ring-closure with medium yield. The solution polymerization of spirolactides using TBD as catalyst and TBBA as initiator at -20 ^{o}C afforded polymers at medium yield with relatively good molecular weight control and narrow PDI. The polyspirolactides showed slightly higher decomposition temperature (≥ 255 ^{o}C) than polylactide. The glass transition temperature of polyspirolactides depends on the cyclic ring substituents along backbone. Cyclo- pentyl and hexyl groups substituted polyspirolactides exhibited T_g with values at 65 and 71 ^{o}C, respectively, which are higher than polylactide. This indicates the bulky and rigid cyclic structure

along polymer backbone can raise their T_g by increasing their rotation barrier. However, cycloheptyl group, a bigger ring substituent, did not raise the T_g. Instead, it resulted in polyspirolactide with similar T_g to polylactide probably due to the disruption of dipole-dipole interactions between chains and more flexible ring structure. These results demonstrated the direct attachment of rigid and bulky substituents can be used to tune the T_g and thermal properties of polylactides.

4.4 Experimental Section

Materials. Bromopropionyl bromide, 4-*tert*-butylbenyl alcohol (TBBA), triazabicyclodecene (TBD), cyclopentanone, cyclohexanone and cycloheptanone were purchased from Sigma-Aldrich and used directly. THF was dried over sodium/benzophenone and distilled before use. Dichloromethane and triethyl amine were dried over calcium hydride and distilled before use. The silica gel (60 Å porosity) for column chromatography was purchased from SiliCycle Inc. All other reagents and solvents were ACS grade and used as received unless specified.

Characterization. Melting points were measured on Electrothermo® melting point apparatus. ^{1}H NMR and ^{13}C NMR were recorded on a VXR-500 MHz instrument in $CDCl_3$ unless otherwise noted. $CDCl_3$ was used as the internal standard for both ^{1}H NMR (δ = 7.24) and ^{13}C NMR (δ = 77.0). Analytical thin-layer chromatography (TLC) was performed on silica gel plates with F-254 indicator. FT-IR spectra were taken with Mattson Galaxy 3000 FT-IR. HRMS were taken on Waters Xevo G2-S TOF UPLC/TOF

MS. Thermogravimetric analysis (TGA) was recorded on Perkin-Elmer TGA 7 at a heating/cooling rate of 10 °C under air. Differential scanning calorimetry analyses of the polymers (DSC) was recorded on DSC-Q100 at a heating/cooling rate of 10 °C under nitrogen and the second heating scan was used for analysis. The molecular weights of polymers were determined by gel permeation chromatography (GPC) at 35 °C using two PLgel 10μ mixed-B columns in series with THF as the eluting solvent at a flow rate of 1 mL/min. A Waters 2410 differential refractometer was used as the detector, and monodisperse polystyrene standards were used to calibrate the molecular weights.

Synthesis of α-hydroxy acid (70a, 70b and 70c). A mixture of 190 mL of water and cycloketones (**69**, 0.5 mol) was mixed with a aqueous solution of NaCN (49 g, 1 mol) in 75 mL of water and cooled down in ice bath. After the addition of sodium metabisulfite ($Na_2S_2O_5$, 95 g, 1 mol) in 160 mL of water at 0 ^oC, the mixture was vigorously stirred overnight to give a light yellow suspension. After extracted with dichloromethane (4 x 100 mL), the organic layer was dried, filtered and concentrated. The resulted oily product was directly hydrolyzed in concentrated HCl under reflux for 12 h. Then the mixture was extracted continuously with dichloromethane and recrystallized with dichloromethane/hexne (1:10) to afford products as white solids.

1-Hydroxycyclopentanecarboxylic acid (**70a**), 71 g, 78%. m. p. 99-101 ^oC. ^1H NMR (500 MHz, $CDCl_3$) δ 2.10-2.22 (m, 2H), 1.75-1.95 (m, 6H); ^{13}C NMR (125 MHz, $CDCl_3$) δ 182.30, 81.76, 39.88, 24.94; IR 3308, 3186, 2960, 2875, 2596, 1733, 1429, 12811198, 1099, 1066, 1030, 947, 886 cm^{-1}.

Hydroxycyclohexanecarboxylic acid (**70b**), 81 g, 82%. m. p. 102-105 ^oC. ^1H NMR

(500 MHz, $CDCl_3$) δ 1.75-1.87 (m, 2H), 1.54-1.72 (m, 7H), 1.20-1.34 (m, 1H); ^{13}C NMR (125 MHz, $CDCl_3$) δ 181.87, 73.69, 34.41, 25.01, 20.98; IR 3407, 2960, 2933, 2872, 2856, 2635, 1735, 1454, 1377, 1278, 1234, 1154, 1041, 994, 743, 674 cm^{-1}.

1-Hydroxycycloheptanecarboxylic acid (**70c**), 80 g, 76%. m. p. 67-69 °C. ^1H NMR (500 MHz, $CDCl_3$) δ 1.97-2.07 (m, 2H), 1.75-1.85 (m, 2H), 1.47-1.75 (m, 8H); ^{13}C NMR (125 MHz, $CDCl_3$) δ 182.94, 76.95, 38.87, 29.54, 22.56; IR 3247, 2922, 2856, 2600, 1700, 1463, 1418, 1267, 1253, 1179, 1063, 895cm^{-1}.

Synthesis of spirolactide monomers (72a, 72b and 72c). α-Hydroxy acids (**70**, 0.1 mol) and 300 mL of dry THF were added to a round bottom flask under nitrogen. 2-Bromopropionyl bromide (11.6 mL, 0.11 mol) was added at 0 °C. Then a solution of Et_3N (19 mL) in THF (75 mL) was added dropwise. After stirring overnight, the mixture was filtered to remove white precipitate and the filtrate was concentrated and dissolved in ethyl acetate (350 mL). After washed with 1 M HCl (4 x 100 mL), saline (2 × 100 mL) and dried over $MgSO_4$, filtration and removal of the solvent *in vacuo* gave the crude linear acid ester as a white solid which was used directly. The ester was dissolved in acetone (1.8 L) and refluxed for 24 h in the presence of $NaHCO_3$. After filtration, the filtrate was concentrated *in vacuo*. The residue was dissolved in ethyl acetate (400 mL), washed with 1 M HCl (3 x 100 mL), saturated $NaHCO_3$ (2 x 150 mL) and saturated NaCl (5 × 100 mL), and then dried over $MgSO_4$. After recrystallization from ethyl

acetate/hexane, the product was purified by flash chromatography with CH_2Cl_2 and dried under vacuum to give white solids and kept in dry box

72a, R_f = 0.80. 11.4 g, 62%. m. p. 68-71 ^oC. ^1H NMR (500 MHz, $CDCl_3$) δ 5.03 (q, 1H, *J* = 6.5 Hz), 2.58 (m, 1H), 2.25 (m, 1H), 2.14 (m, 2H), 1.82-2.00 (m, 4H), 1.69 (d, 3H, *J* = 6.5 Hz); ^{13}C NMR (125 MHz, $CDCl_3$) δ169.35, 167.30, 89.30, 72.64, 38.51, 38.29, 25.03, 24031, 16.88; IR 2971, 2883, 1438, 1383, 1327, 1267, 1154, 1103, 1071, 1044, 1000, 925, 787cm^{-1}; HRMS(m/z) calcd for $C_9H_{13}O_4$ 185.0869, $[M+H]^+$, found 185.0864.

72b, R_f = 0.80. 10.9 g, 55%. m. p. 73-75 ^oC. ^1H NMR (500 MHz, $CDCl_3$) δ 5.06 (q, 1H, *J* = 6.5 Hz), 2.14 (m, 1H), 1.95-2.0.8 (m, 2H), 1.90 (m, 1H), 1.65-1.80 (m, 8H), 1.39(m, 1H); ^{13}C NMR (125 MHz, $CDCl_3$) δ; IR 2966, 2938, 2856, 1769, 1738, 1449, 1374, 1339, 1319, 1261, 1275, 1132, 1071, 1046, 994, 964, 917, 724 cm^{-1}; HRMS(m/z) calcd for $C_{10}H_{15}O_4$ 199.0957, $[M+H]^+$, found 199.0955.

72c, R_f = 0.80. 12.3 g, 58%. m. p. 62-64 ^oC. ^1H NMR (500 MHz, $CDCl_3$) δ 5.02 (q, 1H, *J* = 6.5 Hz), 2.40 (m, 1H), 2.20 (m, 1H), 2.09 (m, 2H), 1.56-1.82 (m, 11H); ^{13}C NMR (125 MHz, $CDCl_3$) δ169.21, 166.87, 85.61, 72.68, 38.03, 36.73, 29.53, 29.41, 22.25, 21.91, 17.63; IR 3004, 2933, 2856, 1755, 1463, 1355, 1289, 1380, 1250, 1115, 1063, 1033, 986, 939, 727 cm^{-1}; HRMS(m/z) calcd for $C_{11}H_{17}O_4$ 213.1174, $[M+1]^+$, found 213.1178.

Solution polymerizations of spirolactides. Solution polymerizations were carried out in a glass bulb prepared from 3/8 in. diameter glass tubing which was sealed by connecting to another one-end closed 3/8 in. glass tubing via cajon fitting. The general procedure is as follows. In a dry box, a catalyst solution (0.04 M) was prepared by adding TBD (13.9 mg, 0.1 mmol) into 2.5 mL of dichloromethane and used freshly. The initiator solution (0.04 M) of TBBA was prepared by dissolving TBBA (131 mg, 0.8 mmol) in 20 mL of dichloromethane. The desired amount of spirolactides was added to one 5-ml vial, then predetermined catalyst solution, initiator solution and dichloromethane were transferred into the vial to make the monomer concentration at 1 M. Then the solution was transferred to polymerization apparatus and taken out of the dry box for polymerization in -20 ^{o}C cooler. At required polymerization time, the apparatus was taken out and quenched immediately by adding excess of benzoic acid. The polymers were collected by precipitating their dichloromethane solution to ice-clod methanol and dried under vacuum to give white solid. For polymerization kinetics, one polymerization mixture ([M]/[I] = 100) was prepared and separated to different polymerization apparatus for desired polymerization time before quenching for conversion and GPC measurement.

P72a: Yield 45%. ^{1}H NMR (500 MHz, $CDCl_3$) δ 4.97-5.17 (br, 1H), 2.35-2.55 (br, 1H), 2.16-2.35 (br, 1H), 1.92-2.15 (br, 2H), 1.65-1.82 (br, 4H), 1.45-1.55 (br, 3H).

P72a: Yield 51%. ^{1}H NMR (500 MHz, $CDCl_3$) δ 5.02-5.21 (br, 1H), 2.05-2.28 (br, 2H), 1.87-1.99 (br, 1H), 1.40-1.87 (br, 9H), 1.24-1.37 (br, 1H).

P72a: Yield 43%. ^{1}H NMR (500 MHz, $CDCl_3$) δ 4.97-5.17 (br, 1H), 2.23-2.45 (br,

1H), 1.95-2.23 (br, 3H), 1.40-1.83 (br, 11H).

CHAPTER 5 SURFACE FUNCTIONALIZATION OF SMALL SILICA NANOPARTICLES VIA CLICK CHEMISTRY

5.1 Introduction

Nanoparticles are characterized by their size which is in the range of several nanometers to several hundred nanometers, well below the micrometer range. Because of their nanoscale dimensions and hence large specific surface area, nanoparticles exhibit remarkable physicochemical properties, which are usually not observed in their bulk materials. Among them, silica nanoparticles (SiNPs) have attracted much attention due to their chemical inertness, low or non toxicity and excellent thermal stability. Particularly, SiNPs have been widely studied in applications such as drug/gene delivery,[179] imaging agents,[180] immnunoassay agents,[181] because of the easy access of surface functionalization. The silanol surface of SiNPs has been modified by introducing functional groups such as amino, thiol, epoxy, carboxy, azido or alkyne groups.[182,183,184,185] The latter two allow for the efficient functionalization of SiNPs by copper-catalyzed 1,3-dipolar cycloaddition reaction (click chemistry) between an organic azido group and an alkyne group.[184,185] This click reaction is now widely used in biosciences because they proceed with high efficiency at room temperature, in aqueous solution over a wide range of pH and functionalities. Click chemistry has not only been used in the fields of homogenous reactions, but also moved into areas such as nanoparticle surface chemistry with promising applications in controlled drug delivery,[186] diagnostics,[187] fluorescent labeling.[184]

The properties of nanoparticles can be modified based one surface functionalization. For example, poly(ethylene glycol) (PEG), one of the best known surface coating agents, has been reported to reduce the non-specific protein binding and enable nanoparticles stealth characteristics to enhance permeation, retention and circulation time of nanoparticles.[188,189] Aggregation is a common and complex phenomenon for small particles and makes, which can be overcome by suitable surface coating. Surface coating can change the surface charge of the colloidal suspension of nanoparticles to stabilize the particles via electrostatic repulsion. The surface layer can also create a barrier between particles to stabilize nanoparticles, which is often referred to as steric stabilization. In many cases, particle stabilization is attributed to a combination of electrostatic repulsion and steric repulsion.

We prepared a series of small and monodisperse silica nanoparticles, which were surface modified with different PEG chains and different functionalities via click chemistry. The surfaces of monodisperse silica nanoparticles were directly coated with alkynyl-substituted triethoxysilanes via condensation with silanol groups, which enabled click function of SiNPs surfaces. Since the click reaction is the final step in the synthesis, the particles are identical except for the surface chemistry, which allows the preparation of surface functionalized SiNPs in a reproducible fashion.

5.2 Results and Discussion

5.2.1 Synthesis of Clicking Reagents

As shown in **Scheme 45**, silane coupling reagent (**74**) containing terminal alkyne group was synthesized from one-step addition reaction between difunctional

organosilane (**73**) and propargyl alcohol in 90% yield leaving the condensable site untouched for further SiNPs surface functionalization.[190, 191] Linear azido clicking reagents with different functionalities (**76**, **78**, **79**, **83**) were synthesized using the corresponding starting materials oligo- or polyethylene glycol monomethyl ether (**75**), tetraethylene glycol (**77**) or triethylene glycol monochlorohydrin (**80**) without column purification as shown in **Scheme 45**.[192,193] All of these compounds were characterized by ^{1}H NMR, ^{13}C NMR and FT-IR.

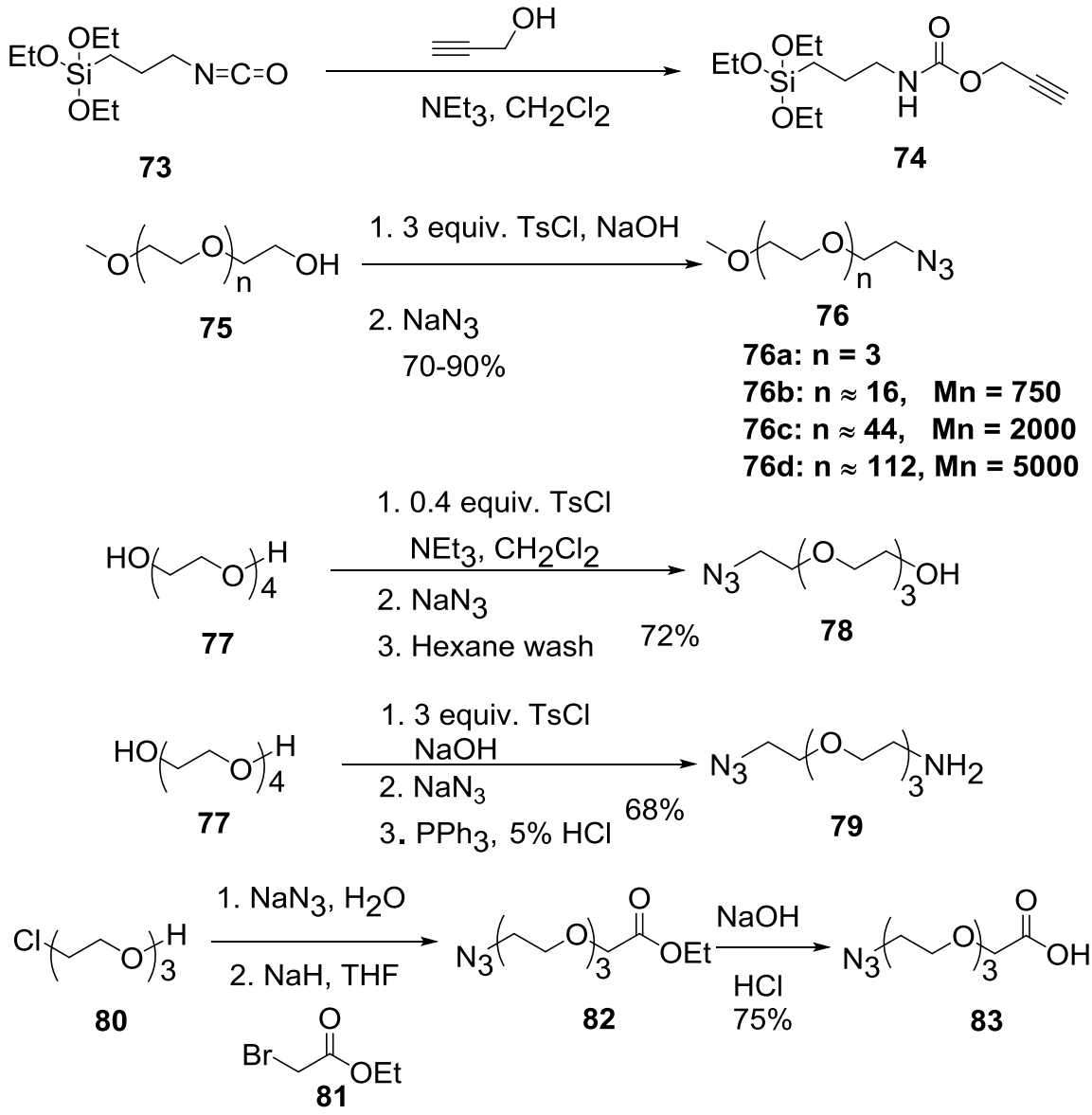

Scheme 45. Synthesis of linear clicking reagents.

5.2.2 SiNPs Surface Modification with mPEG Azides (76)

Commercially available bare silica nanoparticles with different sizes were condensed with triethoxysilane **74** in basic EtOH-H_2O mixture for three days, as shown in **Scheme 46.** After condensation, the alkyne modified silica nanoparticles were purified using dialysis tubing with different molecular weight cut off (**MWCO**) based on size of the

particles for 1.5 to 8 days. This thorough purification was confirmed by the absence of organic chemicals in ^{1}H NMR spectra of dialysate and particle suspension in dialysis tubing after removal of the solvent. The alkyne moiety was condensed on the surface successfully and also confirmed by TGA weight loss. Second, the clicking reagents (**76a,b,c,d, 78**, **79** and **83**) were attached onto the silica particles surface by click reaction (copper catalyzed azide alkyne cycloaddition) to afford the designed monodisperse particles with specific surface functionalities and sizes. To avoid aggregation, the modified particles were purified by dialysis and kept in the corresponding solvent until further characterization or application. As shown in **Figure 49**, the surface chemistry of nanoparticles was tracked by normalized FTIR spectra of silica nanoparticles using characteristic absorbance of silica at 806 cm^{-1}, which allows semi-quantitative comparison of the nanoparticles during the syntheses. Alkynyl modified SiNPs (25 nm, **SiNP25/74**) show an increased absorption band at 2900-3300 cm^{-1} and two new bands at 1700cm^{-1} and 1430 cm^{-1}, which correspond to the alkyl group and the carbonyl group, confirming successful surface condensation. Although the characteristic of triple bond was not observed probably due to the low content of organic layer and small change of dipole moment of triple bond, the subsequent click modification with different mPEG azides (**76**) resulted in particles. The Ft-IR of the resulting particles clearly showed three sets of stronger absorption bands at 2930, 1460 and 1630 cm^{-1} (**SiNP25/76a-d**, **Figure 49**) due to more methylene groups from mPEG units and formed triazole rings,[194] indicating successful PEG functionalization on the particle surface. Those absorption bands corresponding to methylene groups from

mPEG units became stronger with increasing PEG chain length due to the higher surface mPEG grafting. The higher surface grafting for longer mPEG units was also confirmed by their TGA data in **Table 12** and **Figure 50**, which will be discussed later. The zeta potential of the pegylated particles (-6 to -15 mV) was higher than bare SiNPs in buffer (-25 mV, 100 mM KCl and 10 mM HEPES), which indicates the surface modification by mPEG units shields the silica core and reduced the surface charges.[195] Because of the steric hindrance of grafting layers on surface, not all the hydroxyl groups on the particle surface reacted with alkynyl triethoxy silanes (**74**) and then clicked with azides, thus the zeta potentials were not zero.[196]

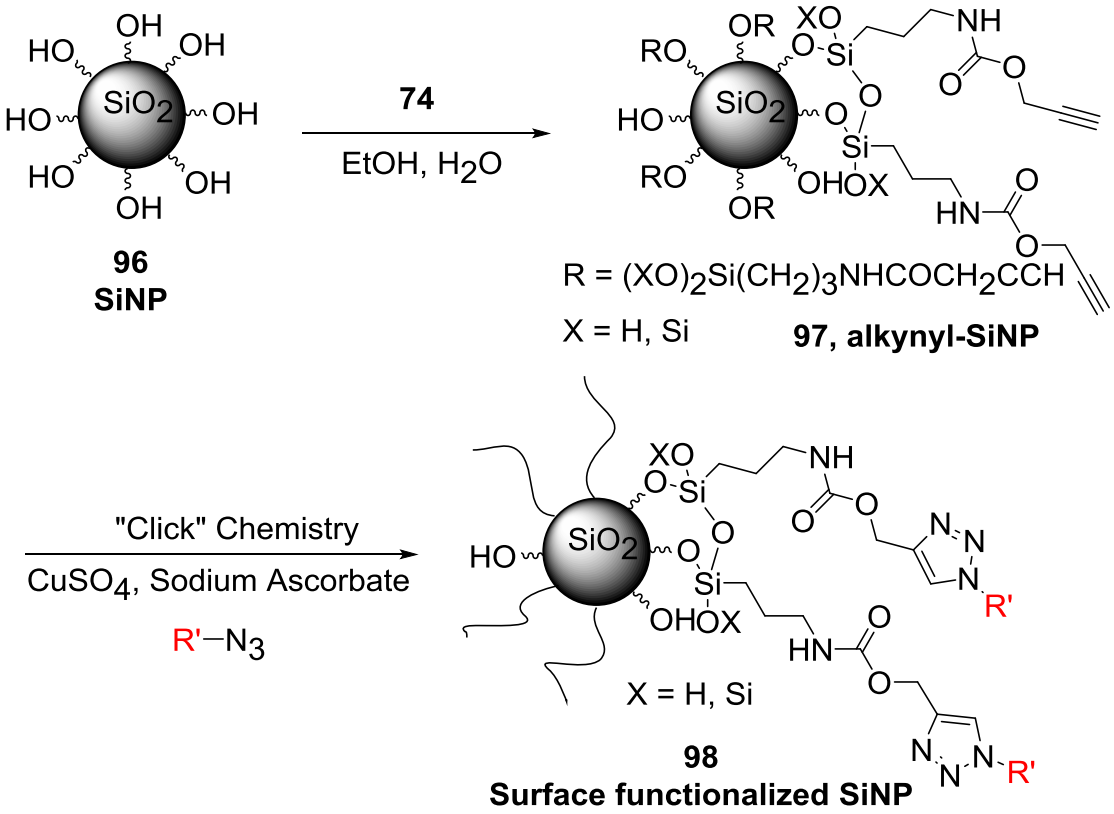

Scheme 46. Surface modification of silica nanoparticles using click chemistry.

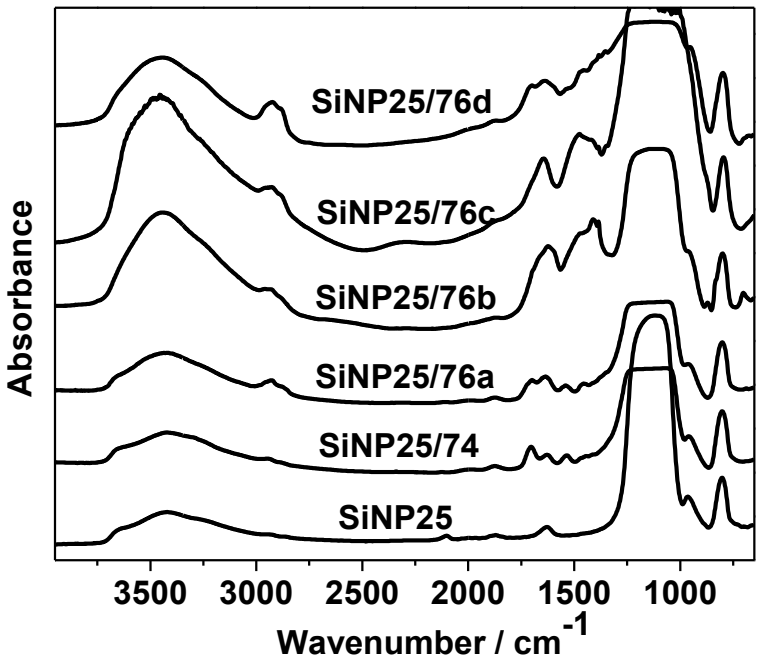

Figure 49. Normalized FT-IR spectra of bare SiNP (**SiNP25**, 25 nm), alkynyl SiNP (**SiNP25/74**) and SiNPs click-modified with different mPEG azides (**76a**: 4PEG; **76b**: PEG750; **76c**: PEG2000; **76d**: PEG5000).

The TGA data in **Table 12** and **Figure 50** confirm the step-by-step modification of silica particles with different surface functionalities. The grafting amount on the particle surface can be calculated by dividing the TGA weight losses by the molecular weight of the corresponding organic compound, which correspond to oxidation of the organic layer on the nanoparticles. Table 1 shows a 5% weight loss for alkyne-modified nanoparticles (**SiNP25/74**), which corresponds to a grafting amount of 0.36 mmol/g on silica. The pegylation step shows 7.6-25% weight loss for peglyated silica particles corresponding to a grafting amount of 0.03 - 0.33 mmol/g on silica, and this indicates the successful click surface modification and synthesis of water-soluble nanoparticles. However, the grafting amount dramatically decreased from 0.33 to 0.03 mmol/g with increasing the length of mPEG units from PEG750 to mPEG5000. This is a typical self-

limiting process of grafting process due to the steric hindrance which makes it more difficult for the longer polymer chains penetrate through existing polymer layer to reach the reactive sites on the surface.[197]

Table 12. Surface grafting of silica nanoparticles (25 nm)

NP	Weight Loss[a] %	Grafting amount[a] mmol/g	Click Conv.[a] %	Size[b] nm	Zeta Potential[d] mV
SiNP25	--	--	--	30	-25
SiNP25/74	5	0.36	--	37[c]	--[e]
SiNP25/76a	7.6	0.33	91	44	-10
SiNP25/76b	17	0.22	61	63	-15
SiNP25/76c	25	0.12	34	56	-13
SiNP25/76d	17	0.03	10	66	-6

[a] Weight loss, grafting amount, and click conversion were calculated for each modification step, not for total modification. [b] Size was measured in H_2O by DLS after sonication for 4 h. [c] Size was measured in EtOH. [d] Measured in a buffer of 100 mM KCl and 10 mM HEPES. [e] Data are not available.

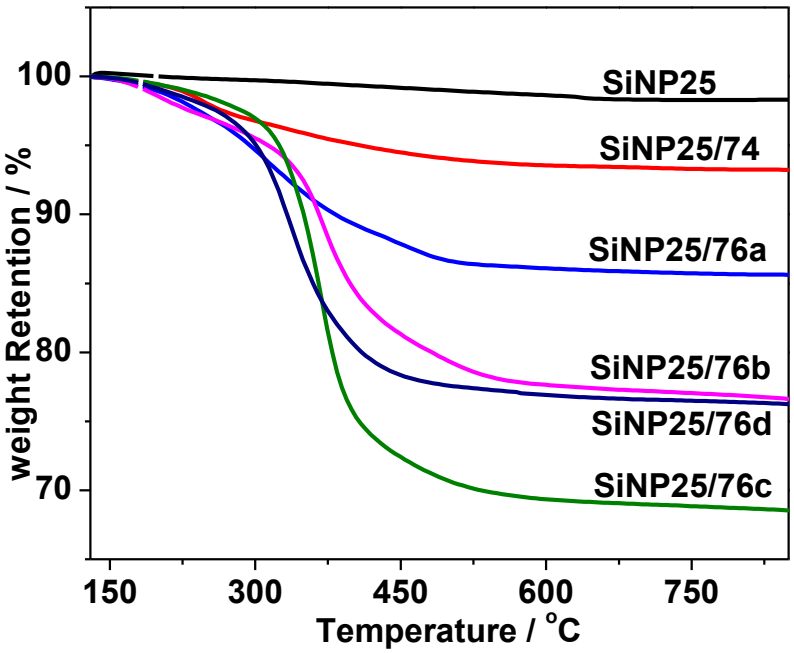

Figure 50. Normalized TGA curves of bare SiNP (**SiNP25**, 25 nm), alkynyl SiNP (**SiNP25/74**) and click-modified silica particles with different mPEG azides (**76a**: 4PEG; **76b**: PEG750; **76c**: PEG2000; **76d**: PEG5000).

The DLS measurements were conducted after each modification step of **SiNP25**, as shown in **Table 12** and **Figure 51**. All surface modified nanoparticles showed monomodal dispersity by intensity in aqueous solution and the hydrodynamic diameters of the particles increased after each modification. The diameter of bare **SiNP25** was 30 nm, and after alkyne modification, the diameter increased to 37 nm. After the pegylation step, the size of particles increased to 44, 63, 56, and 66 nm for different mPEG azides (**76a**: 4PEG; **76b**: PEG750; **76a**: PEG2000; **76b**: PEG5000) with longer mPEG units giving slightly larger hydrodynamic diameters, which indicates the swelled surface layer increases the micro viscosity around SiNPs and then changes their hydrodynamic impermeability during the Brownian diffusion resulting in larger diameters from DLS.[198,199] The effect of thicker surface mPEG layer on DLS size should also not be

omitted due to the higher grafting amount and denser surface layer structure. However, the TEM results (data not shown here) measured from dry particles show that the particle sizes are almost the same as those without surface modification, confirming that the TEM sizes only provide a good measure of the individual nanoparticle cores after thin surface layer collapses during drying on TEM copper grid and have no relevance to solution behavior before and after surface modification.[196,199]

The solution dispersion stability of mPEG modified SiNPs in water was studied by monitoring the DLS size distribution versus aging time. The hydrodynamic particle size distributions were narrow and confirmed the monodispersity. As shown in **Figure 52**, the hydrodynamic diameters of all modified SiNPs from DLS were almost similar during aging in the lab up to 4 days. This long term disperse stability might be due to the combination of electrostatic stabilization (negatively charged surface for all particles) and steric stabilization (surface layer coating) to increase repulsive forces between particles. Thus agglomeration is suppressed or kinetically slow.[200] The slight decrease of sizes might be due to the sediment of larger particles or dust in the solution.

We have also investigated the structural stability of surface layer grafted to SiNPs surface when the modified particles were sonicated for 4 h at 60 ^{o}C. As shown in **Figure 53**, both alkynyl **SiNP25/74** and **SiNP25/76a** showed no obvious loss of grafting amount of surface layer following ultrasound sonication. This is consistent with the results reported by Bielawski et al., which demonstrated that short polymers (up to 36 kDa) linked through 1,2,3-triazole moiety (which is often prepared using the click coupling of azides and alkynes) do not undergo cycloreversion[201] or any other bonds breaking.

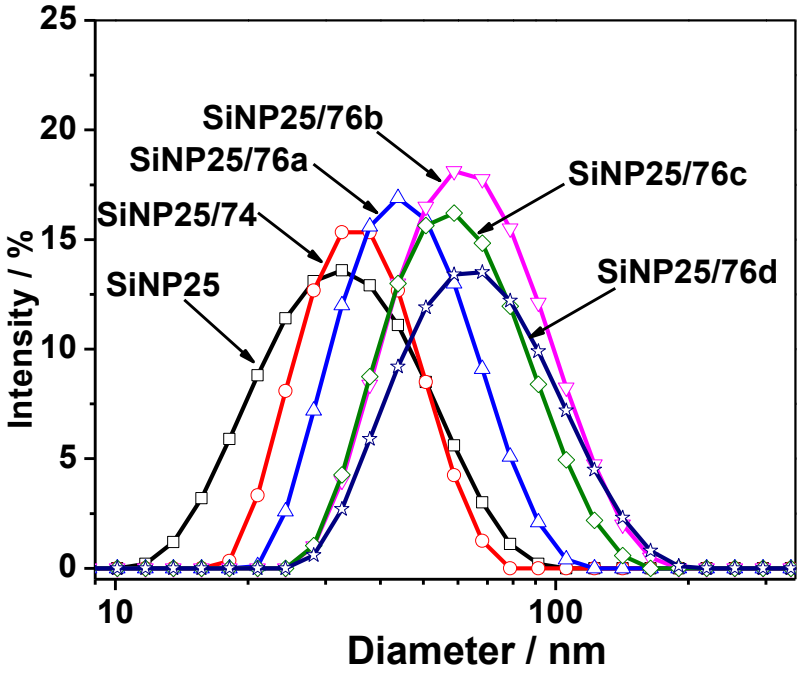

Figure 51. DLS p

ofiles (size distribution by intensity) of bare SiNP (**SiNP25**, 25 nm), alkynyl SiNP (**SiNP25/74**) and SiNPs click-modified with different mPEG azides (**76a**: 4PEG; **76b**: PEG750; **76c**: PEG2000; **76d**: PEG5000) after 4 h sonication at 60 °C.

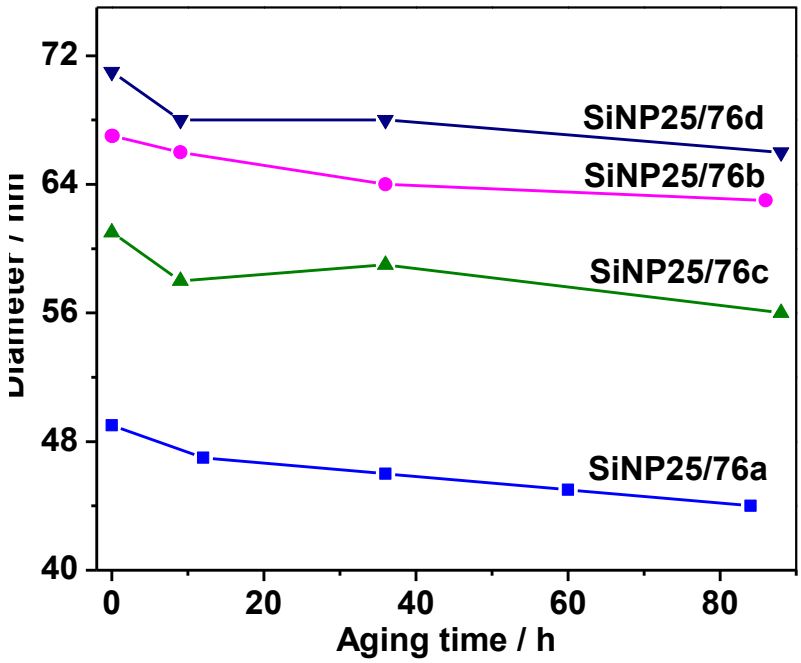

Figure 52. Dispersion stability of silica particles (**SiNP25**) click-modified with different mPEG azides (25 nm; **76a**: 4PEG; **76b**: PEG750; **76c**: PEG2000; **76d**: PEG5000) in aqueous solution.

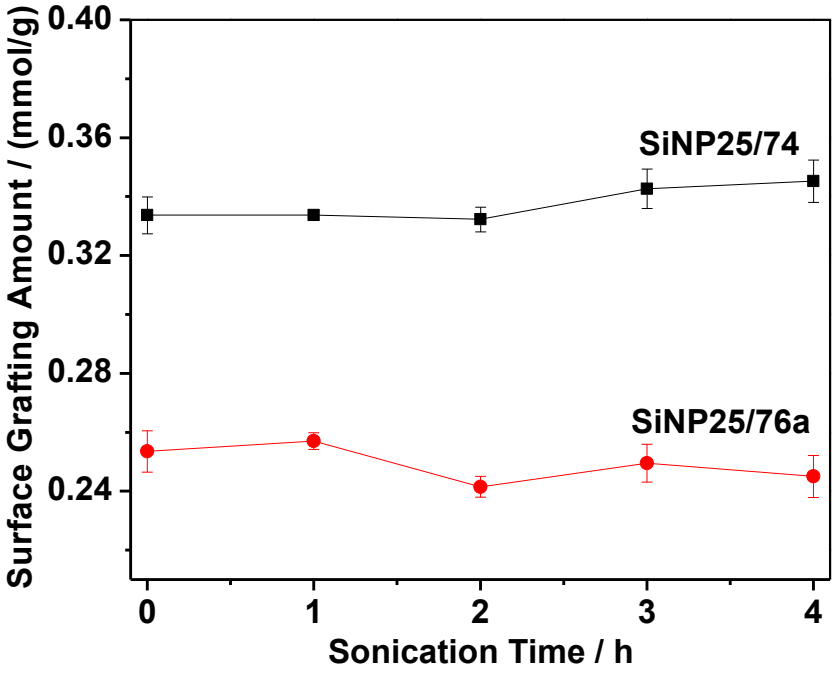

Figure 53. Structural stability of click-grafted surface layer of silica particles modified with alkynyl silane (**SiNP25/74**) and mPEG azide (**SiNP25/76a**, 4PEG) during 4 h sonication at 60 ^{o}C.

5.2.3 SiNPs Surface Modification with Different Functionalities

The surface chemistry of nanoparticles was tracked by normalized FT-IR (**Figure 54**) of silica nanoparticles (**SiNP25**) after modification with different organic azides (**76a**: 4PEG-OMe; **78**: 4PEG-OH; **79**: 4PEG-NH_2; **83**: 4PEG-COOH). After "click" modification of particles, two stronger bands at 2930 and 1640 cm^{-1} appeared corresponding to higher methylene groups content of PEG units and triazole ring. The TGA weight loss of clicked surface layers (7.2 – 8.7 %) and the calculated grafting amount on the surface in **Table 13** were very close to the grafted alkyne layer before clicking. These results

indicate the successful click chemistry on the particle surface. FT-IR and TGA is not very useful for characterizing surface functionalities (-OMe, -OH, -NH_2 and –COOH terminated particles), but the zeta potential of modified particles showed higher values than bare SiNPs, indicating the shielding effect of grafted surface layer on silanol group from bare silica surface, as shown in **Table 13**. -NH_2 terminated particles (**SiNP25/79**) showed highest zeta potential, which indicates highly negative zeta potential of bare SiNPs was compensated by both PEG layer and -NH_2 (+) surface charge. And -COOH terminated particles (**SiNP25/83**) in buffer gave the lowest zeta potential. The zeta potential was higher than that of bare **SiNP25** due to both of PEG layer shielding and negative charged carboxylate group. The DLS showed sizes of modified particles increased slightly from 37 nm before clicking to ~50-60 nm after clicking due to the click grafting and thus microenvironment changes around particles. Only one particle population was observed in all DLS measurements, which suggested that the particles were mono-dispersed in aqueous solution (**Figure 55**). These results indicate click chemistry could introduce different surface functionalities and afford monodisperse silica nanoparticles.

Table 13. Surface grafting of SiNPs (25 nm) with different functionalities.

NP	Weight Loss[a] %	Grafting amount[a] mmol/g	Click Conv.[a] %	Size[b] nm	Zeta Potential[d] mV
SiNP25	--	--	--	30	-25
SiNP25/74	5	0.36	--	37[c]	--[e]
SiNP25/76a	7.6	0.33	91	44	-10
SiNP25/78	7.5	0.34	94	50	-14

SiNP25/79	7.2	0.33	90	66	-7
SiNP25/83	8.7	0.37	100	51	-16

[a] Weight loss, grafting amount, and click conversion were calculated for each modification step, not for total modification. [b] Size was measured in H_2O by DLS after sonication for 4 h. [c] Size was measured in EtOH. [d] Measured in a buffer of 100 mM KCl and 10 mM HEPES. [e] Data are not available.

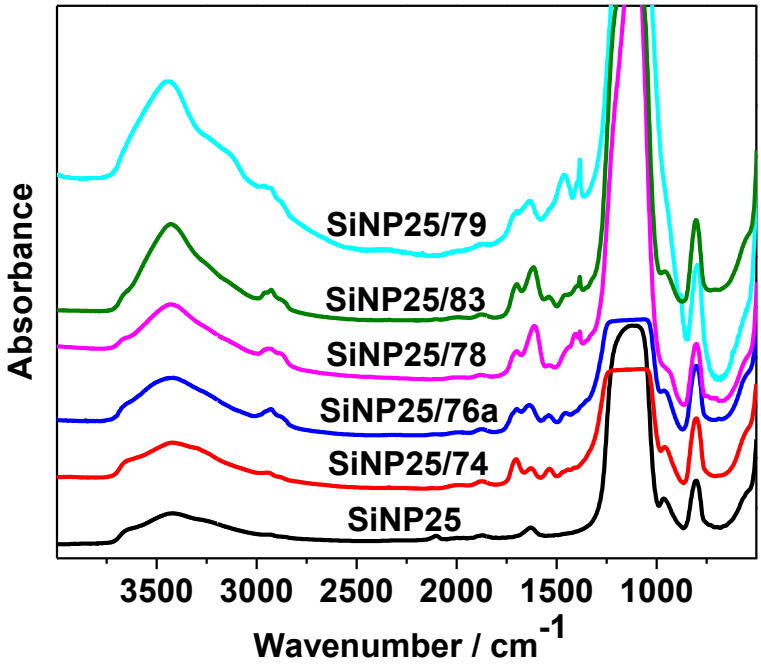

Figure 54. Normalized FT-IR spectra of bare SiNP (**SiNP25**, 25 nm), alkynyl SiNP (**SiNP25/74**) and SiNPs click-modified with different surface functionalities (**76a**: 4PEG-OMe; **78**: 4PEG-OH; **79**: 4PEG-NH_2; **83**: 4PEG-COOH).

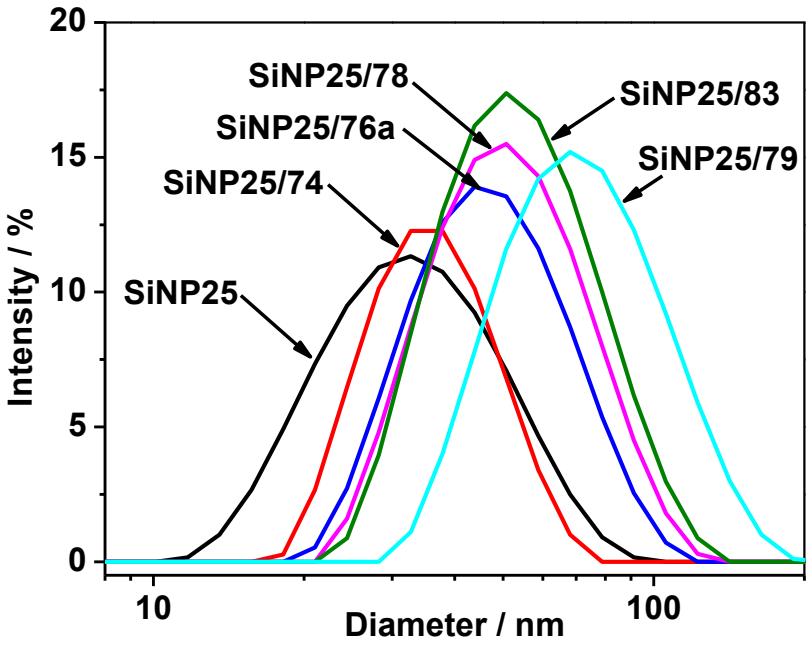

Figure 55. DLS profiles (size distribution by intensity) of bare SiNP (**SiNP25**, 25 nm), alkynyl SiNP (**SiNP25/74**) and SiNPs click-modified with different functional azides (**76a**: 4PEG-OMe; **78**: 4PEG-OH; **79**: 4PEG-NH_2; **83**: 4PEG-COOH).

5.2.4 Click Surface Modification of Different Sized SiNPs with Azido Carboxylic Acid (83)

The surface functionalities of –COOH terminated silica nanoparticles with different sizes (silica core diameter declared by manufacturer: **SiNP8**, 8 nm; **SiNP25**, 25 nm; **SiNP45**, 45 nm; **SiNP70**, 70 nm.) were also tracked by FT-IR (**Figure 56**) normalized by using the IR band at 806 cm^{-1} for semi-quantitative comparison of the nanoparticles during the syntheses. All the pegylated particles showed IR absorption bands at 2900-3300 cm^{-1} and 1700cm^{-1}, which correspond to the alkyl group and carbonyl group, confirming successful modification on the particle surface. Since smaller silica nanoparticles have higher specific surface area, they have higher grafting amount of

organic layers on the surface per gram of particles. As shown in **Figure 56**, with decreasing nanoparticles size, the IR absorption bands at 2900-3300 cm^{-1} and 1700cm^{-1} became stronger, indicating higher grafting amount for smaller silica nanoparticles. TGA results in **Table 14** further confirmed this observation by showing higher weight loss and grafting amount for smaller particles. The click conversion was calculated from TGA data and it showed high conversion for all particles (>80%). The DLS traces and results after click modification of silica nanoparticles were shown in **Figure 57** and **Table 14**. The average hydrodynamic diameters of bare silica particles were measured by DLS in water and they were bigger than the sizes claimed by manufacturers. And all pegylated nanoparticles showed monomodal dispersity (intensity distribution) in aqueous solution with their diameters closer to the corresponding bare SiNPs. This suggests the surface coating, highly negative charged surface and hydrophilicity of the surface modified particles facilitate the dispersion in solution. These results confirm the surface modification of silica nanoparticles with different sizes.

Table 14. Surface grafting of different sized SiNPs with carboxylic acid (**83**).

NP	Weight Loss[a] %	Grafting amount[a] mmol/g	Click Conv.[a] %	Size[b] nm	Size[c] nm	Size[d] nm	Zeta Potential[e] mV
SiNP8/83	13.4	0.57	97	8	20-30	36	-14
SiNP25/83	8.7	0.37	100	25	30	51	-16
SiNP45/83	2.8	0.12	84	45	80	82	-32
SiNP70/83	2.1	0.10	79	70	150	137	-37

[a] Weight loss, grafting amount, and click conversion were calculated from click modification step only. [b] The average diameter of bare SiNPs declared by

manufacturer. [c] The hydrodynamic diameter of bare SiNPs measured in H_2O by DLS.[d] The hydrodynamic diameter of SiNPs modified with **83** measured in H_2O by DLS. [e] Measured in a buffer of 100 mM KCl and 10 mM HEPES.

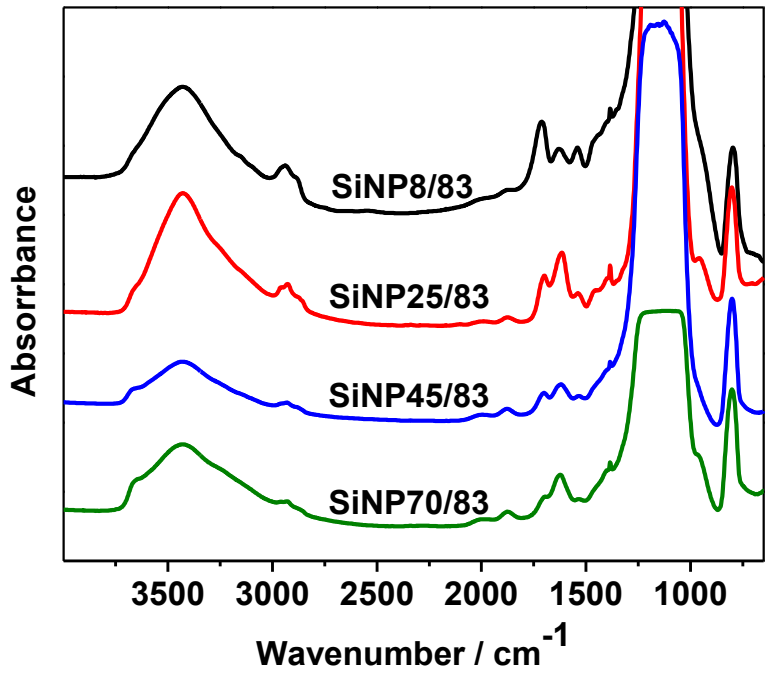

Figure 56. Normalized FT-IR spectra of different sized SiNPs click-modified with **83** (4PEG-COOH after 4 h sonication. Core diameter: **SiNP8**, 8 nm; **SiNP25**, 25 nm; **SiNP45**, 45 nm; **SiNP70**, 70 nm.

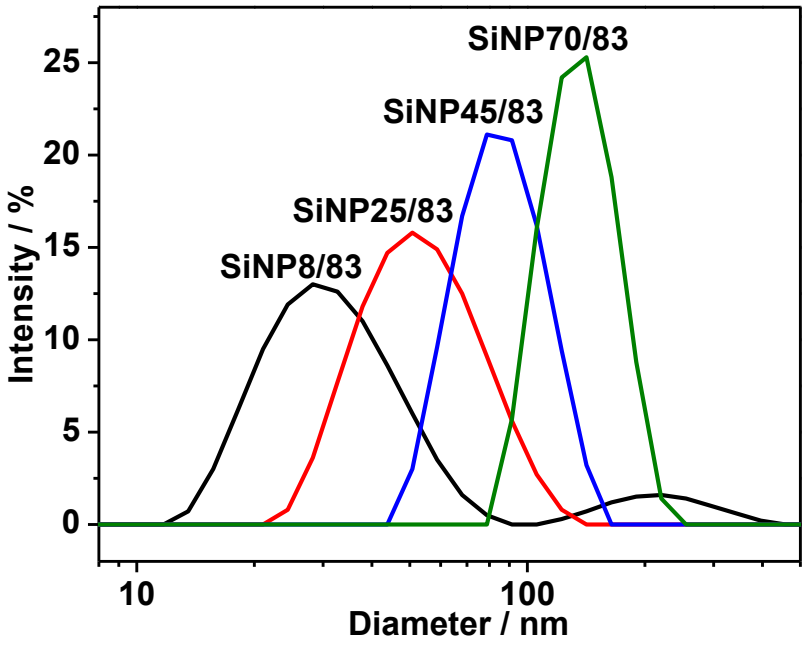

Figure 57. DLS profiles (size distribution by intensity) of different sized SiNPs click-modified with **83** (4PEG-COOH) after 4 h sonication. Core diameter: **SiNP8**, 8 nm; **SiNP25**, 25 nm; **SiNP45**, 45 nm; **SiNP70**, nm.

5.2.5 *In Vitro* Colloidal Stability Studies of SiNPs Modified with Different Surface Functionalities

Colloidal stability under physiological conditions is one of the most important factors relating to the biological applications of nanomaterial.[202,203] The colloidal stability of the silica nanoparticles in RPMI media 1640 with 2% bovine calf serum was investigated by measuring their hydrodynamic sizes by DLS for 3 days at room temperature. As shown in **Figure 58**, **SiNP25/76a** terminated with –OMe group was incubated in the media. DLS profiles of SiNPs only, media only and SiNPs in media (0.1 mg/mL) at different incubation time were recorded to show how the modified particles evolved. The media exhibited one smaller population and a bigger particle population in DLS profile. After incubation for 68 h, the intensity of the peak with larger diameter

grew. It is not clear what these two peaks are corresponding to. The shift of the peak may be due to the protein aggregation. **SiNP25/76a** in media showed a similar particle population during the 68 h incubation. Very similar DLS size distribution behavior was observed for **SiNP25/78** terminated with –OH group (**Figure 59**). Although **SiNP25/83** terminated with –COOH group exhibited very good solution stability in media when incubated for 42 h, it eventually showed gradual size increase in media by presenting a much bigger particle population close to that from media after incubated for 68 h as shown in **Figure 60**. However, **SiNP25/79** terminated with $–NH_2$ group showed immediate size increase from ~66 nm to ~100 nm after mixed with media and its size remained with little changes very close after incubation for 68 h (**Figure 61**). Therefore, the dispersion of surface-modified SiNPs in media crucially depends on their surface functionalities. However, as it is not clear why the two components in media changed with longer incubation time, it is difficult to draw a clear conclusion for the colloidal stability of surface-modified SiNPs. Further studies are needed to evaluate and understand the colloidal stability and the interactions between the media and the modified SiNPs, such as by measuring the change of media components before and after incubation with SiNPs.

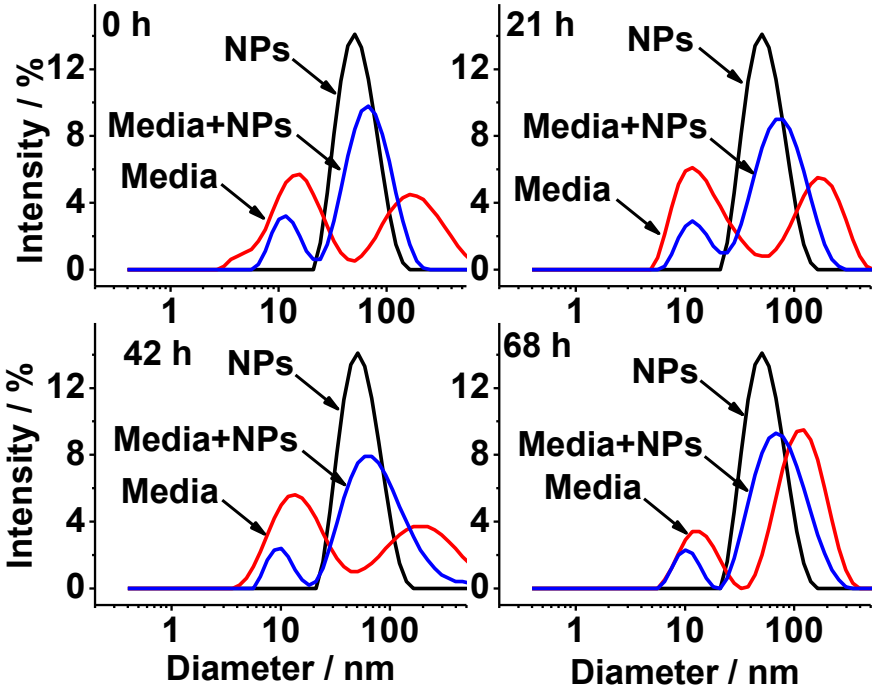

Figure 58. Size distribution of SiNPs (**SiNP25/76a**, -OMe terminated) when incubated in media at 0, 21, 42 and 68 h.

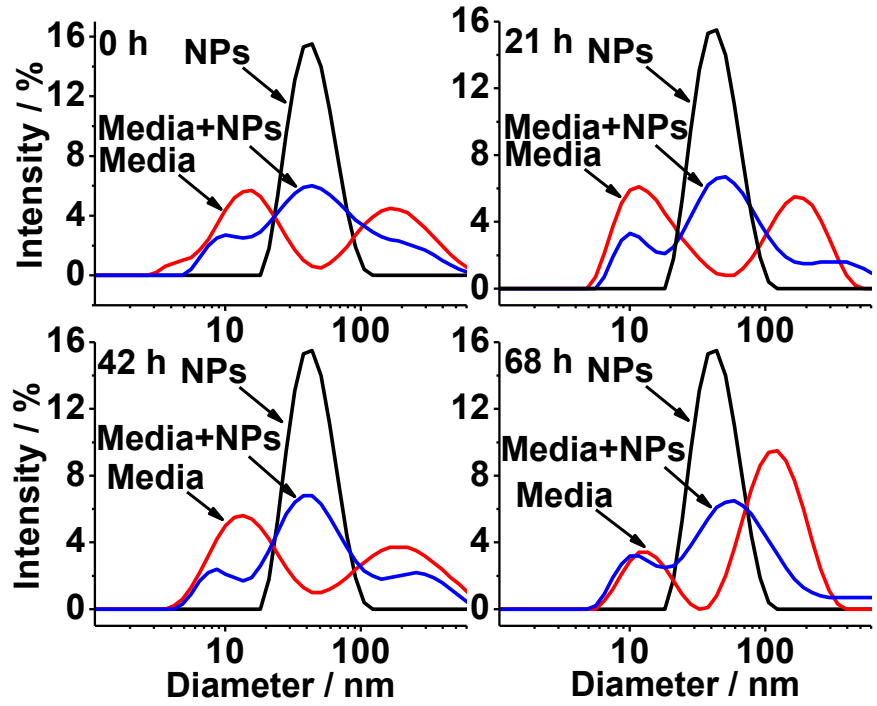

Figure 59. Size distribution of SiNPs (**SiNP25/78**, -OH terminated) when incubated in media at 0, 21, 42 and 68 h.

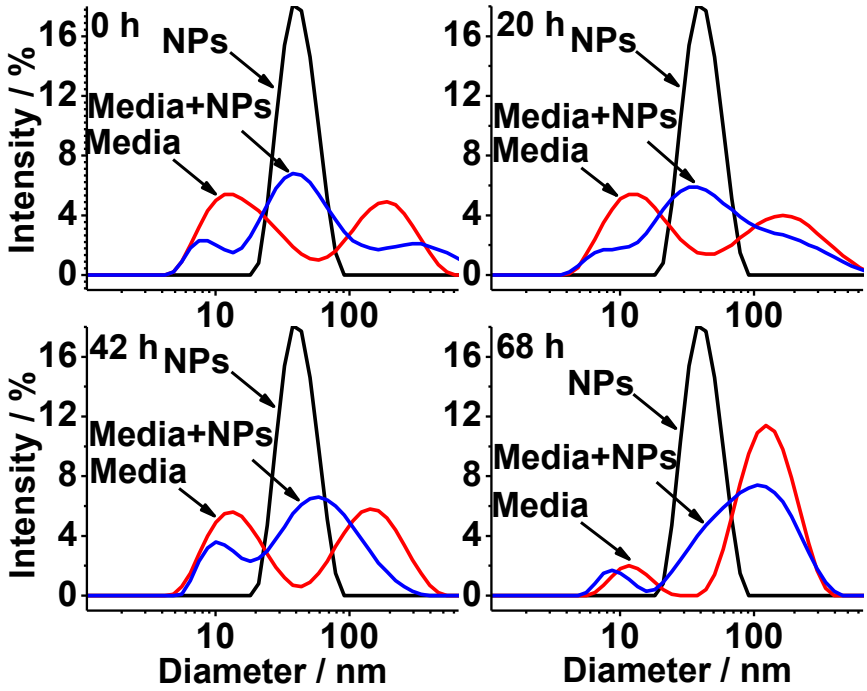

Figure 60. Size distribution of SiNPs (**SiNP25/83**, -COOH terminated) when incubated in media at 0, 20, 42 and 68 h.

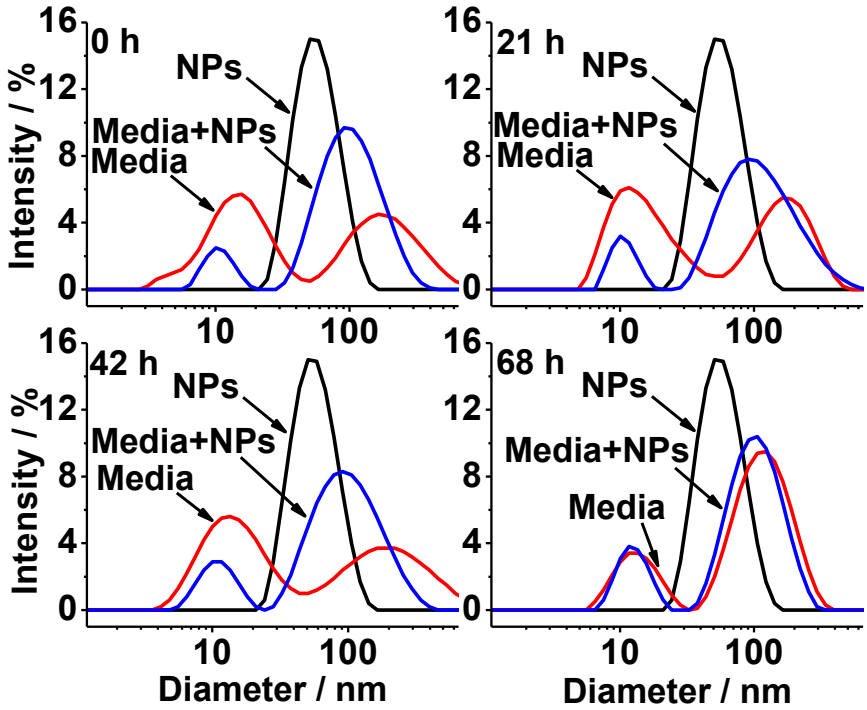

Figure 61. Size distribution of SiNPs (**SiNP25/79**, -NH_2 terminated) when incubated in media at 0, 21, 42 and 68 h.

5.3 Conclusion

We developed a facile route to synthesize stable mono-disperse SiNPs with specific sizes and surface chemistries. SiNPs were grafted with an alkynyl-substituted triethoxysilane (**74**) to afford alkynyl silica nanoparticles, which enable the modification of particle surfaces via click chemistry, the Cu-catalyzed azide-alkyne cycloaddition. Subsequent click reactions with different organic azides provide nanoparticles with a broad range of surface chemistries (carboxylic acids, amines, alcohols, and methoxy-terminated polyethylene glycol chains) and narrow size distributions. The click modification on different sized silica nanoparticles was also investigated. The surface modification was characterized by FT-IR, TGA and DLS. The DLS of surface modified nanoparticles in water confirmed that the nanoparticles did not aggregate. The colloidal stability studies of modified nanoparticles in cell culture media showed the different dispersion behavior depending on the surface functionalities, but further study is needed to evaluate the interactions between the media and the modified SiNPs. This surface modification of silica nanoparticles provides one facile and general method to produce engineered nanoparticles with specific surface functionalities.

5.4 Experimental Section

Materials. LUDOX TM-40 colloidal silica (25 nm, **SiNP25**, 40 wt% suspension in H_2O), 3-(triethoxysilyl)propyl isocyanate, propargyl alcohol, tetraethylene glycol monomethyl ether, poly(ethylene glycol) monomethyl ether (M_n = 750, 2000, 5000),ethyl bromoacetate, tosyl chloride, sodium ascorbate and sodium azide were

purchased from Sigma-Aldrich and used as received. Colloidal silica SNOWTEX S (8 nm, **SiNP8**, 40 wt% suspension in H_2O), SNOWTEX 20L (45 nm, **SiNP45**, 20 wt% suspension in H_2O), and SNOWTEX ZL (70 nm, **SiNP70**, 40 wt% suspension in H_2O) were received as gifts from Nissan Chemical Industries, Ltd. [2-[2-[2-chloroethoxy]ethoxy]ethanol (**80**) was purchased from TCI America. Other reagents and solvents were used as received. Dialysis membrane (Spectra/Por® Biotech Cellulose ester, MWCO: 300K, 50K, 12-14K) was purchased from Spectrum Laboratories Inc. Ion exchange resin (Amberlite® IRC-748) was purchased from Alfa Aesar.

Instruments and Characterization. ^{1}H NMR and ^{13}C NMR spectra were recorded in $CDCl_3$ on a VXR-500 MHz instrument. The $CDCl_3$ resonance was used as the internal standard for ^{13}C NMR (δ = 77.0 ppm) and residual $CHCl_3$ for ^{1}H NMR (δ = 7.24 ppm). Fourier transform infrared (FT-IR) spectra were recorded on a Mattson Galaxy series FT-IR 3000. Thermogravimetric analyses (TGA) were obtained in air from a Perkin-Elmer TGA 7. Samples were held at 120 °C for 30 min to remove absorbed water from particle surfaces, and then heated to 850 °C at a rate of 10 °C/min. All samples for FT-IR and TGA were dried from water solution and dried under vacuum at room temperature for 24 h.

Dynamic Light Scattering (DLS) was performed in a Malvern NanoZS ZetaSizer with a 178 degree backscattering detection. Intensity average diameters were calculated from the autocorrelation function using Malvern's Zetasizer Software 6.12. Nanoparticles dispersion stability in media was measured by adding particles to fresh

media and vortex them, then the DLS was taken at certain time.

Synthesis of ((2-propynylcarbamate)propyl)triethoxysilane (74). Propargyl alcohol (12.0 g, 210 mmol) and triethylamine (19.0 g, 190 mmol) were dissolved in 120 mL of dry CH_2Cl_2 and cooled in an ice bath. A solution of 3-(triethoxysilyl)propyl isocyanate (**73**, 46.0 g, 180 mmol) in 60 mL of dry CH_2Cl_2, was added dropwise under nitrogen. The reaction mixture was stirred for 24 h at room temperature and then filtered. CH_2Cl_2, excess propargyl alcohol, and NEt_3 were evaporated under reduced pressure to afford 50 g of **74** as colorless oil. ^{1}H NMR (500 MHz, $CDCl_3$): δ 4.55 (s, 2H), 3.71 (q, 6H, *J* = 7 Hz), 3.08 (m, 2H), 2.37 (s, 1H), 1.52 (m, 2H), 1.11 (t, 9H, *J* = 8 Hz), 0.52 (t, 2H, *J* = 8Hz); ^{13}C NMR (125 MHz, $CDCl_3$) 155.4, 78.40, 74.40, 58.46, 52.26, 43.47,23.14, 18.25, 7.56. IR 3310, 2981, 2936, 2891, 1718, 1536, 1443, 1249, 1107, 1079, 957 cm^{-1}.

Synthesis of 1-azido-2-(2-(2-(2-methoxyethoxy)ethoxy)ethoxyethane (76a). A solution of NaOH (6.00 g, 150 mmol) in a water/THF mixture (6:4 , 30 mL) was added to tetraethylene glycol monomethyl ether (5.2 g, 25 mmol) in 50 mL of THF dropwise at 0 °C. The mixture was stirred for 30 minute and then tosyl chloride (9.5 g, 50 mmol) in 50 mL of THF was added dropwise. The mixture was stirred at 0 °C for 3 hours and then for 6 hours at room temperature. The mixture was poured into ice water and the water layer was extracted with ether (3 x 50 mL). The combined organic layer was washed with saturated aqueous NaCl, dried over Na_2SO_4 and concentrated. The resulted tosylate was used without further purification (8.0 g, 91 %). The prepared tosylate (8 g,

22 mmol), NaI (1 g) and sodium azide (4.8 g, 70 mmol) were dissolved in 50 ml of DMF and heated at 60 °C for 24 h. The solution was cooled and added to 100 mL of water. The solution was extracted with ether (4 x 50 mL) and the combined organic layer was washed with saturated NaCl (2 x 100 ml) and dried over Na_2SO_4. The ether was evaporated to give product (**76a**) as light yellow oil, 4.3 g, 85 %. ^{1}H NMR (500 MHz, $CDCl_3$): δ 3.69–3.64 (m, 12 H), 3.52 (m, 2 H), 3.36-3.34 (m, 5H); ^{13}C NMR (75 MHz, $CDCl_3$): δ 72.87, 70.75, 70.72, 70.66, 70.63, 70.50, 70.02, 59.05, 50.7; IR 2928, 2874, 2094, 1441, 1329, 1245, 1130, 956, 852 cm^{-1}.

Synthesis of mPEG azides (76b-d). Polyethylene glycol monomethyl ether (25 mmol) and TsCl (14 g, 75 mmol) were dissolved in 150 ml of dry CH_2Cl_2. Then 28 mL of triethylamine was added dropwise. The mixture was stirred for 48 h at room temperature. After washed with $NaHCO_3$ (100 mL), 1 M HCl (3 x 200 mL) and water (200 mL), CH_2Cl_2 layer was dried over Na_2SO_4 and concentrated. The resulted tosylate was used directly by mixed with NaI (1 g) and sodium azide (6.5 g, 100 mmol) in 150 mL of DMF and the suspension was heated at 90 °C for 24 h. The solution was cooled and concentrated to remove DMF under vacuum. After dissolved in 100 mL of CH_2Cl_2 (caution: be careful for the possible explosive risk from CH_2Cl_2 and NaN_3), the product was washed with water, dried and concentrated to give light yellow liquid or white solid.

76b: light yellow liquid, 17 g, 90%. ^{1}H NMR (500 MHz, $CDCl_3$): δ 3.56–3.75 (m, 70 H), 3.50-3.54 (m, 2 H), 3.34-3.38 (m, 5H); ^{13}C NMR (75 MHz, $CDCl_3$): δ 72.44, 71.85,

70.61-70.36 (br), 70.13, 69.94, 61.53, 58.94, 50.61; IR 2872, 2111, 1460, 1352, 1300, 1250, 1118, 953, 853 cm^{-1}.

76c: white solid, 37 g, 75%. ^{1}H NMR (500 MHz, $CDCl_3$): δ 3.45–3.77 (m, 200 H), 3.32-3.38 (m, 5H); ^{13}C NMR (75 MHz, $CDCl_3$): δ 71.88, 70.60-70.45 (br), 69.97, 58.98, 50.67; IR 2889, 2106, 1468, 1361, 1278, 1146, 1115, 1063, 950, 842 cm^{-1}.

76d: white solid, 87 g, 70%. ^{1}H NMR (500 MHz, $CDCl_3$): δ 3.48–3.77 (m, 520 H), 3.35-3.39 (m, 5H); ^{13}C NMR (75 MHz, $CDCl_3$): δ 71.91, 70.68-70.30 (br), 70.00, 59.00, 50.67; IR 2889, 2100, 1471, 1358, 1344, 1278, 1148, 1112, 1066, 950, 845 cm^{-1}.

Synthesis of 2-[2-[2-[2-azidoethoxy]ethoxy]ethoxy]ethanol (78). A solution of TsCl (14 g, 71 mmol) in 250 mL of THF was added dropwise to a solution of tetraethylene glycol (34 g, 180 mmol), triethylamine (14 mL) and THF (250 mL). After stirring the resulting solution for 36 h at room temperature, THF was removed by rotary evaporation and the crude product was dissolved in 200 mL of CH_2Cl_2. The organic layer was washed with water (3 × 150 mL), aqueous $NaHCO_3$ (200 mL), and brine (200 mL). After drying over Na_2SO_4, the solution was concentrated and dried under vacuum to give 18 g of a light yellow liquid comprised of a mixture of mono-tosylate (85%) and di-tosylate (15%), 58% yield. The product was used in the next step without further purification. ^{1}H NMR (500 MHz, $CDCl_3$) δ 7.77 (m, 2H), 7.32 (m, 2H), 4.29 (m, 2H), 3.69-3.50 (m, 14H), 2.5 (br, 1H), 2.42 (s, 3H). The tosylates were dissolved in DMF, (210 mL), treated with NaN_3 (10.4 g, 15 mmol), and then heated to 60 °C for 24 h. Then

the mixture was concentrated, re-dissolved in ethyl acetate, filtered to remove the solid, and concentrated under reduced pressure. The resulting oily product was dissolved in water and washed with hexane until α,ω-diazido tetraethylene glycol was not detected in the aqueous layer. Drying under vacuum gave the product as a light yellow liquid (8.0 g, 72%). ^{1}H NMR (500 MHz, $CDCl_3$) δ 3.69 (m, 2H), 3.64 (m, 10H), 3.58 (m, 2H), 3.36 (t, 2H, *J* = 5.5 Hz), 2.8 (br, 1H); ^{13}C NMR (125 MHz, $CDCl_3$) 72.41, 70.55, 70.51, 70.43, 70.18, 69.90, 61.56, 50.54; IR 3412, 2872, 2106, 1457, 1350, 1284, 1123, 944 cm^{-1}.

Synthesis of 2-[2-[2-[2-azidoethoxy]ethoxy]ethoxy]ethyl amine (79). A solution of TsCl (39.9 g, 210 mol) in THF (150 mL) was added dropwise into an ice-cold mixture of tetraethylene glycol (13.5 g, 70 mol), aqueous KOH (100 g, 47%, w/w), and THF (100 mL). After stirring for 36 h at room temperature, THF was removed by rotary evaporation, and then CH_2Cl_2 (200 mL) was added to the residue. The organic layer was washed with water (3 × 150 mL), aqueous $NaHCO_3$ (200 mL), and brine (200 mL). After drying the organic layer over Na_2SO_4, the solution was concentrated and dried under vacuum to give 32 g of a light yellow liquid (91%). ^{1}H NMR (300 MHz, $CDCl_3$) δ 7.81(m, 4H), 7.36 (m, 4H), 4.20 (m, 4H), 3.70-3.65 (m, 12H), 2.47 (s, 6H). The di-tosylate of tetraethylene glycol was treated with NaN_3 (11.7 g, 180 mmol) in DMF (300 mL) at 90 °C for 24 h. The mixture was concentrated, dissolved in water, and extracted with CH_2Cl_2 (4 × 100 mL). The solution was dried over anhydrous Na_2SO_4 and concentrated under reduced pressure to give 12 g of a yellow liquid. Aqueous HCl (5%,

100 mL) was added to the yellow liquid, and under vigorous stirring at room temperature, a solution of PPh_3 (11.4 g, 41.0 mmol) in 75 mL of ether was added dropwise. After stirring for 24 h, the ether was removed by rotary evaporation and the aqueous layer was extracted with CH_2Cl_2 until triphenylphosphine oxide was not detected in the aqueous layer. The aqueous layer was adjusted to pH=12, and amine (**79**) was extracted from the aqueous layer with CH_2Cl_2 (6 × 50 mL). Drying under vacuum gave the product as a light yellow liquid (9.0 g, 68%). ^{1}H NMR (500 MHz, $CDCl_3$) δ 3.72-3.58 (m, 10H), 3.48 (t, 2H, *J* = 5 Hz), 3.35 (t, 2H, *J* = 5 Hz), 2.84 (t, 2H, *J* = 5Hz), 2.24 (s, 2H); ^{13}C NMR (125 MHz, $CDCl_3$) 72.79, 70.50, 70.47, 70.43, 70.07, 69.85, 50.50, 41.44; IR 3350, 2872, 2111, 1589, 1460, 1347, 1297, 1123, 939, 859 cm^{-1}.

Synthesis of 2-[2-[2-[2-azidoethoxy]ethoxy]ethoxy]acetic acid (83). A solution of [2-[2-[2-chloroethoxy]ethoxy]ethanol (**80**, 16.8 g, 100 mmol) and NaN_3 (13 g, 200 mmol) in 75 mL of water was heated at 75 °C with stirring for 24 h. Water was removed by rotary evaporation and the crude product was extracted from the salts with 200 mL of CH_2Cl_2. Concentration and drying under vacuum gave the product as a light yellow liquid (17 g, 97%), which was used without further purification. ^{1}H NMR (500 MHz, $CDCl_3$) δ 3.72-3.62 (m, 8H), 3.58 (m, 2H), 3.37 (t, 2H, *J* = 5 Hz). The light yellow liquid product (14 g, 80 mmol) was added to NaH (100 mol) in 350 mL of dry THF cooled in an

ice bath. After stirring for 1 h at room temperature, ethyl bromoacetate (17.7 mL, 160 mmol) was added dropwise and then stirred for 48 h at room temperature. The THF was removed, and 150 mL of water was added. The aqueous layer was extracted with CH_2Cl_2 (3 × 50 mL), dried over anhydrous Na_2SO_4, and concentrated under reduced pressure at 55 °C to give an amber liquid (26 g), which was used without further purification. ^{1}H NMR (500 MHz, $CDCl_3$) δ 4.24 (q, 2H, *J* = 10 Hz), 4.17 (s, 2H), 3.77-3.65 (m, 10H), 3.41 (t, 2H, *J* = 5 Hz). The ester was hydrolyzed with 53 mL of 3M NaOH at room temperature for 18 h. After extracting the aqueous layer with CH_2Cl_2 (10 × 30 mL) to remove mineral oil and other impurities, the aqueous layer was acidified to pH=1 and extracted with EtOAc (1 × 80 mL, 7 × 30 mL). After dred over anhydrous Na_2SO_4, the residue was concentrated to a pale red liquid (14 g, 75%). ^{1}H NMR (500 MHz, $CDCl_3$) δ 4.18 (s, 2H), 3.78-3.67 (m, 10H), 3.41 (t, 2H, *J* = 5 Hz); ^{13}C NMR (125 MHz, $CDCl_3$) 177.88, 76.71, 75.95, 75.69, 75.48, 75.31, 74.02, 55.9; IR 3120, 2927, 2853, 2536, 2111, 1741, 1443, 1354, 1289, 1123, 936, 853 cm^{-1}.

Surface modification of SNPs

Synthesis of alkynyl SiNP. commercial available SiNPs (9.0 g of 40% or 20% suspension in water) were diluted with 37.5 mL of water followed by addition of 37.5 ml of ethanol and sonicated. The pH of the silica suspension was adjusted to ~9 by adding drops of aqueous ammonia followed by the addition of a solution of **74** (3.0 g, 10 mmol) in 10 mL of ethanol dropwise. After stirring for 3 days, the suspension was diluted with EtOH until it was homogeneous. The modified particles were purified by dialysis in

EtOH and water (9:1) using dialysis tubing (**SiNP8**, MWCO: 50 K; other **SiNPs**, MWCO: 300K). The surface coverage of the alkyne functional group was evaluated by TGA and FT-IR. The hydrodynamic diameters were measured by DLS. The particle concentration (mg/g) was determined by evaporating 2 - 4 mL of purified particle solutions.

Click surface modification of SiNPs. Click chemistry between alkynyl SiNPs and clicking reagents is described using the synthesis of **SiNP25/76a** as example. A **SiNP25** suspension in 13.8 g of EtOH/water (9:1) (100 mg of **SiNP25**, 0.036 mmol of alkyne functional groups) was diluted with 30 mL of DMF/water (3:1), then **76a** (41.9 mg, 0.180 mmol, 5 equiv.) and sodium ascorbate (14.3 mg, 2 equiv.) were added to the mixture. After trace O_2 was removed by three freeze-pump-thaw cycles, aqueous $CuSO_4$ (72 μL, 0.10 M, 0.2 equiv.) was added to the solution followed by a final degassing process, and the solution changed to light brown-yellow. After stirring at room temperature for 36 h, 1 mL of aqueous EDTA (0.1M) was added and the solution was stirred for another 6 h. The resulting particles were dialyzed against (MWCO:12-14K) EtOH/water (9:1, 5 × 2 L) and against distilled water to afford purified surface-modified SiNPs with different sizes and surface chemistry. For the synthesis of -NH2 modified **SiNP25/79**, 1 mL of aqueous EDTA (0.1M) was not added after click chemistry, instead, it was dialyzed directly as mentioned above followed by sonication of the **SiNP25/79** suspension to be homogeneous. Then ion exchange resin (2 g, Amberlite® IRC-748) was added to remove Cu^{2+} under gentle stirring, and this resin was removed via filtration through cotton after stirring for 8 hours. All modified SiNPs were kept in deionized water until further characterization. The surface coverage of surface functional groups after each

step modification was evaluated by TGA. DLS samples were prepared by diluting solutions to 0.1 or 1 mg/mL. The particle concentration (mg/g) was determined by evaporating 2-4 mL of purified particle solutions.

.

APPENDIX

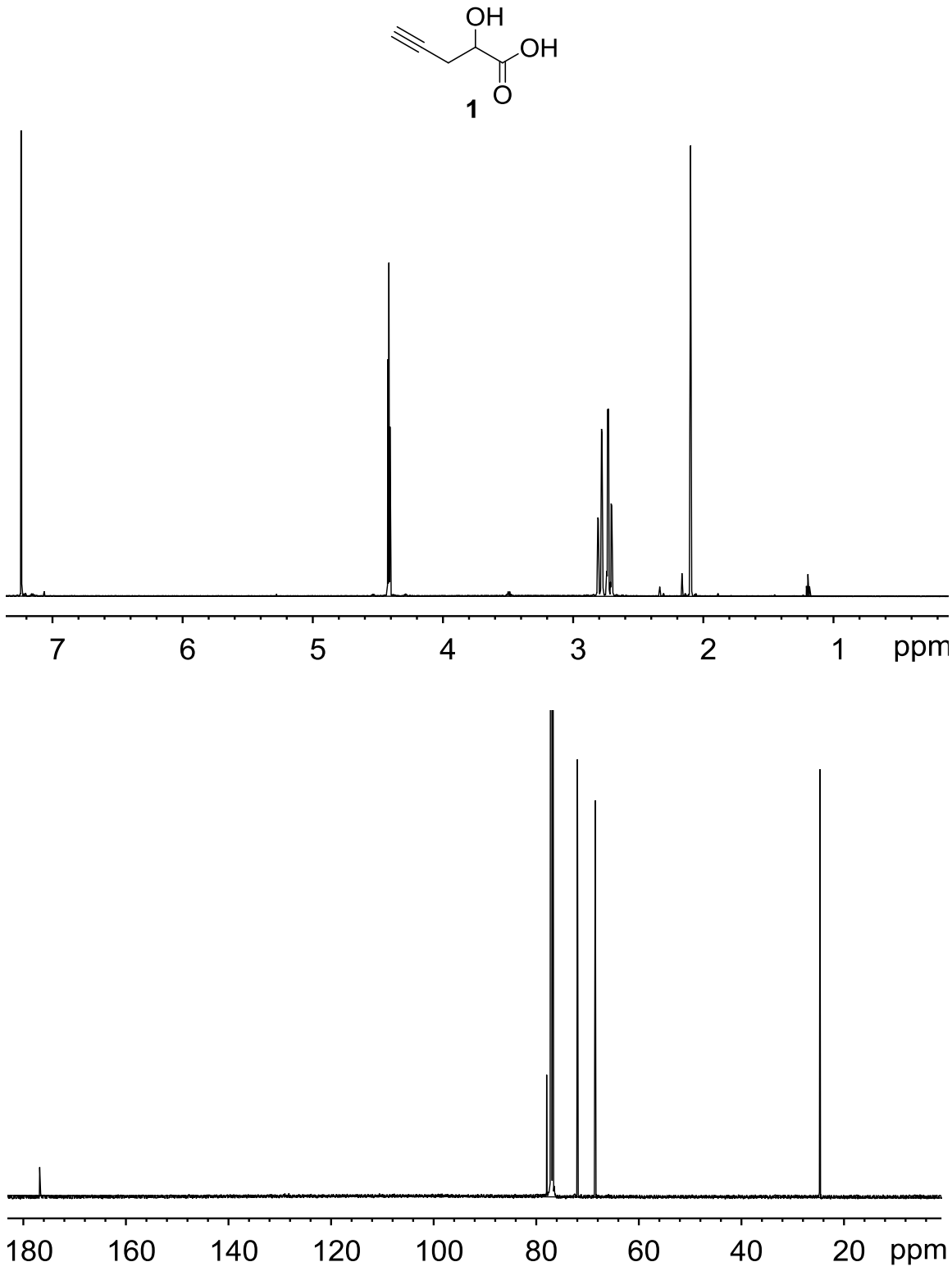

Figure A 1. ^{1}H and ^{13}C NMR spectra of propargyl glycolic acid (**1**) in $CDCl_3$.

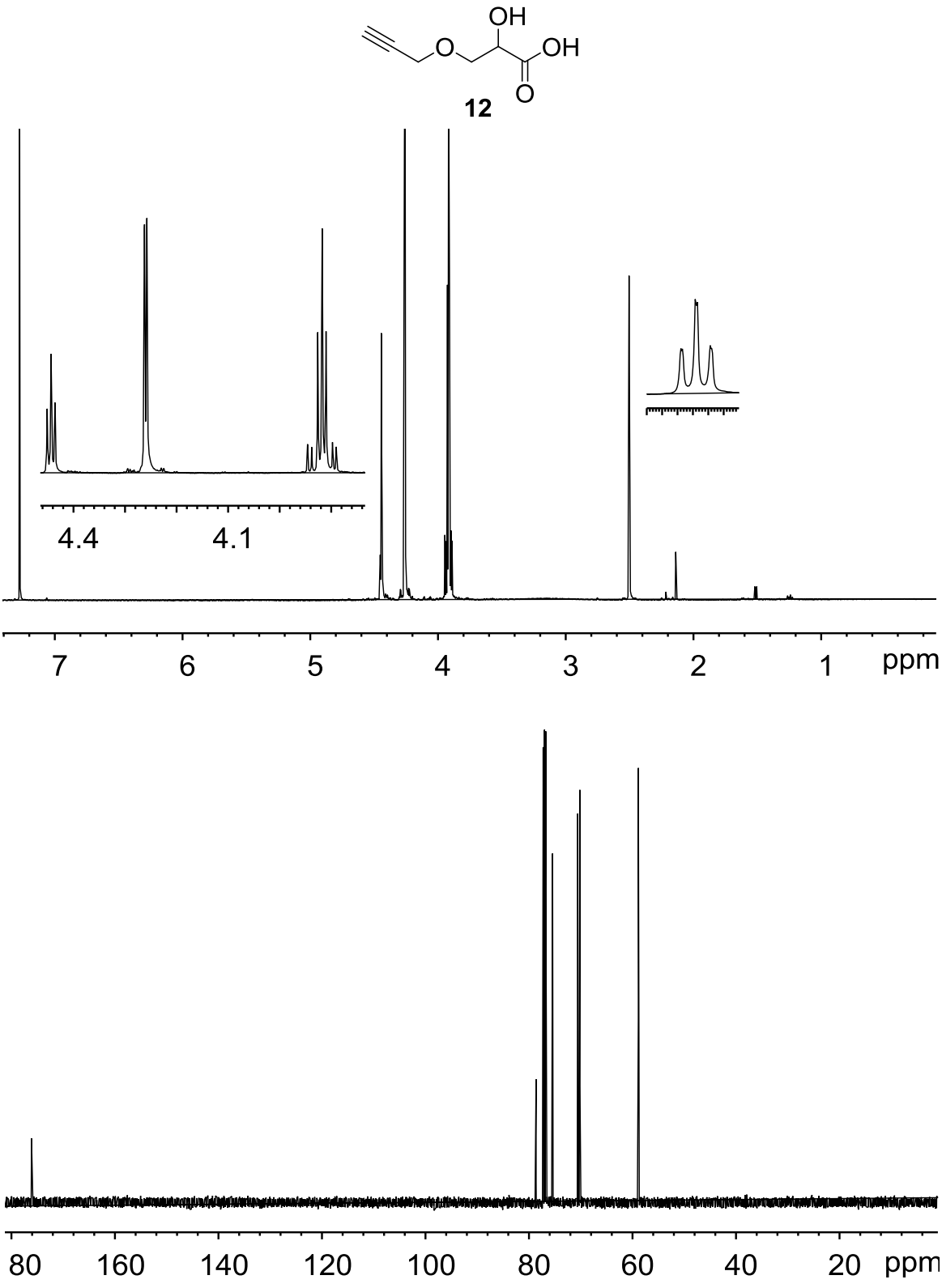

Figure A 2. ^{1}H and ^{13}C NMR spectra of propargyloxy lactic acid (**12**) in $CDCl_3$.

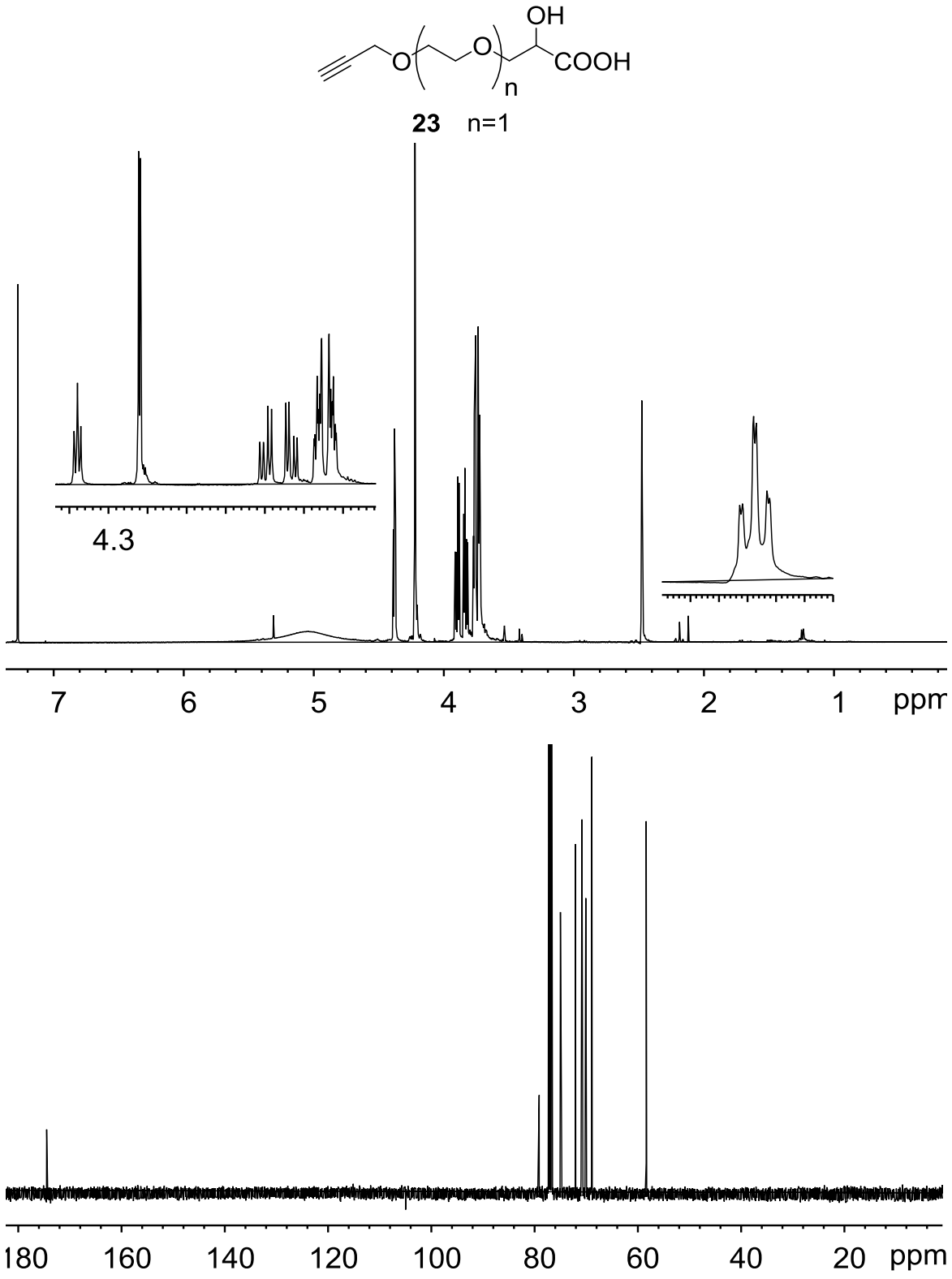

Figure A 3. ^{1}H and ^{13}C NMR spectra of poly(ethylene glycol) monopropargy lether lactic acid (**23**, n =1) in $CDCl_3$.

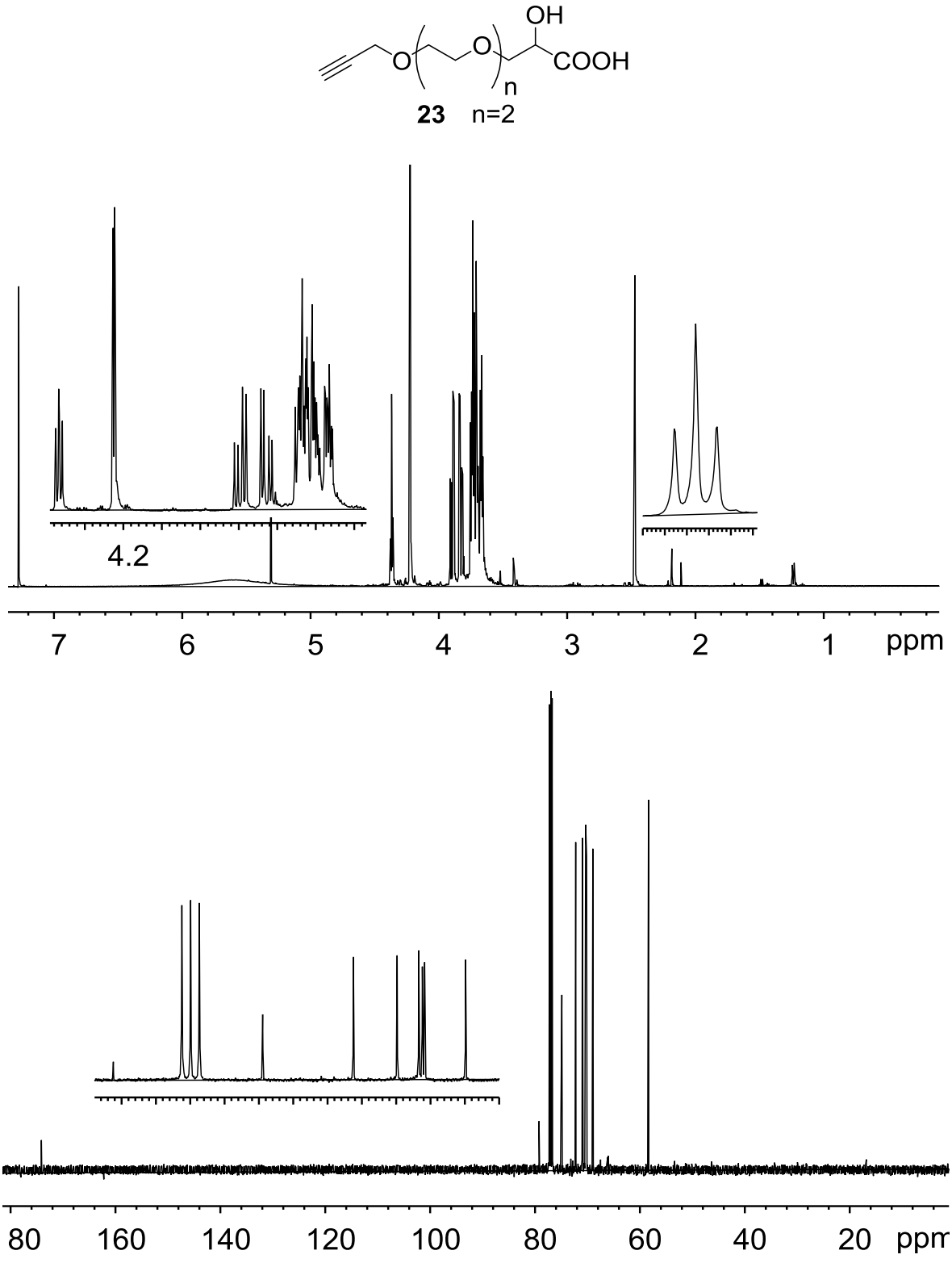

Figure A 4. ^{1}H and ^{13}C NMR spectra of poly(ethylene glycol) monopropargyl ether lactic acid (**23**, n =2) in $CDCl_3$.

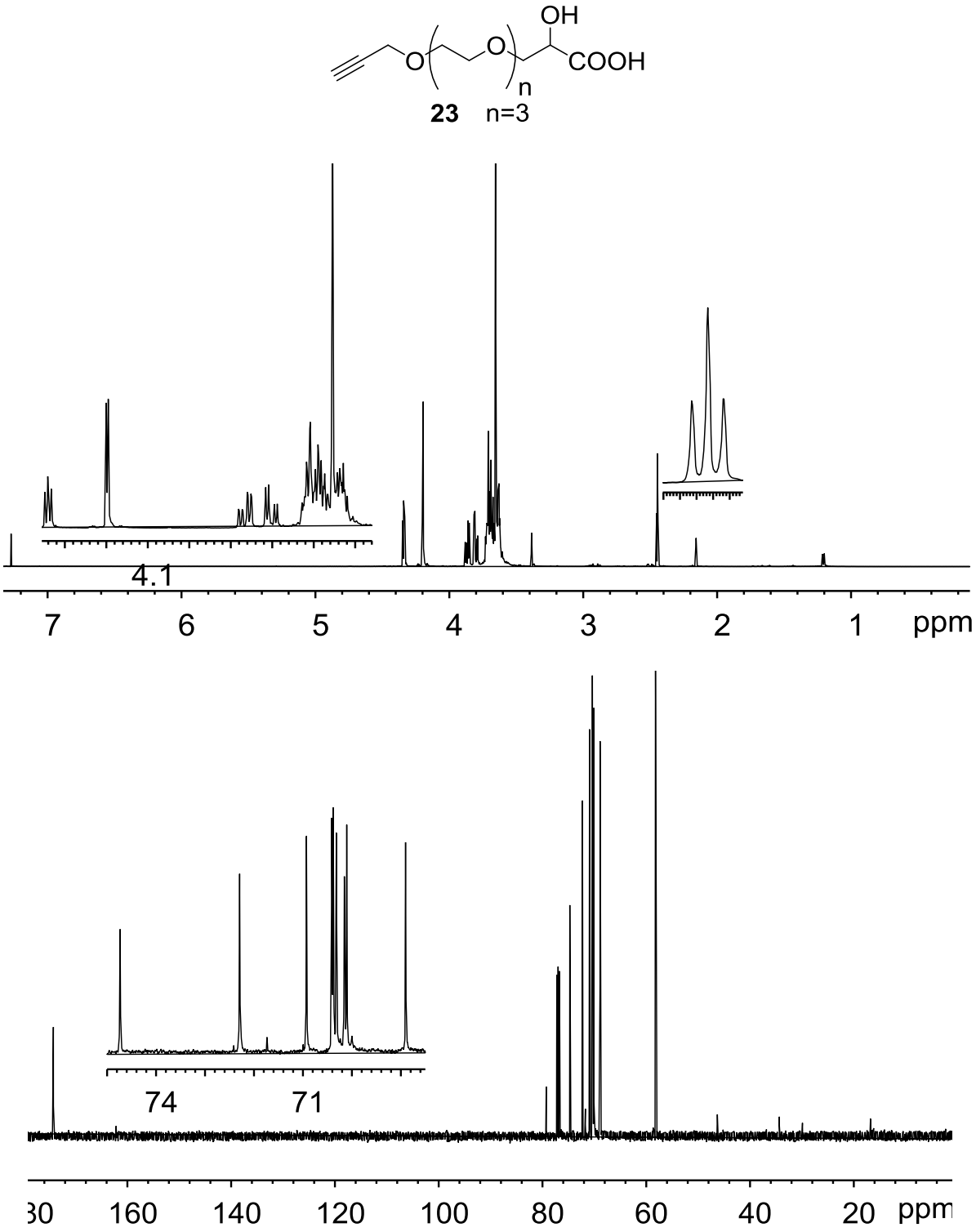

Figure A 5. ^{1}H and ^{13}C NMR spectra of poly(ethylene glycol) monopropargyl ether lactic acid (**23**, n =3) in $CDCl_3$.

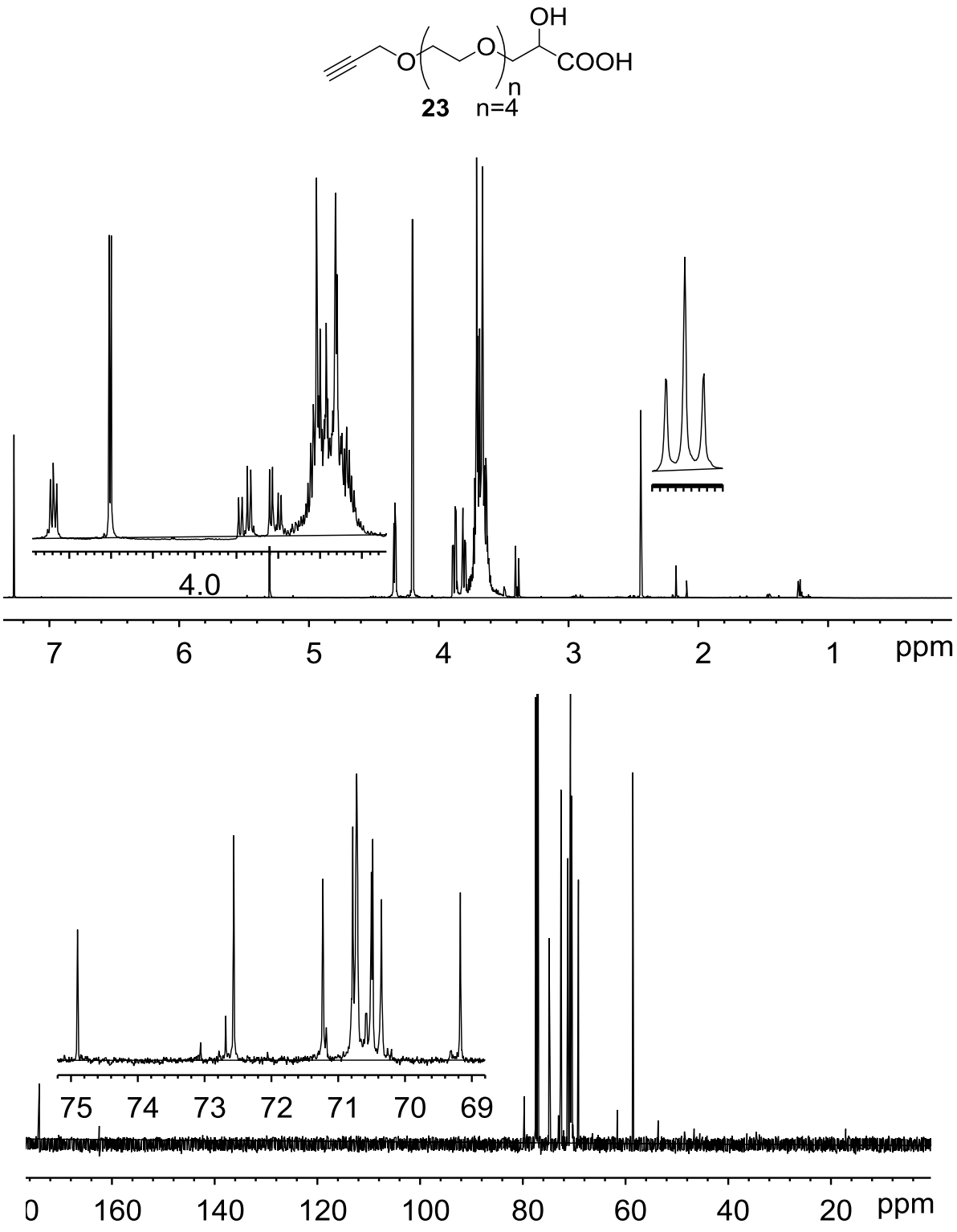

Figure A 6. ^{1}H and ^{13}C NMR spectra of poly(ethylene glycol) monopropargyl ether lactic acid (**23**, n =4) in $CDCl_3$.

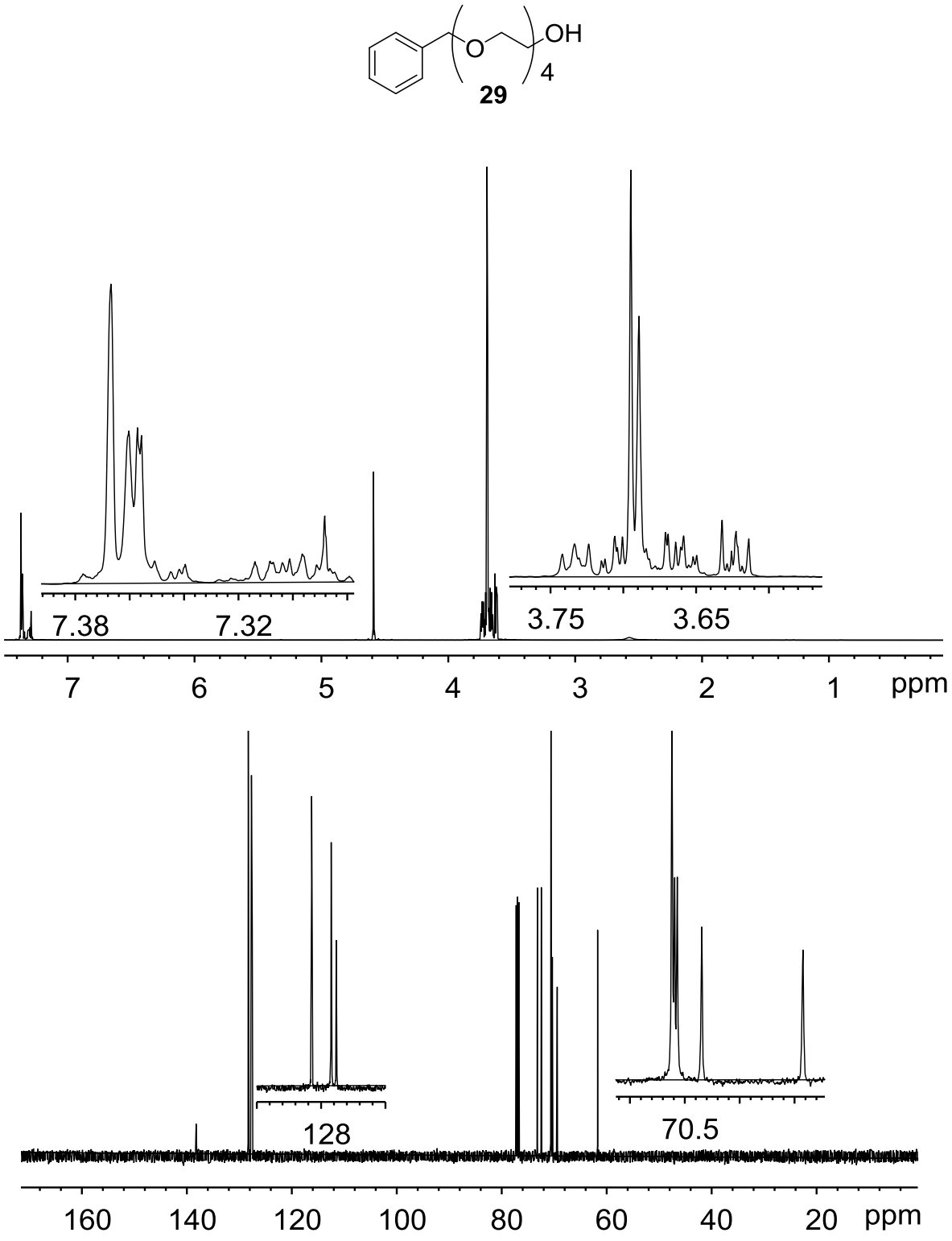

Figure A 7. ^{1}H and ^{13}C NMR spectra of tetraethylene glycol monobenzyl ether (**29**) in $CDCl_3$.

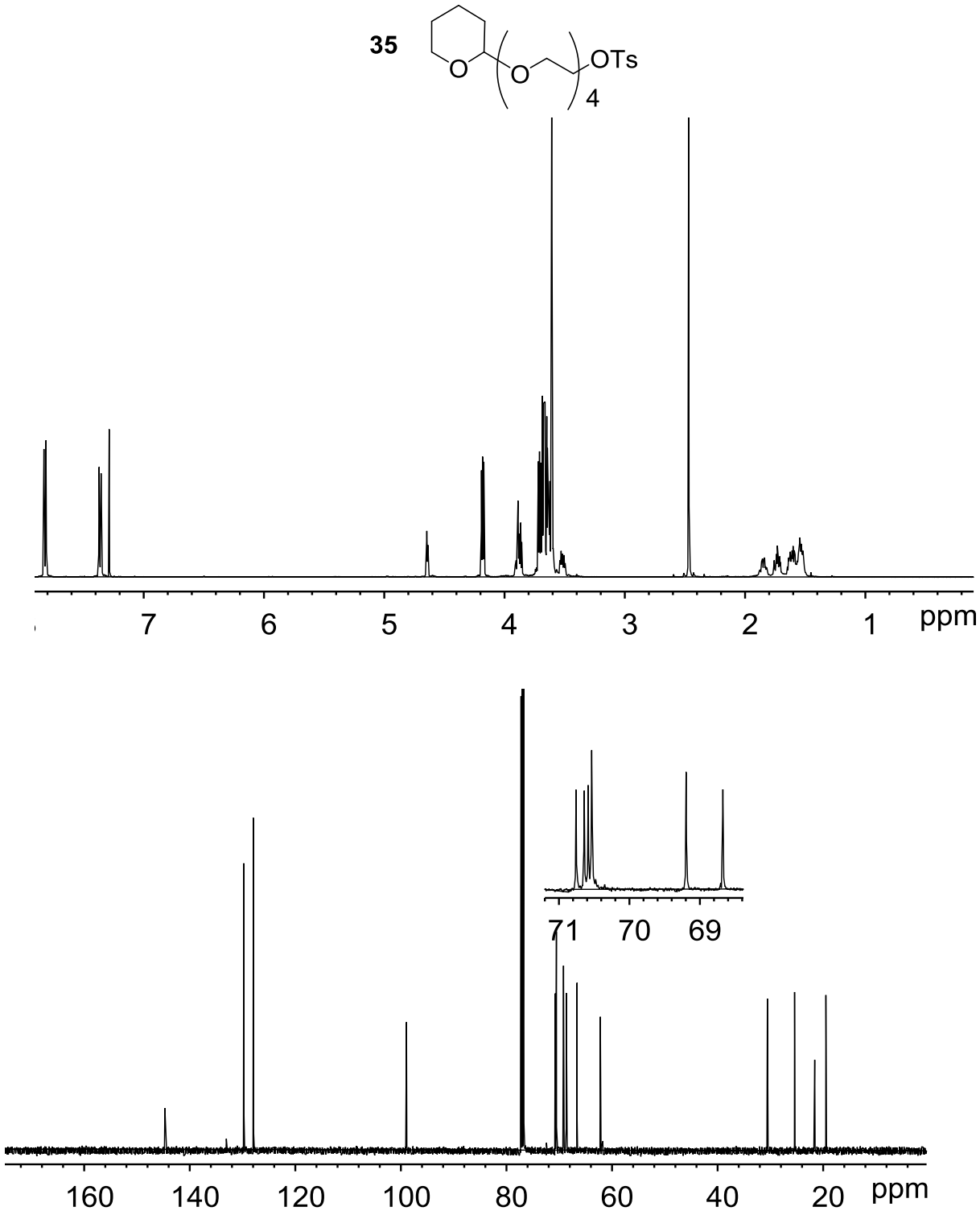

Figure A 8. ^{1}H and ^{13}C NMR spectra of monotetrahydropyran-protected tetraethylene glycol monotosylate (**35**) in $CDCl_3$.

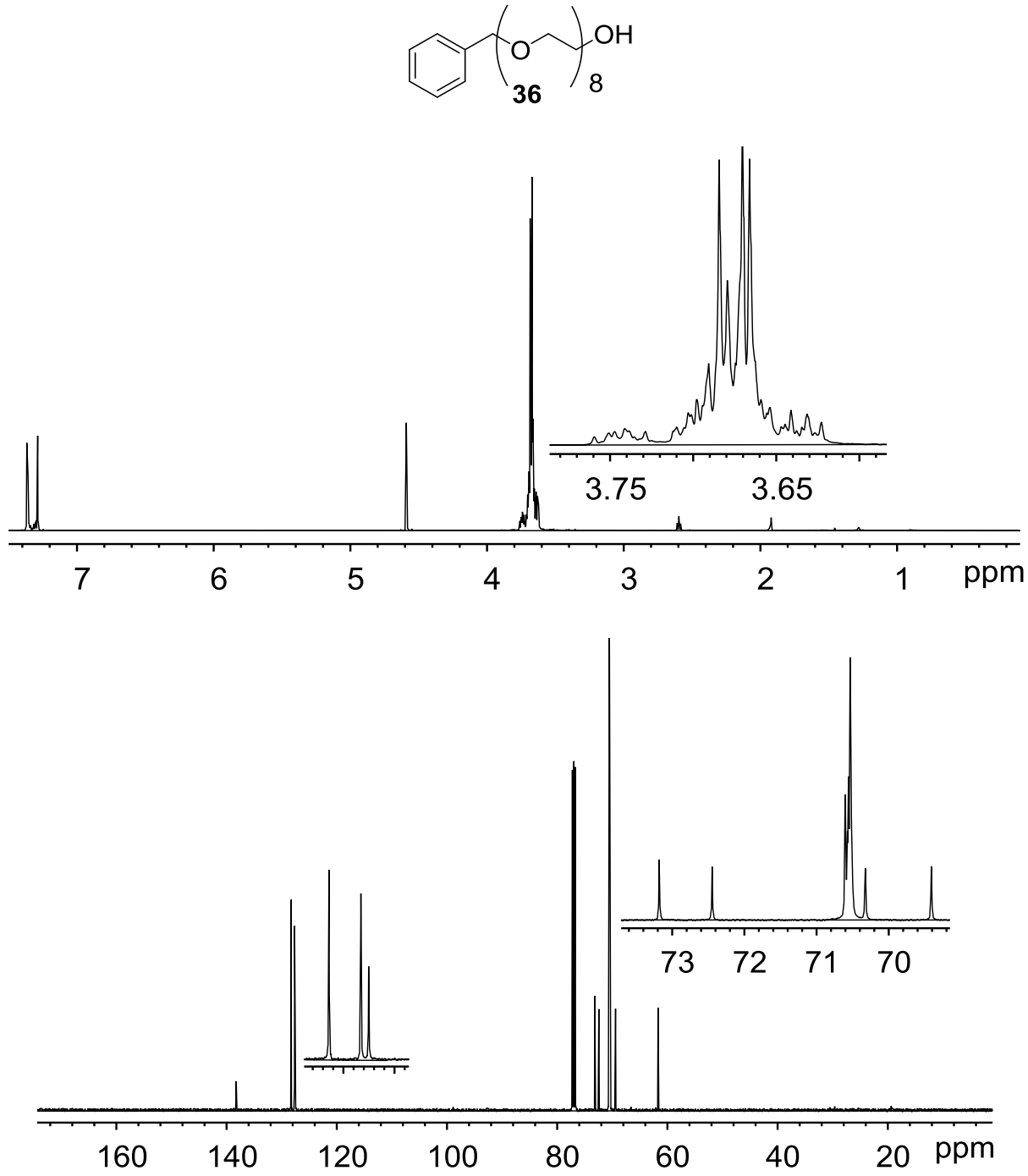

Figure A 9. ^{1}H and ^{13}C NMR spectra of octa(ethylene glycol) monobenzyl ether (**36**) in $CDCl_3$.

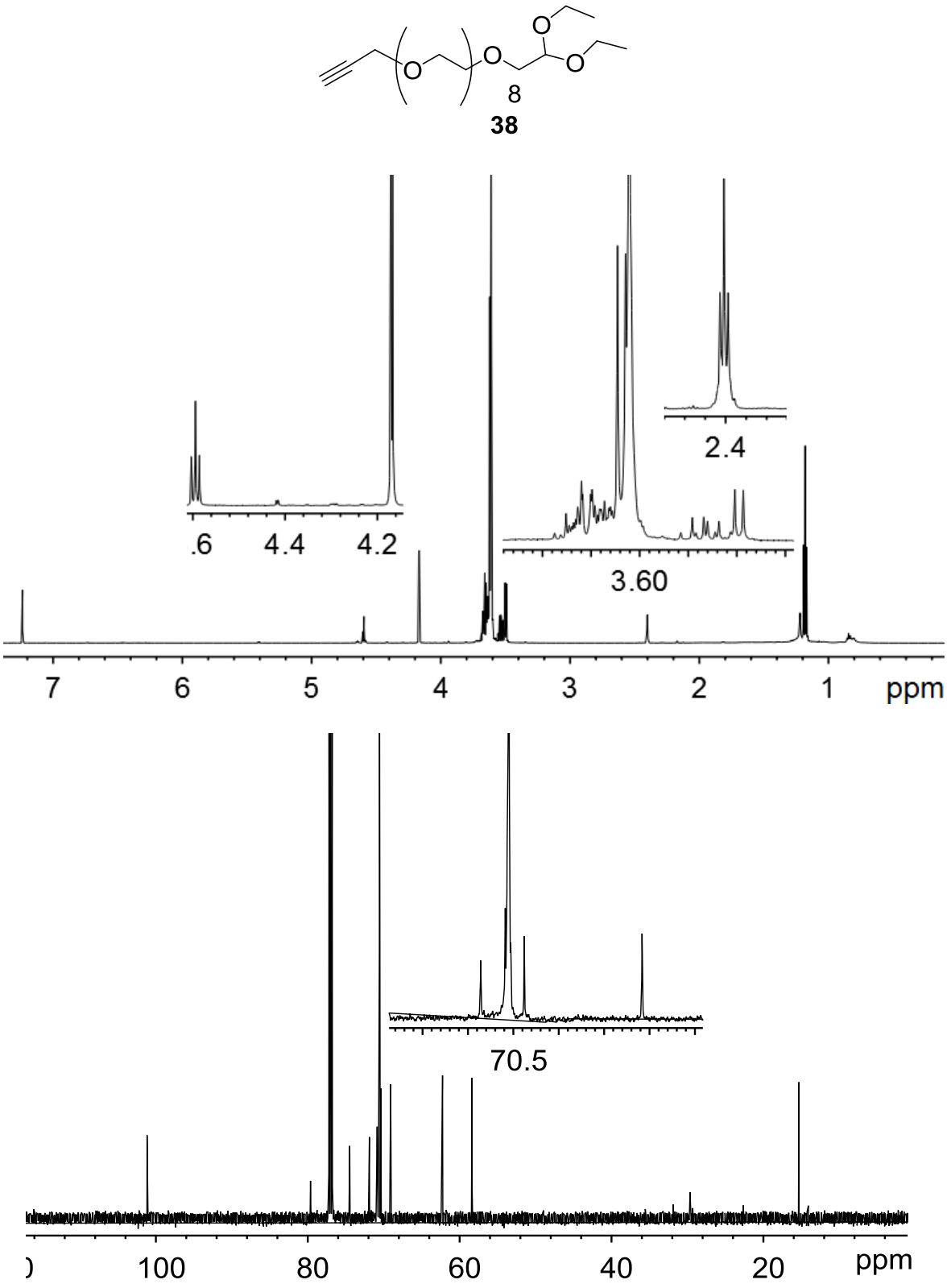

Figure A 10. ^{1}H and ^{13}C NMR spectra of **38** in $CDCl_3$.

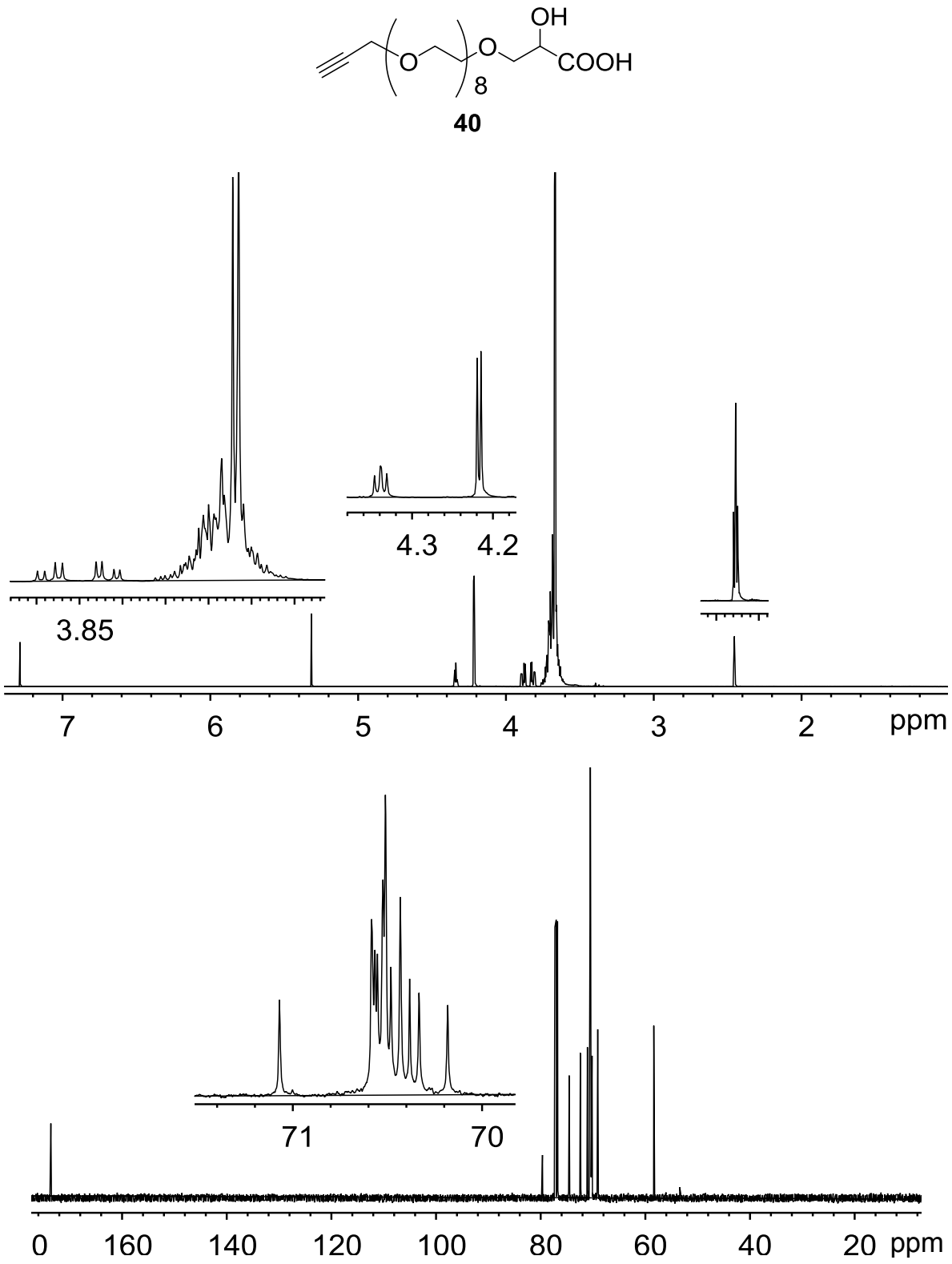

Figure A 11. ^{1}H and ^{13}C NMR spectra of octa(ethylene glycol) monopropargyl ether lactic acid (**40**) in $CDCl_3$.

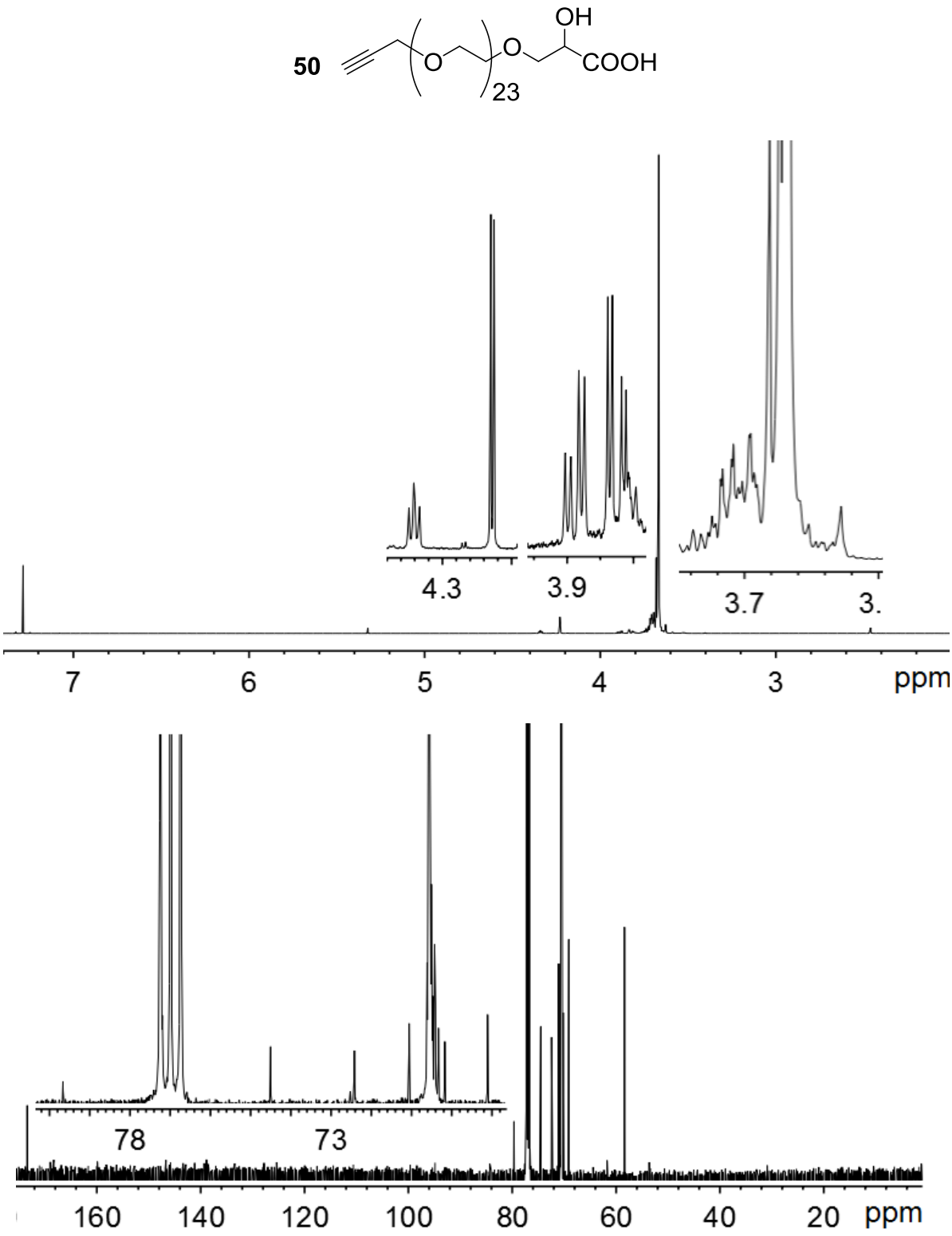

Figure A 12. ^{1}H and ^{13}C NMR spectra of poly(ethylene glycol) monopropargyl ether lactic acid (**50**) in $CDCl_3$.

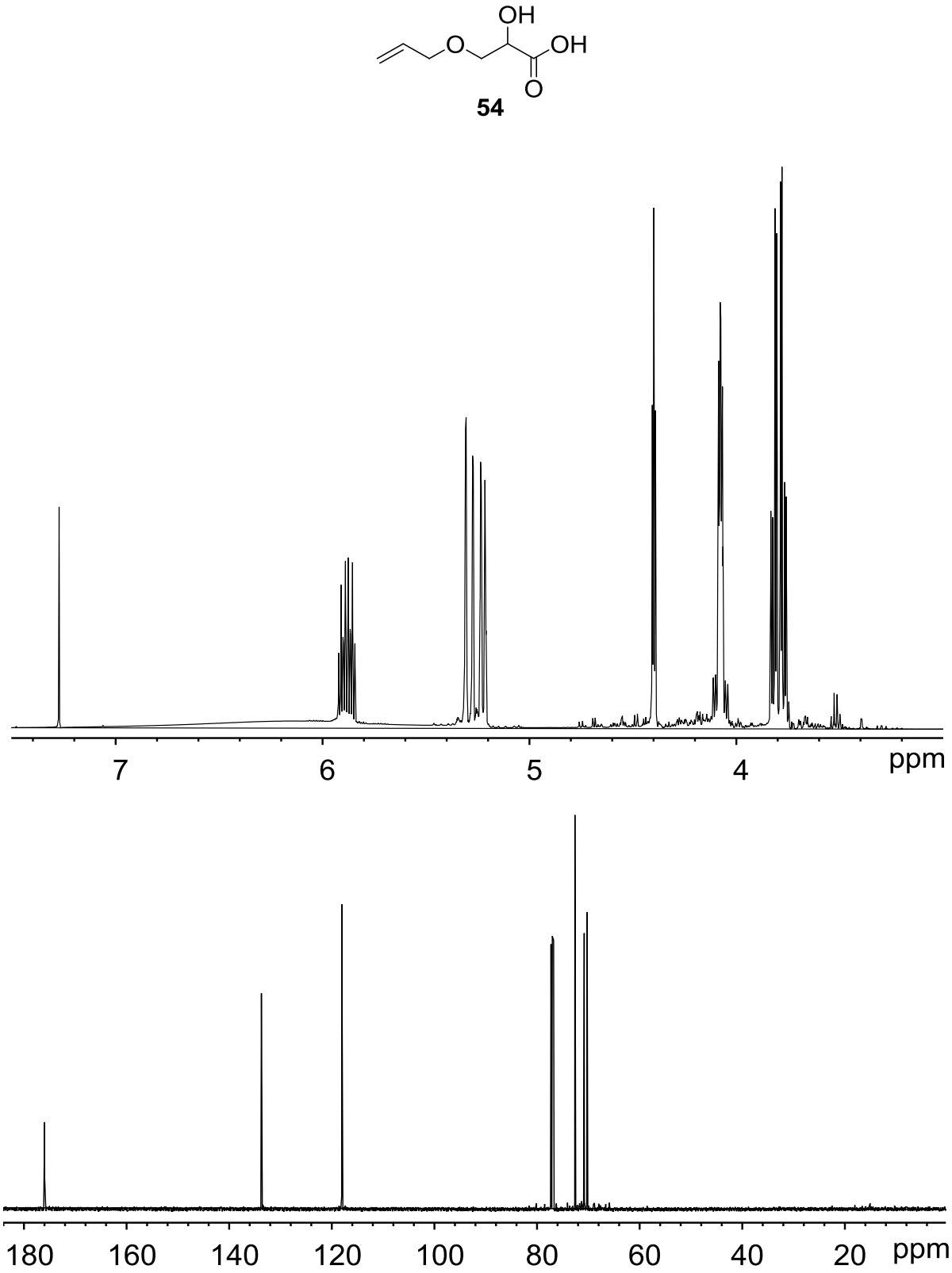

54

Figure A 13. ^{1}H and ^{13}C NMR spectra of allyloxy lactic acid (**54**) in $CDCl_3$.

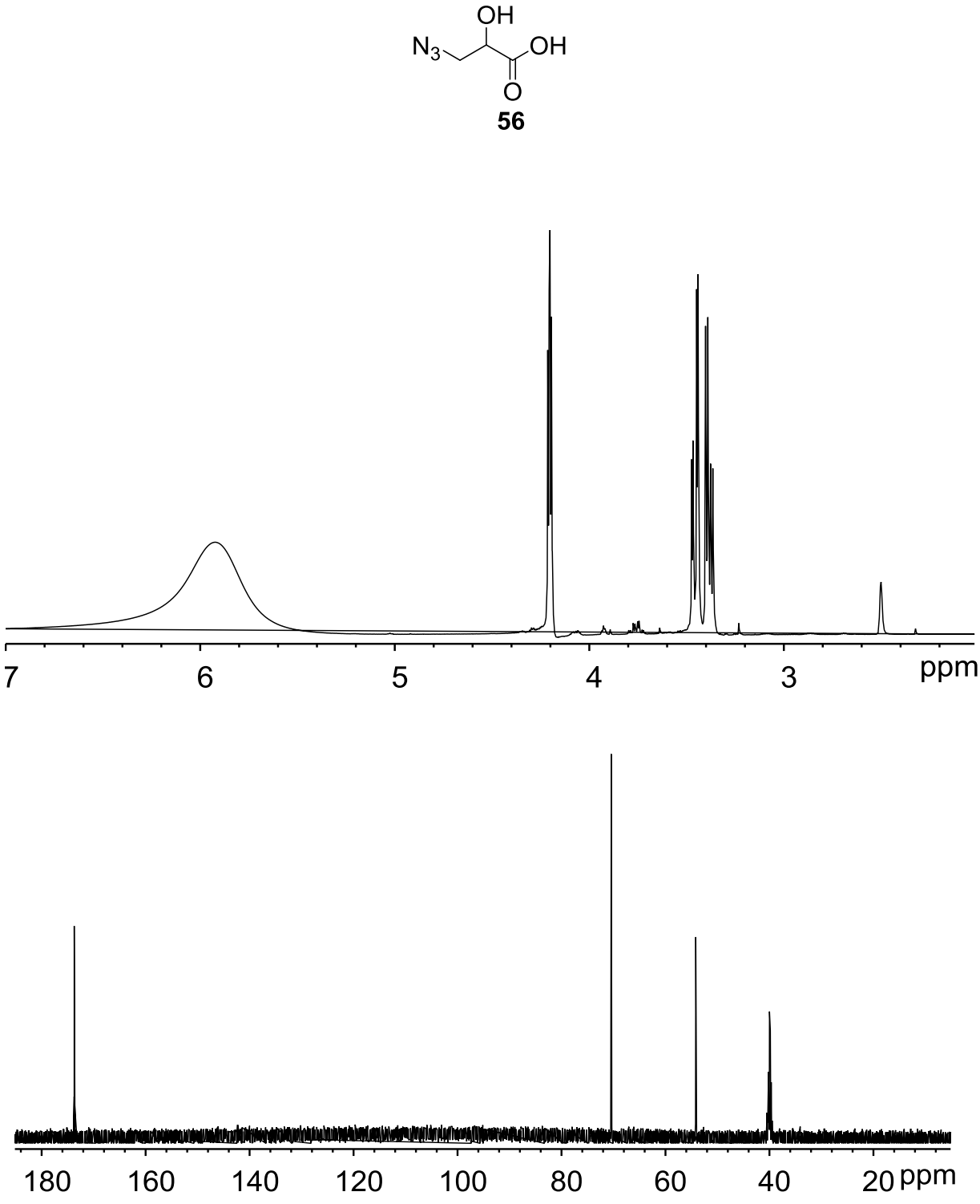

Figure A 14. ^{1}H and ^{13}C NMR spectra of azido lactic acid (**56**) in DMSO-d_6.

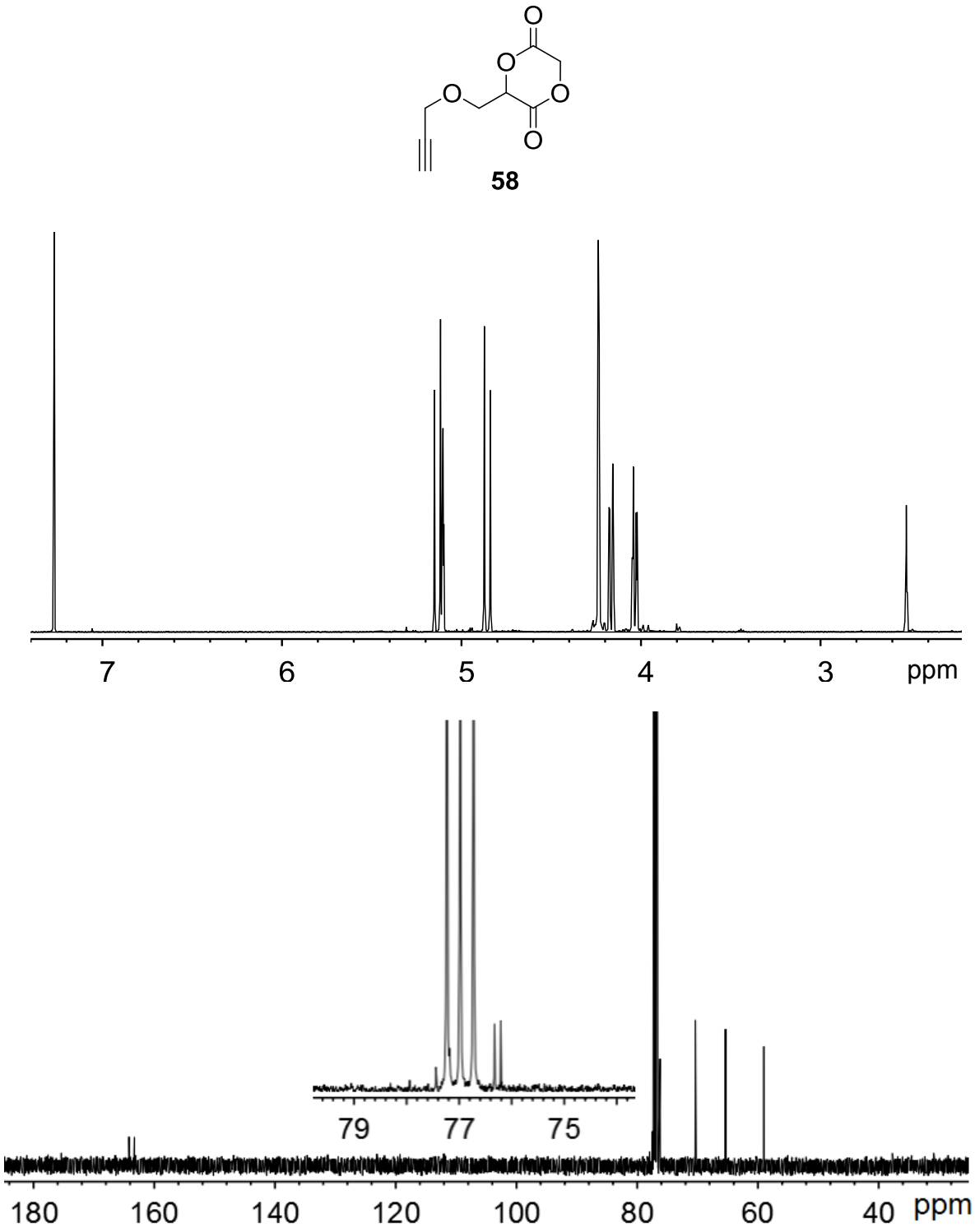

Figure A 15. ^{1}H and ^{13}C NMR spectra of hetero-monomer (**58**) in $CDCl_3$.

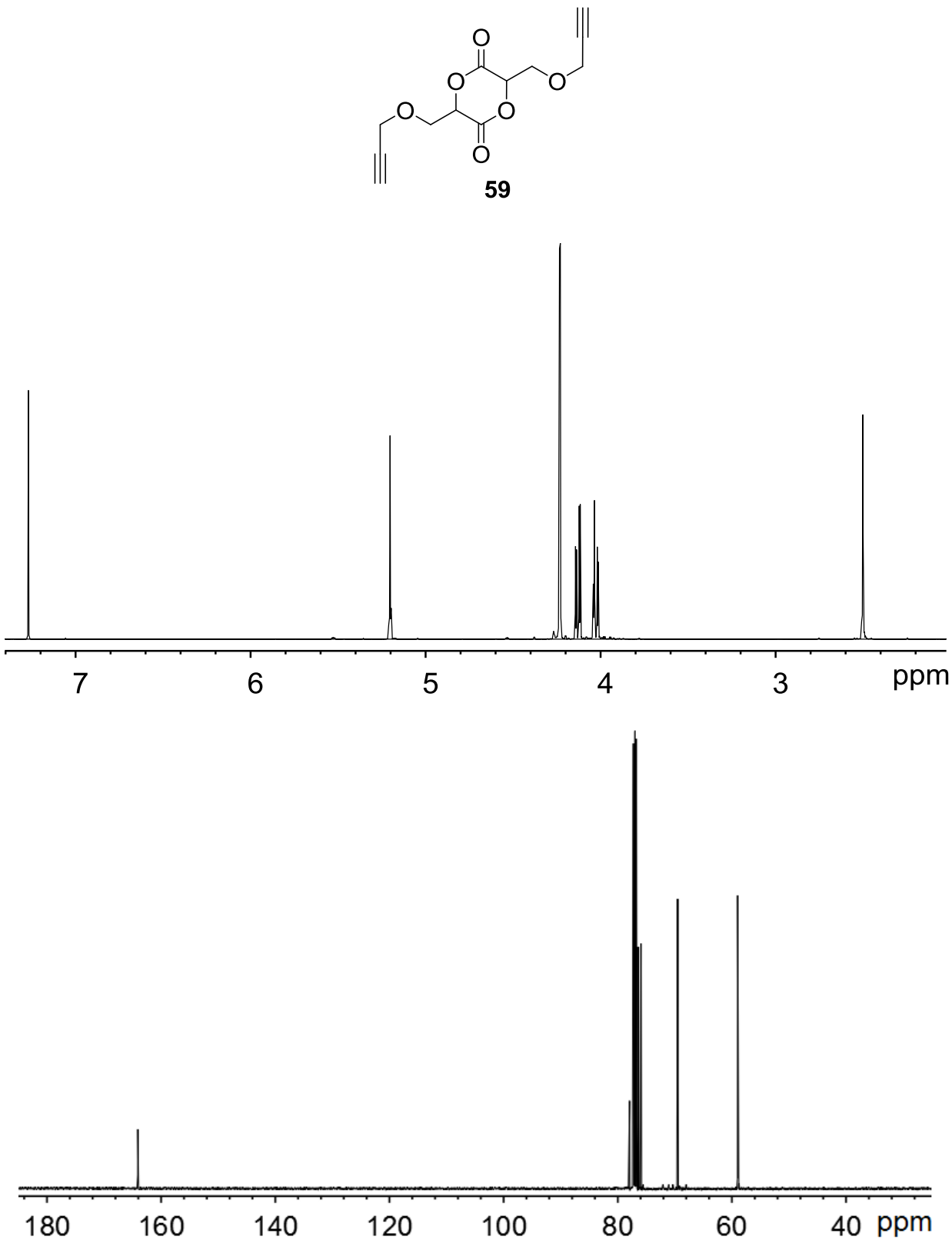

Figure A 16. ^{1}H and ^{13}C NMR spectra of homo-monomer (**59**) in $CDCl_3$.

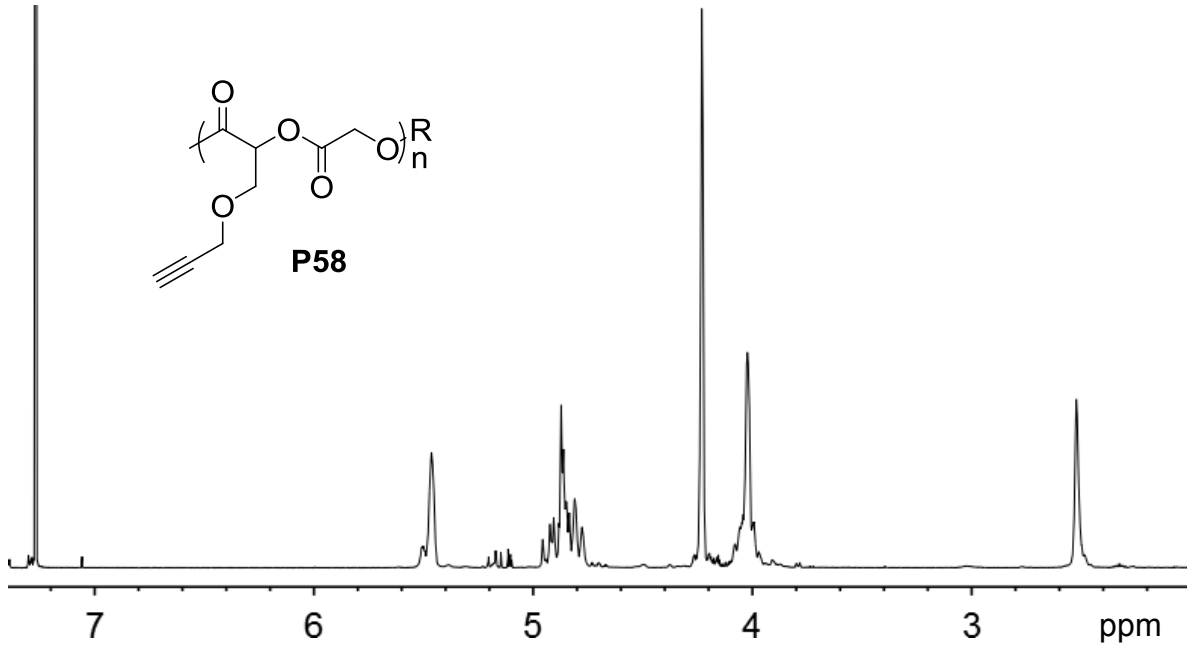

Figure A 17. ^{1}H NMR spectra of polymer **P58A** in $CDCl_3$.

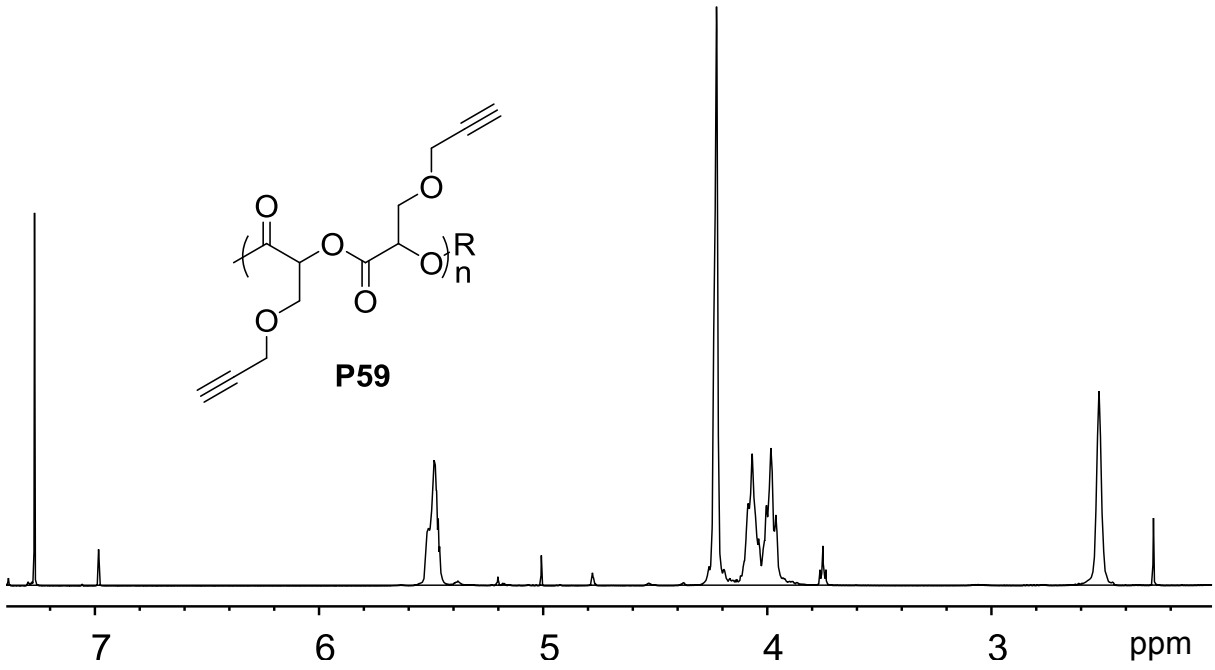

Figure A 18. ^{1}H NMR spectra of polymer **P59A** in $CDCl_3$.

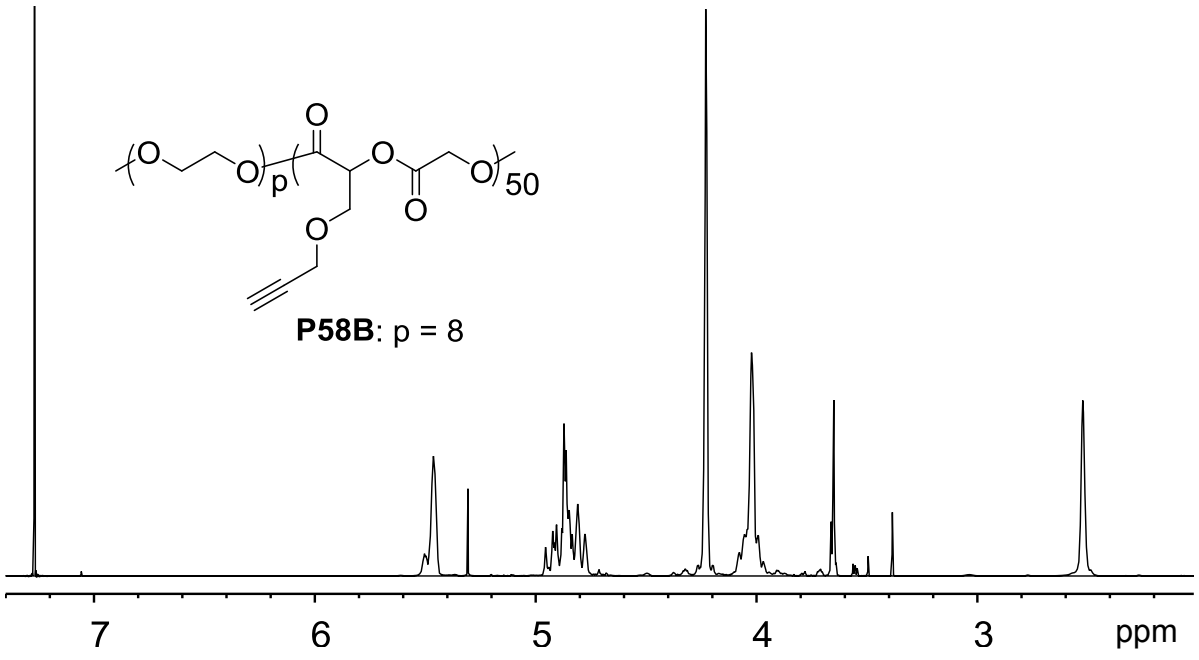

Figure A 19. ^{1}H NMR spectra of polymer **P58B** in $CDCl_3$.

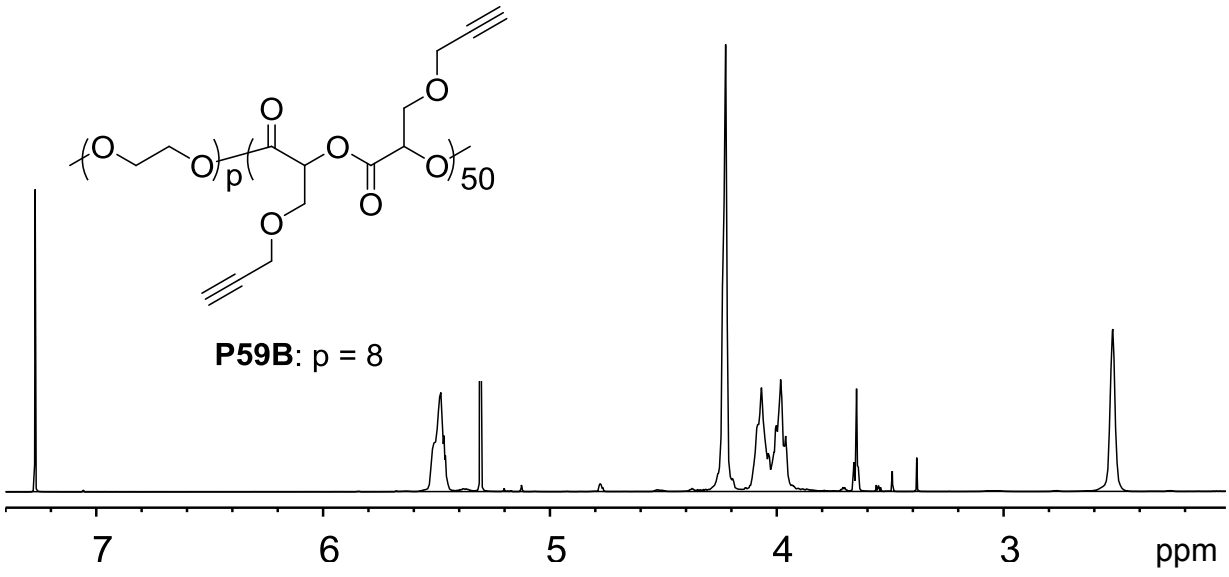

Figure A 20. ^{1}H NMR spectra of polymer **P59B** in $CDCl_3$.

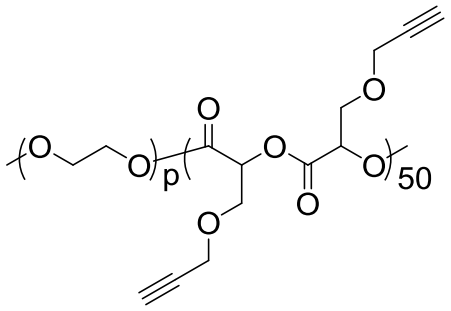

P59C: p = 44

Figure A 21. ^{1}H NMR spectra of polymer **P59C** in $CDCl_3$.

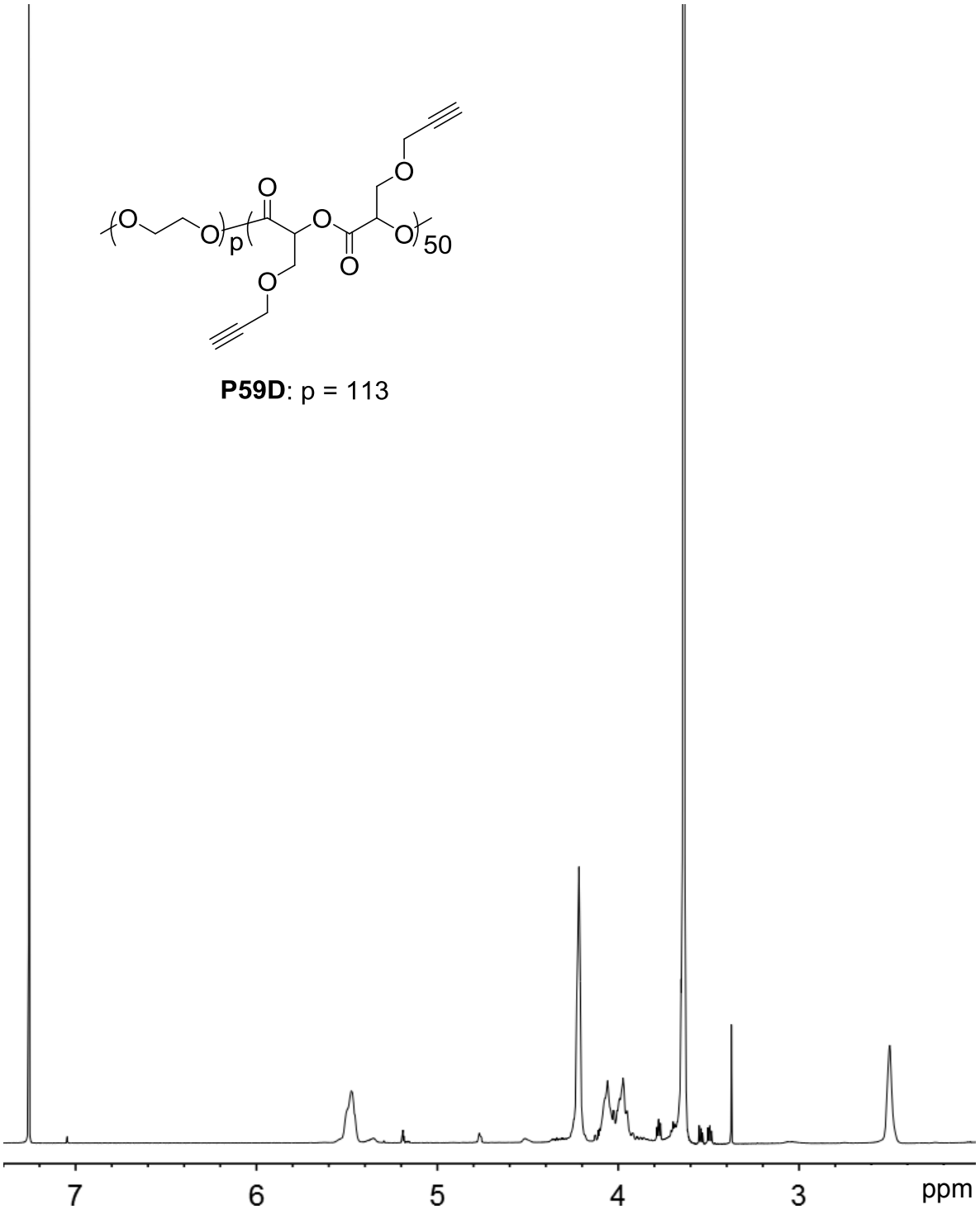

P59D: p = 113

Figure A 22. ^{1}H NMR spectra of polymer **P59D** in $CDCl_3$.

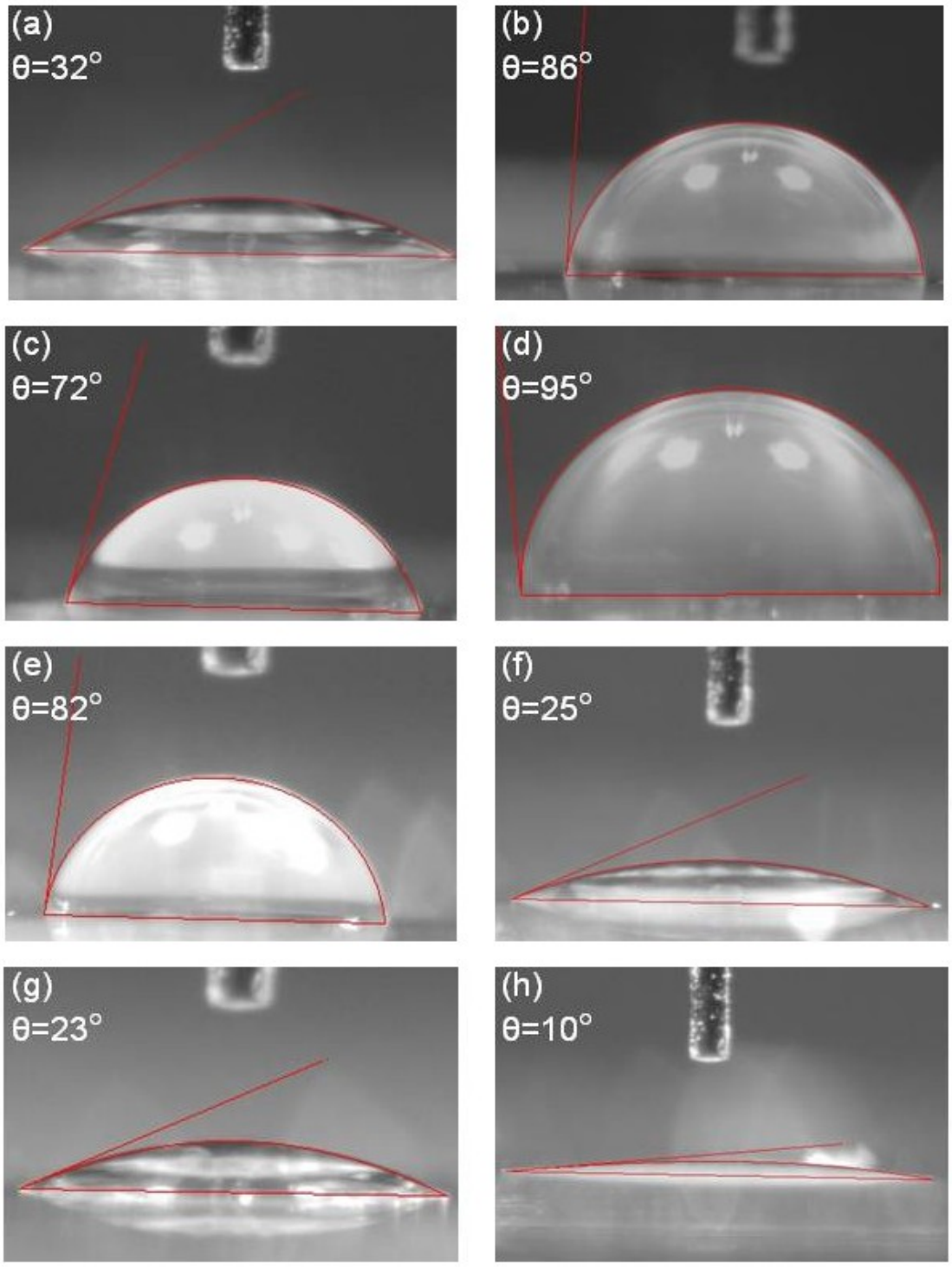

Figure A 23. Water contact angle of glass substrate (**a**); **P58** film (**b**); **P58B** film (**c**); **P59** film (d); **P59B** film (e); **P59C** film (**f**); **P59D** film (**g**); **P60** film (**h**).

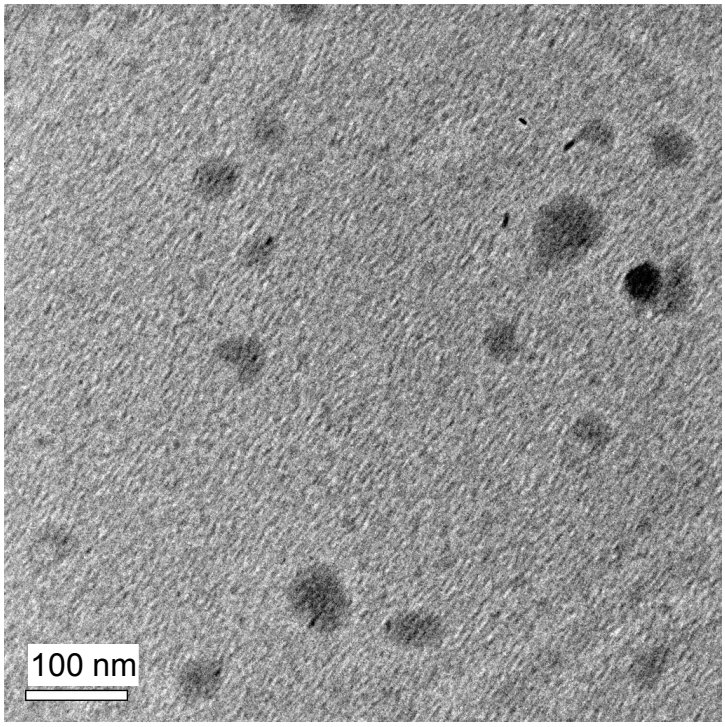

Figure A 24. TEM of **UCMP58B**. Scale bar: 100 nm.

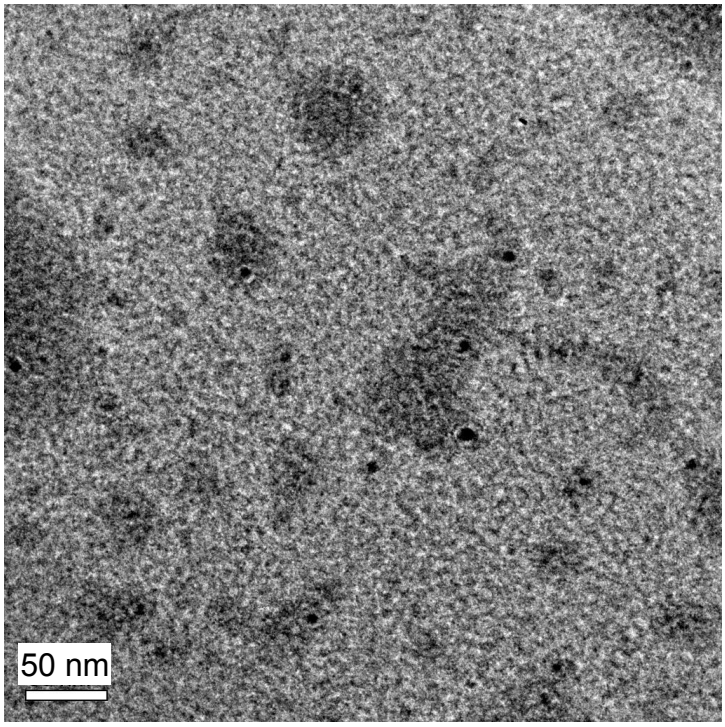

Figure A 25. TEM of **UCMP59B** Scale bar: 50 nm.

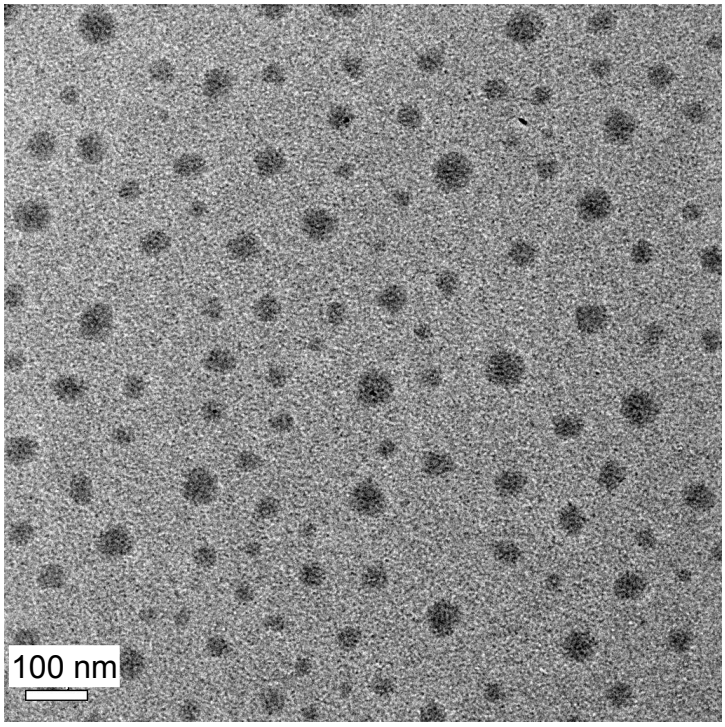

Figure A 26. TEM of **UCMP59C** Scale bar: 100 nm.

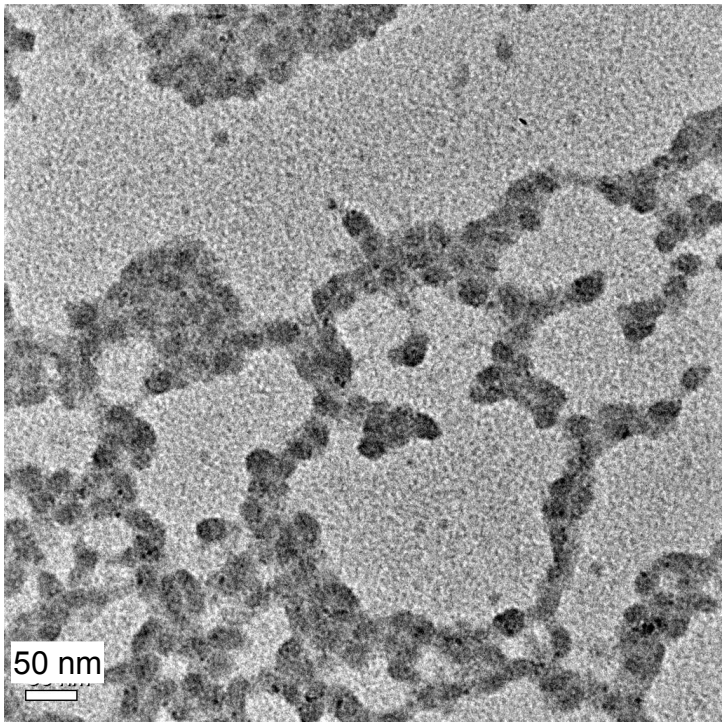

Figure A 27. TEM of **CMP59C** from cross-linker **63**. Scale bar: 50 nm.

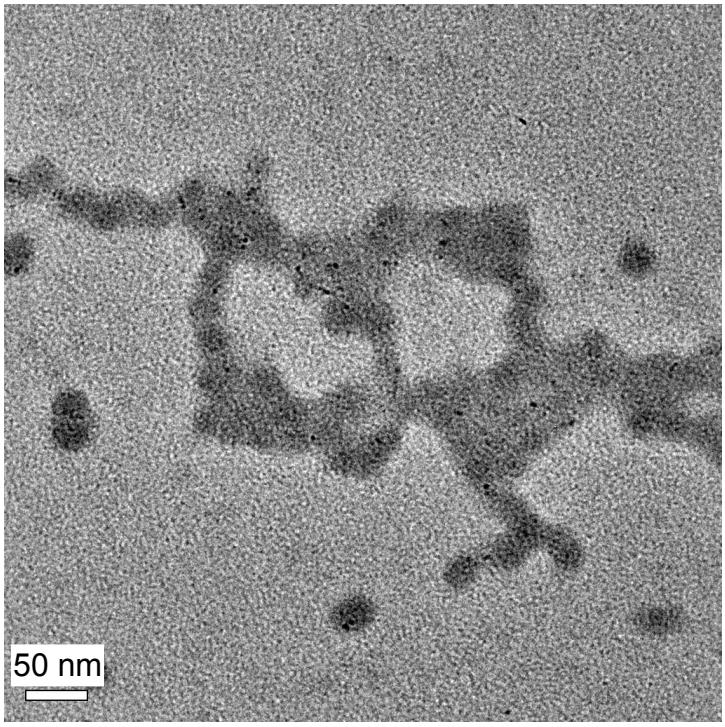

Figure A 28. TEM of **CM*P59C** from cross-linker **64**. Scale bar: 50 nm.

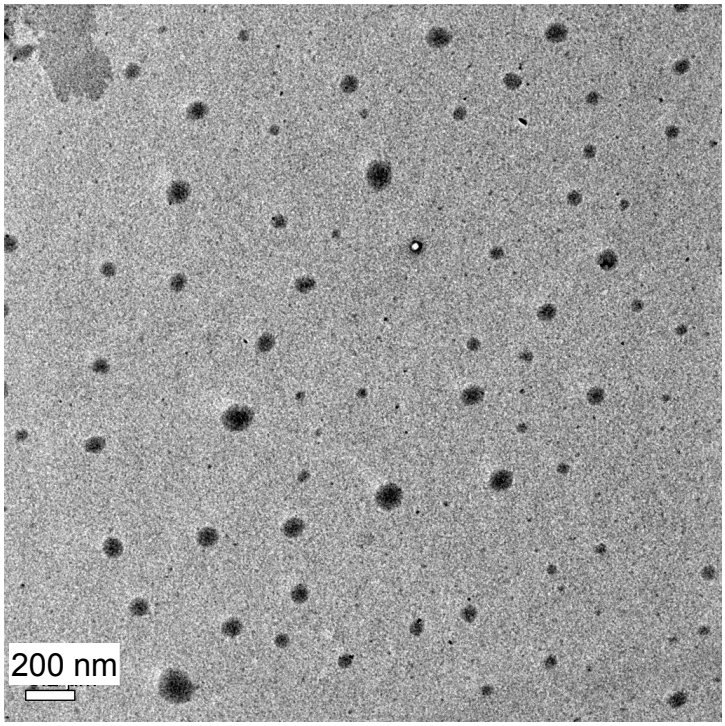

Figure A 29. TEM of **UCMP59D**. Scale bar: 200 nm.

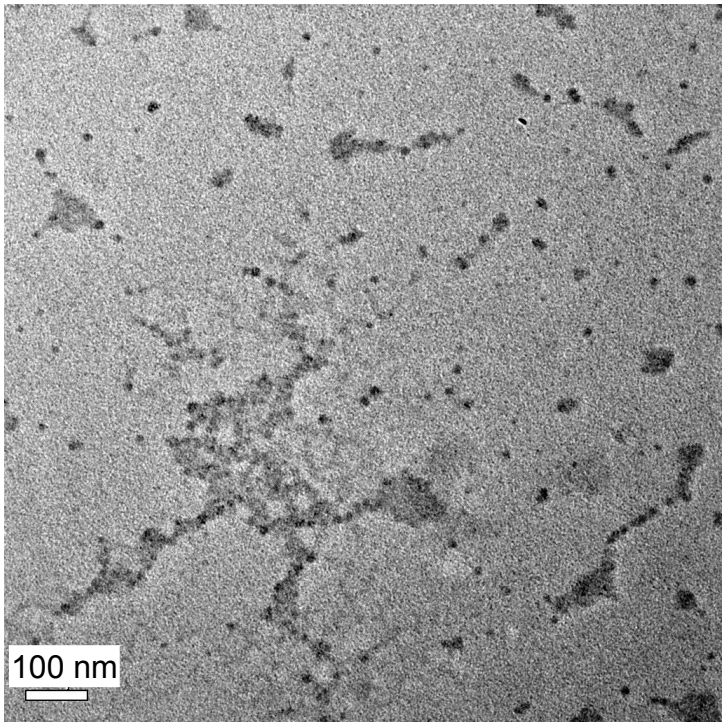

Figure A 30. TEM of **CMP59D** from cross-linker **63**. Scale bar: 100 nm.

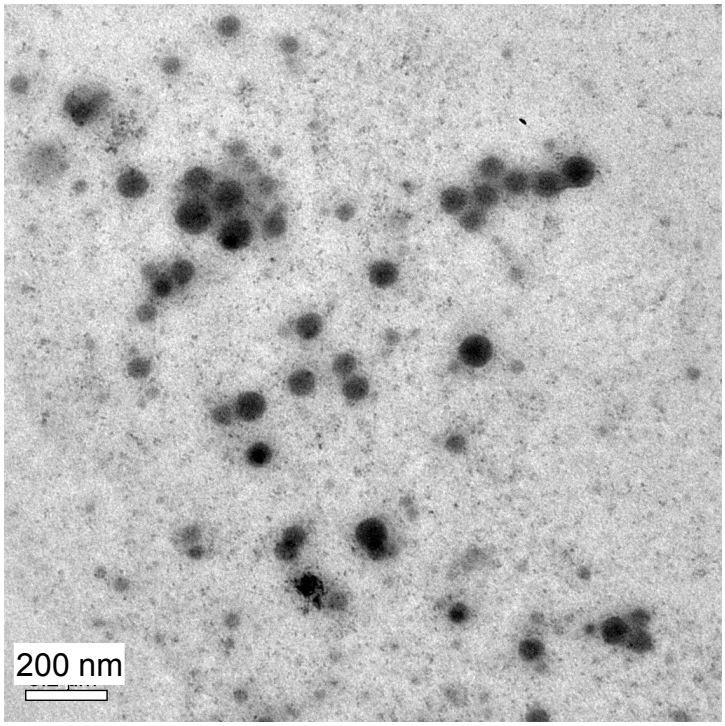

Figure A 31. TEM of **CM*P59D** from cross-linker **64**. Scale bar: 200 nm.

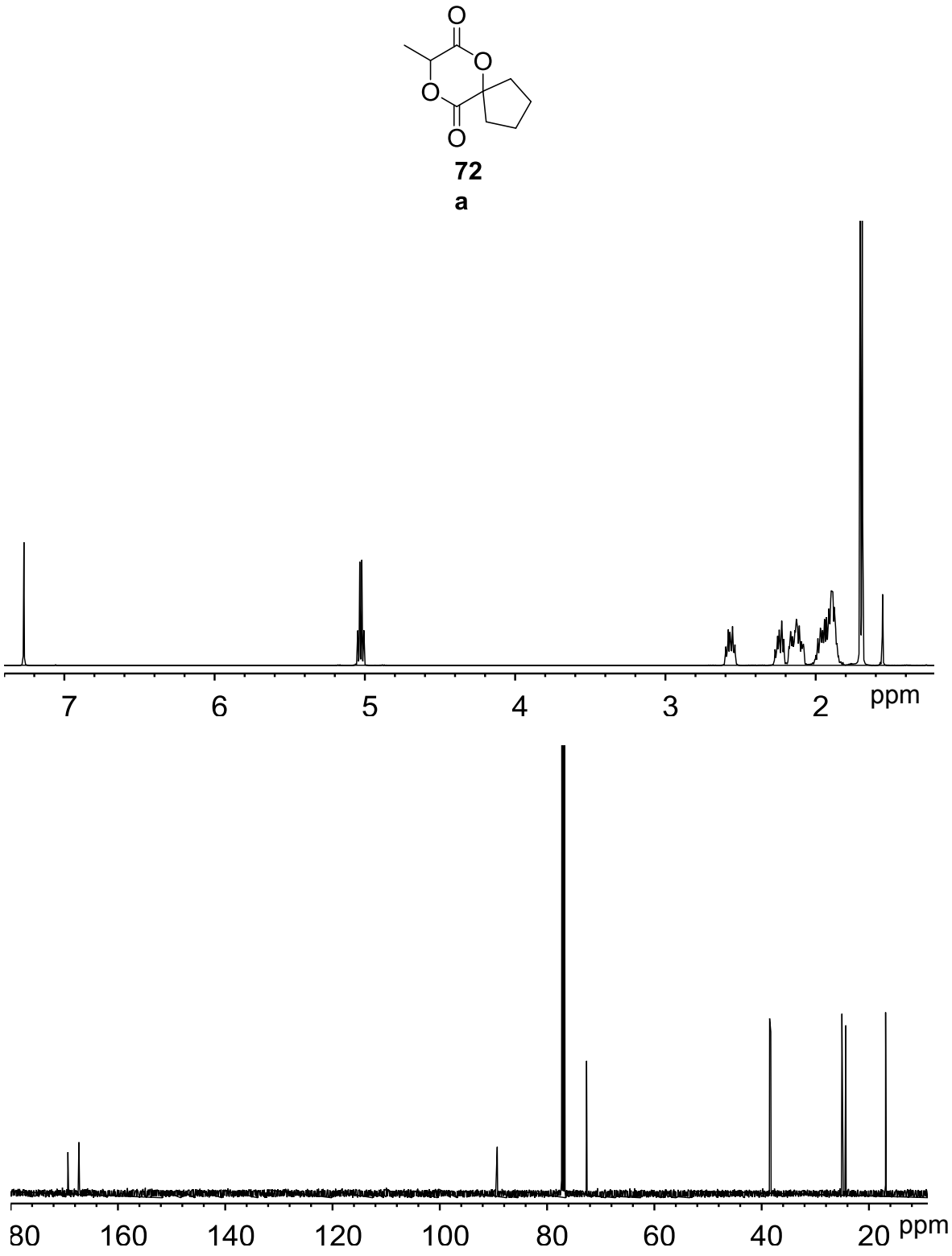

Figure A 32. ^{1}H and ^{13}C NMR spectra of monomer (**72a**) in $CDCl_3$.

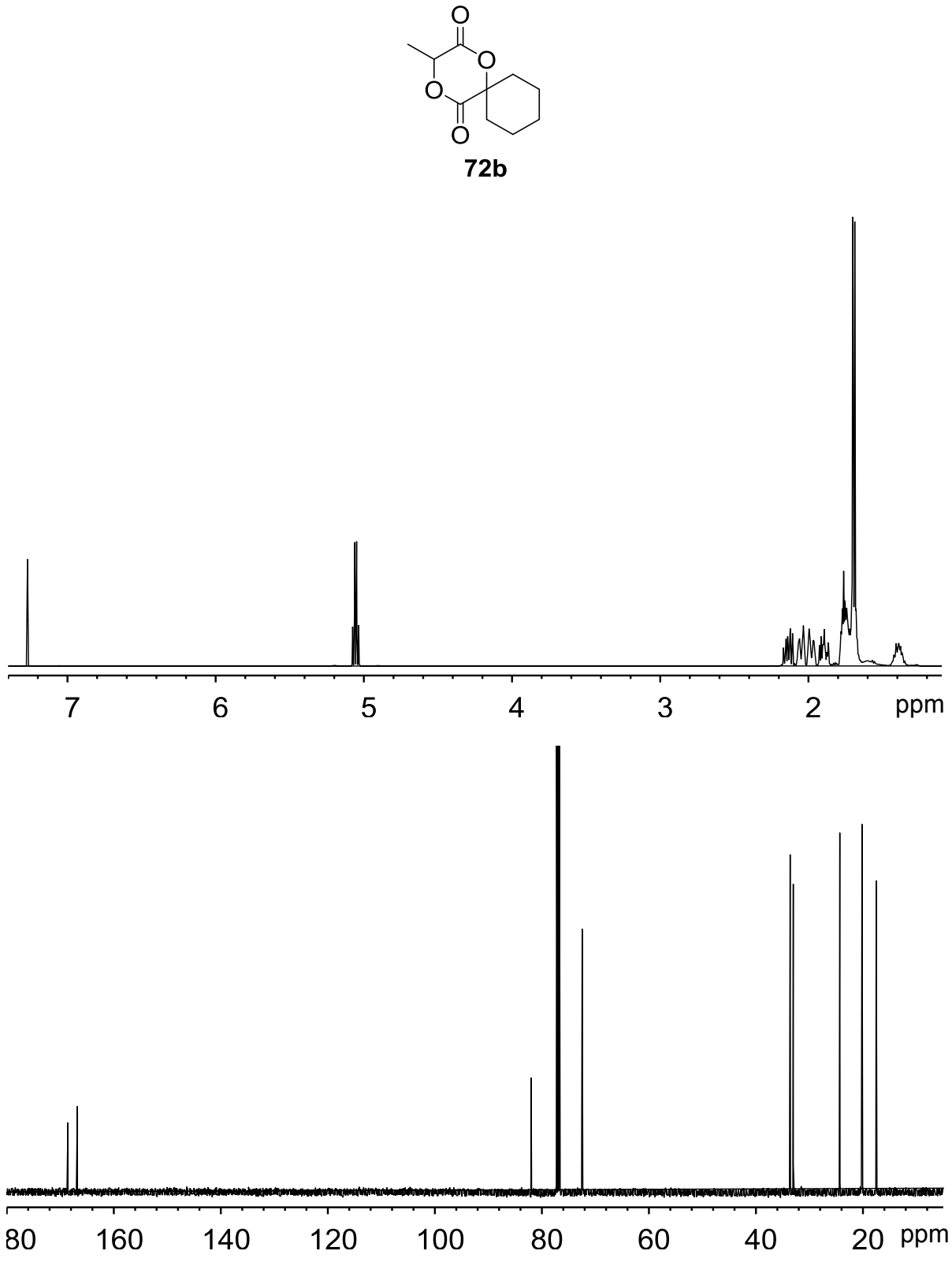

72b

Figure A 33. ^{1}H and ^{13}C NMR spectra of monomer (**72b**) in $CDCl_3$.

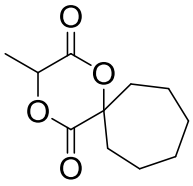

72c

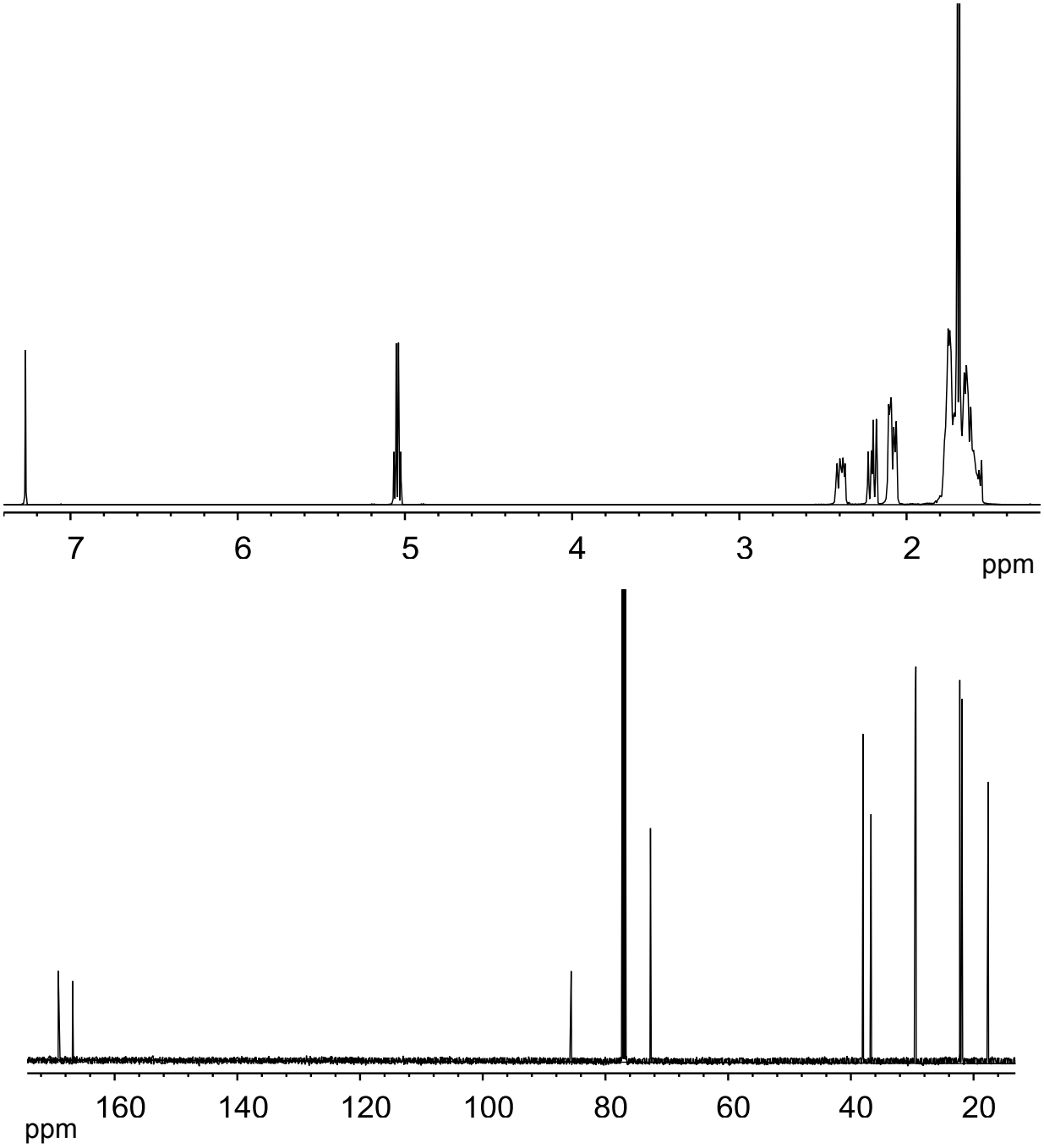

Figure A 34. ^{1}H and ^{13}C NMR spectra of monomer (**72c**) in $CDCl_3$.

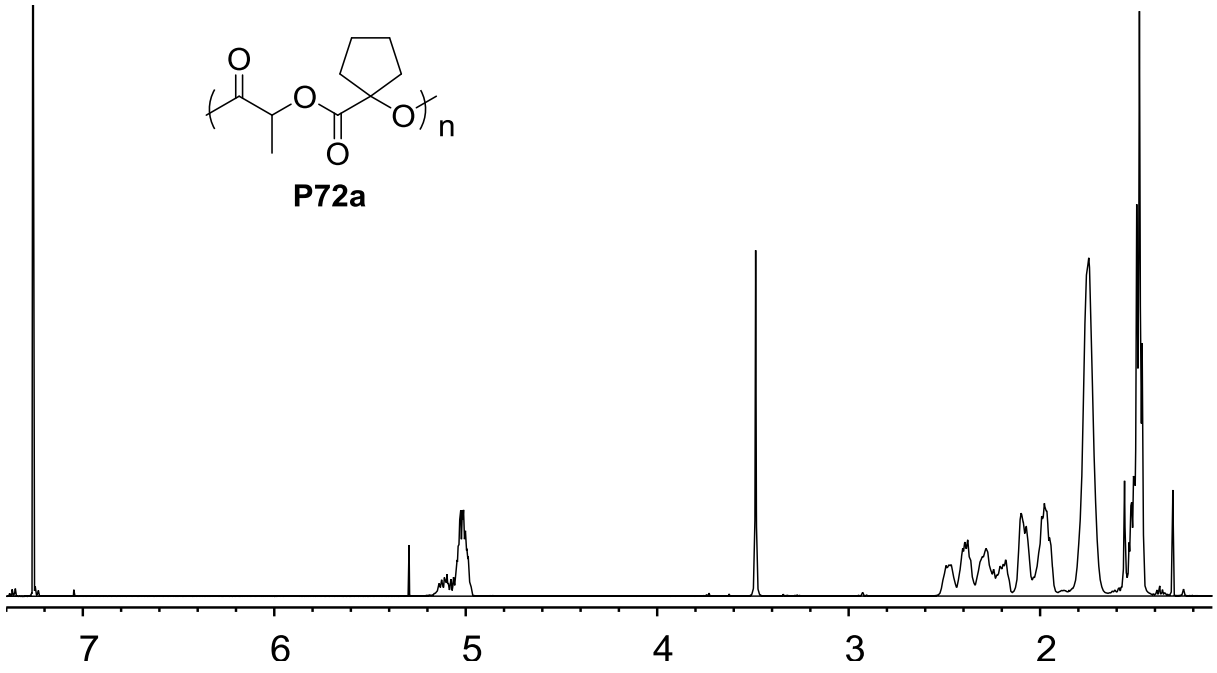

Figure A 35. ^{1}H NMR spectra of polymer (**P72a**) in $CDCl_3$.

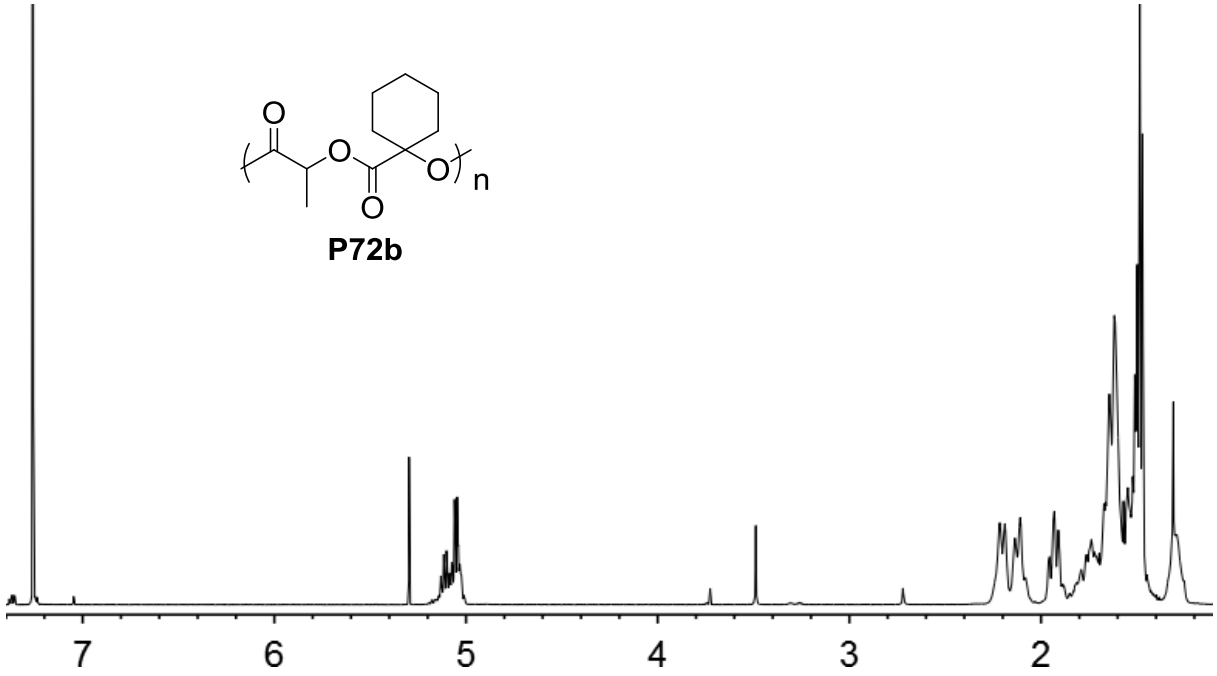

Figure A 36. ^{1}H NMR spectra of polymer (**P72b**) in $CDCl_3$.

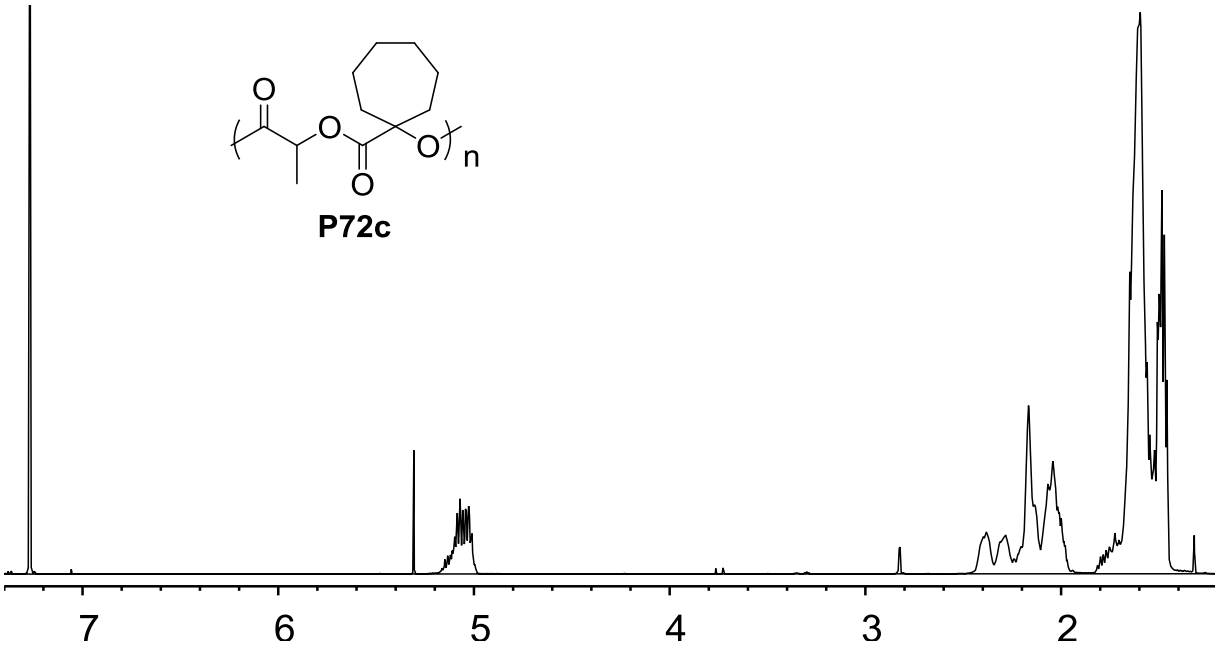

Figure A 37. ^{1}H NMR spectra of polymer (**P72c**) in $CDCl_3$.

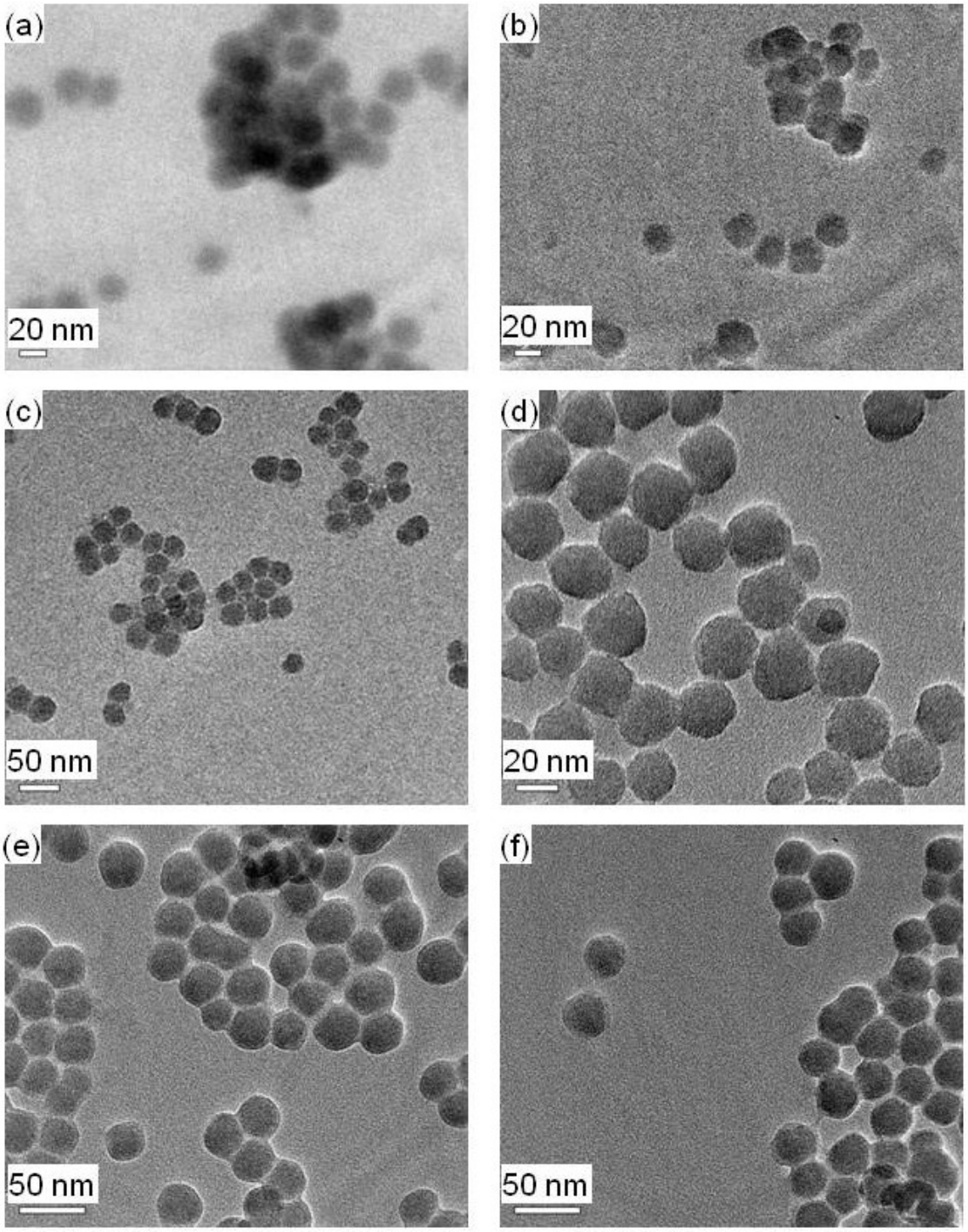

Figure A 38. TEM images of **SiNP25** (**a**); **SiNP25/74** (**b**); **SiNP25/76a** (**c**); **SiNP25/78** (**d**); **SiNP25/83** (**e**); **SiNP25/79** (**f**).

REFERENCES

REFERENCES

1. Datta, R.; Henry, M. J. *Chem. Technol. Biotechnol.* **2006**, *81*, 1119-1129.

2. Dechy-Cabaret, O.; Martin-Vaca, B.; Bourissou, D. *Chem. Rev.* **2004**, *104*, 6147–6176.

3. Drumright, R. E.; Gruber, P. R.; Henton, D. E. *Adv. Mater.* **2000**, *12*, 1841–1846.

4. Sinclair, R.G. *J. Macromol. Sci., Pure Appl. Chem.* **1996**, *33*, 585–597.

5. Prokop, A.; Jubel, A.; Helling, H. J.; Eibach, T.; Peters, C.; Baldus, S. E.; Rehm, K. E. *Biomaterials* **2004**, *25*, 259–267.

6. Claes, L. E.; Ignatius, A. A.; Rehm, K. E.; Scholz, C. *Biomaterials* **1996**, *17*, 1621–1626.

7. Meyer, D. C.; Fucentese, S. F.; Ruffleux, K.; Jacob, H. A. C.; Gerber, C. *Arthroscopy* **2003**, *19*, 188-193.

8. Albertsson, A. C.; Varma, I. K. *Biomacromolecules* **2003**, *4*, 1466-1486.

9. Pan, Z.; Ding, J. *Interface Focus* **2012**, rsfs20110123; doi:10.1098/rsfs.2011.0123 2042-8901.

10. Vij, N.; Min, T.; Marasigan, R.; Belcher, C. N.; Mazur, S.; Ding, H.; Yong, K-T.; Roy, I. *J. Nanobiotechnol.* **2010**, *8*:22.

11. Cao, Z.; Yu, Q.; Xue, H.; Cheng, G.; Jiang, S. *Angew. Chem. Int. Ed.*, **2010**, *49*, 3771–3776.

12. Acharya, S.; Sahoo, S. K. *Adv. Drug Deliver. Rev.* **2011**, *63*, 170-183.

13. Khanna, A.; Sudha, S. S.; Pillai, S.; Rath, S. S. *J. Mol. Model.* **2008**, *16*, 367-374.

14. Chen, G.; Kim, H.; Kim, E.; Yoon, J. *Eur. Polym. J.* **2006**, *42*, 468-472.

15. Moon, S. II; Lee, C. W.; Miyamoto, M.; Kimura, Y. *J. Polym. Sci., Part A: Polym. Chem.* **2000**, *38*, 1673-1679.

16. Marques, D. S.; Gil, M. H.; Baptista, C. M. S. G. *J. Appl. Polym. Sci.* **2012**, *128*, 2145–2151.

17. Ryner, M.; Stridsberg, K.; Albertsson, A.-C.; von Schenk, H.; Svensson, M. *Macromolecules* **2001**, *34*, 3877-3881.

18. Kowalski, A.; Duda, A.; Penczek, S. *Macromol*. *Rapid Commun*. ***1998****, 19*, 567-572.

19. Kricheldorf, H. R.; Kreiser-Saunders, I.; Stricker, A. *Macromolecules* **2000**, *33*, 702-709.

20. Nederberg, F.; Connor, E. F.; Moller, M.; Glauser, T.; Hedrick, J. L. *Angew. Chem. Int. Ed.* **2001**, *40*, 2712-2715.

21. Blakey, I.; Yu, G.; Howdle, S. M.; Whittaker, A. K.; Thurech, K. J. *Green Chem.* **2011**, *13*, 2032–2037.

22. Pratt, R. C.; Lohmeijer, B. G.G.; Long, D. A.; Waymouth, R. M.; Hedrick, J. L. *J. Am. Chem. Soc.* **2006**, *128*, 4556-4557.

23. Coady, D. J.; Engler, A. C.; Horn, H. W.; Bajjuri, K. M.; Fukushima, K.; Jones, G. O.; Nelson, A.; Rice, J. E.; Hedrick, J. L. *ACS Macro Lett.* **2012**, *1*, 19−22.

24. Nederberg, F.; Connor, E. F.; Glausser, T.; Hedrick, J. L. *Chem. Commun.* **2001**, 2066-2067.

25. Grasa, G. A.; Kissling, R. M.; Nolan, S. P. *Org. Lett.* **2002**, *4*, 3583–3586.

26. Connor, E. F.; Nyce, G. W.; Myers, M.; Mock, A.; Hedrick, J. L. J. Am. Chem. Soc 2002, 124, 914-915.

27. Nyce, G. W.; Glauser, T.; Connor,. E. F.; Mock, A.; Waymouth, R. M.; Hedrick, J. L. *J*. *Am*. *Chem*. *Soc*. **2003**, *125*, 3046–3056.

28. Myers, M.; Connor, E. F.; Glauser, T.; Mock, A.; Nyce, G.; Hedrick, J. L. *J. Polym. Sci., Part A: Polym. Chem.* **2002**, *40*, 844-851.

29. Dove, A. P.; Pratt, R. C.; Lohmeijer, B. G.; Waymouth, R. M.; Hedrick, J. L. *J. Am. Chem. Soc.* **2005**, *127*, 13798 -13799.

30. Kricheldorf, H. R.; Dunsing, R. *Makromol. Chem.* **1986**, *187*, 1611-1625.

31. Kricheldorf, H. R.; Kreiser, I. *Makromol. Chem*. **1987**,*188*, 1861-1873.

32. Bhaw-Luximon, A.; Jhurry, D.; Spassky, N.; Pensec, S.; Belleney, J. *Polymer* **2001**, *42*, 9651-9656.

33. Xie, W.; Chen, D.; Fan, X.; Li, J.; Wang, P. G.; Cheng, H. N.; Nickol, R. G. *J. Polym. Sci., Part A: Polym. Chem.* **1999**, *37*, 3486-3491.

34. Kricheldorf, H. R.; Lee, S.R. *Polymer* **1995**, *36*, 2995-3003.

35. Padovani, M.; Hilker, I.; Duxbury, c. J.; Heise, A. *Macromolecules* **2008**, *41*,

2439-2444.

36. Matsumura, S.; Mabuchi, K.; Toshima, K. *Macromol. Rapid Commun.* **1997**, *18*, 477-482.

37. Matsumura, S.; Tsukada, K.; Toshima, K. *Int. J. Biol. Macromol.* **1999**, *25*, 161-167.

38. Kobayashi, S.; Uyama, H. *Macromol. Symp.* **1999**, *144*, 237-246.

39. Parrish,; B.; Breitenkamp, R. B.; Emrick, T. *J. Am. Chem. Soc*. **2005**, *127*, 7404-7410.

40. Li, S.; Vert, M. *Macromolecules*, **2003**, *36*, 8008–8014.

41. Yang, L.; El Ghzaoui, A.; Li, S. *Int. J. Pharm.* **2010**, 96-103.

42. Ohya, Y.; Maruhashi, S.; Ouchi, T. *Macromolecules* **1998**, *31*, 4662-4665.

43. Ouchi, T.; Uchida, T.; Ohya, Y. *Macromol. Biosci.* **2001**, *1*, 371-375.

44. Stassen, S.; Archambeau, S.; Dobois, Ph.; Jerome, R.; Teyssie, Ph. *J. Polym. Sci. Part A: Polym. Chem.* **1994**, *32*, 2443-2455.

45. Tessmar, J. K.; Mikos, A. G.; Göpferich, A. *Biomacromolecules* **2002**, *3*, 194-200.

46. Nguyen, C. A.; Allémann, A.; Schwach, G.; Doelker, E.; Gurny, R. *Eur. J. Pharm. Sci.* **2003**, *20*, 217–222.

47. Kang, E-H.; Lee, I-H.; Choi, T-L. *ACS Macro Lett.* **2012*,*** *1*, 1098-1102.

48. Liu, X.; Li, K.;Feng, X.; Cao, Y*. J. Macromol. Sci., Pure Appl. Chem.***2009**, *46*, 937-942.

49. Basko, M.; Bednarek, M. *React. Funct. Polym.* **2012**, *72*, 213-220.

50. Lav, T.; Lemechko, P.; Renard, E.; Amiel, C.; Langlois, V.; Volet, G. *React. Funct. Polym.* **2013**, *73*, 1001-1008.

51. Molla, M. R.; Ghosh, S. *Macromolecules* **2012**, *45*, 8561-8570.

52. Barker, I. A.; Hall, D. J.; Hansell, C. F.; Du Prez, F.; O'Reilly, R. K.; Dove, A. P. *Macromol. Rapid Commu.* **2011**, *32*, 1362–1366.

53. Hwang, J. J.; Iyer, S. N.; Li, L. S.; Claussen, R.; Harrington, D. A.; Stupp, S. I. *PNAS* **2002,** *99*, 9662-9667.

54. Klok, H.-A.; Hwang, J. J.; Hartgerink, J. D.; Stupp, S. I. *Macromolecules* **2002**,

35, 6101-6111.

55. Stendahla, J. C.; Lia, L.; Claussen, R.; Stupp, S. I. *Biomaterials* **2004**, *25*, 5847–5856.

56. Klok, H. A.; Hwang, J. J.; Iyer, S. N.; Stupp, S. I. *Macromolecules* **2002**, *35,* 746-759.

57. Baker, G. L.; Vogel, E.B.; Smith III, M. R. *Polym. Rev.* **2008**, *48*, 64–84.

58. Yin, M.; Baker, G. L. *Macromolecules* **1999**, *32*, 7711–7718.

59. Simmons, T. L.; Baker, G. L. *Biomacromolecules* **2001**, *2*, 658–663.

60. Liu, T. Q.; Simmons, T. L.; Bohnsack, D. A.; Mackay, M. E.; Smith III, M. R.; Baker, G. L. *Macromolecules* **2007**, *40*, 6040–6047.

61. Jing, F.; Smith III, M. R.; Baker, G. L. *Macromolecules* **2007**, *40*, 9304-9312.

62. Gerhardt, W. E.; Noga, D. E.; Hardcastle, K. I.; García, A. J.; Collard, D. M.; Weck, M. *Biomacromolecules* **2006**, *7*, 1735-1742.

63 . Leemhuis, M.; van Nostrum, C. F.; Kruijtzer, J. A. W.; Zhong, Z. Y.; Breteler, M. R.; Dijkstra, P. J.; Feijen, J.; Hennink, W. E. *Macromolecules* **2006**, *39*, 3500-3508.

64. Noga, D. E.; Petrie, T. A.; Kumar, A.; Weck, M.; García, A. J.; Collard, D. M. *Biomacromolecules* **2008**, *9*, 2056–2062.

65. Ghassemi, A. H.; van Steenbergen, M. J.; Talsma, H.; van Nostrum, C. F.; Crommelin, D. J. A.; Hennink, W. E. *Pharm. Res.* **2010**, *27*, 2008-2017.

66. Lu, Y.; Yin, L.; Zhang, Y.; Zhang, Z.; Xu, Y.; Tong, R.; Cheng. J. *ACS Macro Letters* **2012**, *1,* 441-444.

67. Taguchi, K. Y., S.; Hiratani, K.; Norikio, M.; Okahata, Y. *Macromolecules* **1988**, *21*, 3338-3340.

68. Ouchi, T.; Fujino, A. *Makromol. Chem.* **1989**, *190*, 1523-1530.

69. Porjazoska, A.; Dimitrov, P.; Dimitrov, I.; Cvetkovska, M.; Tsvetanov, C. B. *Macromol. Symp.* **2004**, *210*, 427-436.

70. Lutz, J. F.; Hoth, A. *Macromolecules* **2006**, *39*, 893-896.

71. Jiang, X.; Smith III, M. R.; Baker, G. L. *Macromolecules* **2008**, *41*, 318-324.

72. Jiang, X.; Vogel, E. B.; Smith, M. R.; Baker, G. L. *J. Polym. Sci. A Polym.*

*Chem.***2007**, *45*, 5227–5236.

73. Castillo, J. A.; Borchmann, D. E.; Cheng, A. Y.; Wang, Y.; Hu, C.; García, A. J.; Weck, M. *Macromolecules* **2012**, *45*, 62-69.

74. Jing, F.; Hillmyer, M. A. *J. Am. Chem. Soc.* **2008**, *130*, 13826-13827.

75. Leemhuis, M.; Akeroyd, N.; Kruijtzer, J. A. W.; van Nostrum, C. F.; Crommelin, D. J. A.; Hennink, W. E. *Eur. Polym. J.* **2008**, *44*, 308-317.

76. Zou, J.; Hew, C. C.; Themistou, E.; Li, Y.; Chen, C.-K.; Alexandridis, P.; Cheng, C. *Adv. Mater.* **2011**, *23*, 4274–4277.

77. Jiang, X.; Vogel, E. B.; Smith III, M. R.; Baker, G. L. *Macromolecules* **2008**, *41*, 1937-1944.

78. Rubinshtein, M.; James, C. R.; Young, J. L.; Ma,Y. J.; Kobayashi, Y.; Gianneschi, N. C.; Yang, J. *Org. Lett.* **2010**, *12*, 3560–3563.

79. Gutiérrez-Villarreal, M. H.; Guzmán-Moreno, J. G.; *J. Polym. Res.* **2013**, 20:149.

80. Carlisle, E. S.; Mariappan, M. R.; Nelson, K. D.; Thomes, B. E.; Timmons, R. B.; Constantinescu, A.; Eberhart, R. C.; Bankey, P. E. *Tissue Eng.* **2000**, *6*, 45-52.

81. Edlund, U.; Källrot, M.; Albertsson, A. C. *J. Am. Chem. Soc.* **2005**, *127*, 8865-8871.

82. Källrot, M.; Edlund, U.; Albertsson, A. C.*Biomacromolecules* **2007**, *8*, 2492-2496.

83. Pan, J.; Wang, Y. L.; Qin, S. H.; Zhang, B. B.; Luo, Y. F. *J. Biomed. Mater. Res. Part B* **2005**, *74B*, 476-480.

84. Porter, K.; Hossain, M.; Wang, M.; Radano, C. P.; Baker, G.; Smith, M. R.; McCabe, L. R. *Mol. Biol. Rep.* **2006**, *33*, 1-12.

85. du Boullay, O. T.; Bonduelle, C.; Martin-Vaca, B.; Bourissou, D. *Chem. Commun.* **2008**, 1786-1788.

86. Kolb, H. C.; Finn, M. G.; Sharpless, K. B. *Angew. Chem. Int. Ed.* **2001**, *40*, 2004–2021.

87. Ott, C.; Hoogenboom, R.; Schubert, U. S. *Chem. Commun.* **2008**, 3516–3518.

88. Becer, C. R.; Babiuch, K.; Pilz, K.; Hornig, S.; Heinze, T.; Gottschaldt, M.; Schubert, U. S. Macromolecules **2009**, *42*, 2387–2394.

89. Killops, K. L.; Campos, L. M.; Hawker, C. J. *J. Am. Chem. Soc.* **2008**, *130*, 5062-5064.

90. Witczak, Z. J.; Lorchak, D.; Nguyen, N.; *Carbohydr. Res.* **2007**, *342*, 1929–1933.

91. Stanford,, M. J.; Dove, A. P.*Macromolecules* **2009**, *42*, 141–147.

92. Dag, A.; Durmaz, H.; Hizal, G.; Tunca, U. *J. Polym. Sci. Part A Polym. Chem.* **2008**, *46*, 302–313.

93. Williams, R. J.; Barker, I. A.; O'Reilly, R. K.; Dove, A. P. *ACS Macro Lett.* **2012**, *1*, 1285−1290.

94. Chen, C.-K.; Law, W.-C.; Aalinkeel, R.; Nair, B.; Kopwitthaya, A.; Mahajan, S. D.; Reynolds, J. L.; Zou, J.; Schwartz, S. A.; Prasad, P. N.; Cheng, C. *Adv. Healthcare Mater.* **2012**, *1*, 751-761.

95. Jones, C. H.; Chen, C. K.; Jiang, M.; Fang, L.; Cheng, C.; Pfeifer, B. A. *Mol. Pharm.* **2013**, *4,* 1138-1145.

96. Zhang, Z.; Yin, L.; Tu, C.; Song, Z.; Zhang, Y.; Xu, Y.; Tong, R.; Zhou, Q.; Ren, J.; Cheng, J. *ACS Macro Lett.* **2013**, *2*, 40–44.

97. Zhang, Z.; Yin, L.; Xu, Y.; Tong, R.; Lu, Y.; Ren, J.; Cheng, J. *Biomacromolecules* **2012**, *13*, 3456−3462.

98. Dimitrov, I.; Trzebicka, B.; Müller, A. H. E.; Dworak, A.; Tsvetanov, C. B. *Prog. Polym. Sci.* **2007**, *32*, 1275–1343.

99. Nalluri, S. K. M.; Voskuhl, J.; Bultema, J. B.; Boekema, E. J.; Ravoo, B. J. *Angew. Chem. Int. Ed.* **2011**, *50*, 1–6.

100. Akhoury, A.; Bromberg, L.; Hatton, T. L. *ACS Appl. Mater. Interfaces* **2011**, *3*, 1167–1174.

101. Jeong, B.; Bae, Y. H.; Lee, D. S.; Kim, S. W. *Nature* **1997**, *388*, 860–862.

102. Cunningham, A.; Oh, J. K. *Macromol. Rapid Commun.* **2013**, *34*, 163–168.

103. Fujishige, S.; Kubota, K.; Ando, I. *J. Phys. Chem.* **1989**, *93*, 3311–3313

104. Chen, G. H.; Hoffman, A. S. *Nature* **1995**, *373*, 49–52.

105. Chen, S.; Pieper, R.; Webster, D. C.; SinghInt. J. *Int. J. Pharm.* **2005**, *288*, 207–218.

106. Feil, H.; Bae, Y. H.; Feijen, J.; Kim, S. W. *Macromolecules* **1993**, *26*, 2496–2500.

107. Verma, A.; Simard, J. M.; Worrall, J. W. E.; Rotello, V. M. *J. Am. Chem. Soc.* **2004**, *126*, 13987-13991

108. Fiore, G. L.; Jing, F.; Young, Jr., V. G.; Cramer, C. J.; Hillmyer, M. A. *Polym. Chem.* **2010**, *1*, 870-877.

109. The routes shown in Scheme 30 are unpublished and will not be presented in this thesis.

110. Downs, A. J. Chemistry of Aluminium, Gallium, Indium and Thallium, 1st ed., 1993,pp. 372 Springer.

111. Murray, T. F.; Samsel, E. G.; Varma, V.; Norton, J. R. *J. Am. Chem. Soc.* **1981**, *103,* 7520–7528.

112. Buser, D.; Pauling, H.; Thum, A.; Bonrath, W**.** *Molecules* **2002**, *7*, 341-352.

113. Holmes, A. B.; Sporikou, C. N. *Org. Synth.***1987**, *65*, 61-65.

114. Suzuki, T.; Saimoto, H.; tomioka, H.; Oshima, K.; Nozaki, H. *Tetrahedron Lett*. **1982**, *23,* 3597-3600.

115. Roush, W. R.; Blizzard, T. A.; Basha, F. *Tetrahedron Lett*. **1982**, *23*, 2331-2334.

116. Akita, H.; Matsukura, H.; Oishi, T. *Tetrahedron Lett.* **1986**, *27*, 5397-5400.

117. Larcheveque, M.; Peit, Y. *Bul.l Soc. Chim. Fr.* **1986**, 130-139.

118. Mole, T,; Surtee, J. R. *Chem. Ind.* **1963**, *43*, 1727-1728.

119. Srinivasan, R.; Uttamchandani, M.; Shao Q. Yao, S. Q. *Org. Lett.* **2006**, *8*, 713-716.

120. Brea, R. J.; López-Deber, M. P.; Castedo, L.; Granja, J. R. *J. Org. Chem.* **2006**, *71,* 7870-7873.

121. Dragovich, P. S.; Prins, T.J.; Zhou, R. et al. *J. Med. Chem.* **2003**, *46*, 4572–4585.

122. Feifel, S. C.; Schmiederer, T.; Hornbogen, T.; Berg, H.; Sssmuth, R. D.; Zocher, R. *ChemBioChem* **2007**, *8*, 1767–1770.

123. Davison, E. C.; Fox, M. E.; Holmes, A. B. et al. *J. Chem. Soc. Perkin Trans. 1* **2002**, 1494-1514.

124. Nishida, H.; Miyazaki, Y.; Mukaihira, T.; Saitoh, F.; Fukui, M.; Harada, K.; Itoh, M.; Muraoka, A.; Matsusue, T.; Okamoto, A.; Hosaka, Y.; Matsumoto, M.; Ohnishi, S.; Mochizuki, H. *Chem. Pharm. Bull.* **2002**, *50*, 1187-1194.

125. Liu, C. F.; Tam, J. P. *Proc. Natl. Acad. Sci. U.S.A.* **1994**, *91,* 6584-6588.

126. Vugts, D. J.; Aktas, H.; Al-Mafraji, K.;Orru, R. V. A. et al. *Eur. J. Org. Chem.*

2008, 1336-1339.

127. Compernolle, F.; Toppet, S. *J. Heterocyclic Chem.* **1986**, *23*, 541–544.

128. Bitan,G.; Muller, D.; Kasher, R.; Gluhov, E. V.; Gilon, C. *J. Chem. Soc., Perkin Trans. 1* **1997**, 1501-1510.

129. Plank, C.; Mechtler, K.; Szoka, F. S. Jr.; Wanger, E. *Hum. Gene Ther.* **1996**, *7*, 1437-1446.

130. Pozzo, A. D.; Vigo, A.; Donzelli, G. *Makromol. Chem.* **1989**, *190*, 2457–2461.

131. Chen, Y.; Baker, G. L. *J. Org. Chem.* **1999**, *64*, 6870-6873.

132. Bhattacharya, B.; Dileep, P. V. *Bioconjugate Chem.* **2004**, *15*, 508-519.

133. Wang, C.; Zhang, H. *Synth. Commun.* **2002**, *32*, 3465-3468.

134. Ahmed, S. A.; Tanaka, M. *J. Org. Chem.* **2006**, *71*, 9884-9886.

135. Liang, C.; Feng, Y.; Vojkovsky, T. *PCT Int. Appl.* WO2006127961, **2006**.

136. Krasovskiy, A.; Knochel, P. *Synthesis* **2006**, *5*, 890–891.

137. Torchilin, V. P. *Pharm. Res.* **2007**, *24*, 1–16.

138. O'Reilly, R. K.; Hawker, C. J.; Wooley, K. L. *Chem. Soc. Rev.* **2006**, *35*, 1068–1083.

139. Weaver, J. V. M; Tang, Y. Q.; Liu, S. Y.; Iddon, P. D.; Grigg, R.; Billingham, N. C.; Armes, S. P.; Hunter, R.; Rannard, S. P. *Angew. Chem. Int. Ed.* **2004**, *43*, 1389–1392.

140. Jiang, X. Z.; Liu, S. Y.; Narain, R. *Langmuir* **2009**, *25*, 13344–13350.

141. Opsteen, J. A. and van Hest, J. C. M., *Chem. Commun.* **2005**, 57-59.

142. Malkoch, M., Schleicher, K., Drockenmuller, E., Hawker, C. J., Russell, T. P., Wu, P., and Fokin, V. V., *Macromolecules*, **2005** *38,* 3663-3678.

143. Parrish, B., Breitenkamp, R. B., and Emrick, T., *J. Am. Chem. Soc.*, **2005** *127,* 7404-7410.

144. Dubois, P.; Ropson, N.; Jerome, R.; Teyssie, P. *Macromelecules*, **1996**, *29*, 1965-1975.

145. Yin, M.; Baker, G. L. *Macromolecules* **1999**, *32*, 7711-7718.

146. Settle, F. A. *Handbook of Instrucmental Techniques for Analytical Chemsitry*; Prentice Hall: 1997, p 856, Chapter 4.

147. Khosravi, E.; Yagci, Y.; Savelyev, Y. *New Smart Materials via Metal Mediated Macromolecular Engineering*; Springer: 2009, p 157.

148. Bertini, F.; Audisio, G.; Kiji, J.; Fujita, M. *J. Anal. Appl. Pyrolysis* **2003**, *68–69*, 61–81.

149. Fournier, D.; Du Prez, F. *Macromolecules* **2008**, *41*, 4622-4630.

150. Leemhuis, M.; van Nostrum, C. F.; Kruijtzer, J. A. W.; Zhong, Z. Y.; Feijen, J.; Hennink, W. E. *Macromolecules* **2006**, *39*, 3500-3508.

151. Kim, J. H.; Jang, J.; Lee, D-Y.; Zin, W-C. *Macromolecules*, **2002**, *35*, 311–313.

152. Tsai, Y.; Fan, C.-H.; Hung, C.-Y.; Tsai, F.-J. *J. Appl. Polym. Sci.* **2008**, *109*, 2598–2604.

153. Hiemenz, P. C.; Lodge, T. P. *Polymer Chemistry*; Boca Raton, CRC Press, 2007, p 493.

154. Sperling, L.H. *Glass-Rubber Transition Behavior, in Introduction to Physical Polymer Science*, Fourth Edition, John Wiley & Sons, Inc., Hoboken, NJ, USA: 2005, p 401.

155. Kraus, G.; Childers, C. W.; Gruver, J. T. *J. Appl. Polym. Sci.* **1967**, *11*, 1581–1591.

156. Guo, M.; Yu, T.; Xue, Z. *Makromol. Chem., Rapid Commun.* **1987**, *8*, 601–605.

157. Zhou, X.-M; Jiang, Z.-H. *J. Polym. Sci. B Polym. Phys.* **2005**, *43*, 1624–1630.

158. Parrish, B.; Breitenkamp, R. B.; Emrick, T. *J. Am. Chem. Soc.* **2005**, *127*, 7404-7410.

159. Silvers, A. L.; Chang, C.-C.; Emrick, T. *J. Polym. Sci. A Polym. Chem.* **2012**, *50*, 3517–3529.

160. Lu, C.; Shi, Q.; Chen, X.; Lu, T.; Xie, Z.; Hu, X.; Ma, J.; Jing, X. *J. Polym. Sci. A Polym. Chem.* **2007**, *45*, 3204-3217.

161. Khosravi, E. et al. Editor, *New Smart Materials via Metal Mediated macromolecular Engineering,* Springer Science: 2009, p 77.

162. Tachibana, Y.; Kurisawa, M.; Uyama, H.; Kobayashi, S. *Biomacromolecules* **2003**, *4,* 1132-1134.

163. Shimokuri, T.; Kaneko, T.; Akashi, M. *J. Polym. Sci. A Polym. Chem.* **2004**, *42*, 4492-4501.

164. Chen, C.; Wang, Z.; Li, Z. *Biomacromolecules* **2011**, *12,* 2859-2863.

165. Rijcken, C. J. F.; Soga, O.; Hennink, W. E.; van Nostrum, C. F. *J. Control. Release* **2007**, *120*, 131-148.

166. Behnke, T.; Würth, C.; Hoffmann, K.; Hübner, M.; Panne, U.; Resch-Genger, U. *J Fluoresc.* **2011**, *21*, 937-944.

167. Zhang, Y.; Zhang, Q.; Zha, L.; Yang, W.; Wang C.; Jiang, X.; Fu, S. *Colloid Polym. Sci.* **2004**, *282*, 1323-1328.

168. Ren, J.; Hong, H.; Song, J.; Ren, T. *J. Appl. Polym. Sci*. **2005**, *98*, 1884–1890.

169. Li, Y.; Qi, X. R.;Matani, Y.; Nagai, T. *Nanotechnology* **2009**, *20*, 055106.

170. Govender, T.; Stolnik, S.; Garnett, M. C.; Illum, L.; Davis, S. S. *J. Control. Release* **1999**, *99*, 171–185.

171. Gref, R.; Mück, M.; Quellec, P.; Marchand, M.; Dellacherie, E.; Harnisch, S.; Blunk, T.; Müller, R. H. *Colloids Surf., B* **2000**, *18*, 301-313.

172. Wu, Y.; Chen, W.; Meng, F.; Wang, Z.; Cheng, R.; Deng, C.; Liu, H.; Zhong, Z. *J. Control. Release* **2012**, *164*, 338-345.

173. Liu, T.; Simmons, T. L.; Bohnsack, D. A.; Mackay, M. E.; Smith, M. R.; Baker, G. L. *Macromolecules* **2007**, *40*, 6040-6047.

174. Rudine, A. B.; Walter, M. G.; Wamser, C. C. *J. Org. Chem.* **2010**, *75*, 4292-4295.

175. Mills, J. E.; Maryanoff, C. A.; McComsey, D. F.; Stanzione, R S.; Scott, S. *J. Org. Chem.* **1987**, *52*, 1857-1859.

176. McQuillin, F. J.; Baird, M. S. *Acycli Chemistry*, Second Edition, Cambridge University Press, 1983, p 10.

177. Settle, F. A. *Handbook of Instrucmental Techniques for Analytical Chemsitry*; Prentice Hall: 1997, p 856, Chapter 4.

178. Zhang, J. M.; Sato, H.; Tsuji, H.; Noda, I.; Ozaki, Y. *Macromolecules* **2005**, *38*, 1822−1828.

179. Ravi Kumar, M. N.; Sameti, M.; Mohapatra, S. S.; Kong, X.; Lockey, R. F.; Bakowsky, U.; Lindenblatt, G.; Schmidt, H.; Lehr, C. M. *J. Nanosci. Nanotechnol.*

2004, *4*, 876-881.

180. Mahtab, F.; Lam, J. W. Y.; Yu, Y.; Liu, J.; Yuan, W.; Lu, P.; Tang, B. Z. *Small*, **2011**, *7*, 1448–1455.

181. Wang, T,; Jiang, H.; Zhao, Q.; Wang, S.; Zou, M.; Cheng, G. *Int. J. Pharm.* **2012**, *436*, 351-358.

182. Mader, H.; Li, X.; Saleh, S.; Link, M.; Kele, P.; Wolfbeis, O. S. *Ann. N.Y. Acad. Sci.* **2008**, *1130*, 218–223.

183. Bagwe, R. P.; Hilliard, L. R.; Tan, W. *Langmuir* **2006**, *22*, 4357–4362.

184. Achatz, D. E.; Heiligtag, F. J.; Li, X.; Link, M.; Wolfbeis, O. S. *Sens. Actuators, B* **2010**, *150*, 211-219.

185. Lu, X.; Sun, F.; Wang, J.; Zhong, J.; Dong, Q. *Macromol. Rapid Commu.* **2009**, *30*, 2116-2120.

186. Chen, C., Geng, J., Pu, F., Yang, X., Ren, J. and Qu, X. *Angew. Chem. Int. Ed.* **2011**, *50*, 882–886.

187. Kele, P., Mezö, G., Achatz, D. and Wolfbeis, Otto S. *Angew. Chem. Int. Ed.* **2009**, *48*, 344–347.

188. Howard, M. D.; Jay, M.; Dziublal, T. D.; Lu, X. L. *J. Biomed. Nanotechnol.* **2008**, *4*, 133-148.

189. Karakoti, A.; Das, S.; Thevuthasan, S.; Seal, S. *Angew. Chem. Int. ed.* **2011**, *50*, 2-17.

190. Choualeb, A.; Ros, J.; Braustein, P.; Welter, R. *Organometallics* **2003**, *22*, 2688-2693.

191. Lu, X.; Sun, F.; Wang, J.; Zhong, J.; Dong, Q. *Macro. Rapid Commun.* **2009**, *30*, 2116-2120.

192. Li, G.; Bhosale, Sh. V.; Wang, T.; Hackbarth, S.; Roeder, B.; Siggel, U.; Fuhrhop, J-H *J. Am. Chem. Soc.* **2003**, *125*, 10693-10702.

193. James, M.; Ciampi, S.; Darwish, T. A.; Hanley, T. L.; Sylvester, S.O.; Gooding, J. J. *Langumir* **2011**, *27*, 10753-70762.

194. Pandey, P.; Farha, O.; Spokoyny, A.; Mirkin, C.; Kanatzidis, M.; Hupp, J.; Nguyen, S. *J. Mater. Chem.* **2011**, *21*, 1700-1703.

195. Yildirim, A.; Ozqur, E.; Bayindir, M. *J. Mater. Chem. B* **2013**, *1*, 1909-1920.

196. Wang, J.; Meng, G.; Tao, K.; Feng, M.; Zhao, X.; Li, Z.; Xu, H.; Xia, D.; Lu, J. R. *PLoS ONE* **2012**, *7*, e43478.

197. Zdyrko, B.; Luzinov, I. *Macromol. Rapid Commun.***2011**, *32*, 859–869.

198. Bevan, M. A.; Prieve, D. C. *Langmuir* **2000**, *16*, 9274-9281.

199. Ito, T.; Sun, L.; Bevan, M. A.; Crooks, R. M. *Langmuir* **2004**, *20,* 6940–6945.

200. Jiang, J.K.; Oberdorster, G.; Biswas, P. *J. Nanopart. Res.* **2009**, *11*, 77–89.

201. Brantley, J. N.; Wiggins, K. M.; Bielawski, C. W. *Science* **2011**, *16*, 1606-1609.

202. Kamart, M.; El-Boubbou, K.; Zhu, D.; Lansdell, T.; Lu, X.; Li, W.; Huang, X. *Bioconjugate Chem.* **2010**, *21*, 2128-2135.

203. Hu, F.; MacRenaris, K. W.; Waters, E. A.; Liang, T.; Schultz-Sikma, E. A.; Eckermann, A. L.; Meade, T. J. *J. Phys. Chem. C* **2009**, *113*, 20855–20860.